Title
Evaluating Climate Impacts and Inequities in Regions Prone to Human Displacement and Out-Migration

Author
Depsky, Nicholas J

Publication Date
2023

Peer reviewed|Thesis/dissertation

Evaluating Climate Impacts and Inequities in Regions Prone to Human Displacement and Out-Migration

By

Nicholas J. Depsky

A dissertation submitted in partial satisfaction of the

requirements for the degree of

Doctor of Philosophy

in

Energy and Resources

in the

Graduate Division

of the

University of California, Berkeley

Committee in charge:

Professor Solomon Hsiang, Co-Chair
Professor Andrew Jones, Co-Chair
Professor Rachel Morello-Frosch

Spring 2023

Evaluating Climate Impacts and Inequities in Regions Prone to Human Displacement and Out-Migration

Abstract

Evaluating Climate Impacts and Inequities in Regions Prone to Human Displacement and Out-Migration

By

Nicholas J. Depsky

Doctor of Philosophy in Energy and Resources Group

University of California, Berkeley

Professor Solomon Hsiang, Co-Chair
Professor Andrew Jones, Co-Chair

As climate hazards and their associated socioeconomic impacts become more severe, individuals and governments across the globe are reckoning with how best to adapt. For some, this might entail staying in place and altering their behaviors, livelihoods and investments as temperatures rise and rainfall becomes more variable. For others, however, the increased risk of physical harm, economic loss and social instability wrought by worsening climatic conditions may compel them to migrate in search of security elsewhere. Identifying how climate phenomena influence human movement can be straightforward, such as forced displacement that occurs following the physical destruction of a storm, flood or fire; however, in many instances, the climate-migration relationship is more opaque. Impacts on economic productivity, health and wellbeing from chronic stressors like drought, heatwaves, desertification and sea level rise may spur certain members of an afflicted region to out-migrate, while limiting the ability of others to do so, and will occur amidst a multitude of other, non-climatic influencing factors. Therefore, disentangling the manner and extent to which climate has driven human migration in the past, and the potential for it to do so in the future, is a challenging yet critical priority to shaping robust, proactive adaptation policies and humane migration governance frameworks moving forward.

This dissertation helps address this need by investigating the intersection of climate impacts, inequities and human displacement in various contexts. It is segmented into three distinct chapters based on relevance to i) Central America, ii) the United States and iii) global coastlines, regions in which climate-migration dynamics are likely to become increasingly relevant. The chapters are comprised of the following project-based subsections: (i) assessing 21st century drought projections in Central America's Dry Corridor, which finds that seasonal and annual-scale droughts in the region are projected to lengthen, intensify and increase in frequency throughout the remainder of the century; (ii) modeling of international emigration and internal migration, as reported in the Guatemalan 2018 national census, using sociodemographic, physical and climatic covariates, finding various sociodemographic variables and drought stress as significant predictors of out-migration from the country; (iii) reviewing literature linking climate hazards, internal displacement, movement and inequities in the United States, which assesses the complex manner by which acute and chronic climatic hazards impact human displacement and exacerbate social inequality; (iv) producing high-resolution dasymetric maps of population in

California using the 2020 census for various demographic subgroups, which are publicly available and useful in evaluating geospatial population distributions across the state for any number of research applications, and which to date have included numerous climate change, environmental justice and health equity studies; (v) conducting geospatial analysis of Hurricane Maria's impact on Puerto Rican power supply, recovery and re-electrification and correlational relationships to subsequent out-migration, with constructed models explaining up to 82% of observed variance in post-storm power outage patters, indicating both physical and socioeconomic variables as being significant predictors of prolonged recovery; and (vi) creating an open-source coastal impacts and adaptation modeling platform along fine-scale global coastlines for multiple scenarios of 21st century sea level rise, which was used to inform the U.S. Environmental Protection Agency's updated social cost of carbon estimate and suggests that, globally, between 16-46 million people are expected to relocate inland by 2100 if optimal adaptation strategies are undertaken and up to 200 million people under high-end sea level rise and sub-optimal adaptation pathways.

Contents

Acknowledgements

The majority of the work, sacrifice and support it took to complete this PhD is not articulated in the words, tables or charts on the following pages. Although these chapters serve as the 'physical' manifestation of my accomplishments over the course of the last five and a half years, they do not reflect the unyielding support from the countless friends, family and colleagues it took to me to stay motivated, to stay sane. In many ways, the knowledge, skills and lessons I have learned as a graduate student and the ways in which I have grown are largely unrelated to the actual number-crunching and paper writing I did whilst affixed to a screen.

I would therefore like to start by acknowledging all of the academic advising and guidance I received. Special thanks to my dissertation committee for the many hours they spent teaching, reading my work, writing letters of recommendation and providing motivation over the years. Thank you to Solomon Hsiang for the unparalleled care, attention and excitement you showed me these last few years and for providing me with an incredibly rich academic home since my joining the Climate Impact and Global Policy Labs. To Andy Jones, thank you for your superb academic mentorship, genuine enthusiasm towards my work, meticulous feedback and for your consistent convening of much-needed happy hours. To Rachel Morello-Frosch, you have been one of my biggest advocates and mentors since I joined your lab in 2019. Thank you for entrusting me with such important work, encouraging my new ideas and more broadly for your tireless leadership in the environmental justice field.

To ERG faculty that have toiled over designing courses, providing instruction and maintaining the unique community that is the Energy and Resources Group. Special thanks to Isha Ray for being a wellspring of exquisite insight on all topics, to her and the entire Water Group Plus community all those end-of-semester WG+ parties at her house. To Lara Kueppers, thank you for your guidance early on in my graduate school career, especially for your invaluable comments and suggestions for my first, first-authored publication. Also, I want to profusely thank Kay Burns for her frontline support of myself and my fellow ERG students on all issues large and small, from navigating UC's bureaucratic foibles to showing selfless emotional support for all manner of personal and professional challenges. Thank you to all ERG students, faculty and staff for being integral parts of this incredible community.

I would also like to thank all the collaborators with whom I crafted much of this work. For the Central American drought and migration studies presented in Chapter 1, thank you first and foremost to Diego Pons for being a great collaborator and co-author, for inviting me to participate in the the Climate Change and Migration conference at the Universidad de la Valle de Guatemala and for being a wonderful host and tour guide in Guatemala City. Thanks also to Edwin Castellanos for connecting Diego and I and for highlighting our work in various academic fora. Many thanks also to the whole team at the Urban Displacement Project for their support and contribution to the climate and displacement review featured in Chapter 2.1, with special thanks to Anna Cash for directing the bulk of the final research and writing efforts and to Shazia Manji for her collaborative work during this phase of the project as well. For Chapter 2.2, thank you to Lara Cushing, Rachel Morello-Frosch for your support, as well as in many other environmental justice, public health and state policy-relevant work not featured in these pages.

Thank you again to Solomon Hsiang for teaching a great spatial data course and for encouraging me to continue to expand upon my final project in that class on hurricane impacts in Puerto Rico, which evolved into Chapter 2.3. Finally, thanks to the whole Climate Impact Lab team for their critical efforts to update the federal government's social cost of carbon estimates and for giving me the opportunity to contribute to such an important initiative. I want to explicitly thank Ian Bolliger for his skillful guidance, mentorship and vision throughout the coastal impacts analysis on which I was principally involved, and which served as the foundation for Chapter 3. Thanks also to Daniel Allen and Junho Choi for their tireless contributions to this project and to Solomon Hsiang and Robert Kopp for their thorough review and feedback on resultant publication. I also want to thank Ted Grantham, Iryna Dronova, Andy Jones, Lara Cushing, Rachel Morello-Frosch and Solomon Hsiang for advising research projects on which I contributed but are not reflected in the following pages. Thank you to the many collaborators who contributed to those efforts.

To my parents, thank you for the continued support to pursue my intellectual interests and for exposing me to the beauty of the natural world from a young age. The countless hours spent traversing the ridgelines, peaks and forests of Southern California and roasting marshmallows in national park campsites across the country taught me how unique - and fragile - our ecosystems are. Infinite thanks to my older sister for being the person who knows me better than anyone and for being a much needed outlet for venting, silly chatting, essential memes and all forms of hilarious content and for showing me around your incredible, bustling home in the southern hemisphere.

To all of my amazing friends and housemates that have been the glue to my mental wellbeing over the years and who continue to show me the love and companionship that gives me life. To everyone with whom I've shared a home over the years. To Thornton for making this house possible. To Betsy and Henry for being the best living partners someone could wish for during the bleakest months of the pandemic. To Suz for being so reliable, caring and hilarious during my Master's and beyond. To Peter for teaching me the proper way to pronounce 'Reese's' and for having the best mullet in town. And finally to Ben, who continues to be the antidote to any dour mood, purveyor of amazing music recommendations and generally the most steadfast friend and supportive advocate anyone could want.

Thank you to Emma for sharing your brilliant curiosities, deep thoughts, lazy crosswords, sunset longboard rides and Alaskan adventures with me. To Lily, Nandy and Noah, thank you for being incredible friends and for making Sacramento my home in the Central Valley these past years. To Toby, Steve and Roger, thanks for the decade of chuckles and the decades to come. To my entire Davis friend group, many of whom have stayed immeasurably important to me. To all of my amazing friends in L.A., who remind me where my true home is and always will be. And to Sean, my oldest and dearest friend, with whom I've shared more years of friendship than I can quite literally remember. I would also be remiss to not thank the trails, trees and sunsets of the East Bay and the hummingbirds who twice chose to build their nests outside my bedroom window. Finally, thank you to my ERG 2017 Newbies cohort. Without the mutual support and camaraderie we provided one another throughout our shared grad school experience, none of this would have been possible.

Introduction

The following chapters of this dissertation showcase a wide variety of different intellectual, investigative avenues that I undertook during my time as a M.S. and PhD student in the Energy and Resources Group and UC Berkeley. The overarching theme that undergirds my work is regarding **climate impacts and inequities, specifically with respect to human migration**, an increasingly important subfield of climate science and human geography that require improved scientific understanding, communication and global decision-making as society grapples with shifting climatic regimes in the coming decades. Throughout my time as a doctoral student, the specific topical focus of my work within this broader theme varied due to changing curiosities, funding and collaborative opportunities on campus. Therefore, while some of my projects more clearly complement one another, the full collection of work presented here spans a number of different disciplines and objectives. In this dissertation, I attempt to weave each project together in a cohesive way, reflecting the intellectual throughline that motivated my research throughout.

As such, the following introductory section represents a contextual, theoretical framing surrounding the challenges associated with observing, identifying and ultimately governing climate influences on human migration and global priorities for achieving sustainable governance of increased transnational and internal migrant flows in the context of climate change. This narrative framing motivates the bulk of my research work and underscores the gaps in research understanding my research attempts to address.

The Collective Challenge of Climate Migration

The concept of 'climate migrants' or 'climate refugees' is not new. Major paleoclimatic events, such as transitions between ice ages, changing sea levels and prolonged droughts have driven the movement of human societies for millennia. However, the dramatic rate at which global climate systems are changing, in conjunction with the fragility of our interconnected, built societies and the complex structure of states, borders and policy regimes make the issue of modern-day climate-migration uniquely challenging, requiring both scientific and governance solutions.

Mass movements of people, especially across international borders, have posed difficult challenges for the international community from humanitarian, logistical, legal and governance standpoints. This concluding section outlines the current state of global climate-migration governance, major challenges to improving existing frameworks and presents recommendations for future action and policymaking in this realm. It does so in four parts: i) a definition of climate migrants in the context of migration theory ii) detailing the major framing lenses used to motivate migration and refugee policy, iii) summarizing existing legal and governance frameworks and iv) recommendations for improved governance moving forward.

Theories of Migration and Attempting to Define 'Climate Migrants'

One of the biggest challenges of studying climate-influenced migration is how to classify a given individual or group as a 'climate migrant(s)' or not. Some scholars argue that attempts at such a definition are so convoluted and fraught with confounding factors as to be essentially arbitrary (Mayer, 2015). Both the wide variety of climate hazard severity as well as the vast spectrum of

migrant types makes identification of any marginal influence that the climate may have on observed human movement difficult to establish. However, attempting to demarcate who is, at least partially, displaced due to (changing) climate and related environmental phenomena is imperative if future legal and political frameworks are to be structured to acknowledge and respond to past and future climate trends, making the identification of climate-driven migrants an important endeavor, however challenging (Williams, 2008; Bardsley and Hugo, 2010; Gemenne and Blocher, 2017).

Therefore, for purposes of discussion here, "climate-displaced persons" (CDPs) are defined as all refugees, internally-displaced persons or international migrants for whom climatic stress or related environmental degradation served as a major push factor. This could be those fleeing loss of homes or territory in the wake of an acute major climate disaster such as a flood or fire, those facing a gradual but severe loss of land or livelihoods due to incremental environmental change such as sea level rise or desertification, or those for whom climatic stressors have borne any other substantial adverse impacts, directly or indirectly. This definition does not encompass those for whom the decision to move is largely voluntary, though the continuum of personal agency in personal migration decision-making is often difficult to distinguish.

It should also be noted that the concept of "indirect" climate impacts is inherently nebulous and can in theory encompass a wide array of different economic, political, social, or private actor driven actions or outcomes that in turn influence migration. Examples include decreased income or employment due to impacts to regional crop yields in periods of heat stress or drought, or displacement resulting from violence over the appropriation of resources made scarce under changing climate conditions. However, the chain of causality between climate stress and human movement in such cases can quickly become complex, with many intermediary layers, making it difficult to identify climate-migration links with certainty. Therefore, "indirect" climate-migration drivers in this discussion are limited to those for which compelling empirical links have already been made, generally corresponding to cases with few intermediary "links" in the chain of climate migration causality.

Once the definition of CDPs is made, the manner in which they are accounted for and eventually governed will ultimately be premised by the theoretical frameworks of migration to which relevant policymakers ascribe. Different theories prescribe varying degrees of importance to different migration-influencing factors and, in turn, the likely impacts that certain climatic changes may have on migration flows. The relative validity of these theories as perceived by policymakers will in turn inform their sense of urgency and importance regarding climate-driven migration.

Largely following the evolution of migration theoretical frameworks as described in Massey (1999), the following represents a summary of dominant theories in the field, with each of them representing an arguably generalizable schema as to the most important causes of migration. Early attempts by Ravenstein (1885) were built upon by Lee (1966), which ultimately assert that migration is largely dictated by travel distance, existing currents of migrants, rural-urban status (high rates of rural-to-urban migration), gender (high rates of women migrants to industrial zones), the balance of push factors in the source location and pull factors in destinations,

advancement of technology (e.g. transportation), barriers or 'intervening obstacles' to movement, and various economic factors.

Many of these factors would come to inform subsequent, formalized theories of migration, beginning with the neoclassical migration theory, which posits that migration is the product of rational decisions made autonomously by individual migrants, each calculating the economic costs and benefits of migrating, ultimately choosing the action that will be most likely to maximize their income (Massey, 1999). Eventually, the theory known as the New Economics of Labor Migration (NELM) theory emerged, which placed greater emphasis on the role of groups of people, such as households, as the primary decision making agents with respect to migration. NELM states that a given household seeks to minimize the collective risk of its members, perhaps by sending someone to work in another country, rather than each individual within the household making personal migration decisions autonomously (Massey, 1999). Stark and Taylor (1989) point out that migration decisions made by individuals and households may also be driven by a sense of "relative deprivation", that is the perceived potential gains from migration conditioned on their present status relative to the community around them, not simply in absolute terms.

The Segmented Labor Market Theory of migration underscores the importance of labor demands in destination communities, specifically as they form in relation to the 'segmenting' of sectors of production into 'capital-intensive' versus 'labor-intensive' industries, with the former associated with more stable, higher-paying jobs and the latter consisting of volatile, low-paying employment, often explicitly catering to a migrant workforce eager to secure any form of employment in a new location. This hierarchical structure becomes increasingly entrenched as corporations become more accustomed to the segmenting of their workforce in their way, in turn reinforcing the demand for such labor and hence the "pull" of migrants from sending communities (Massey, 1999). This theory is related to the World Systems Theory of migration, which centers the importance of global, economic interdependence between nations and the subordination of poorer, developing economies relative to richer, wealthier ones (Massey, 1999). World systems theorists argue that proper attention must be paid to the complex dynamics that arise from processes such as foreign investment and industrialization of migrant-sending nations, which may produce paradoxical outcomes with respect to migration flows (Sassen, 1988).

Social Capital migration theory states the importance of social networks in determining migration patterns, such as familial ties in destination countries. This is related in part to the theory of Cumulative Causation, which states that migration trends are self-reinforcing and largely increase as networks, experience and volumes of migrants corresponding to a given pathway (e.g. Guatemala to the U.S.) increase, not dissimilar to aspects of the original theoretical frameworks put forth by Ravenstein and Lee (Massey, 1999).

Another important determinant in the flows of migrants, largely omitted from the theories listed above, is related to state policies and action regarding immigration. In many cases, as Zolberg (1999) argues, changing national immigration policies, such as the 1965 Immigration and Nationality Act, were actually the *primary* determinants of subsequent migration flows. Massey (1999) acknowledges the fact that the influence of the state is under-explored but also minimizes its likely impact relative to the myriad of theoretical explanations detailed above. There is no

single “correct” theory of migration, each of them potentially more valid than others from one context to another. However, as Sassen (1988) and Zolberg (1999) point out, much of the existing political discourse and paradigmatic framing of migration reflected in receiving-country policies fail to adequately account for the complexities inherent in migration, often simply assuming it is the product of autonomous decisions by individuals out of their control, opting often for a strategy of deterrence.

When designing policies aimed at accommodating or alleviating climate-driven migration, a full accounting of relevant factors, drawn from the aforementioned theories, is crucial. For example, failing to anticipate the unintended consequences that certain types of economic investment in migrant-sending countries could exacerbate declining livelihoods and employment opportunities of some of the most climate-vulnerable communities in those countries. Furthermore, it’s important to bear in mind the relevance of each of these theories when framing discourse around climate and migration, so as to resist the temptation to over-ascribe the relative influence of climate variables upon migration in a reductive manner.

Relevant Legal and Governance Frameworks

The following is a summary of existing migration and refugee governance frameworks and agreements that could be restructured to accommodate CDPs, or in which they are already explicitly acknowledged. However, there remains no single international agreement in place that specifically governs with CDPs.

1951 Convention Relating to the Status of Refugees and its 1967 Protocol
International legal protections under the 1951 Refugee Convention are focused primarily on those who are fleeing persecution based on “race, religion, nationality, membership of a particular social group or political opinion” (UNHCR, 1951). Sarah Song (2018) notes that those facing persecution based on gender or sexual orientation have also been generally accepted as warranting refugee status under the Convention. However, forced migrants due to environmental degradation or natural disasters have not been granted refugee status under the auspices of the Convention, and in fact, their specific exclusion has been repeatedly upheld in refugee jurisprudence (Williams, 2008). The 1951 Convention remains the authoritative framework dictating international refugee protections to this day, leaving CDPs without legal protection in either “spirit or language” under the current international legal landscape (Burkett, 2018).

United States Temporary Protected Status (U.S. Immigration Act of 1990)
In the United States there is no official system in place for granting asylum to CDPs, even for those fleeing acute natural disasters. Temporary Protected Status (TPS) was granted to residents of Honduras, Nicaragua and El Salvador following the impacts of Hurricane Mitch in 1998 and deportations of Central American immigrants were slowed or paused in subsequent years due to the storm’s destruction. However, this represents the only instance in which TPS was applied to accommodate CDPs (other natural disasters such as earthquakes are not considered “climate hazards”) since the program’s inception in 1990 (Wilson, 2021).

1994 Addis Ababa Document on Refugees and Forced Population Displacements in Africa
Due to the narrow definition of refugees laid out in the 1951 Refugee Convention, many African states wanted to improve upon the classification of refugees given common issues that plagued

the continent, such as widespread, generalized violence, environmental degradation and sociopolitical instability. They therefore drafted and adopted this framework to expand the refugee classification within the African Union, specifically citing 'physical environmental degradation' as a 'root cause' of migration and internal displacement (OAU, 1994). However, it does not explicitly embed climate or environmental impacts into any of its articles or recommendations, but rather limits it to contextual discussion in the foreword and introductory sections.

2009 African Union Convention for the Protection and Assistance of Internally Displaced Persons in Africa (Kampala Convention)
This update to the 1994 Addis Ababa Document framework explicitly cites climate change, stating "States Parties shall take measures to protect and assist persons who have been internally displaced due to natural or human made disasters, including climate change". Significantly, it also stipulates circumstances in which compensation should be provided to "internally displaced persons in the event of natural disasters", if a state "refrains from protecting" against such threats (African Union, 2009). This language is ambiguous, however, and lacks an enforcement mechanism. Furthermore, it is likely that a state will not have the capacity to compensate internal CDPs if it was unable to safeguard them against such threats to begin with.

2010 Cancún Outcome Agreement (COP16)
The final language of the 16th UNFCCC Conference of the Parties (COP16) agreement explicitly acknowledges climate-induced migration and displacement and frames it as an adaptation issue in need of further attention. It also calls for "measures to enhance understanding, coordination and cooperation with regard to climate change induced displacement, migration and planned relocation, where appropriate, at the national, regional and international levels" from State Parties (UNFCCC, 2017). However, no specific plan or systems of accountability are detailed for how to realize these goals.

2016 New York Declaration for Refugees and Migrants
Drafted in light of the UN's 2030 Agenda for Sustainable Development, this declaration specifically cites climate change and climate change-related natural disasters as a driving force behind migration. It commits to "creating conditions for balanced, sustainable and inclusive economic growth and employment, combating environmental degradation and ensuring effective responses to natural disasters and the adverse impacts of climate change". It explicitly states, however, that it is not expanding the definition of 'refugee' to apply to CDPs, but includes them under the auspices of the protections laid out in the declaration as a means to address this gap (UN General Assembly, 2016). That said, the document lacks specificity regarding the nature of climate hazards it considers as drivers of displacement and provides no substantive updates to the 1951 Refugee Convention in terms of specific legal or governance measures to accommodate and prevent CDPs.

2016 Paris Agreement (COP21)
This is the current guiding international agreement regarding climate change. Article 7 of the agreement sets long-term goals for global adaptation and specifically highlights the issues of human mobility and migration, imploring states to "promote the rights of migrants" (Ionesco,

2017). Nonetheless, it lacks specific goals and enforcement mechanisms for achieving this and does not amend or introduce any expanded legal protections or recognition of CDPs.

2018 Global Compact for Safe, Orderly and Regular Migration (GCM)
Stemming from the 2016 New York Declaration for Refugees and Migrants, its goal is to 'enhance cooperation on international migration in all its dimensions". Importantly, it lays out 23 objectives, which include collection and analysis of increased quantity and quality of migration and mobility data, and by reducing adverse push factors that drive outmigration, specifically citing "climate mitigation and adaptation" as a key strategy. It lays out provisions for how migrants should be accounted for in natural disaster planning, the adverse effects of climate change and environmental degradation, and calls for early warning systems, improving pathways for "regular" migration (McAdam, 2019). Though this agreement represents a significant step forward towards coordinating international action to mitigate and accommodate CDPs, it still lacks specificity regarding responsibilities, accountability and enforcement, and is not legally binding.

2018 Global Compact for Refugees (GCR)
This agreement aims to "provide a basis for predictable and equitable burden- and responsibility-sharing among all United Nations Member States" regarding refugee flows. It acknowledges that "climate, environmental degradation and natural disasters increasingly interact with the drivers of refugee movements", though reaffirming that CDPs are not classified as refugees nor afforded the associated legal protections (UNHCR, 2018). And like the GCM, this compact lacks specific obligations for signatories and is not binding.

The language and objectives detailed in these agreements, especially the explicit language surrounding CDPs in the Paris Agreement (PA) and the Global Compact for Migration (GCM), represents important progress in international acknowledgement of climate as a driver of forced migration. However, without catalyzing tangible policy and governance initiatives, these non-binding agreements will remain largely discursive rather than actionable. There have been a number of research initiatives and policy responses at regional and national scales that have occurred in conjunction and in response to these agreements. These include the European Union's Environmental Change and Forced Migration Scenarios program, The Nansen Initiative, Platform of Disaster Displacement, and the United Nations' Task Force on Displacement. These important efforts focus on CDP-related data collection, modeling and research, as well as policy advocacy, but lack the power to enact legal or governance-level reform themselves.

Framing Lenses for Governing Climate-Induced Displacement

Motivations behind the enacting governance frameworks for refugees and forced migrants, including CDPs, can be broadly categorized using the conceptual framing detailed by Mayer (2015), which posits that some blend of i) humanitarian/human rights, ii) responsibility and iii) security lenses drive the migration policymaking discourse. This section characterizes each of these lenses and highlights the promise and pitfalls they hold in the context of CDP governance.

Humanitarian and Human-Rights

Through a humanitarian and human rights-based lens, more robust and sympathetic governance of CDPs is needed simply because it is the moral course of action. It would be unethical for the global community to allow massive volumes of CDPs to remain stateless without assistance and to allow environmental conditions to worsen unabated. This approach converges most closely with the framing of the 1951 Refugee Convention, which is based on the International Declaration of Human Rights and which grants refugees international legal protection on a humanitarian basis. Therefore, the 1951 Convention, its 1967 Protocol and the 2018 Global Compact for Refugees can be classified as falling largely in a humanitarian-motivated framework.

Responsibility

The second lens of motivation relevant to CDP governance centers on the concept of responsibility, recognizing that CDPs are influenced by climate change, for which countries have differentiated responsibilities based on past emissions. This framing has served as the central basis for determining emissions mitigation commitments in agreements such as The Paris Climate Accord, where 'Nationally Determined (emissions) Contributions' largely dictated national mitigation requirements. This logic has yet to be largely applied to the discussion of CDPs and there are no proposals that place responsibility on historically high-emitting countries to ameliorate displacement pressures or to admit higher volumes of CDPs (Mayer, 2015). This responsibility framing is an important one, however, because it is inadequate to leave individual nations/regions to grapple with large CDP fluxes on their own (Mayer, 2015; Warner, 2010).

Security

One of the most common motivating lenses for the need to enact governance specific to CDPs is that of national security. Though this framing is valid in the sense that large fluxes of displaced peoples can pose challenges for regions already grappling with political instability and potentially threaten the security of neighboring states, it may also fuel protectionist or xenophobic responses in receiving countries, and serve as justification for increased securitization of CDP source regions (Mayer, 2015; Selby et al., 2017; Buhaug, 2016).

While all three lenses detailed above are valid to some extent, it is unlikely that centering an international CDP governing framework around any single one of them will lead to comprehensive buy-in from all nation states. Solely focusing on the humanitarian lens may rely too narrowly on altruism and may fail to inspire buy-in from all countries, especially those with limited capacity to fund relief or provide employment. Sole focus on the responsibility framing could lead to a geographic imbalance in prescribed 'responsibility' and a potentially uncoordinated approach. Sole focus on the security narrative would be the most dangerous of all in that it can validate protectionism and/or militarized interventions in sending regions. Therefore, discussions of governance at any scale must strategically balance these motivations and in order to achieve the most support from relevant parties without fomenting nativism, a driving force behind many immigration policies, both recent (e.g. Donald Trump's ban on Muslim-majority nations) and old (U.S. Immigration Act of 1917).

Goals for Governance

The global community could strive to enact an international agreement specifically dedicated to the research, definition, and governance of CDPs. A new international agency, potentially under the auspices of the UN might also be created whose explicit mandate is to coordinate the research, collaboration and implementation of CID-responsive policies. Currently, the UN's High Commission on Refugees (UNHCR) is focused solely on refugees, as CDPs do not qualify. Mayer (2015) discusses the limitations of other existing UN and non-UN international agencies, such as the IOM and others. Sasnal (2018) advocates for a consolidation of the existing agencies as a means to reconcile each of their shortcomings in being able to address the issue of CID on their own.

Crucially, increasingly acknowledging climate-driven migration as a valid, and in some cases optimal, adaptation response to shifting climate patterns, rather than a product of some inherent failure to adapt properly, could facilitate progress in humane governance of human movement (Gemenne and Blocher, 2016; Bardsley and Hugo, 2010). Such a re-framing could help combat protectionist tendencies to demonize or blame migrants broadly for their plight (Gemenne and Blocher, 2016), a reactionary trend that has fueled many seismic political backlashes in affluent receiving nations, such as Brexit and the steady rise of right-wing nationalist populism in the United States and Europe.

Costs and barriers facing CDPs could be minimized with the support of a UN-funded mechanism to assist in movement (Gemenne and Blocher, 2016; Bardsley and Hugo, 2010). This can be designed and implemented under the auspices of a new international agreement and could be used to help facilitate well-managed flows of CDPs, potentially prioritizing receiving communities based on local labor needs and the capacity to adequately house and harbor individuals in a humane manner (Bardsley and Hugo, 2010; Ramji-Nogales, 2016).

From a legal perspective, an acknowledgment needs to be made as to the inherent limitations of the current system in effectively and equitably representing the needs of CDPs (Williams, 2008). Burkett (2018) points out that the sheer scope and complexity of climate change and climate-influenced migration means that it intersects a vast number of different legal domains, such as international refugee law, local property law, environmental law, international economic and commercial law. This makes coordinated legal response, in terms of definition of CDPs and proper redress for those subject to harms exceedingly difficult. Cases like the loss of an entire nation state's land area to sea level rise and the resultant CDPs lay bare the poorly-defined rights guarantee under international refugee and rights structures (Burkett, 2018). Therefore, a radical restructuring of current legal regimes need to be undertaken in order to expand rights and legal protections to the various forms of CDPs likely to increasingly emerge in the coming years, especially those displaced from definitive, direct climate.

How to apportion assistance or accommodate CDPs under a hypothetical global governance framework is a difficult but key question. Song (2018) makes the case for those CDPs forcibly and permanently displaced by climate hazards, such as small island states in the face of sea level rise, being afforded refugee status under the 1951 Convention, citing the expansive interpretation with which it has been applied to social groups not explicitly referenced in its text. Indeed, the case could be made for a comprehensive inclusion of all CDPs under the refugee banner if the

climate is considered a persecuting "actor", targeting those social groups residing in climate-vulnerable regions. However, such an approach would be difficult to justify and apply across the wide variety of CDPs, some facing more dire circumstances than others.

A global governing framework that accounts for CDPs outside of the auspices of the Refugee Convention might, therefore, be structured in such a way as to account for this variability in relative plight across different groups of CDPs. Williams (2008) suggests that CDPs be "*identified along a graduating scale would allow for differing degrees of protection to be accorded depending on the severity of the situation"*. In conjunction with the varying degrees of situational severity facing CDPs, it will also be important to account for the varying levels of past responsibility to global climate change that each potential receiving nation bears, as well as their relative "integrative capacity" to admit CDPs (Song 2018). Accounting for each of these aspects (severity of situation, nationally-differentiated responsibility, and integrative capacity) will be essential to enacting "fair" policies, such that participating nations will feel that the commitments to which they adhere are as equitably determined as possible.

However, securing a globally-agreed upon governing framework for CDPs will be difficult and lengthy. Therefore, the development of regional frameworks, brokered by groups of nations facing similar climatic challenges, could serve as a helpful fora for collaborative dialogue and policy progress. Many regional agreements in non-migration sectors exist, as do a limited number of migration/displacement related ones, such as the Kampala Convention. These examples can serve as roadmaps for continued regional agreement-making regarding CDPs, the success and structures of which can be used to inform future efforts and establish continuing norms. Regional agreements can more easily secure buy-in from regional partners where global agreements may stall, and can serve as "norm entrepreneurs", laying the groundwork for a global framework in the long run (Williams, 2008; Rother, 2019).

Dissertation Research

As discussed above, grappling with the physical and sociopolitical impacts of global climate change, specifically with respect to potential increased human migration and displacement, is a pressing challenge faced by modern society. The ways in which physical climate regimes evolve in the coming years, and how we collectively react and reshape the structure of our political and economic systems in response, will largely determine the relative stability and wellbeing of our ecological and social fabric for centuries to come. Effective mitigation and adaptation in response to these growing threats requires an improved understanding of the complex physical processes at play and a detailed evaluation of likely socioeconomic impacts in order to motivate the collective action necessary to address this global problem.

The latest comprehensive assessment report (AR6) released by the Intergovernmental Panel on Climate Change (IPCC) predict global mean surface temperature (GMST) increases of roughly 3.2° C by 2100, asserting with nearly unequivocal certainty that anthropogenic greenhouse gas emissions are the primary driver of this rise (IPCC, 2022) and not barring the possibility of even higher end-of-century increases. Average global mean sea levels (GMSL) are similarly projected to increase, primarily in the latter half of the century, by approximately 0.7-0.9 meters by 2100

under likely GMST pathways (Fox-Kemper et al., 2021). Similarly, acute hazards, such as extreme storms, droughts, wildfires and heatwaves are slated to worsen across the board, either in frequency and/or severity (IPCC, 2022).

These worsening trends are likely to have widespread impacts upon the stability and security of our global ecosystems, economies, political institutions and communities across the globe. One of the most likely symptoms of this climatic stress will be the massive movement of human populations, in both forced displacement and voluntary migratory contexts. However, predicting the magnitude and characteristics of this population re-sorting, which is likely to happen predominantly internally within national borders, is challenging given the uncertain factors at play (McAdam, 2019; Ramji-Nogales, 2016, IPCC, 2022). While there is a fast-growing body of research being done in the field of climate-migration, there remain many unanswered questions and underdeveloped methods for making plausible estimates of future climate-driven human displacement. For example, one migration modeling study, the 'Groundswell' report, is frequently cited in the IPCC AR6 report and postulates between 31-143 million people are likely to become internally displaced in Sub-Saharan Africa, South Asia and Central and South America by 2050, with the IPCC ascribing 'high confidence' to this projected outcome (Riguad et al., 2018; IPCC, 2022).

However, assigning a high-level of confidence to the predictions made by the Groundswell report and others like it can be somewhat misleading, given the wide range of its model results and significant methodological limitations. For example, the study is primarily centered upon a simplified, neoclassical economic assumption-based model of human migration and internal displacement, without integrating historical empirical observations of climate-influenced migration nor does it consider complex decision making processes likely to drive human displacement in the future. Additionally, many of the future climate hazard scenarios implemented in the model are highly-simplified projections of climate hazard exposure, such as the simple assumption that local sea level rise experienced in all study locations by 2050 will be a uniform increase of 1 meter, with population exposure to this projected rise estimated using a digital elevation dataset (SRTM) with known inaccuracies in coastal areas (Kulp and Strauss, 2018).

Although the Groundswell report constitutes a useful resource in the field of climate-driven migration and displacement estimation, its inherent limitations combined with its prominence in the AR6 report in each migration subsection response to climate change, indicates the urgent need for more work to build upon this study. Additional research work, especially that which integrates empirical data, the development of improved methodologies and relevant data products, and a concerted effort to integrate these findings in current climate-migration policy and governance dialogue is needed. As climate models, satellite imagery, and population distribution estimates continue to evolve, becoming increasingly available and highly-resolved, the landscape of potential methodologies for empirically evaluating climate impacts and human migration are rapidly expanding. Leveraging these dataset and modeling advances is critical for contemporary climate-migration research, such that estimates of past and projected climate-displacement are better grounded in empirics and, in theory, narrow the range of uncertainty facing policymakers.

This dissertation presents a collection of research efforts aimed at addressing these needs, by better understanding the past and potential future physical characteristics of hazardous climate phenomena, their socioeconomic impacts, especially regarding human migration, and future adaptation pathways that could be considered in response. It concludes with contextual framing as to how political will and collective policy response can be shaped in the coming decades. While a multitude of physical processes and socioeconomic impacts are presented in the following chapters, the primary theme that motivated the selection of climate hazards, their potential impacts and geographic regions evaluated in the chapters that follow is one of human displacement and migration. Understanding the ways in which climate change will compel a global re-sorting of human populations both within and across national borders is one of the most pressing, and relatively understudied, topics in the current literature. The study locations, methods and results provide useful tools to inform the analytical and policy conversations surrounding human displacement and migration in the wake of changing global climatic conditions.

Project Summaries

My research is segmented into three chapters based on geographical relevance to i) Central America, ii) the United States and iii) global coastlines, all of which have the potential to be sites of significant human migration and displacement as a result of the changing climate. These chapters are comprised of the following project-based sections

Chapter 1 - Central America

- **(1.1) 21st Century Drought Projections in Central America's Dry Corridor**
  The vulnerability of Central American residents to drought, especially small-scale farmers in its 'Dry Corridor' region (CADC), is an increasingly salient topic in academic, policy and media circles, many of which cite rainfall shortages as being a principal driver of migration out of the region. Numerous prior studies have predicted decreases in mean annual precipitation for the CADC and a lengthening and intensification of the region's mid-summer drought (MSD) period, a period of decreased rainfall from July to August (Rauscher et al., 2008; Campbell et al., 2011; Karmalkar et al., 2011; Kitoh et al., 2013, Nakaegawa et al., 2014; Maurer et al., 2017; Pons et al., 2018). However, there remains a lack of research on future drought predictions in the CADC that takes a broader focus outside of MSD and MAP trends, specifically regarding other types of seasonal drought and longer, annual-scale drought characteristics, which would help inform climate vulnerability studies seeking to link out-migration to drought stress.

  This project addresses this gap, consisting of an analysis of projected changes to drought characteristics through the year 2100 under scenarios of moderate and high global greenhouse gas emissions. Results are presented across the 'Dry Corridor' region, which spans portions Guatemala, Honduras, El Salvador and Nicaragua and is known for its high level of poverty, dependence on rainfed agricultural systems and vulnerability to food insecurity. Our findings indicate that seasonal-scale droughts are projected to lengthen by 12-30%, intensify by 17-42% and increase in frequency by 21-24% by end-of-century. Annual-scale, longer-term droughts are projected to lengthen by 68% under moderate emissions, potentially triple in length under high emissions and to

intensify by 27-74%.

These findings were published in Environmental Research Letters in 2021 (Depsky and Pons, 2021) and highlighted in the latest assessment report, AR6, issued by the Intergovernmental Panel on Climate Change (IPCC) as part of the Working Group II report, Chapter 12: Central and South America (Castellanos et al., 2022).

- **(1.2) Predictive modeling of international emigration and internal migration, as reported in the Guatemalan 2018 national census, using sociodemographic, physical and climatic covariates.**
  Complementing the findings Chapter 1.1, which highlight worsening drought projections across the Central American Dry Corridor throughout the 21st-century, this study attempts to illuminate potential linkages between various factors, including drought stress, and migration from and within Guatemala between 2002 and 2018. Very few published studies to date make empirical links between observed migration in Central America and climatic stress, a shortcoming in the literature this project aims to address.

  Using data from the last comprehensive national census, published by the Guatemalan government in 2018, I constructed predictive models of reported international emigration rates from 2002 to 2018 and inter-municipal moves from 2013-2018 at the level of municipality (n=340). The census contains nationally comprehensive individual and household surveys that report instances of household reported international emigration without return and internal movement between municipalities, as well as a multitude of additional sociodemographic variables employed as covariates in the modeling effort. A collection of physical and climatic variables were also used as predictors to complement the census covariate set. I was able to construct a predictive linear model that explains the majority (~55%) of observed variance in reported international emigration from Guatemala between 2002 and 2018, with various sociodemographic variables (e.g. education, employment, proxies for poverty) emerging as significant predictors, as did cumulative exposure to drought stress (positively associated with rates of out-migration). Modeling inter-municipal migration from 2013 to 2018 proved more difficult, with models only reliably explaining roughly a quarter of observed variance, though many of the same sociodemographic covariates appeared as significant predictors.

  This work was presented at a symposium on climate change and migration at the Universidad del Valle de Guatemala on January 23, 2023 and will likely evolve into an academic publication in collaboration with Guatemala research partners.

Chapter 2 - United States

- **(2.1) Review of the literature linking climate hazards, internal displacement, movement and inequities in the United States**
  Assessing the myriad ways in which acute and chronic climatic hazards impact human

displacement requires looking not just at direct, visible impacts, such as storm damage or permanent coastline inundation, but also by analyzing the many potential indirect ways that increased climate stress can impel displacement. Doing so with an eye towards potential social inequities both in terms of hazard exposure, as well as recovery and adaptive resilience, is crucial for comprehensively evaluating climate displacement. However, with the rapid growth of climate and migration/displacement literature in a U.S. context, there is a need for better documentation of the most relevant and contemporary findings in this space, such that communication and amelioration of associated challenges can be carried out.

Therefore, as a member of the Urban Displacement Project at UC Berkeley, I led the authorship of a large-scale literature review of the various linkages between different climate hazards and the displacement of people throughout the United States over the past two decades. Generally, the evidence base we assessed suggests that climate shocks and stressors can contribute directly and indirectly to human movement within the U.S. due to acute physical impacts or by worsening chronic environmental, health and/or economic precarity. Furthermore, certain climate-driven community interventions, such as public transit or open space developments play an important role in addressing climate change but should be done in a manner that does not exacerbate displacement (i.e. gentrification) dynamics.

This synthesis was published as a gray report (Cash et al., 2020) under the Strong, Prosperous and Resilient Communities Challenge (SPARCC), a U.S.-based non-profit initiative focused on housing, climate and health equity at the community level. My primary responsibilities were assisting in review and serving as the primary author of the final report (the report's final author listing order was sorted alphabetically and does not reflect relative writing contribution).

- **(2.2) Producing high-resolution dasymetric maps of population in California using the 2020 census for various demographic subgroups**
  One of the primary challenges of conducting climate-related human geography studies is the common lack of availability of relevant data at a high enough spatial resolution to facilitate meaningful analysis. For environmental justice, climate impacts and migration work, population distribution data at a useful level of granularity is often limited and difficult to produce. Therefore, there remains a vibrant and important subfield of human geography and demographic modeling that is oriented towards producing downscaled estimates of past, present and/or projected future populations at various regional and global scales. As part of my involvement in the Sustainability and Health Equity Lab at UC Berkeley, I created one such population product for the state of California, which models sub-census block gridded population using recent census data. Though initially constructed for use in environmental justice and community pollution exposure studies, the data products and methodological advances this project represents are relevant for any manner of human-based research in California, and have already been used to underpin an analysis of the state's vulnerability to sea level rise and potential contamination

exposure from flooded industrial facilities, which are risk factors likely to serve as drivers of coastal out-migration in the future (IPCC, 2022).

Using values from the 2020 U.S. census, I constructed a novel methodology for creating high-resolution (100m) population grids for the entire state of California for 12 different demographic subgroups. This effort was originally undertaken as part of an effort between UC Berkeley's Sustainability and Health Equity Lab and California state agencies to assist in the analysis and implementation of two pieces of statewide environmental justice-oriented legislation, AB 617 and SB 673. These statewide population grids ("CA-POP") are publicly available and useful in evaluating geospatial population distributions across the state for any number of research applications, which to date have included numerous climate change, environmental justice and health equity studies.

The methods and output of this project, as well as the details of their public-availability were published as a research article in PLoS ONE (Depsky et al., 2022).

- **(2.3) Geospatial analysis of Hurricane Maria's impact on Puerto Rican power supply, recovery and re-electrification and correlational relationships to subsequent out-migration**
  Given the increases in Category 4-5 tropical cyclones (TCs) in the Caribbean projected this century (Knutson et al., 2015), understanding how such extreme events can drive displacement and migration is crucial yet not well-understood (IPCC, 2022). The manner in which the occurrence of extreme weather will compel more people to migrate, both reactively and proactively, is inherently complex and understudied. However, with the increased availability of certain types of high-resolution datasets, such as from remotely-sensed satellite imagery, new methodological frontiers for detecting climate impacts, adaptation and even human movement are becoming increasingly possible.

  Therefore, this project focused on employing novel geospatial methods to assess the impact of Hurricane Maria on the U.S. island territory of Puerto Rico. The storm, which struck in 2017, devastated the island's electricity grid and caused widespread power outages, the magnitudes and durations of which I was able to approximate using satellite imagery of nighttime lights. I then identified certain physical and socioeconomic variables that served as significant predictors of grid recovery times in the months following the storm at a fine-scale spatial resolution (500m), with the distance to the storm's landfall, centerline path were strongly associated with outage severity, as were average education, income and racial composition of the locations assessed. Overall, this model predicted post-storm outages successfully, with one random forests model robustly explaining up to 82% of observed variance. Then, using values from the 2010, 2020 U.S. decennial censuses and additional socioeconomic covariates from the 2013-2017 American Community Survey, I also evaluated the predictive power of these power outages in observed population changes between 2010 and 2020 at the census block group-level following the storm. This modeling exercise, however, proved more

difficult, with models failing to explain a significant share of variance, suggesting the need to better identify, measure and represent migration-relevant push and pull factors at play.

The methods and findings in this research effort are yet to be published but represent the seeds of potential continued work beyond the scope of this dissertation.

Chapter 3 - Global Coastlines

- **Creating an open-source coastal impacts and adaptation modeling platform along fine-scale global coastlines for multiple scenarios of 21st century sea level rise (SLR)** Given that much of the global sea level rise that is in store for the 21st-century is likely to going to manifest from 2050 onwards and has not yet historically occurred in a large magnitudes across the globe, much of the impacts, including coastal out-migration, likely to ensue from SLR have not yet been reliably observed. Therefore, empirical modeling of such potential future impacts is difficult to conduct. Much work on potential SLR-related displacement, such as the Groundswell report on internal displacement that is featured throughout the sixth IPCC Assessment Report (Rigaud et al., 2018), is constrained to making solely theoretical assumptions to model likely adaptation and behavior outcomes. However, much of this prior work has been limited in its utilization of high-quality and high-resolution input data on exposure of populations, exposure of capital assets, physical characteristics of coastlines (e.g. topography) and spatially-explicit SLR and storm surge projections, which inherently limits the confidence of resultant adaptation and out-migration estimates. This project, though still centered upon agent-based and economic theory-based modeling, represents a significant advancement in the realm of state-of-the-art input dataset integration and geospatial modeling of the exposure, impacts and adaptation to SLR along the globe's coastlines throughout the 21st-century.

  Originally conducted as part of an effort with the Climate Impact Lab (CIL) to inform the U.S. Environmental Protection Agency's updated social cost of carbon estimation, this project represents a large, collaborative research effort to provide a powerful, open-source modeling platform and coastal characteristics database for interested users in the coastal impacts research community. This platform, which constitutes the coastal component of CIL's Data-Driven Spatial Climate Impact Model (DSCIM-Coastal), consists of a vastly improved iteration of the pre-existing Coastal Impacts and Adaptation Model (CIAM, Diaz, 2016), with numerous computational improvements and comprehensive updating of all input data sources to the best-available resources at the time of construction. Our results indicate that with 2° C of warming by 2100, annual end-of-century costs associated with climate-driven SLR will be $110-530 billion, depending on emissions and socioeconomic pathways, assuming optimal adaptation. Under low-likelihood, high-impact SLR, these cost estimates range from $420 billion to $1.5 trillion. Additionally, a key component of our model is its estimation of potential migratory retreat from coastlines experiencing rising sea levels and worsening storm surges. Our results suggest that, globally, between 16-46 million people are expected to

relocate inland by 2100 if optimal adaptation strategies are undertaken, depending upon sea level rise, SSP and economic growth model scenarios. However, if no proactive adaptation is employed (i.e. no construction of protective infrastructure or proactive retreat), up to 200 million people are projected to be forced to migrate away from coastal regions under high-end SLR by 2100.

The methods for constructing this modeling platform and its complementary input dataset, along with summary global results regarding projected impacts and adaptation by end-of-century were submitted for publication following final revisions to Geoscientific Model Development in January 2023, with the final publication currently in press (Depsky, Bolliger et al., 2023).

Table 1. Unique research advances made by each project.

Project Chapter	***Research Contributions***
(1.1) Drought Projections in Central America's Dry Corridor *[CLIM, DM]**	● Application of multi-model (*n=20*) ensemble analysis with CMIP5 global climate models for the Dry Corridor region specifically, whereas prior studies focused on older and fewer models and often for limited, disparate geographies ● Assessment of seasonal and annual-scale droughts - not solely mean annual rainfall or mid-summer dry spells - showing projected amplification of future droughts that outpace projected reductions in simple, mean rainfall totals ● Developed a novel, integrated annual drought metric that reflects drought duration, frequency and intensity (AIWD), which better highlights comprehensive drought stress
(1.2) Guatemalan Migration Modeling *[MIG]*	● First known predictive modeling exercise for migration values reported in the latest national census in Guatemala, including using contemporary climate datasets to assess climatic predictors of human movement ● Poverty, education and exposure to drought stress are identified as significant predictors for out-migration
(2.1) Review of Climate Displacement in the U.S. *[MIG]*	● One of the broadest-reaching reviews of U.S.-based climate and displacement literature ● Unique review framing to include expansive consideration of indirect climate impacts on displacement, as well as the inequities in community hazard exposure and recovery
(2.2) High-Resolution California Population Grids *[DM]*	● Novel dasymetric techniques to downscale population in a U.S. context at the sub-census block level for multiple sociodemographic variables, which outperforms many similar datasets in the context of CA ● Utilization of latest (2020) census values ● Provision of publicly available datasets

(2.3) Post-hurricane electricity outages and out-migration modeling in Puerto Rico *[MIG, DM]*	● Novel application of nighttime lights satellite imagery for post-Maria electricity outage detection and development of novel, pixel-scale outage severity index, which enables similar such post-shock assessments in any global region with nighttime lights coverage ● Unique attempt to identify predictors of recovery and out-migration from Puerto Rico following the storm ● Physical factors, such as distance to storm landfall, and socioeconomic factors emerged as strongest predictors of outage severity, with results for out-migration more mixed
(3) Global sea level rise impacts and adaptation modeling *[CLIM, MIG, DM]*	● Fully open-source global coastal impacts and adaptation modeling platform that allows interested researchers to customize coastal research efforts using this architecture ● Integrates the latest sea level change projections developed by the international research community (e.g. CMIP6) and other scenario sets ● Integrates contemporary, high-resolution datasets of different socioeconomic and physical coastal characteristics ● Provides an agent-based framework for modeling potential adaptation behavior for thousands of unique coastal segments, including estimates of proactive and reactive out-migration ● Indicates that up to 200 million people could be displaced by 2100 under high-end sea level rise scenarios and absent proactive adaptation measures, the employment of which (i.e. protection, managed retreat) could reduce coastal displacement by an order of magnitude

**Fields of novel research contribution:*
CLIM - climate modeling
MIG - migration analysis
DM - dataset and methods development

References

African Union: Kampala Convention. (2009). Africa Research Bulletin: Economic, Financial and Technical Series. https://doi.org/10.1111/j.1467-6346.2009.02642.x

Bardsley, D. K., and Hugo, G. J. (2010). Migration and climate change: Examining thresholds of change to guide effective adaptation decision-making. Population and Environment, 32(2), 238–262. https://doi.org/10.1007/s11111-010-0126-9

Buhaug, H., 2016. Climate change and conflict: taking stock. Peace Economics, Peace Science and Public Policy, 22(4), pp.331-338.

Burkett, M., 2018. Behind the veil: Climate migration, regime shift, and a new theory of justice. Harv.

CR-CLL Rev., 53, p.445.

Campbell, J.D., M.A. Taylor, T.S. Stephenson, R.A. Watson, and F.S. Whyte, 2011: Future climate of the Caribbean from a regional climate model. International Journal of Climatology, 31(12), 1866-1878.

Cash, A., Chapple, K., Depsky, N., Elias, R. R., Krnjaic, M., Manji, S., & Montano, H. (2020). Climate Change and Displacement in the U.S. – A Review of the Literature, (April), 70.

Castellanos, E., M.F. Lemos, L. Astigarraga, N. Chacón, N. Cuvi, C. Huggel, L. Miranda, M. Moncassim Vale, J.P. Ometto, P.L. Peri, J.C. Postigo, L. Ramajo, L. Roco, and M. Rusticucci, 2022: Central and South America. In: Climate Change 2022: Impacts, Adaptation and Vulnerability. Contribution of Working Group II to the Sixth Assessment Report of the Intergovernmental Panel on Climate Change [H.-O. Pörtner, D.C. Roberts, M. Tignor, E.S. Poloczanska, K. Mintenbeck, A. Alegría, M. Craig, S. Langsdorf, S. Löschke, V. Möller, A. Okem, B. Rama (eds.)]. Cambridge University Press, Cambridge, UK and New York, NY, USA, pp. 1689–1816, doi:10.1017/9781009325844.014.

Depsky, N., and Pons, D. (2021). Meteorological droughts are projected to worsen in Central America's dry corridor throughout the 21st century. Environmental Research Letters, 16(1). https://doi.org/10.1088/1748-9326/abc5e2

Depsky, N., Bolliger, I., Allen, D., Choi, J.H., Delgado, M., Greenstone, M., Hamidi, A., Houser, T., Kopp, R.E. and Hsiang, S., 2022. DSCIM-Coastal v1.0: An Open-Source Modeling Platform for Global Impacts of Sea Level Rise. Geoscientific Model Development, EGUsphere [accepted pre-print].

Depsky, N, Cushing, L. and Morello-Frosch, R., 2022. High-Resolution Gridded Estimates of Population Sociodemographics from the 2020 Census in California. PLoS One.Diaz, D. B. (2016). Estimating global damages from sea level rise with the Coastal Impact and Adaptation Model (CIAM). Climatic Change, 137(1–2), 143–156. https://doi.org/10.1007/s10584-016-1675-4

Fox-Kemper, B., H. T. Hewitt, C. Xiao, G. Aðalgeirsdóttir, S. S. Drijfhout, T. L. Edwards, N. R. Golledge, M. Hemer, R. E. Kopp, and G. Krinner. 2021. "Ocean, Cryosphere and Sea Level Change." Climate Change 2021: The Physical Science Basis. Contribution of Working Group I to the Sixth Assessment Report of the Intergovernmental Panel on Climate Change [Masson-Delmotte, V., P. Zhai, A. Pirani, S.L. Connors, C. Péan, S. Berger, N. Caud, Y. Chen, L. Goldfarb, M.I. Gomis, M. Huang, K. Leitzell, E. Lonnoy, J.B.R. Matthews, T.K. Maycock, T. Waterfield, O. Yelekçi, R. Yu, and B. Zhou (Eds.)], no. Cambridge University Press, Cambridge, United Kingdom and New York, NY, USA: 1211–1362.
Gemenne, F. and Blocher, J., 2017. How can migration serve adaptation to climate change? Challenges to fleshing out a policy ideal., The Geographical Journal, 183(4), pp.336-347.

Ionesco, Dina, 2017. Climate Migration: From the Paris Agreement to the Global Compact for Migration. UN IOM. Web article.
https://weblog.iom.int/climate-migration-paris-agreement-global-compact-migration

IPCC, 2022: Climate Change 2022: Impacts, Adaptation and Vulnerability. Contribution of Working Group II to the Sixth Assessment Report of the Intergovernmental Panel on Climate Change [H.-O. Pörtner, D.C. Roberts, M. Tignor, E.S. Poloczanska, K. Mintenbeck, A. Alegría, M. Craig, S. Langsdorf, S. Löschke, V. Möller, A. Okem, B. Rama (eds.)]. Cambridge University Press. Cambridge University Press, Cambridge, UK and New York, NY, USA, 3056 pp., doi:10.1017/9781009325844

Karmalkar, A. V., Bradley, R. S., and Diaz, H. F., 2011. Climate change in Central America and Mexico:

Regional climate model validation and climate change projections. Climate Dynamics, 37(3), 605–629. https://doi.org/10.1007/s00382-011-1099-9

Knutson, T.R., Sirutis, J.J., Zhao, M., Tuleya, R.E., Bender, M., Vecchi, G.A., Villarini, G. and Chavas, D., 2015. Global projections of intense tropical cyclone activity for the late twenty-first century from dynamical downscaling of CMIP5/RCP4. 5 scenarios. Journal of Climate, 28(18), pp.7203-7224.

Kitoh, A., H. Endo, K. Krishna Kumar, I.F.A. Cavalcanti, P. Goswami, and T. Zhou, 2013: Monsoons in a changing world: a regional perspective in a global context. Journal of Geophysical Research: Atmospheres, 118(8), 3053-306

Kulp, Scott A., and Benjamin H. Strauss. 2018. "CoastalDEM: A Global Coastal Digital Elevation Model Improved from SRTM Using a Neural Network." Remote Sensing of Environment 206 (March): 231–39.
Maurer, E. P. and Hidalgo, H. G., 2008: Utility of daily vs. monthly large-scale climate data: an intercomparison of two statistical downscaling methods, Hydrology and Earth System Sciences, 12, 551-563.

Mayer, B., 2015. Climate migration governance. Handbook of Climate Change Adaptation. Springer, pp.823-838.

McAdam, J. (2019). Global Compact for Safe, Orderly and Regular Migration. International Legal Materials, 58(1), 160–194. https://doi.org/10.1017/ilm.2019.6

Nakaegawa, T., A. Kitoh, H. Murakami, and S. Kusunoki, 2013b: Annual maximum 5- day rainfall total and maximum number of consecutive dry days over Central America and the Caribbean in the late twenty-first century projected by an atmospheric general circulation model with three different horizontal resolutions. Theoretical Applied Climatology (in press), doi:10.1007/s00704-013-0934-9.

Organization of African Unity (OAU), Addis Ababa Document on Refugees and Forced Population Displacements in Africa, 10 September 1994

Pons, D., Castellanos, E., Conde, D., Brincker, J., Incer, D., and López, A. (2018). Escenarios de aridez para Guatemala para los años 2030 , 2050 y 2070 utilizando modelos de cambio climático . Yu'am, 2(4), 4–16

Ramji-Nogales, J., 2016. Migration emergencies. Hastings LJ, 68, p.609.

Rauscher, S. A., Giorgi, F., Diffenbaugh, N. S., and Seth, A., 2008. Extension and Intensification of the Meso-American mid-summer drought in the twenty-first century. Climate Dynamics, 31(5), 551–571. https://doi.org/10.1007/s00382-007-0359-1

Rigaud, K.K., De Sherbinin, A., Jones, B., Bergmann, J., Clement, V., Ober, K., Schewe, J., Adamo, S., McCusker, B., Heuser, S. and Midgley, A., 2018. Groundswell.

Sasnal, Patrycja, 2018. Domesticating the Giant: The Global Governance of Migration. Council of Foreign Relations. Article. https://www.cfr.org/report/domesticating-giant-global-governance-migration
Selby, J., Dahi, O.S., Fröhlich, C. and Hulme, M., 2017. Climate change and the Syrian civil war revisited. Political Geography, 60, pp.232-244.

UN General Assembly. (2016). New York Declaration for Refugees and Migrants: Comprehensive Refugee Response Framework (CRRF). A/Res/71/1, 16163(October), 1–24. Retrieved from

https://refugeesmigrants.un.org/declaration

UNFCCC (2017). Report of the Task Force on Displacement, (September), 89. Retrieved from https://unfccc.int/node/285

UNHCR. (2018). Report of the United Nations High Commissioner for Refugees - Global Compact on Refugees. https://doi.org/10.4324/9780203146651

Warner, K., 2010. Global environmental change and migration: Governance challenges. Global environmental change, 20(3), pp.402-413.

Williams, A., 2008. Turning the tide: Recognizing climate change refugees in international law. Law and Policy, 30(4), pp.502-529.

Wilson, Jill, 2021. Temporary Protected Status and Deferred Enforced Departure. Congressional Research Service – Report. RS208

Chapter 1 - Central America: Assessing past and projected droughts in the region's Dry Corridor and migration from and within Guatemala.

1.1 - Meteorological Droughts Are Projected to Worsen in Central America's Dry Corridor Throughout the 21st Century

This section is adapted from (Depsky and Pons, 2021). The project formulation, data analysis, majority of the text and all figures were prepared by myself, with observational weather station data provision and portions of the text contributed by my collaborator, Dr. Diego Pons. The published version of this work can be found at https://doi.org/10.1088/1748-9326/abc5e2

Abstract

Understanding past and projected drought patterns across Central America's 'Dry Corridor' (CADC) is crucial for adaptation planning and impact mitigation, especially in small-scale agricultural communities. We analyzed historical and predicted drought patterns in the CADC by calculating Standardized Precipitation Index (SPI) values from local rain gauge records, reanalysis data and a 20-member ensemble of bias-corrected, downscaled CMIP-5 GCMs at both seasonal (3-month) and annual (12-month) scales. Trends in drought frequency, duration, intensity were assessed for three, 30-year future periods compared to historical values. Our results suggest a decrease in mean annual rainfall of 8-14% in the CADC under moderate to high emissions scenarios, respectively, by end-of-century (2071-2100) relative to a historical baseline (1950-2005). However, projected changes to drought characteristics under these scenarios are more pronounced, with seasonal-scale droughts projected to lengthen by 12-30%, intensify by 17-42% and increase in frequency by 21-24% by end-of-century. Annual-scale, longer-term droughts are projected to lengthen by 68% under moderate emissions, potentially triple in length under high emissions and to intensify by 27-74%. These results were similar yet slightly more pronounced for some drought metrics when just considering rainy/cropping season months (May-Oct). End-of-century changes to rainfall reliability and drought occurrence such as these would severely impact millions of vulnerable inhabitants in the CADC and should be considered in adaptation policy-making efforts.

Introduction

Central America's Dry Corridor (CADC) routinely experiences periods of drought that impact the livelihoods of millions of people, especially those living in rainfed agricultural communities. This has been true in recent years throughout the CADC, which spans Guatemala, El Salvador, Honduras and Nicaragua (Figure 1) (Van der Zee Arias et al., 2012).

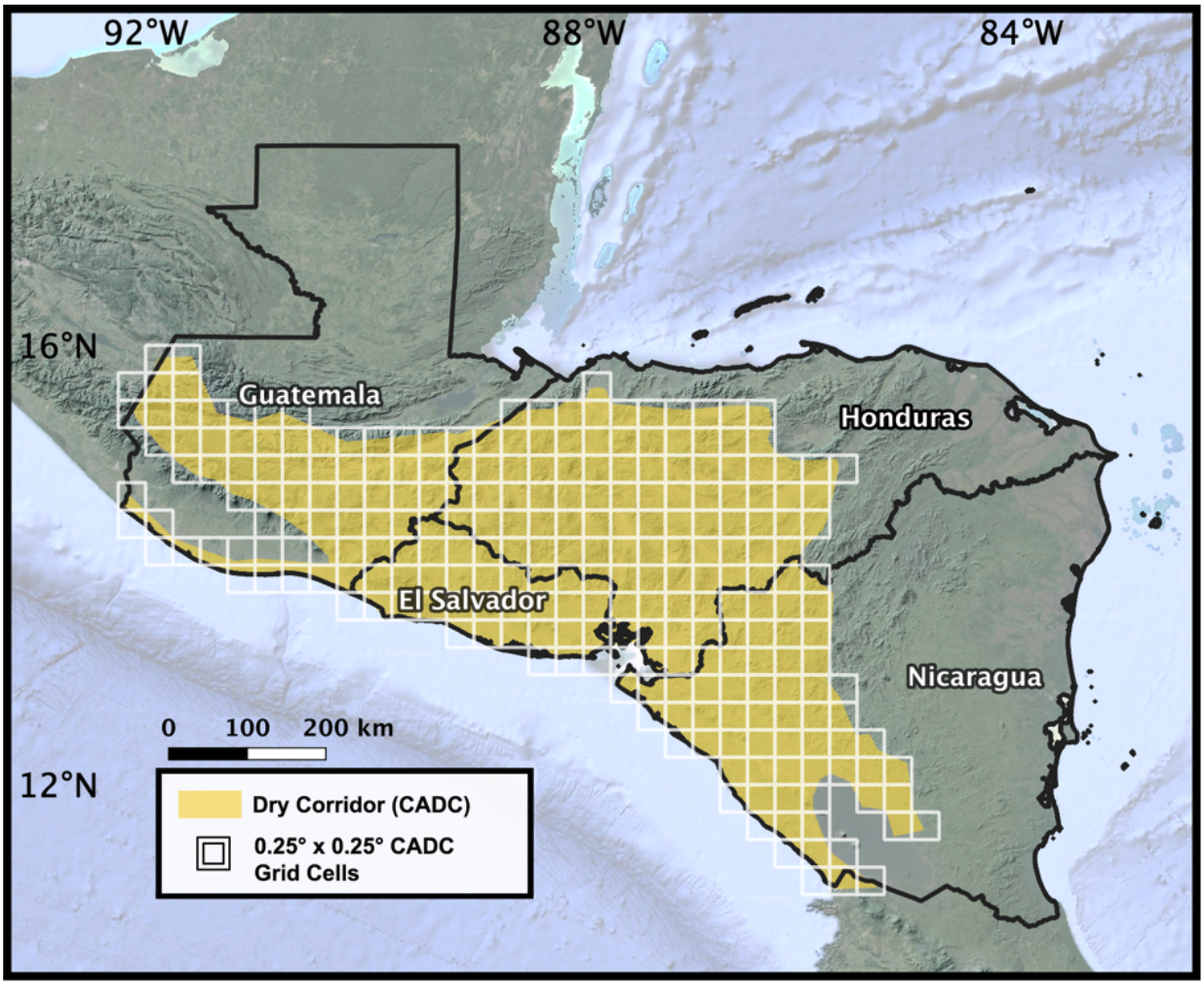

Figure 1. CADC study region with estimated boundaries and corresponding 0.25-degree pixels used from the climate datasets used for CAD-averaged calculations. Spatial extent approximated from Van der Zee Arias et al. (2012) and FAO (2016).

The CADC is home to 10.5 million people, nearly two-thirds of whom live in poverty, primarily in small farming communities (Van der Zee Arias et al., 2012; Hidalgo et al., 2019). In early 2019, the region was entering its fifth consecutive drought year, with 2.2 million people having suffered severe crop losses in previous years and 1.4 million people in urgent need of food aid (Vaqué, 2017; WFP, 2019; WFP, 2020; FAO, 2018). Rural, smallholder farming communities dependent on timely and sufficient rainfall from May to October for the production of both staple grains and cash crops, like coffee, were most impacted by the ongoing drought (Van der Zee Arias et al., 2012; Anderson et al., 2019; Rauscher et al., 2008; Hannah et al., 2017; Marroquín and Gómez, 2019).

Droughts have impacted these communities' crop yields, income and food security and have been linked to internal displacement and migration in the region (Lobell et al., 2008; Arévalo et al., 2015; Nawrotzki et al., 2016; Rivera et al., 2019; IDB, 2017; WFP, 2020). The World Food Programme estimated that emigration from the CADC increased nearly five-fold between 2010

and 2015, with nearly a third of emigrants citing extreme weather as their primary reason for leaving (WFP, 2020). In economic terms, Central America has suffered roughly $5 billion USD in losses due to drought impacts on agriculture in the past 30 years (GWP, 2016).

The CADC receives approximately 1500 mm of rainfall each year, with some regions receiving just 800 mm/year. The annual pattern of precipitation is characterized by a dry season from November to April, followed by a rainy season from May to October with an intermediate period of decreased rainfall from July to August known as the mid-summer drought (MSD), or colloquially as the canícula or veranillo period (Figure 2) (Rauscher et al., 2008; Hannah et al., 2017; Anderson et al., 2019; Marroquín and Gómez, 2019; Inoue et al., 2002; Wang and Lee, 2007). It should be noted that the colloquial definition of this mid-summer decline in rainfall as a "drought" is not equivalent to the meteorological definition of drought employed in this study, which only defines a period as being a drought if it is anomalously dry compared to average historical values. Since the MSD is an annual lull in July-August rainfall, its occurrence would only be classified as a meteorological drought if it was particularly dry compared to the average MSD.

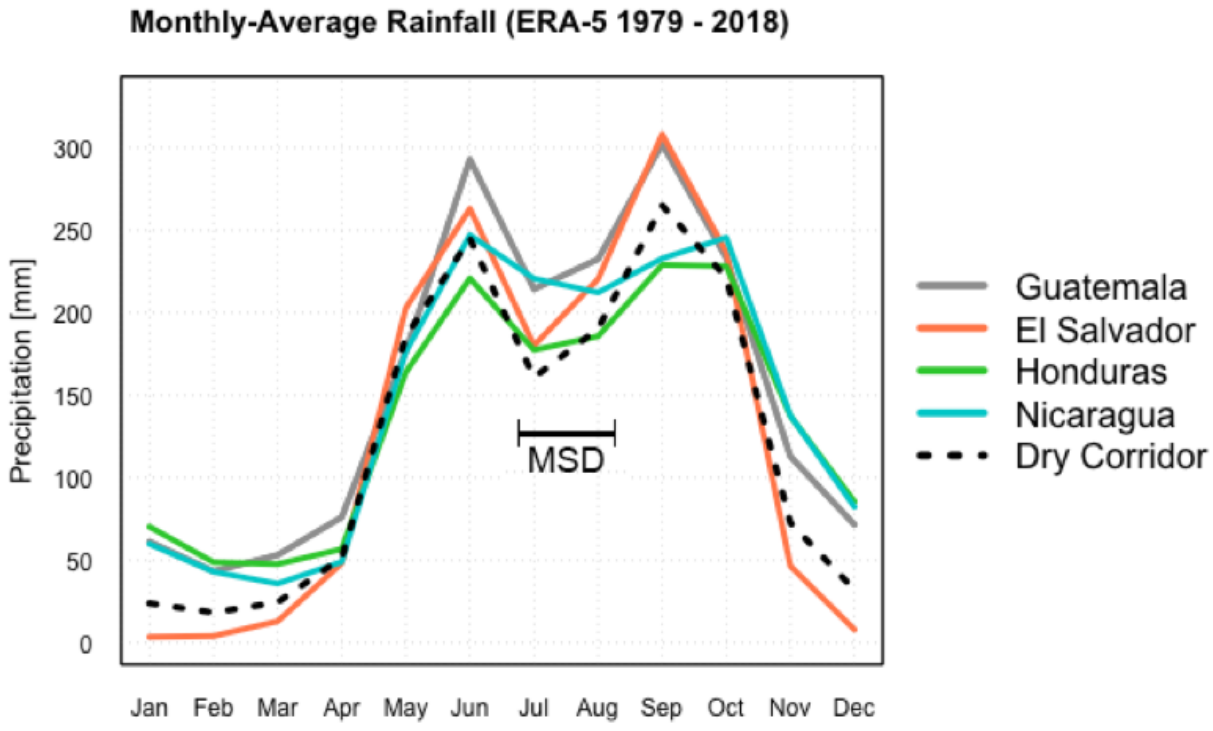

Figure 2. Mean monthly rainfall in the study region derived from ERA-5 reanalysis data. National and CADC-wide values shown. Mid-summer drought (MSD) indicated from July-August.

From Figure 2, we can see that at the national-level, El Salvador exhibits the widest range in monthly average precipitation between the dry and rainy seasons. Its dry season mean precipitation (Nov-Apr) is lower than in Guatemala and Honduras, while its rainy season average monthly values are higher than Honduras in every month and is highest of all three countries in September. At the department-level, the variability in rainfall across different departments in the

region is much more pronounced than it is nationally, with wide variance both in pattern and magnitude of precipitation. Most notable is the fact that the distinct bimodal precipitation pattern diminishes along the Caribbean cost (northern coast of Honduras and eastern coast of Guatemala) and disappears altogether in the Honduras' Islas de la Bahía department – a string of small islands situated approximately 50km north of its northern coastline (Figure 3). Precipitation patterns in this region converge to a unimodal rainfall signal, with peak rainfall occurring in Oct-Nov.

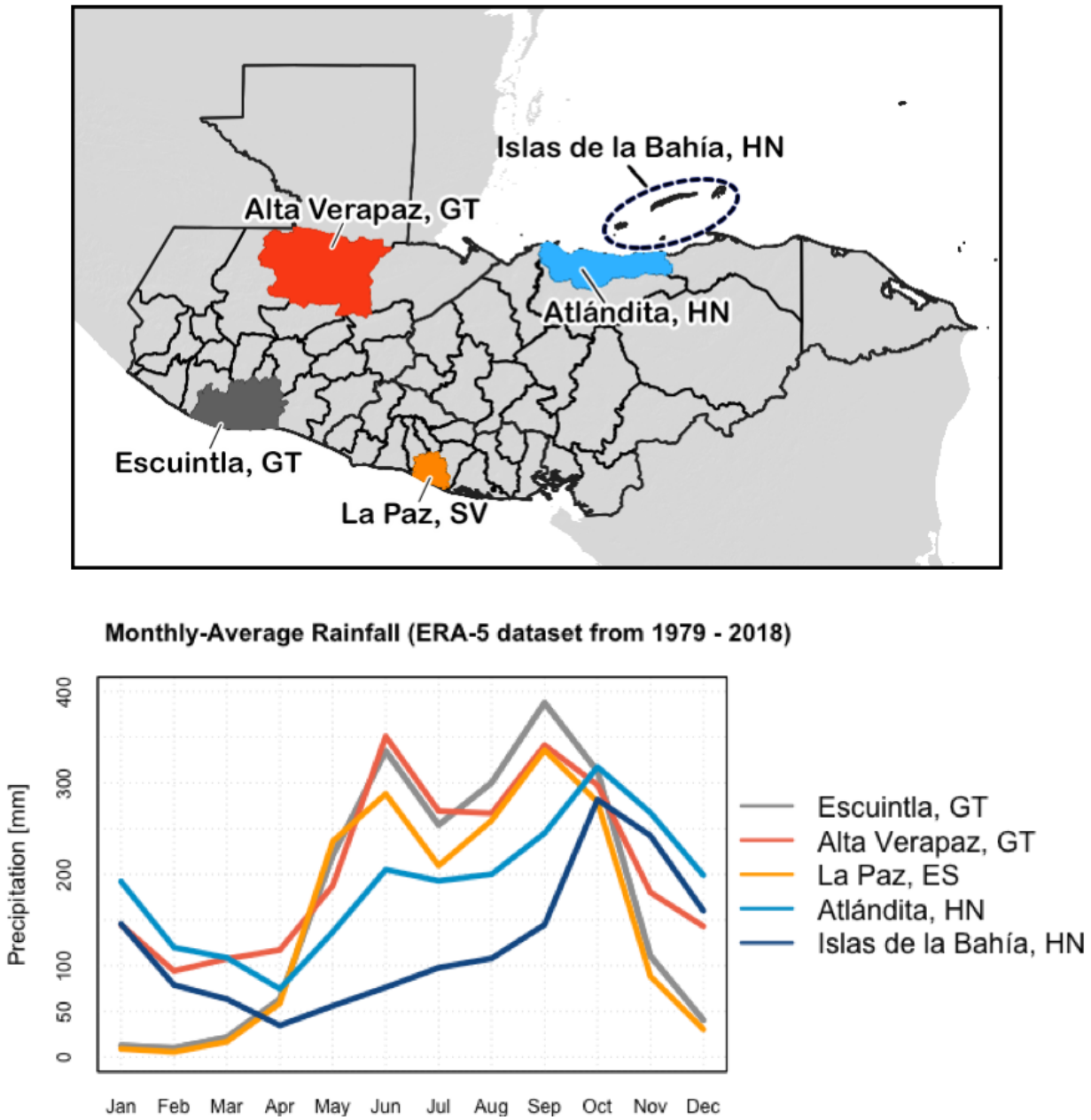

Figure 3. Average rainfall heterogeneity across selected departments across Guatemala, Honduras and El Salvador.

In terms of mean total annual rainfall, there is also considerable variability across the region, with departmental mean annual totals ranging from 1200mm to 3000mm. The lowest mean annual rainfall in the region that spans the Dry Corridor region in the southeastern interior of Guatemala and into much of El Salvador and parts of western and central (Figure 4). In Guatemala, researchers have found that aridity (defined as the ratio between annual precipitation to annual potential evapotranspiration) will likely increase across the country under most future climate scenarios, with the departments in the Dry Corridor becoming especially arid (Pons et al., 2018).

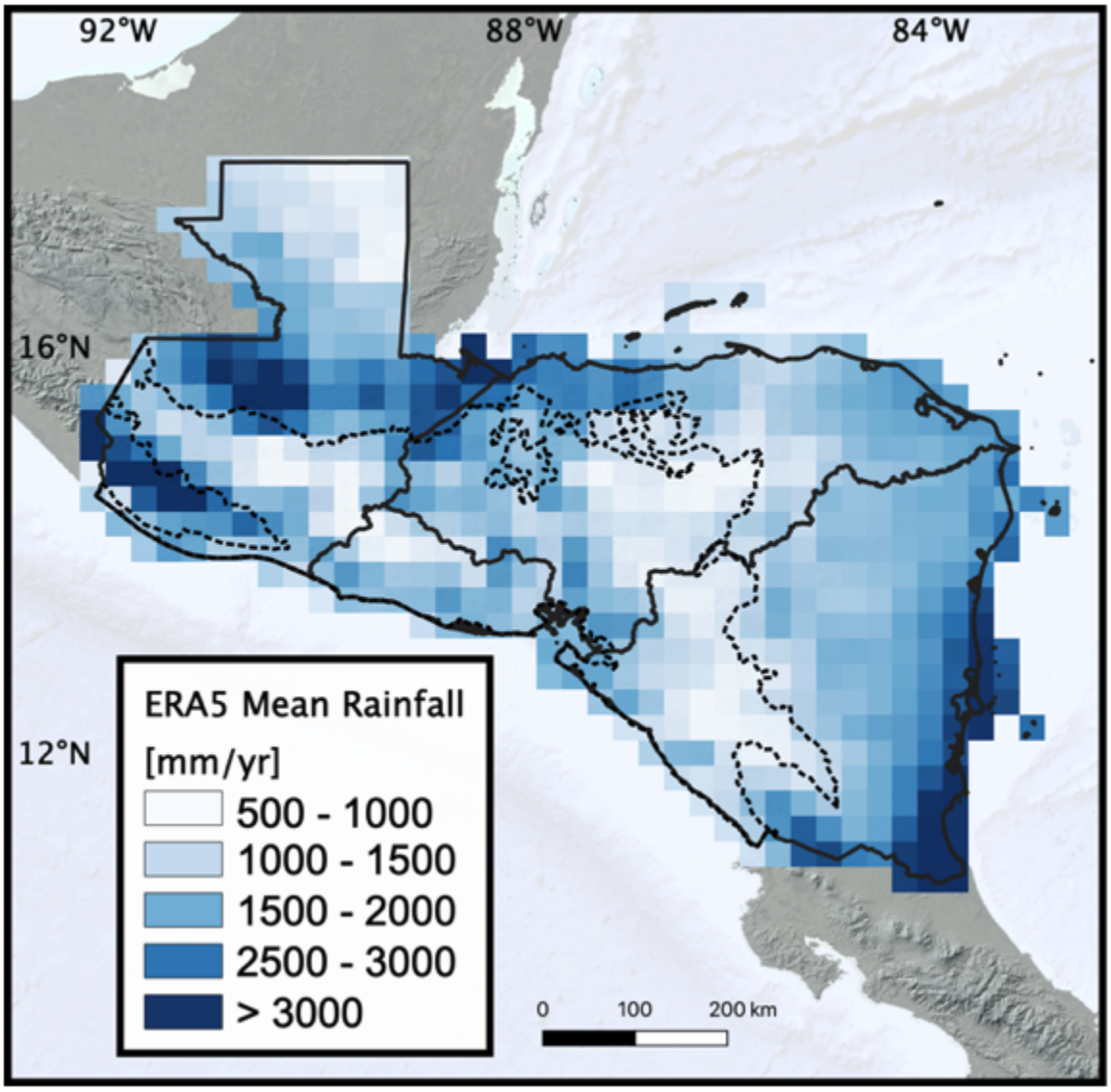

Figure 4. Mean annual rainfall from the ERA-5 dataset (1979-2018).

Numerous studies have predicted decreases in mean annual precipitation (MAP) in Central America by ~10-50% by 2100 for CADC countries (Kitoh et al., 2011; Nakaegawa et al., 2013; Campbell et al., 2011; Karmalkar et al., 2011; Pons et al., 2018). There have also been a growing number of studies of droughts in the region, particularly with respect to future projections of

MSD characteristics. Rauscher et al. (2008) and Maurer et al. (2017) employed multi-model GCM ensembles to show that CADC MSDs are predicted to increase in variability, duration and intensity in coming decades in concert with the expansion of the North Atlantic subtropical high (NASH) and strengthening of low-level easterly winds of the Caribbean Low-Level Jet (CLLJ). Anderson et al. (2019) showed that MSD durations have increased over the past 40 years in the CADC as well. These findings are important, as variability, extension and intensification of MSDs can delay or disrupt cropping practices (Rauscher et al., 2008; Van der Zee Arias et al., 2012; Maurer et al., 2017; Marroquín and Gómez, 2019). Hidalgo et al. (2013) also found statistically-significant decreases in projected precipitation and hydrologic runoff throughout much of Central America by 2100 and other studies of larger-scale climate dynamics project drying trends due to a southward migrating Eastern Pacific Inter-Tropical Convergence Zone (ITCZ) as temperatures warm and a potential increased frequency of El Niño (ENSO) events (Rauscher et al., 2008; Steinhoff et al., 2015; Taylor et al., 2013).

However, there is a lack of research on future drought predictions in the CADC that takes a broader focus than trends of MSDs. While the MSD is one of the most important climate features for CADC communities, there is also a need to understand how rainfall and the occurrence of seasonal and longer-term droughts are projected to change. Lack of rainfall throughout the year can impact water supply and soil moisture leading up to cropping seasons and longer-term droughts can have crippling impacts on the region as a whole. This study complements the growing body of CADC-drought literature by providing the following contributions: i) an analysis of past and projected drought characteristics throughout the CADC using a bias-corrected, statistically-downscaled, 20-member GCM ensemble for both short-term and long-term droughts, ii) assessment of projected changes to drought patterns both during the rainy/cropping season (May-Oct), which encompasses MSD trends, as well as the entire calendar year, iii) application of a suite of drought metrics, including a novel metric that integrates duration, intensity, frequency into one variable, and iv) uses observed station data to validate the GCM ensemble and a relatively new reanalysis dataset (ERA-5) for drought assessments in the CADC.

The analysis was done in two stages, the first being an evaluation of historical droughts through a comparison observational station records, reanalysis and historical climate model data to evaluate the ability of the GCM ensemble to reproduce precipitation and droughts observed over the CADC in the past (1981-2018) and identify model bias. We then assessed projected changes to precipitation and droughts across the GCM ensemble for three, 30-year future periods extending to 2100 compared to reference period (1950-2005) values.

Data

Ground-Based Observational Records

Observational records from 101 rainfall stations maintained by Guatemala's national meteorological agency INSIVUMEH were obtained for the 1981 to 2018 period throughout Guatemala (Supplemental Figure 1). These stations span a range of climate regions both within and outside the Guatemalan portion of the CADC and were used to assess the ability of historical

reanalysis and GCM data to capture historical rainfall and drought patterns. For such comparison purposes, all 101 available stations were utilized – not just those located within the CADC – due to the limited number of station-records available in the study area and the desire to validate gridded reanalysis and climate model data along both the Pacific and Caribbean coasts.

Historical Reanalysis Data (ERA-5)

Historical reanalysis estimates of monthly precipitation were obtained from the European Centre for Medium-Range Weather Forecasts' ERA-5 reanalysis dataset – a global, 0.25° x 0.25° product with data available from 1979 to 2018. Its total precipitation values are estimated from remotely-sensed (satellite) and ground-based radar station estimates (C3S, 2017). The ERA-5 values were compared against both Tropical Rainfall Measurement Mission (TRMM - Version 7) and the Global Precipitation Climatology Centre's (GPCC Version 2018) monthly precipitation values during the period of overlap (01/1998-12/2016) for the three datasets at grid cells corresponding to observed station locations. Monthly averages of all three datasets were compared to observed values for this 19-year period and it was found that ERA-5 performed the best in capturing the seasonal pattern of rainfall observed in the Guatemalan station data, with both TRMM and GPCC over-estimating rainfall, especially during July-August MSD periods (Figure 5).

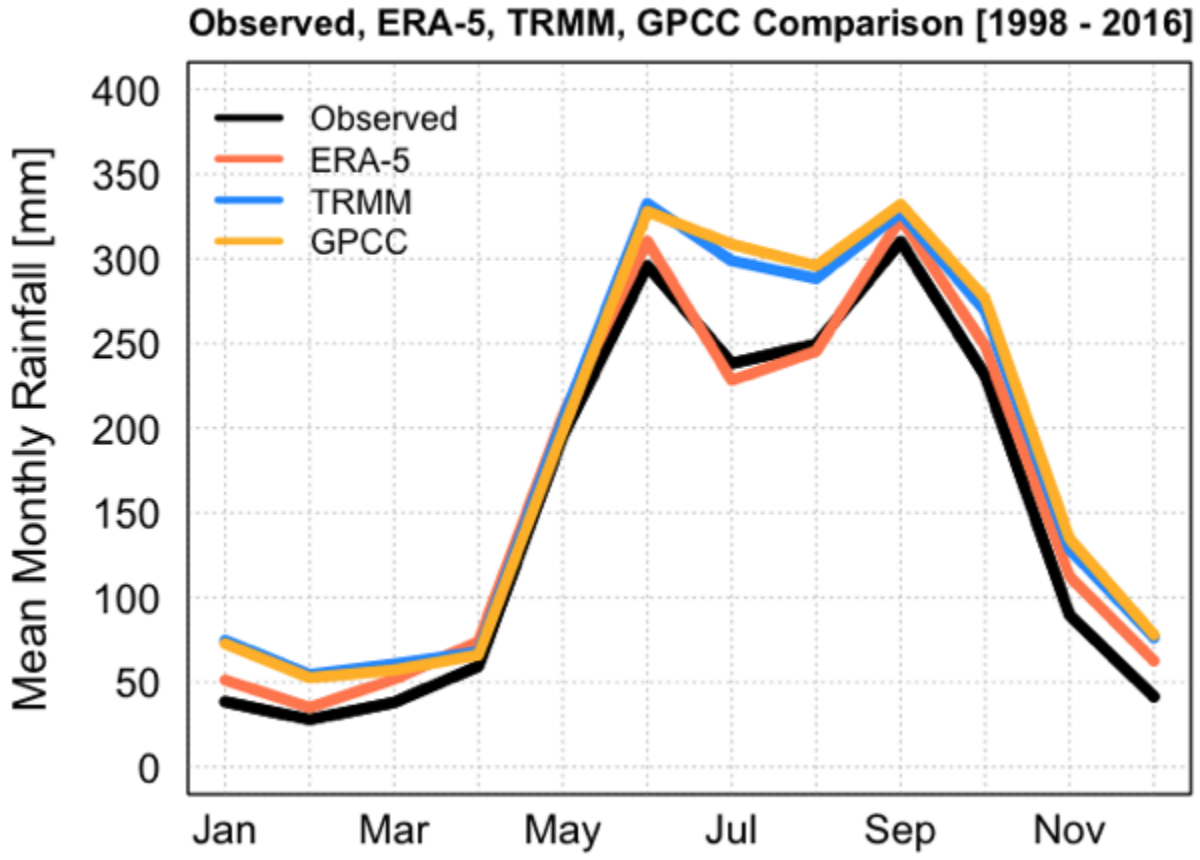

Figure 5. Monthly Average ERA-5, TRMM (Version 7) and GPCC (Version 2018) precipitation values compared to observed station values from 1998-2016.

Data from 20 global climate model implementations (GCMs), included in the Coupled Model Intercomparison Project Phase 5 (CMIP-5) (Taylor et al., 2012), were used to evaluate projected changes in rainfall and drought patterns across the CADC. These data are from the NASA Earth Exchange Global Daily Downscaled Projections (NEX-GDDP), which provides an ensemble of different GCMs, all bias-corrected and statistically-downscaled (BCSD) to a uniform 0.25° x 0.25° grid via a quantile mapping approach between historical forcing data and model outputs as detailed by Thrasher et al. (2012), Wood et al. (2002, 2004), and Maurer et al. (2008). The historical forcing dataset used in this BCSD process was the Global Meteorological Forcing Dataset from Princeton's Terrestrial Hydrology Research Group (Sheffield et al., 2006). The ensemble consists of 3 scenarios for each model – a historical reference baseline from 1950 to 2005, and moderate (RCP 4.5) and high-emissions (RCP 8.5) 'future' scenarios from 2006 to 2100, which roughly correspond to increases in mean global temperatures by 2.4ºC and 4.9ºC by 2100, respectively (Meinshausen et al., 2011; Rogelj et al., 2012; Moss et al., 2010). We did not perform any additional bias correction on these GCM models for use in the CADC region.

Table 1. CMIP-5 global climate models used in study ensemble from the NEX-GDDP dataset.

Model	**Developing Institution**
bcc-csm1-1	Beijing Climate Center, China Meteorological Administration
BNU-ESM	Beijing Normal University
CanESM2	Canadian Centre for Climate Modelling and Analysis
CCSM4	National Center for Atmospheric Research
CESM1-BGC	National Center for Atmospheric Research
CNRM-CM5	National Centre for Meteorologic Research
CSIRO-Mk3-6-0	Commonwealth Scientific and Industrial Research Organisation
GFDL-CM3	Geophysical Fluid Dynamics Laboratory, NOAA
GFDL-ESM2G	Geophysical Fluid Dynamics Laboratory, NOAA
GFDL-ESM2M	Geophysical Fluid Dynamics Laboratory, NOAA
inmcm4	Russian Institute for Numerical Mathematics
IPSL-CM5A-LR	Institute Pierre Simon Laplace
IPSL-CM5A-MR	Institute Pierre Simon Laplace

MIROC-ESM-CHEM	Japan Agency for Marine-Earth Science and Technology
MIROC-ESM	Japan Agency for Marine-Earth Science and Technology
MIROC5	Japan Agency for Marine-Earth Science and Technology
MPI-ESM-LR	Max Planck Institute
MPI-ESM-MR	Max Planck Institute
MRI-CGCM3	Meteorological Research Institute, Japan Meteorological Agency
NorESM1-M	Norwegian Climate Center

Note: the ACCESS1-0 model originally provided in the NEX-GDDP dataset was excluded due to issues in the RCP 8.5 scenario data obtained.

Methods

We used a simple, meteorological drought definition solely based on accumulated precipitation (Mishra and Singh, 2010) due to the high prevalence of rainfed agriculture throughout the CADC (as opposed to highly managed systems with storage and conveyance) and also due to the CADC's location in the tropics, making fluctuations in monthly temperatures and, by partial extension evaporative demand, relatively minimal compared to those in more temperate climes. Monthly station and ERA-5 precipitation data were used to assess both the GCM ensemble's agreement with historical data across the study region and its projected rainfall and drought trends in the future. Drought periods were identified using the Standardized Precipitation Index (SPI), a measure of normalized, accumulated rainfall anomalies. Calculating SPI only requires precipitation data and can be defined for various time-scales (e.g. 3, 6, 12-month), which allows for analysis of both short and long-term periods of accumulated rainfall deficits (Touma et al., 2015; Blain, 2011; Penalba and Rivera, 2013; Svoboda et al., 2012; McKee et al., 1993; Guttman, 1999; Edwards, 1997).

SPI is calculated by converting rainfall time-series to monthly, accumulated values defined by the chosen SPI-scale (e.g. 3-months), fitting these to a probability density function (separately for each calendar month) and ultimately transforming to standard normal values. Resultant SPI values indicate how many standard deviations an accumulated rainfall value is above or below the historical mean for that month (McKee, 1993; Edwards, 1997; Guttman et al., 1999). A 2-parameter gamma (2PG) distribution was utilized with maximum-likelihood estimation for shape and scale parameters (Naresh Kumar et al., 2009; Ukkola et al., 2018; Strzepek et al., 2010; Vincente-Serrano, et al., 2010; Zarch et al., 2015; Penalba and Rivera, 2013; Blain, 2011). Nearly all CADC rainfall values (station, reanalysis and GCMs) fit the 2PG distribution, as determined from application of Kolmogorov-Smirnov tests (p-value < 0.05) (Supplemental Table 1).

Drought periods were defined as any span of continuously negative SPI values with at least one value of -1 or lower (Guttman, 1999; McKee et al., 1997; McKee et al., 1993; Kallis, 2008; Svoboda et al., 2012). This study assesses both 3-month SPI values (SPI3) to assess short-term

droughts as well as 12-month SPI (SPI12), similar to the approach taken by Penalba and Rivera (2013) (Figure 6). SPI3 time-series show more-frequent, shorter droughts and higher variability while the SPI12 series are smoother with less-frequent, longer droughts. For illustrative purposes, example time-series for 3, 6, 9, and 12-month SPI-scales are also shown in Supplemental Figure 2.

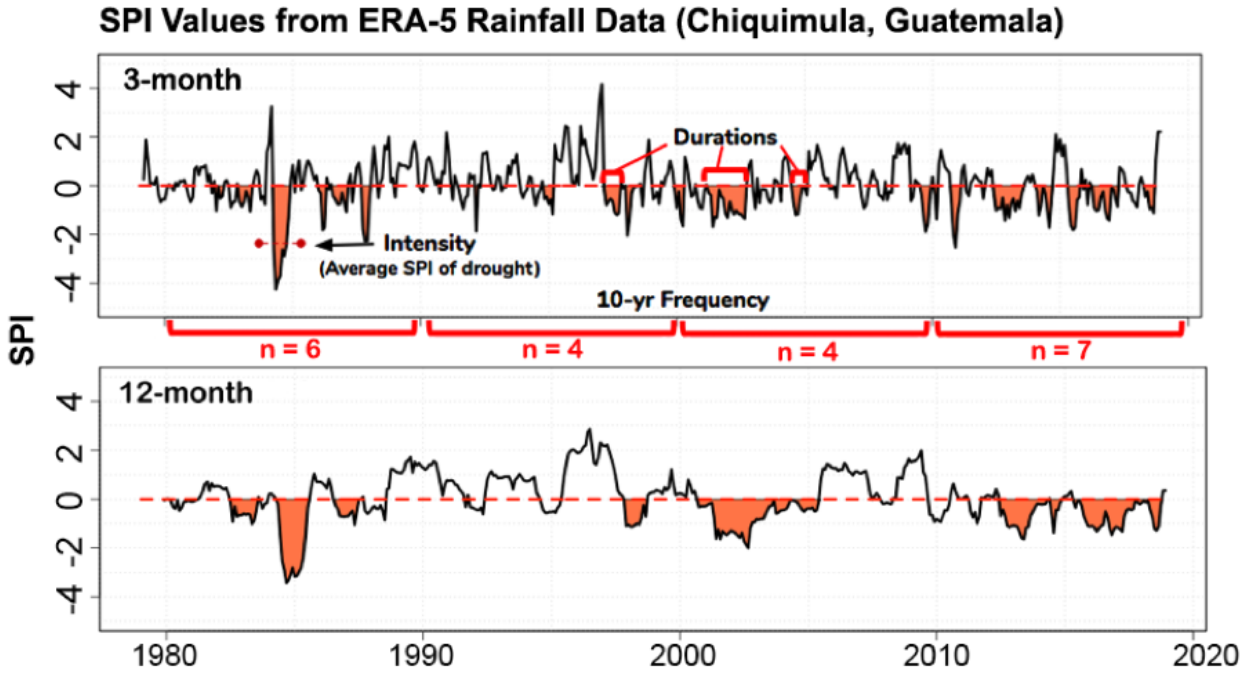

Figure 6. Example of 3 and 12-month historical SPI time-series for Chiquimula Department (Supplemental Figure 3), Guatemala from 1979-2018 using the department-average ERA-5 precipitation. Droughts shaded orange. Drought duration, intensity and decadal frequencies are demonstrated for the SPI3 series.

SPI3 and SPI12 values were derived from station, ERA-5 and GCM data for historical and future periods. These values were used to characterize drought patterns at each station or grid-cell location by calculating the following metrics: i) mean **duration** (DUR), in months, of each drought period ii) mean **intensity** (INT) of each drought, with intensity for a given drought equal to that period's average SPI-value iii) mean **10-year drought frequency** (FREQ10), or the number of droughts per decade, and iv) mean **annual**, **intensity-weighted total drought duration** (AIWD), which is defined as the absolute sum of all SPI-values during droughts over a given period divided by that period's length, in years. AIWD is equivalent to the average number of drought months each year, weighted by intensity (a drought month with an SPI value of -2 would receive twice the weight of a drought month with a value of -1) (Eq. 1).

$$AIWD = \frac{|\sum_{d}^{D}\sum_{m}^{M} SPI_{d,m}|}{Y} \quad \text{(Eq. 1)}$$

D represents the set of each drought period d in the SPI time-series, M is the set of each month m in a given drought d and Y is the record length in years. This metric embeds the duration,

intensity and frequency of drought events and can be thought of as an aggregate of DUR, INT and FREQ10. It is equal to the integrated area of the shaded periods in Figure 6 divided by *Y*.

ERA-5 and GCM ensemble data were compared to the station values from 1981 to 2018 to evaluate their agreement with ground observations. This analysis was split into two periods, one from 1981 to 2005 using the ensemble's historical reference runs, and a second from 2006 to 2018 using the 'future' RCP 4.5 and 8.5 ensemble runs, which span from 2006 to 2100. The second analysis period allowed for a crude assessment of the ability of GCM models to broadly emulate observed rainfall and droughts in their 'future' configurations for 13 years outside of their historical reference period, already subject to bias-correction. Future changes in drought patterns were assessed by calculating SPI from GCM ensemble rainfall during three, 30-year 'future' periods: 2011-2040, 2041-2070 and 2071-2100 (Figure 7).

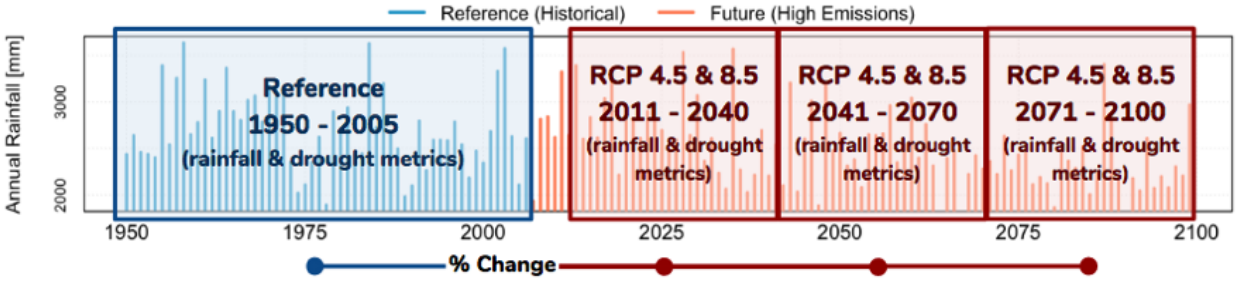

Figure 7. Conceptual schematic illustrating GCM future vs. reference scenario analysis.

In order to evaluate how future rainfall and droughts differ relative to a historical baseline, SPI values in these three periods were calculated using the same shape and scale parameters that were derived from fitting the corresponding historical rainfall from 1950 to 2005 to a 2PG distribution (Touma et al., 2015). Future SPI values therefore represent how many standard deviations each accumulated rainfall value is from the historical mean in that location. Changes from historical averages were evaluated for mean annual rainfall and all drought metrics for SPI3 and SPI12, for the entire year (Jan-Dec) and solely rainy season months (May-Oct). Historical and future rainfall and drought trends were assessed for statistical significance using the non-parametric Mann-Kendall trend test (Mann, 1945; Kendall, 1975).

We should note that we also considered the Standardized Precipitation Evapotranspiration Index (SPEI) as our drought metric of choice, which incorporates potential evapotranspiration (PET) in its calculation. However, reliable calculation of PET can vary depending on the estimation method, the most accurate of which requires additional meteorological variables that were not directly available in our observational records or downscaled GCM ensemble outputs (Da Silva Junior et al., 2017; Quesada-Montano et al., 2019). Additionally, Quesada-Montano et al., (2019) conducted a side-by-side comparison of SPI and SPEI for use in characterizing historical droughts across Central America and found them to produce largely similar results, though they do acknowledge the benefits of accounting for PET when feasible. Given the relative stability of annual PET between months, SPI was deemed sufficient for estimating changes in meteorological drought in the region.

Results and Discussion

Historical Comparisons

Historical mean monthly rainfall patterns for station and ERA-5 data in Guatemala were found to be very similar in both magnitude and seasonality from 1981 to 2018 (Figure 8). The downscaled, bias-corrected GCM ensemble at station locations also captures observed seasonality but consistently overestimates rainfall throughout the year, roughly by +45% during the rainy season (May-Oct) over this historical period and shows a slightly delayed MSD peak, modeled as being most severe in August as opposed to July. However, given that our analysis considers precipitation smoothed across 3 and 12-month periods (SPI3, SPI12), our results are likely less sensitive to this July-August discrepancy than if we had focused on individual monthly values (SPI1). The duration of the MSD and timing of the bimodal precipitation maxima are very consistent between the station, reanalysis and ensemble data.

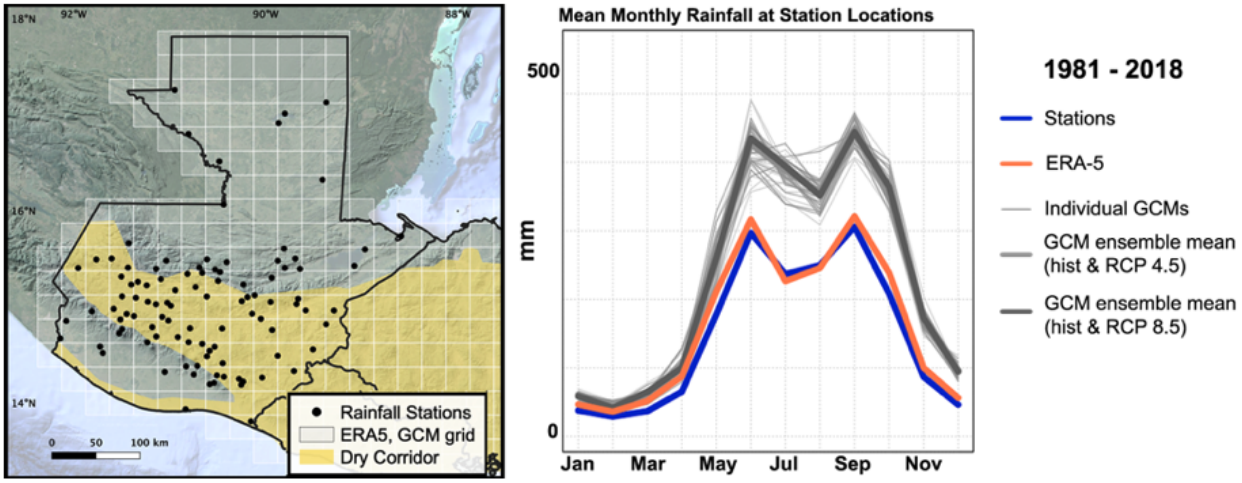

Figure 8. (left) Location of rainfall stations used for comparison. (right) Comparison of mean monthly precipitation values from Guatemalan station data and the ERA-5 reanalysis data and individual GCMs at pixels overlying station locations. Ensemble means for RCP4.5 and 8.5 are shown in bold and are nearly identical., Period of comparison 01/1981-06/2018.

The ensemble was found to produce similar monthly mean rainfall values at the gauge locations during both the 1981-2005 and 2006-2018 periods, which provides crude validation of their ability to capture local rainfall pattern outside of the bias-correction period, though there is slightly higher model variance in the 2006-2018 period (Supplemental Figure 4). Additionally, there is some spatial heterogeneity in the bias of the ensemble mean's average annual rainfall across the study region as compared to ERA-5 (Figure 9a). The ensemble is biased-high compared to ERA-5 in most regions, especially along the northern slope of Guatemala's Pacific Coast range. Overall, mean annual rainfall bias between the GCM data and ERA-5 throughout the CADC from 1979 to 2018 was +18% for the historical/RCP4.5 ensemble and +21% for the historical/RCP8.5 ensemble for that period, and are assumed to be generally unvarying during future modeling periods. Mean monthly rainfall patterns are well-represented by the ensemble (Figure 9b).

The rainfall bias produced by the GCMs from 1979 to 2018 in the eastern regions of Guatemala, Nicaragua, and Honduras suggests the ensemble may be modeling a slightly more intense Caribbean low-level jet (CLLJ) than observed in reality. This is potentially due to overrepresentation of the westward move of the NASH (Wang and Lee, 2007) or to an overactive convective precipitation parameterization, causing some incorrect moisture fluxes over the region. This pattern has been observed before in GCMs assessments of CLLJ historical representations (Martin and Schumacher, 2011). Enhanced divergence of moisture in the Caribbean by the CLLJ could result in enhanced rainfall via orographic lifting, which may explain the overestimation of rainfall observed along the eastern slope of the Pacific coastal range, especially in southeastern Guatemala. However, these observed biases may also be partly due to an under-representation of the region's orographic rainfall more generally in the ensemble compared to ERA-5, potentially due to a low density of observational data used in the original BCSD process.

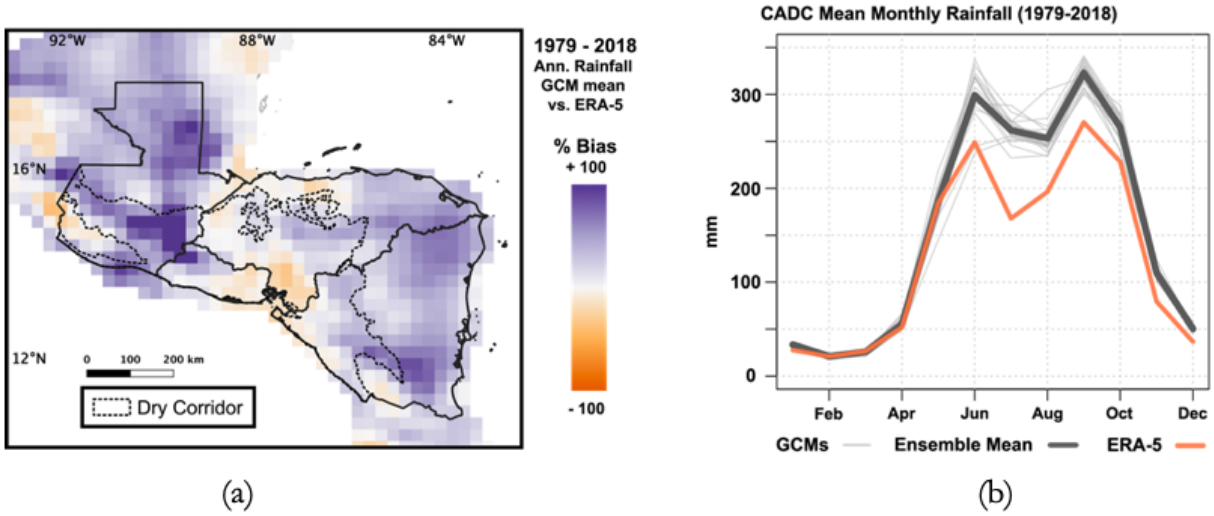

Figure 9. (a) Percent difference in annual mean rainfall between the GCM ensemble mean (average of both RCP scenarios) and ERA-5 from 1979 to 2018. (b) Dry Corridor (CADC) mean monthly rainfall for the GCM ensemble and ERA-5 reanalysis data from 1979 to 2018.

Both the GCM ensemble and ERA-5 reanalysis data also reflect historical DUR, INT, FREQ10, AIWD compared to station values from 1981 to 2018 at the SPI3 and SPI12 scales fairly well (Figure 10). ERA-5 drought metrics diverge from station values more than the ensemble, though still in general agreement for AIWD. The most notable differences are ERA-5's overestimate of DUR and, therefore, its underestimate of FREQ10 for SPI3 and SPI12 droughts during the 1981-2005 period (fewer, longer events than observed in station data). It should be noted that the low frequency of SPI12 droughts means that its metrics are calculated from smaller sample sizes than SPI3 metrics, making values between datasets prone to higher variability. This comparison was also done for solely rainy season months (May-Oct), for which there is similarly high-accuracy of ensemble drought metrics relative to observed values (Supplemental Figure 5), which provides validation for its use in analyzing future drought patterns.

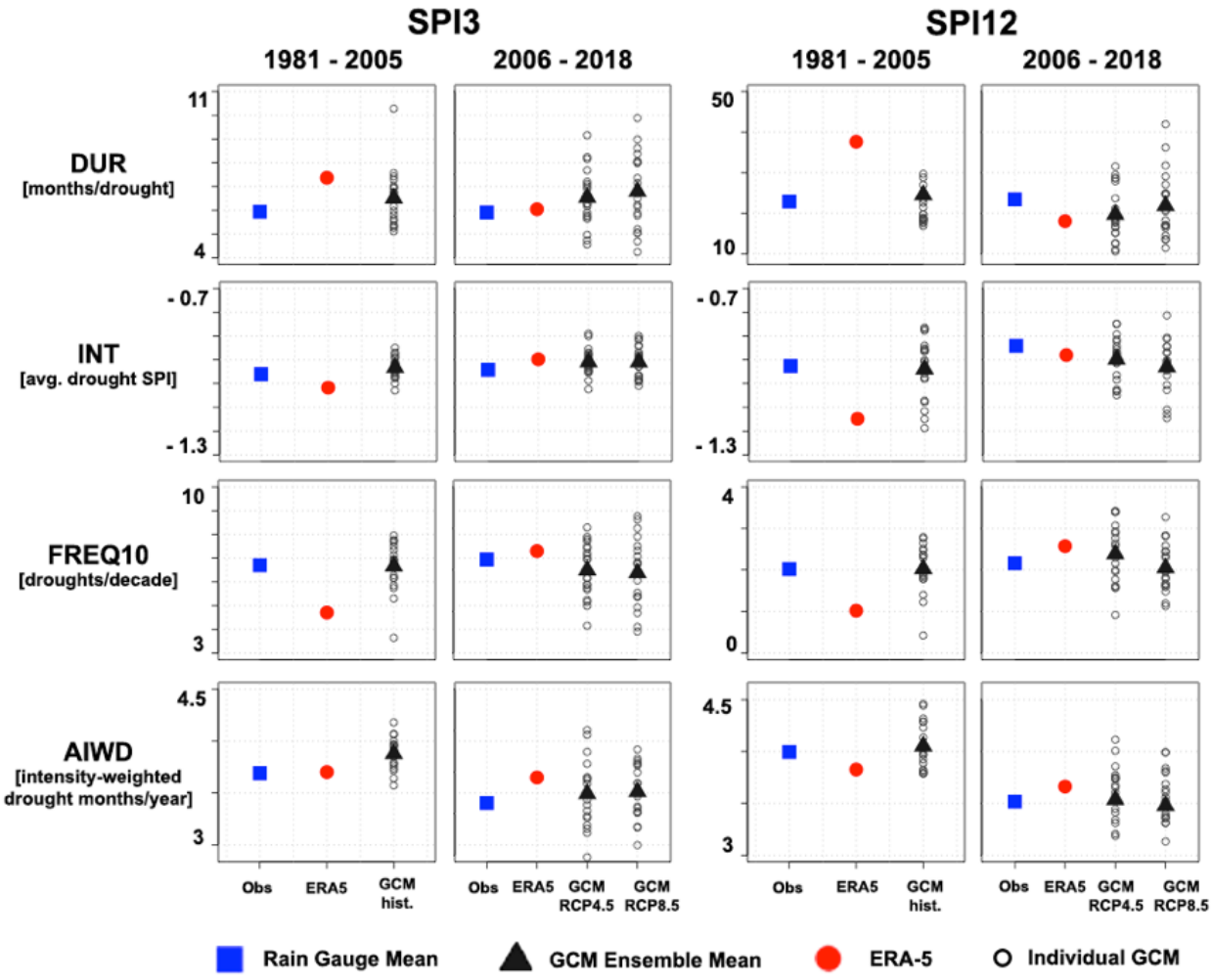

Figure 10. Comparison of average drought metrics across all calendar months observed across the gauging station network and at the ERA-5 and GCM ensemble datasets at these station locations. Results provided for both SPI-scales (3, 12-month) and for each sub-period of the historical analysis. DUR = mean drought duration in months, INT = mean drought intensity in SPI values, FREQ10 = mean number of droughts per decade, AIWD = mean number of intensity-weighted drought months each year.

Department-level historical mean drought metrics from ERA-5 between 1979-2018 are also presented in Supplemental Figures 6-8 for the three Northern Triangle countries of the study region (Guatemala, El Salvador and Honduras) for both SPI-3 and SPI-12.

Projected Rainfall and Drought Patterns

For each GCM ensemble-member, non-parametric Mann-Kendall tests were performed to assess the statistical significance of trends in CADC-averaged mean annual precipitation (MAP) and mean annual DUR, INT, and AIWD values during the historical (1950-2005) and full 'future' (2011-2100) periods (Anderson et al., 2019; Hidalgo et al., 2019). Since FREQ10 is a decadal measure, it was not assessed due to its low sample size (<6 decades in historical period), but is partially represented in AIWD. Statistically significant ($p < 0.05$) MAP trends from 1950 to 2005 were found in only 4 of 20 ensemble members, each of which was negative. CADC-mean ERA-5 MAP values from 1979 to 2018 also showed no significant trend. These findings

corroborate Hidalgo et al. (2017)'s study, which similarly found no significant trends in MAP in the CADC from 1970 to 1999, and gives some credence to our implicit assumption of rainfall stationarity during the reference period. For historical drought metrics, very few significant trends were found – just 2 to 3 members exhibiting (increasing) significant trends for each SPI3 and SPI12 metric.

From 2011 to 2100, 6 and 13 ensemble members displayed significant trends in MAP under moderate (RCP 4.5) and high (RCP 8.5) emissions, respectively. However, the direction of these trends was more mixed under RCP 4.5 as compared to RCP 8.5, the former with 4 of 6 of its significant members showing declining rainfalls by end-of-century and the latter with 11 of 13. For drought metrics, the total number of significant trends amongst ensemble-members was similar to the number of significant MAP trends under each emissions scenario, and there was strong agreement regarding the direction (increasing) of these metrics, especially with respect to drought intensity and all SPI3 metrics. This is likely partly due to the fact that a number of GCMs (e.g. MIROC-5) projected no appreciable change in mean precipitation, but showed a higher frequency of extreme rainfall events, including droughts and intense storms (Figure 11).

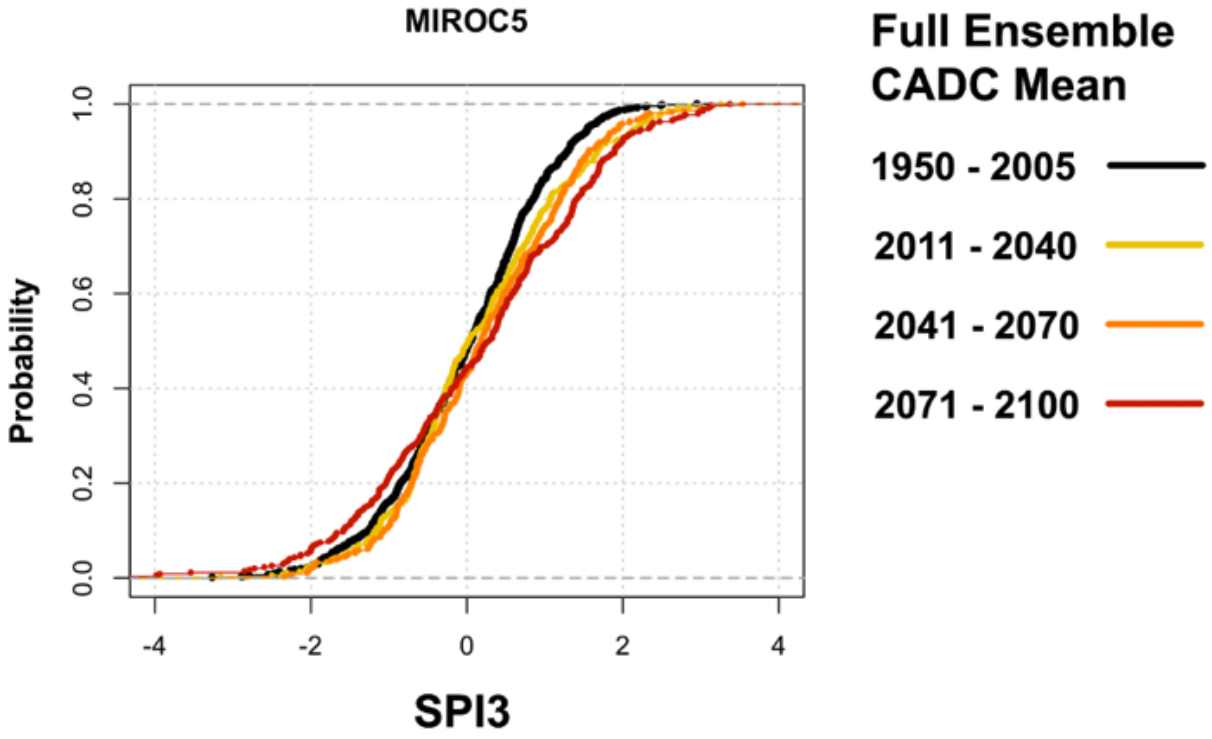

Figure 11. Example of a GCM model (MIROC-5) for which mean precipitation does not dramatically change, but both dry and wet extremes become more common by end-of-century

In terms of magnitudes of change, the projected decrease in ensemble-mean MAP throughout the CADC is -8.1% (-155 mm/yr) and -14.1% (-270 mm/yr) by end-of-century (2071-2100) compared to 1950-2005 under RCP 4.5 and RCP 8.5 emissions scenarios, respectively. Declines in solely rainy season precipitation changes by end-of-century were slightly higher at -8.5% (-165 mm/yr) and -15.5% (-300 mm/yr) (Figure 12). These results are in general agreement with other multi-model climate change assessments conducted in the region focused on projected

changes in annual average rainfall (Giorgi and Diffenbaugh, 2008; Karmalkar et al., 2011; Hidalgo et al., 2013). Reductions are fairly uniform across the study region, though with higher reductions projected in inland regions compared to coastal zones (Supplemental Figure 9).

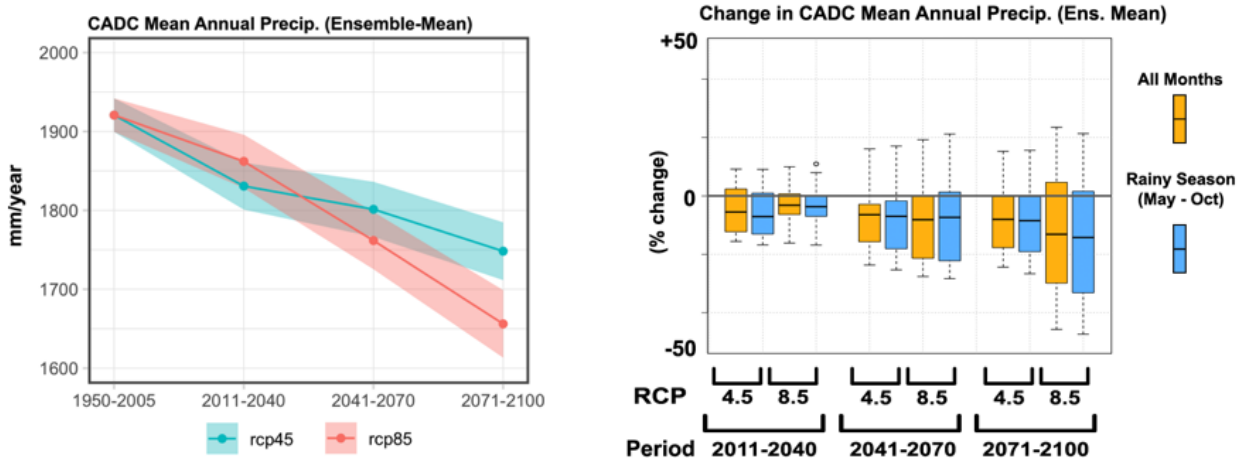

Figure 12. (left) Predicted changes in mean annual precipitation for the entire calendar year under RCP 4.5 and RCP 8.5. Point values represent the ensemble-mean and shading represents 95% confidence intervals derived from the 20-member population standard deviations. (right) Average percent changes to mean annual and rainy season precipitation. Box-and-whiskers plots represent the mean of all individual GCM ensemble members, with whisker ends at the 5th and 95th percentile ensemble values.

Changes in mean monthly rainfall are most pronounced during the rainy season, especially during midsummer months (Figure 13). Slight increases in October and November rainfall are observed by 2071-2100 primarily under the high emissions scenario, possibly from extension and intensification of the CLLJ from July to November (Rauscher et al., 2008; Steinhoff et al., 2015; Taylor et al., 2013; Maurer et al., 2017). However, the mean monthly rainfall pattern emerging by 2071-2100 is distributionally more similar to observed values in terms of July currently experiencing the midsummer rainfall minimum followed by a slight increase in August. Therefore, projected changes in the distribution of rainfall for certain individual months may be more difficult to decipher than annual or rainy season totals due to ensemble bias of monthly distributions. Changes in mean annual precipitation at the department-level for the Northern Triangle are displayed in Supplemental Figure 10.

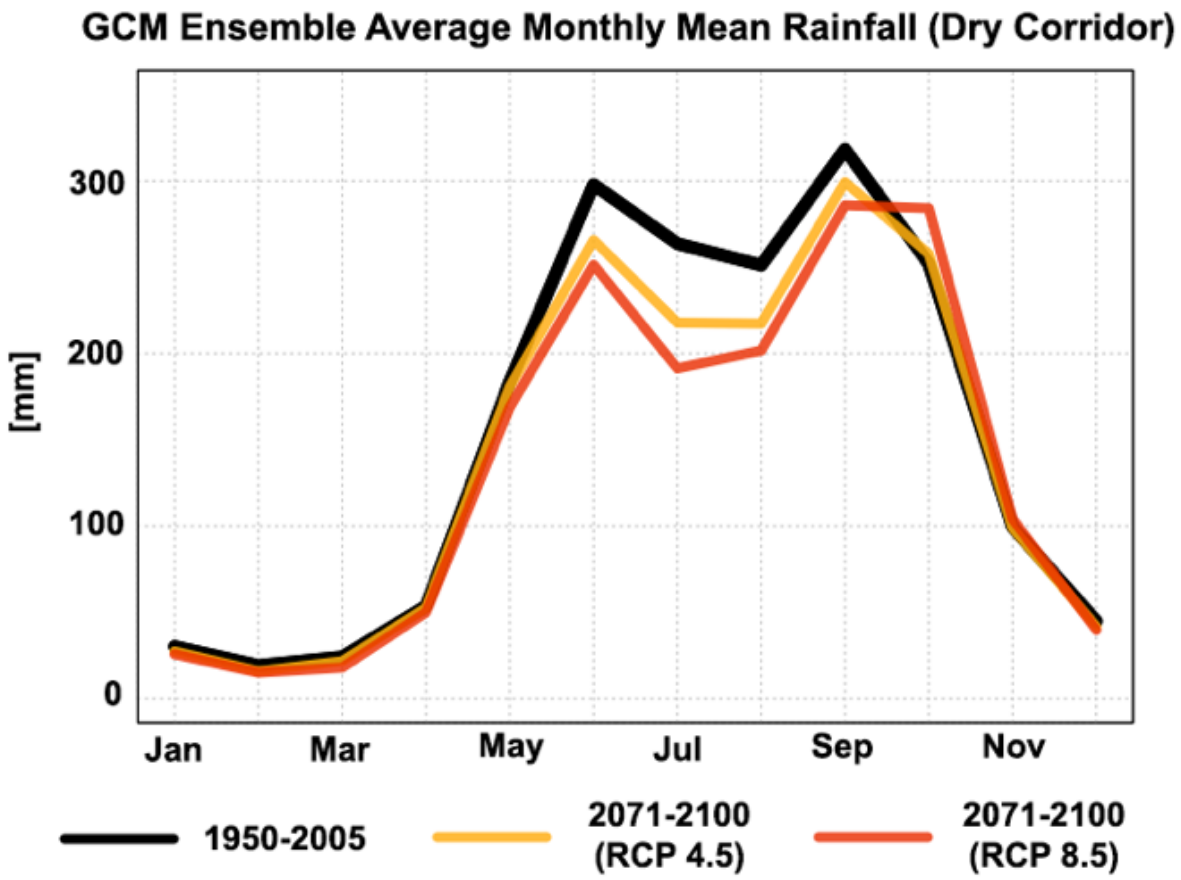

Figure 13. GCM ensemble-mean, monthly rainfall over the historical reference period and end-of-century 30-year period for both moderate and high emissions scenarios.

Changes in annual drought metric averages, however, are more substantial than those predicted for MAP (Figures 14-15). By end-of-century, short-term droughts across all months are projected to lengthen by roughly 12 to 30% (0.7-1.8 months) under moderate to high emissions and by 11 to 23% (0.5-1.1 months) during the rainy season. They are projected to intensify by 17-42% across all months and by 21-51% during the rainy season. Increased frequencies are also projected, with models showing 21-24% (+1.3-1.5 per decade) more events throughout the year and 42-52% more often (+1.7-2.1 per decade) during the rainy season.

Long-term droughts are projected to intensify by 27-73% across all months and by 27-75% during the rainy season by end-of-century. These droughts are shown to lengthen as well, with some models showing a more than tripling (>+300%) in average duration during both the rainy season and entire calendar year (from 2.2 years to >6.6 years per SPI12 drought). Frequencies of SPI12 droughts are shown as decreasing by end-of-century, though this is primarily due to the fact that many GCMs project substantial drying by this time, some projecting much of the 2071-2100 period to be in semi-continuous, SPI12 drought conditions. Therefore, the predicted decrease in frequency of SPI12 droughts corresponds to a dramatic increase in projected duration per drought.

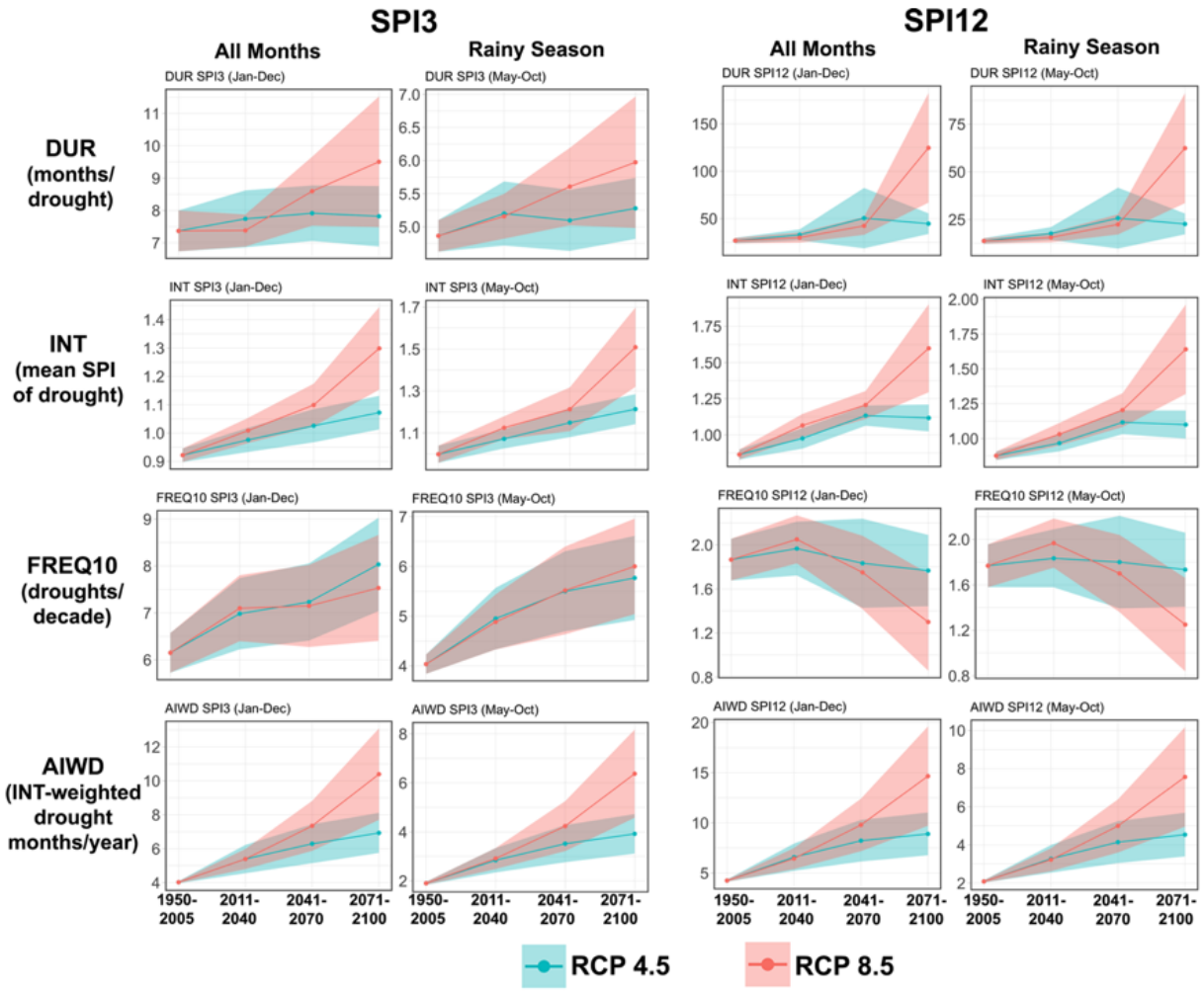

Figure 14. Projected changes in drought metrics throughout the study period. All values are CADC averages, with point values representing ensemble means and shading represents 95% confidence intervals derived from the 20-member population standard deviations and are tabulated in Supplemental Table 2.

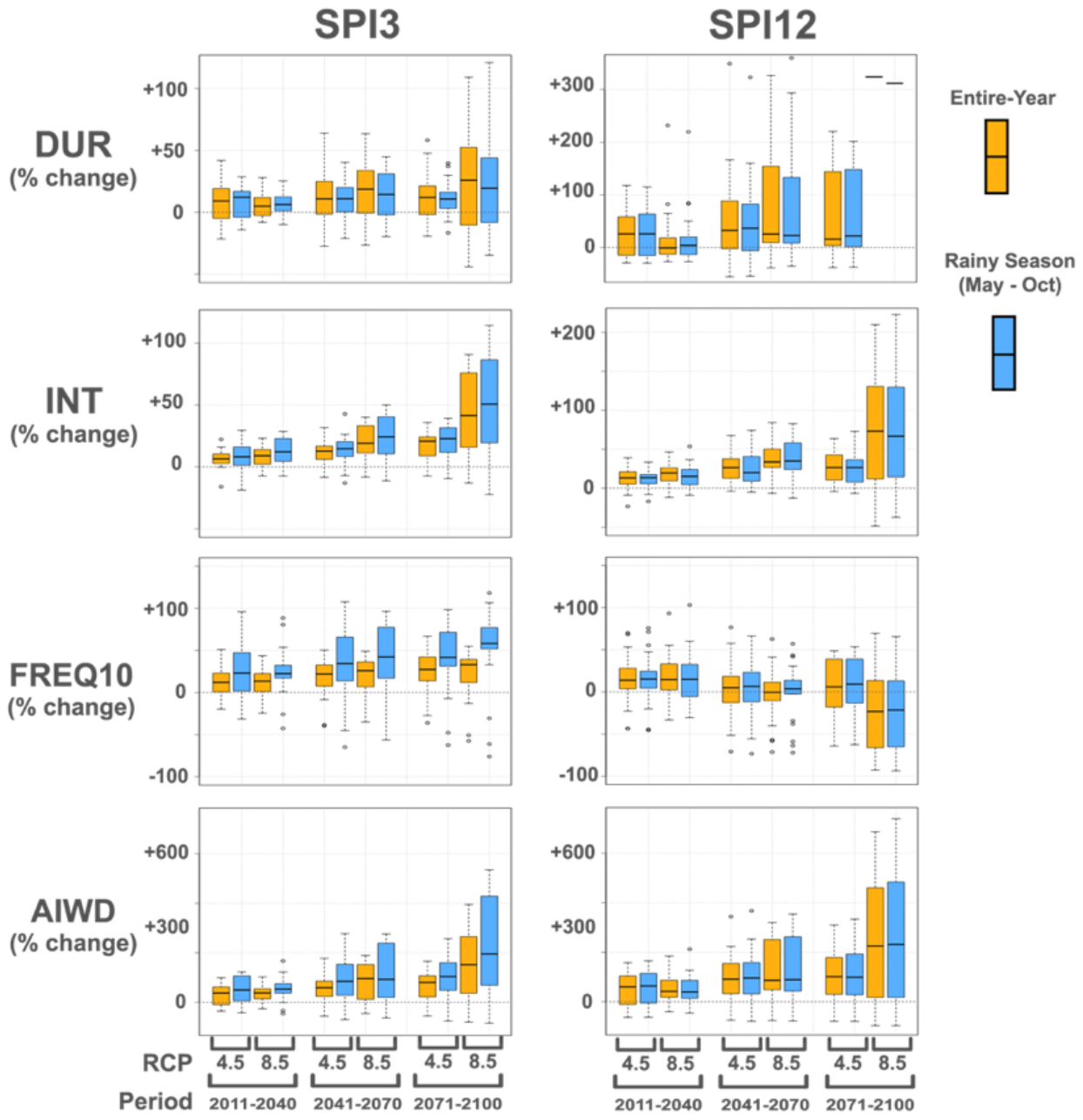

Figure 15. Percent changes in average CADC drought metrics in future periods compared to 1950-2005 for GCM ensemble members. NOTE: Only the ensemble-mean values for percent change in SPI12-drought durations are shown for 2071-2100, to exclude large outliers due to extremely high model variation from small sample sizes of SPI12 droughts in this period.

It should be noted that SPI12 drought metrics are generally more variable between different ensemble-members compared to SPI3 metrics due to the relatively small sample size of long-term droughts compared to short-term ones – the GCM ensemble averaged just 3.9 SPI12 droughts during 2071-2100 under high emissions compared to 22.6 for SPI3 (Figure 16). Therefore, end-of-century results for longer drought events are more difficult to interpret than results for earlier future periods or for short-term droughts.

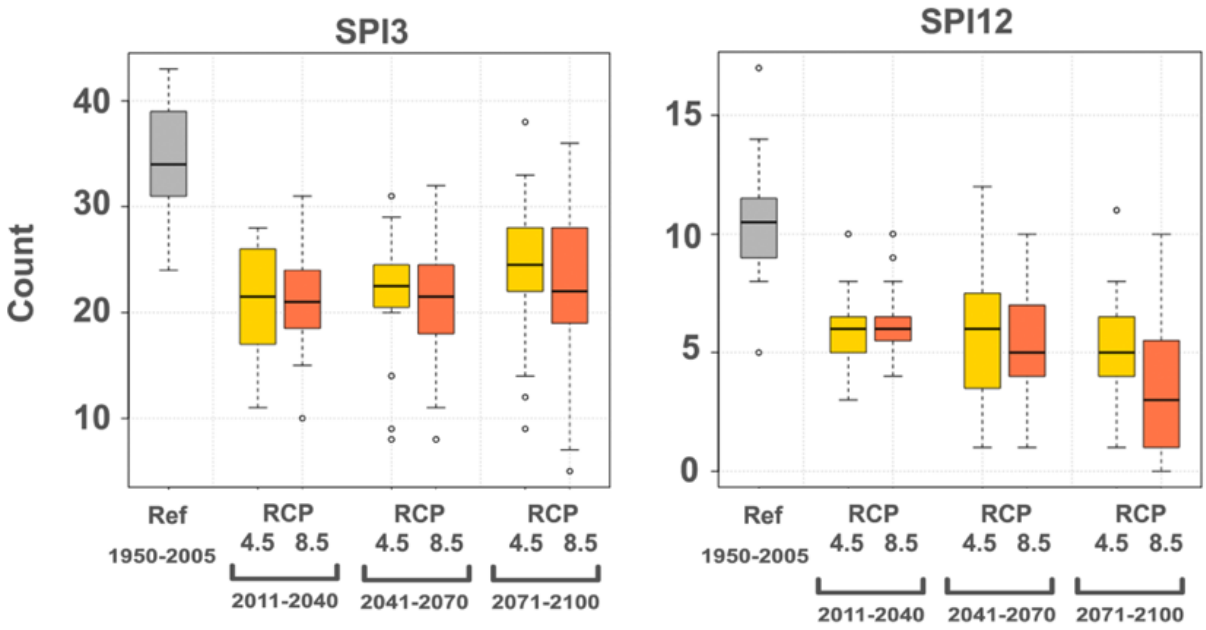

Figure 16. Number of SPI3 and SPI12 drought events present in each period of comparison across the GCM ensemble.

The AIWD metric, which incorporates DUR, INT and FREQ10, offers more comprehensive insight into overall drought conditions, and we can see from this metric that droughts are predicted to worsen over time, particularly in rainy season months, and more so under high emissions relative to moderate. End-of-century changes to AIWD are on the order of 69-150% for short-term droughts across all months and (100-230% during the rainy season), and 110-240% for long-term events over all months (120-250% during the rainy season).

For all metrics, near-term (2011-2040) changes are comparable between both emissions scenarios. Gridded, end-of-century changes for the entire study region reveal fairly homogeneous spatial trends in drought metrics across the CADC (Figure 17).

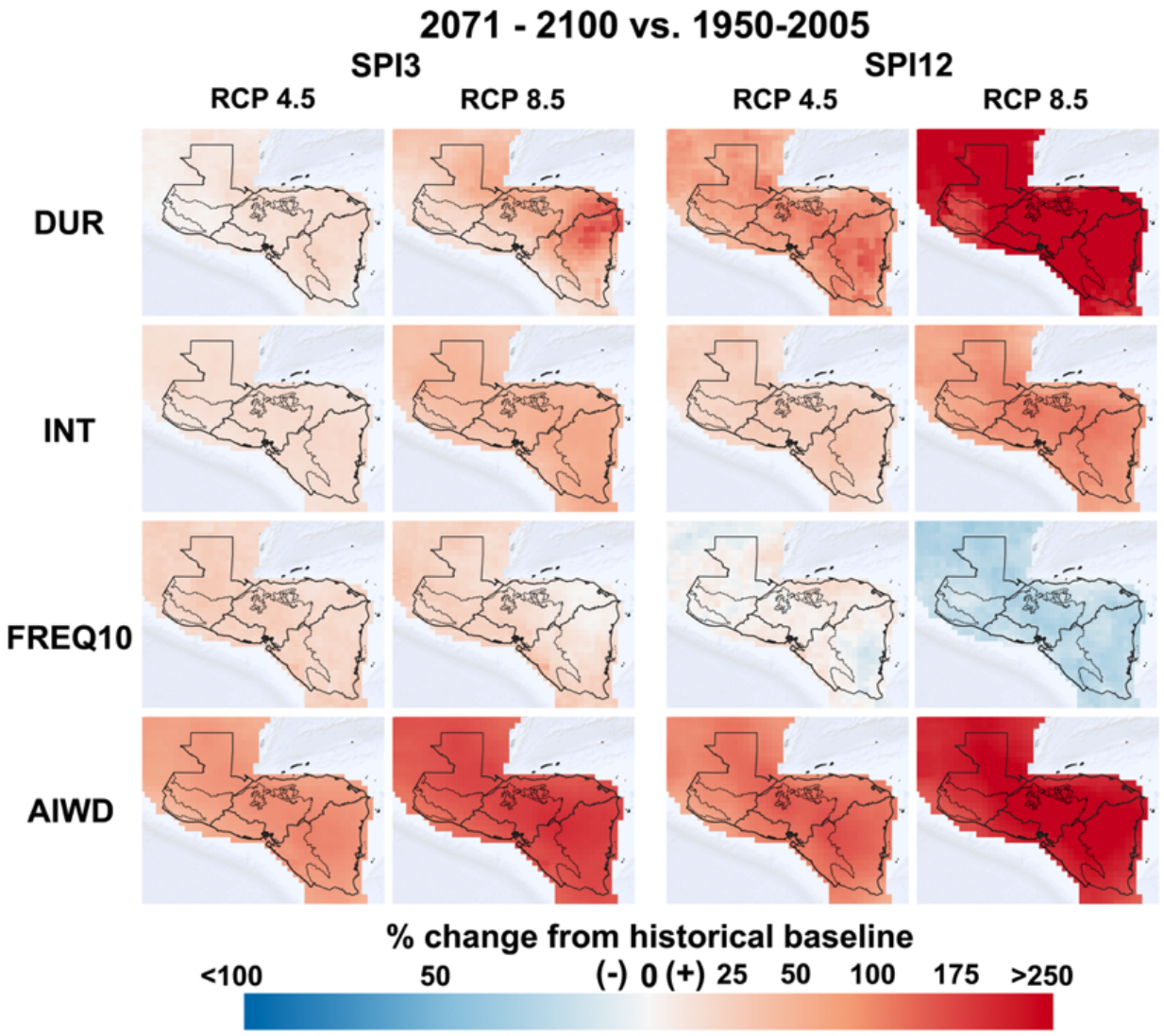

Figure 17. Projected changes in 2071-2100 drought metrics compared to baseline (all months).

Changes in the cumulative distribution functions (CDFs) of SPI3 and SPI12 values over time under each emissions scenario show the extent to which low SPI-values are projected to increase in frequency (Figure 18). Department-level changes for SPI-3 drought metrics are shown in Supplemental Figures 11-13.

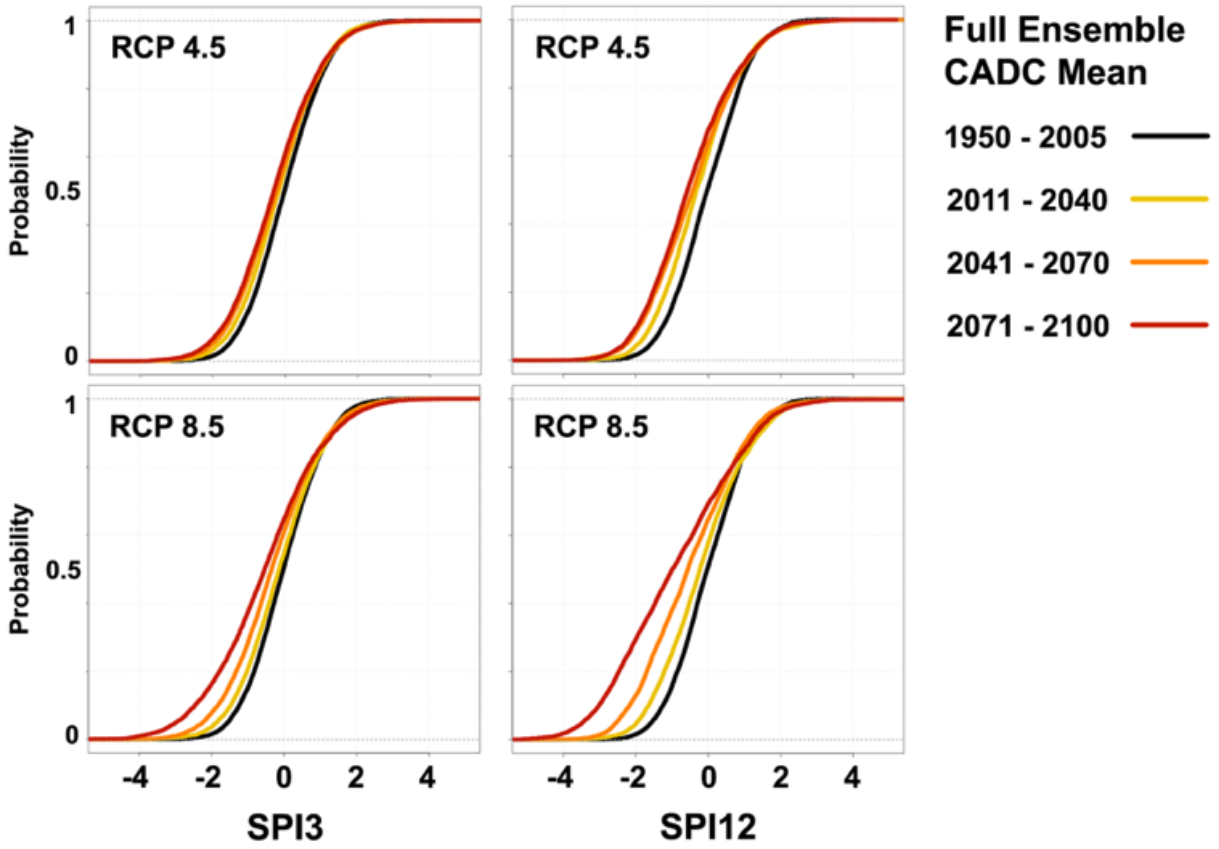

Figure 18. Changes to the cumulative probability distribution functions (CDF) of SPI3 and SPI12 values for the entire GCM ensemble under moderate and high emissions.

From a physical mechanism perspective, the projected increase in duration, intensity, and frequency of droughts are potentially due to the intensification of the CLLJ in the future (Rauscher et al., 2008; Maurer et al., 2017) and also potentially to a shifting ENSO regime (Steinhoff et al., 2015; Taylor et al., 2013). Aside from the annual cycle, ENSO is the main forcing mechanism of climate variability in Central America (Karmalkar et al., 2011). Though the future frequency and intensity of El Niño events overall remains uncertain in climate models (AchutaRao and Sperber, 2006; Wang et al., 2019; Lim et al., 2019), there is broad model agreement regarding the mean-state trend of warming sea-surface temperatures (SSTs) over the eastern Pacific (Rojo Hernández et al., 2020). This increase in SSTs corresponds to robust model predictions of increasingly frequent *extreme* El Niño events under future periods, though overall trends remain less clear (Cai et al., 2014). It is possible that this increase in the sea-surface temperature anomaly (SSTA) amplitude in the equatorial Pacific condition could contribute to a drier mean-state under conditions of higher radiative forcing in the future (Cai et al., 2014). However, the additional influence of amplitude, frequency, and location of the maximum SST anomalies needs to be better understood as well as the non-linearity of the ENSO system and the consistency of its teleconnections with rainfall in Central America (Steinhoff et al., 2015; Lim et al., 2019).

Conclusions

Central America's CADC has been prone to droughts of varying length and severity in the past, which have impacted the livelihoods and food security of the region's large, subsistence farming population. According to this analysis, both short and long-term droughts are projected to worsen substantially across the region under both moderate and high emissions scenarios by end-of-century. Despite somewhat modest projected reductions in mean annual rainfall by 2071-2100 compared to historical (1950-2005) conditions, relative changes in drought characteristics (duration, intensity, frequency, intensity-weighted drought months per year) are projected to be more pronounced.

Throughout the rainy season, during which farmers are most dependent upon stable rainfall patterns, short-term droughts are slated to lengthen, intensify and become more frequent, with the majority of these changes proportionately higher than predicted changes to mean annual precipitation. Long-term droughts, which can have severe regional impacts, are also projected to worsen by 2100. Across all months, they are projected to potentially more-than-triple in length, making for longer but fewer individual events, and to intensify. This entails that though annual, total rainfall may decline modestly by the end of the century, droughts (and their impacts) will likely be disproportionately more severe.

Insufficient water supply, particularly those projected during the midsummer months, could have severe impacts on crops like maize and beans in the CADC, whose first planting season or *Primera* determines the agricultural calendar for the season. Both staple crops and cash crops, like coffee, are affected by diminished rainfall and worsening drought patterns, which could result in not only a shortage of staples for subsistence farmers but also reduced incomes and potential food insecurity for cash crop farm workers (Tucker et al., 2010).

Better understanding of projected, worsening drought conditions information can assist policy-making throughout the CADC. Adaptation-oriented policies could proactively increase resilience of agricultural systems throughout the coming decades. Such programs could help farmers gradually shift from one crop to another, or to more drought-resistant varieties. However, expected near-term worsening of droughts could have more immediate impacts on an already vulnerable agricultural community and may require more urgent resiliency planning efforts.

Further research should be done to better understand the specific atmospheric dynamics underlying each of these projected changes in rainfall and drought metrics in this ensemble. It is important to note that meteorological drought projections such as those derived from SPI do not account for likely some future climatic changes, such as warming temperatures and subsequent increases in evapotranspiration. Exploring such factors with more comprehensive drought metrics (e.g. SPEI) would also be a good topic of complementary research and would potentially produce even more dire drought projections for rainfed agricultural systems in the CADC, as rising temperatures would serve to reduce soil moisture in conjunction with the worsening rainfall deficits displayed in this study.

Similar analysis should also be done both using large ensemble (LENS) GCM datasets to better understand the role of internal variability. Conducting similar analysis for the CADC using new, CMIP-6 GCM model outputs is also needed, although an assessment by Cook et al. (2020) found

remarkable consistency between CMIP-5 and CMIP-6 drought predictions for various drought 'hotspots' across the globe, including Central America. Analysis of socioeconomic impacts of projected drought trends would also help to further inform important adaptation policymaking in the region and should be pursued as well.

Acknowledgments

The authors would like to thank Dr. Edwin Castellanos for providing initial versions of the observational precipitation dataset. Thank you also to Dr. Lara Kueppers and Zeke Hausfather from the University of California, Berkeley and Drs. Andrew Jones and William Collins from the Lawrence Berkeley National Laboratory for providing helpful feedback and guidance. Thanks as well to Richard Barnes and Nicholas Clarke of UC Berkeley, who provided valuable technical support.

References

Anchukaitis, K., Sperber, K.R. ENSO simulation in coupled ocean-atmosphere models: are the current models better?. Clim Dyn 27, 1–15 (2006). https://doi.org/10.1007/s00382-006-0119-7

Anderson, T.G., Anchukaitis, K.J., Pons, D. and Taylor, M., 2019. Multiscale trends and precipitation extremes in the Central American Midsummer Drought. Environmental Research Letters, 14(12), p.124016.

Blain, G. C., 2011. Standardized precipitation index based on pearson type III distribution. Revista Brasileira de Meteorologia, 26(2), 167–180. https://doi.org/10.1590/s0102-77862011000200001

Cai, W., Borlace, S., Lengaigne, M. et al., Increasing frequency of extreme El Niño events due to greenhouse warming. Nature Clim Change 4, 111–116 (2014). https://doi.org/10.1038/nclimate2100

Campbell, J.D., M.A. Taylor, T.S. Stephenson, R.A. Watson, and F.S. Whyte, 2011: Future climate of the Caribbean from a regional climate model. International Journal of Climatology, 31(12), 1866-1878.

Copernicus Climate Change Service (C3S), 2017. ERA5: Fifth generation of ECMWF atmospheric reanalyses of the global climate. Copernicus Climate Change Service Climate Data Store (CDS), April 14, 2019.

Da Silva Junior, Renato O. et al., Three decades of reference evapotranspiration estimates for a tropical watershed in the eastern Amazon. An. Acad. Bras. Ciênc. [online]. 2017, vol.89, n.3, suppl. [cited 2020-09-18], pp.1985-2002

Edwards, D. C., 1997. Characteristics of 20th Century drought in the United States at multiple time scales. Air Force Institute of Tech. Wright-Pattersion OH (Thesis).

Food and Agriculture Organization of the United Nations (FAO), 2018. FAO and WFP concerned about the impact of drought on the most vulnerable in Central America. FAO (Article).

Food and Agriculture Organization of the United Nations (FAO), 2016. Dry Corridor Central America Situation Report - June 2016. FAO (Article).

Giorgi, F., and Diffenbaugh, N., 2008. Developing regional climate change scenarios for use in assessment of effects on human health and disease. Climate Research, 36(2), 141–151.

Global Water Partnership (GWP) - Central America, 2016. Socio-economic Analysis of the Sectoral Impacts of the 2014 Drought in Central America. Water, Climate and Development Programme (WACDEP). https://www.droughtmanagement.info/literature/GWP_CAM_Drought-2014-Impact_eng.pdf

Guttman, N. B., 1999. Accepting the standardized precipitation index: A calculation algorithm. Journal of the American Water Resources Association, 35(2), 311–322. https://doi.org/10.1111/j.1752-1688.1999.tb03592.x

Hannah, L., Donatti, C. I., Harvey, C. A., Alfaro, E., Rodriguez, D. A., Bouroncle, C., Solano, A. L., 2017. Regional modeling of climate change impacts on smallholder agriculture and ecosystems in Central America. Climatic Change, 141(1), 29–45.

Hidalgo, H. G., Amador, J. A., Alfaro, E. J., and Quesada, B., 2013. Hydrological climate change projections for Central America. Journal of Hydrology, 495, 94–112. https://doi.org/10.1016/j.jhydrol.2013.05.004

Hidalgo, H.G., Alfaro, E.J. and Quesada-Montano, B., 2017. Observed (1970–1999) climate variability in Central America using a high-resolution meteorological dataset with implication to climate change studies. Climatic Change, 141(1), pp.13-28.

Hidalgo, H.G., Alfaro, E.J., Amador, J.A. and Bastidas, Á., 2019. Precursors of quasi-decadal dry-spells in the Central America Dry Corridor. Climate Dynamics, 53(3-4), pp.1307-1322.

Inoue, M., Handoh, I., and Bigg, G., 2002. Bimodal Distribution of Tropical Cyclogenesis in the Caribbean : Characteristics and Environmental Factors, (Dunn 1940), 2897–2905.

Inter-American Development Bank (IDB), 2017. Food Security and Emigration - Why People Flee and the impact on family members left behind in El Salvador, Guatemala and Honduras. IDB (Report).

Kallis, G., 2008. Droughts. Annual Review of Environment and Resources, 33(1), 85–118. https://doi.org/10.1146/annurev.environ.33.081307.123117

Karmalkar, A. V., Bradley, R. S., and Diaz, H. F., 2011. Climate change in Central America and Mexico: Regional climate model validation and climate change projections. Climate Dynamics, 37(3), 605–629. https://doi.org/10.1007/s00382-011-1099-9

Kendall MG, 1975. Rank correlation methods, 4th edn. Charles Grif- fin, London

Kitoh, A., H. Endo, K. Krishna Kumar, I.F.A. Cavalcanti, P. Goswami, and T. Zhou, 2013: Monsoons in a changing world: a regional perspective in a global context. Journal of Geophysical Research: Atmospheres, 118(8), 3053-3065

Lim, E., Hendon, H.H., Hope, P. et al., Continuation of tropical Pacific Ocean temperature trend may weaken extreme El Niño and its linkage to the Southern Annular Mode. Sci Rep 9, 17044 (2019). https://doi.org/10.1038/s41598-019-53371-3

Lobell, D.B., Burke, M.B., Tebaldi, C., Mastrandrea, M.D., Falcon, W.P. and Naylor, R.L., 2008. Prioritizing climate change adaptation needs for food security in 2030. Science, 319(5863), pp.607-610.

Mann HB, 1945. Non-parametric tests against trend. Econometrica 13:163–171

Marroquín, Alfaro G., and Gómez, R., 2019. Antecedentes y contexto del cambio climático en Guatemala. En E. J. Castellanos, A. Paiz-Estévez, J. Escribá, M. Rosales-Alconero, and A. Santizo (Eds.), Primer reporte de evaluación del conocimiento sobre cambio climático en Guatemala. Guatemala: Universidad Del Valle de Guatemala.

Martin, E. R., and C. Schumacher, 2011: The Caribbean Low-Level Jet and Its Relationship with Precipitation in IPCC AR4 Models. J. Climate, 24, 5935–5950, https://doi.org/10.1175/JCLI-D-11-00134.1.

Maurer, E. P. and Hidalgo, H. G., 2008: Utility of daily vs. monthly large-scale climate data: an intercomparison of two statistical downscaling methods, Hydrology and Earth System Sciences, 12, 551-563.

McKee, T.B., Doesken, N.J. and Kleist, J., 1993. Analysis of Standardized Precipitation Index (SPI) data for drought assessment. Water (Switzerland)., 26, pp.1-72.

Meinshausen, M. S.J. Smith, K. Calvin, J.S. Daniel, M.L.T. Kainuma, and et al., 2011: The RCP greenhouse gas concentrations and their extensions from 1765 to 2300. Climatic Change, 109, 213-241.

Mishra, A. K., and Singh, V. P., 2010. A review of drought concepts. Journal of Hydrology, 391(1–2), 202–216. https://doi.org/10.1016/j.jhydrol.2010.07.012

Moss, R. H., Edmonds, J. A., Hibbard, K. A., Manning, M. R., Rose, S. K., Van Vuuren, D. P., … Wilbanks, T. J., 2010. The next generation of scenarios for climate change research and assessment. Nature, 463(7282), 747–756. https://doi.org/10.1038/nature08823

Nakaegawa, T., A. Kitoh, H. Murakami, and S. Kusunoki, 2013b: Annual maximum 5- day rainfall total and maximum number of consecutive dry days over Central America and the Caribbean in the late twenty-first century projected by an atmospheric general circulation model with three different horizontal resolutions. Theoretical Applied Climatology (in press), doi:10.1007/s00704-013-0934-9.

Naresh Kumar, M., Murthy, C.S., Sesha Sai, M.V.R. and Roy, P.S., 2009. On the use of Standardized Precipitation Index (SPI) for drought intensity assessment. Meteorological Applications: A journal of forecasting, practical applications, training techniques and modelling, 16(3), pp.381-389.

Nawrotzki, R.J., Runfola, D.M., Hunter, L.M. and Riosmena, F., 2016. Domestic and international climate migration from rural Mexico. Human ecology, 44(6), pp.687-699.

Penalba, O. C., and Rivera, J. A., 2013. Future Changes in Drought Characteristics over Southern South America Projected by a CMIP5 Multi-Model Ensemble. American Journal of Climate Change, 02(03), 173–182. https://doi.org/10.4236/ajcc.2013.23017

Pons, D., Castellanos, E., Conde, D., Brincker, J., Incer, D., and López, A. (2018). Escenarios de aridez para Guatemala para los años 2030 , 2050 y 2070 utilizando modelos de cambio climático . Yu'am, 2(4), 4–16.

Quesada-Montano, B., Wetterhall, F., Westerberg, I.K., Hidalgo, H.G. and Halldin, S., 2019. Characterising droughts in Central America with uncertain hydro-meteorological data. Theoretical and Applied Climatology, 137(3-4), pp.2125-2138.

Rauscher, S. A., Giorgi, F., Diffenbaugh, N. S., and Seth, A., 2008. Extension and Intensification of the Meso-American mid-summer drought in the twenty-first century. Climate Dynamics, 31(5), 551–571. https://doi.org/10.1007/s00382-007-0359-1

Rivera, Solis, Daniela Pedraza, and Paula M. Perez Briceño, 2019. Climate Migration in the Dry Corridor of Central America - Integrating a Gender Perspective. Christian Aid (Report).

Rogelj, J., Meinshausen, M., and Knutti, R., 2012. Global warming under old and new scenarios using IPCC climate sensitivity range estimates. Nature Climate Change, 2(4), 248–253. https://doi.org/10.1038/nclimate1385

Rojo Hernández, J. D., Ó. J. Mesa, and U. Lall, 2020: ENSO Dynamics, Trends, and Prediction Using Machine Learning. Wea. Forecasting, 35, 2061–2081, https://doi.org/10.1175/WAF-D-20-0031.1.

Sheffield, J., G. Goteti, and E. F. Wood, 2006: Development of a 50-yr high-resolution global

dataset of meteorological forcings for land surface modeling, J. Climate, 19 (13), 3088-3111.

Svoboda, Hayes, M., and Wood, D., 2012. Standradized Precipitation Index User Guide, 21(6), 1333–1348. https://doi.org/10.1175/2007JCLI1348.1

Steinhoff D, Monaghan A, Clark M, 2015. Projected impact of twenty-first century ENSO changes on rainfall over Central America and northwest South America from CMIP5 AOGCMs. Clim Dyn 44:1329–1349. doi:10.1007/s00382-014-2196-3

Strzepek, K., Yohe, G., Neumann, J. and Boehlert, B., 2010. Characterizing changes in drought risk for the United States from climate change. Environmental Research Letters, 5(4), p.044012.

Taylor, Karl E., Ronald J. Stouffer, Gerald A. Meehl, 2012: An Overview of CMIP5 and the

Experiment Design. Bull. Amer. Meteor. Soc., 93, 485–498.

Taylor, M.A., Whyte, F.S., Stephenson, T.S. and Campbell, J.D., 2013. Why dry? Investigating the future evolution of the Caribbean low level jet to explain projected Caribbean drying. International Journal of Climatology, 33(3), pp.784-792.

The World Food Program USA (WFP), 2020. The Dry Corridor in Central America. WFP (Article).

The World Food Programme (WFP), 2019. Erratic weather patterns in the Central American Dry Corridor leave 1.4 million people in urgent need of food assistance. WFP (News Release).

Thrasher, B., Maurer, E. P., McKellar, C., and Duffy, P. B., 2012: Technical Note: Bias correcting

climate model simulated daily temperature extremes with quantile mapping. Hydrology and

Earth System Sciences, 16(9), 3309-3314.

Touma, D., Ashfaq, M., Nayak, M. A., Kao, S. C., and Diffenbaugh, N. S., 2015. A multi-model and multi-index evaluation of drought characteristics in the 21st century. Journal of Hydrology, 526, 196–207. https://doi.org/10.1016/j.jhydrol.2014.12.011

Tucker, C.M., Eakin, H. and Castellanos, E.J., 2010. Perceptions of risk and adaptation: coffee producers, market shocks, and extreme weather in Central America and Mexico. Global Environmental Change, 20(1), pp.23-32.

Ukkola, A.M., Pitman, A.J., De Kauwe, M.G., Abramowitz, G., Herger, N., Evans, J.P. and Decker, M., 2018. Evaluating CMIP5 model agreement for multiple drought metrics. Journal of Hydrometeorology, 19(6), pp.969-988.

Vicente-Serrano, S.M., Beguería, S. and López-Moreno, J.I., 2010. A multiscalar drought index sensitive to global warming: the standardized precipitation evapotranspiration index. Journal of climate, 23(7), pp.1696-1718.

Wang, C., and Lee, S. K., 2007. Atlantic warm pool, Caribbean low-level jet, and their potential impact on Atlantic hurricanes. Geophysical Research Letters, 34(2), 1–5. https://doi.org/10.1029/2006GL028579

Wang, Y., Luo, Y., Lu, J. et al., Changes in ENSO amplitude under climate warming and cooling. Clim Dyn 52, 1871–1882 (2019). https://doi.org/10.1007/s00382-018-4224-1

Wood, A.W., E.P. Maurer, A. Kumar, and D.P. Lettenmaier, 2002: Long-range experimental

hydrologic forecasting for the eastern United States. J. Geophysical Research-Atmospheres,

107, 4429, doi:10.1029/2001JD000659.

Wood, A.W., L.R. Leung, V. Sridhar, and D.P. Lettenmaier, 2004: Hydrologic implications of

dynamical and statistical approaches to downscaling climate model outputs. Climatic

Change, 15,189-216.

Van der Zee Arias, A., Meyrat, A., Picado, L., Poveda, C. and Van der Zee, J., 2012. Estudio de caracterización del corredor seco centroamericano Tomo I. FAO (Report).

Van der Zee Arias, A., Meyrat, A., Picado, L., Poveda, C. and Van der Zee, J., 2013. Estudio de caracterización del corredor seco centroamericano Tomo II. FAO (Report).

Vaqué, Jordi, 2017. Chronology of the Dry Corridor: The impetus for resilience in Central America. Information and Communications Management at the FAO Investment Centre, Latin Ameica and the Caribbean Division (Article).

Zarch, M.A.A., Sivakumar, B. and Sharma, A., 2015. Droughts in a warming climate: A global assessment of Standardized precipitation index (SPI) and Reconnaissance drought index (RDI). Journal of Hydrology, 526, pp.183-195.

Supplemental Material

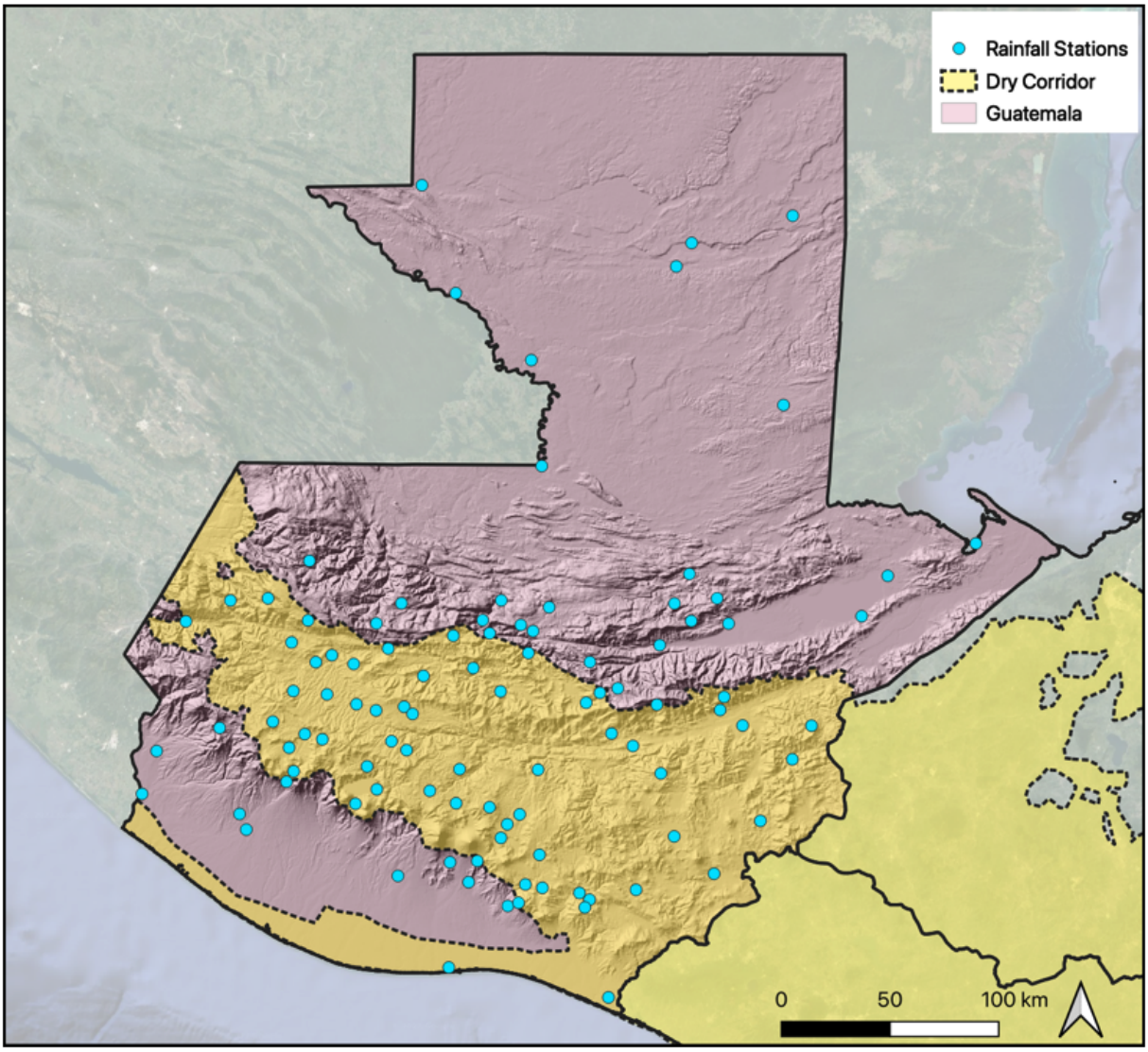

Supplemental Figure 1. Map of INSIVUMEH rainfall gauges with observational records from 1981-2018

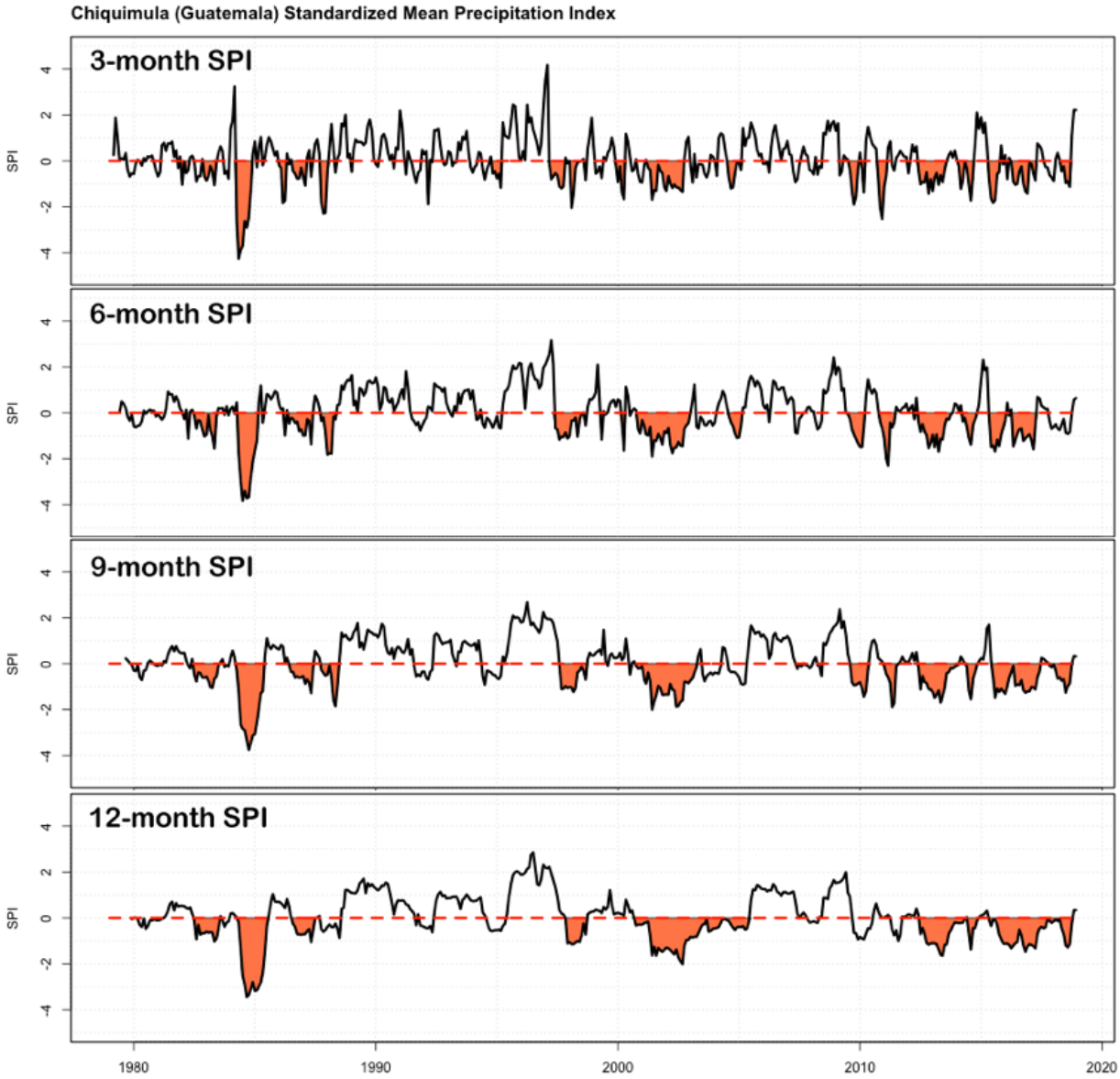

Supplemental Figure 2. Example 3, 6, 9 and 12-month historical SPI time-series for Chiquimula Department, Guatemala from 1979-2018 using the department-average ERA-5 precipitation. Drought events are shaded.

Supplemental Figure 3. Guatemala's Chiquimula department within the CADC is highlighted in yellow. Example SPI3 and SPI12 time-series are shown for this department area in the Methods section.

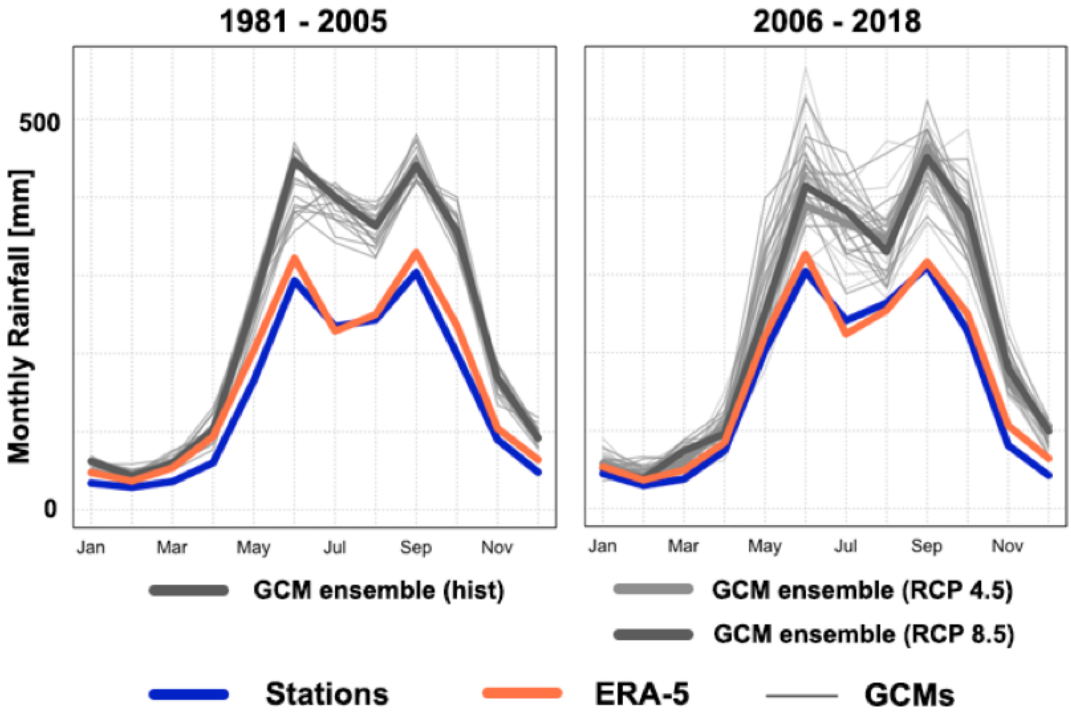

Supplemental Figure 4. Comparison of mean monthly rainfall at the station locations for the period of historical overlap with the historical reference GCM ensemble runs (left) and the first 13 years of their RCP 4.5 and 8.5 runs (right).

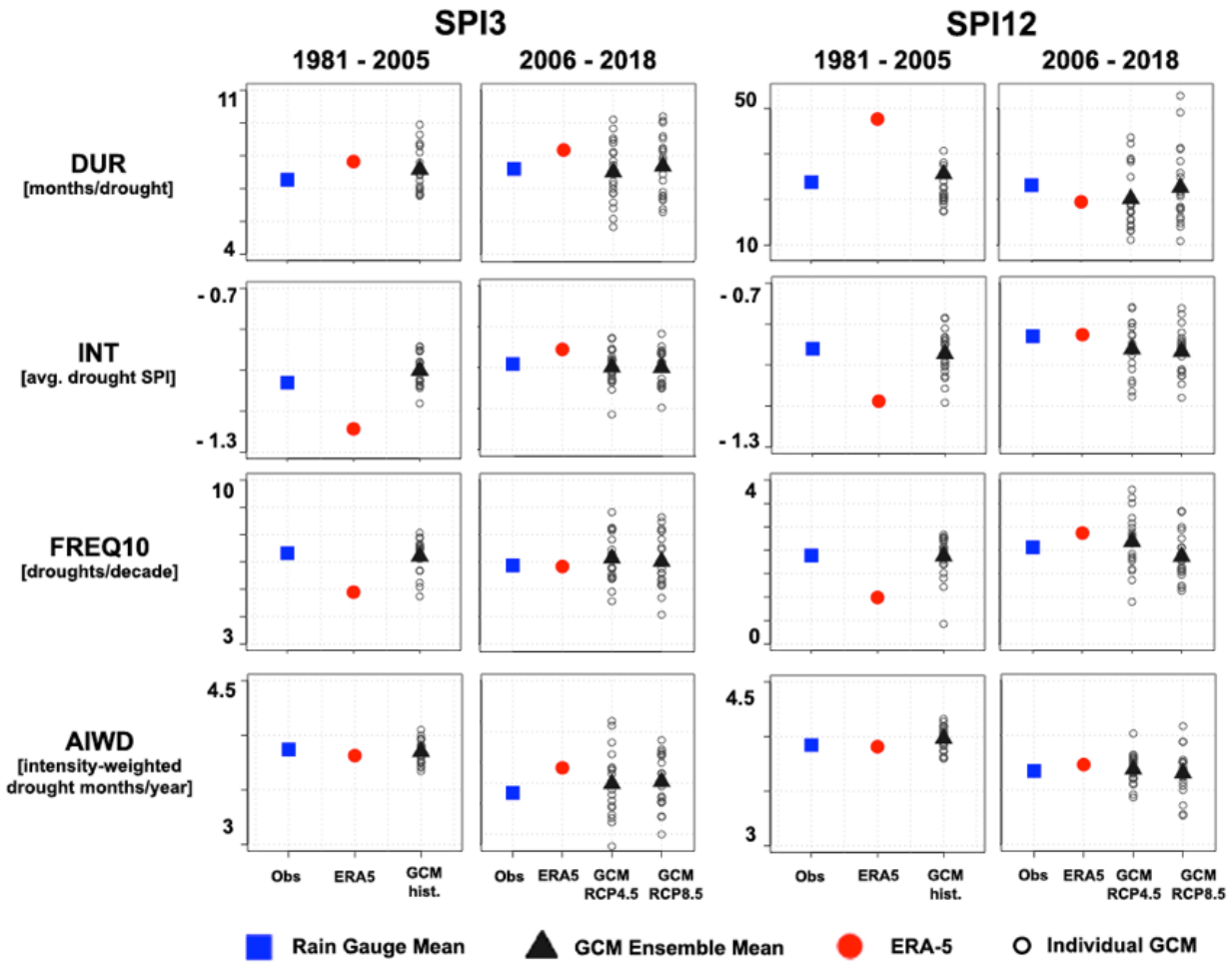

Supplemental Figure 5. Comparison of average rainy season drought metrics from May-Oct observed across the gauging station network and at the ERA-5 and GCM ensemble datasets at these station locations. Results provided for both SPI-scales (3, 12-month) and for each sub-period of the historical analysis. DUR = mean drought duration in months, INT = mean drought intensity in SPI values, FREQ10 = mean number of droughts per decade, AIWD = mean number of intensity-weighted drought months each year.

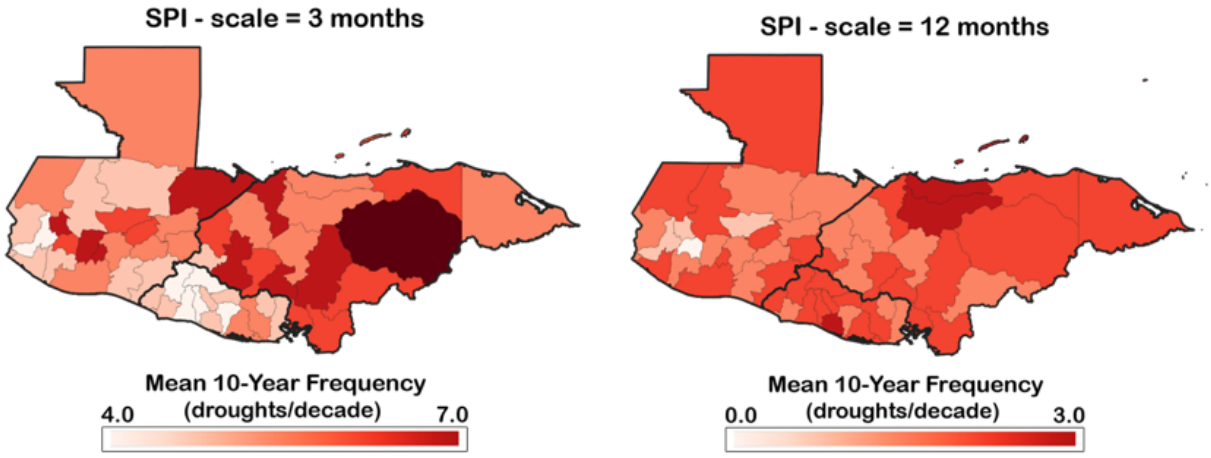

Supplemental Figure 6. Historical (ERA-5, 1979 – 2018) mean 10-year drought frequency by SPI-scale and department

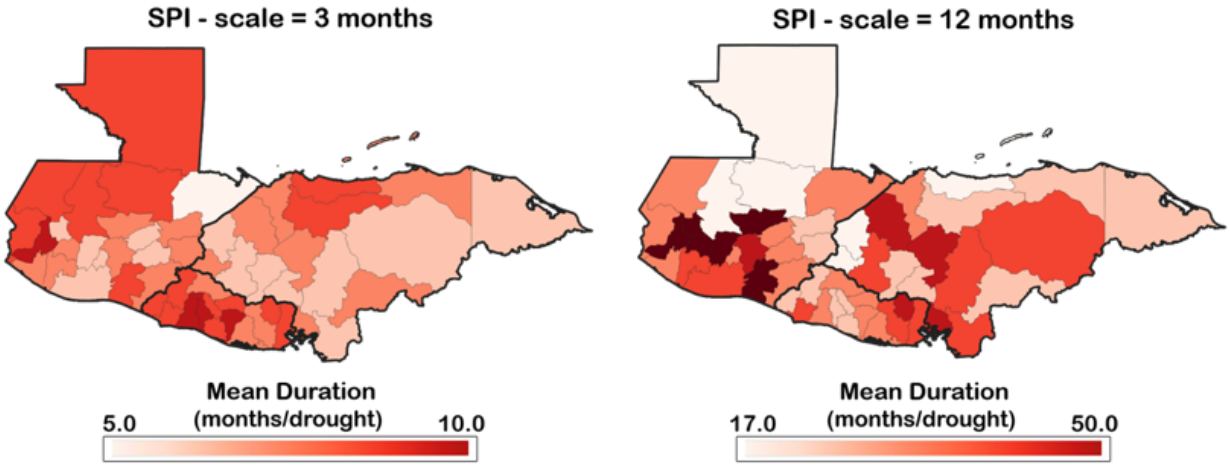

Supplemental Figure 7. Historical (ERA-5, 1979 – 2018) mean drought duration by SPI-scale and department

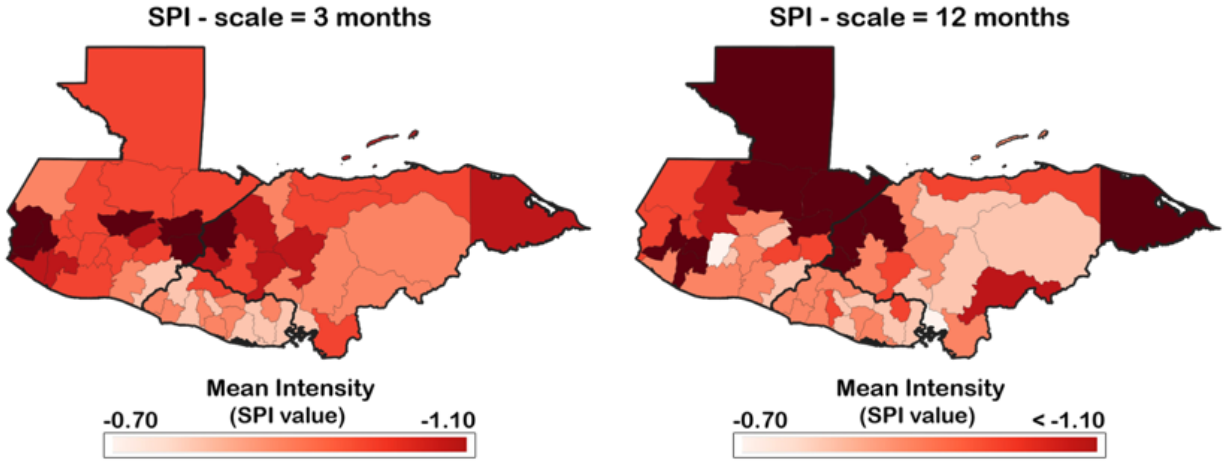

Supplemental Figure 8. Historical (ERA-5, 1979 – 2018) mean drought intensity by SPI-scale and department

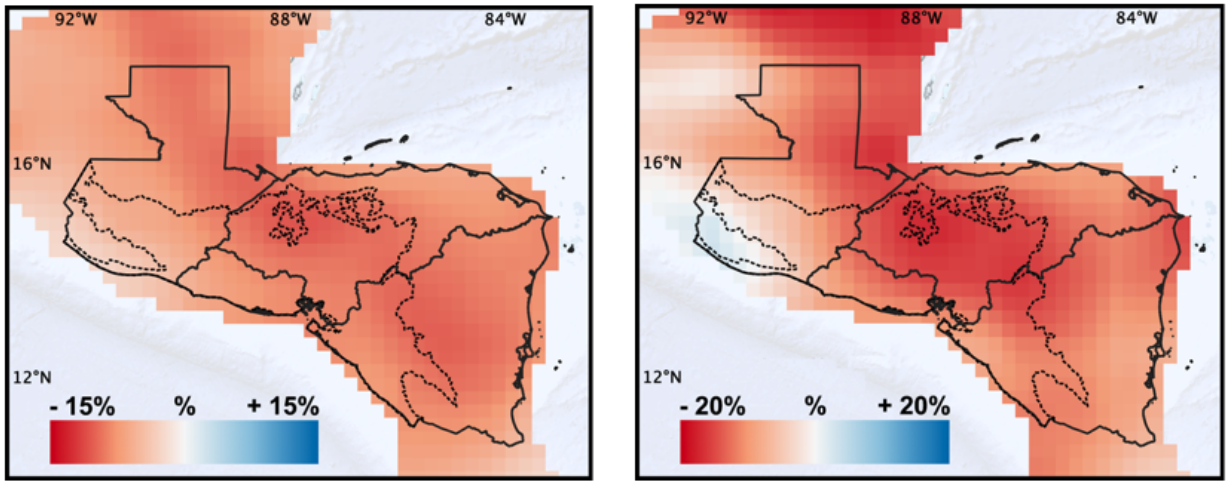

Supplemental Figure 9. Percent change in mean annual rainfall between 2071-2100 and 1950-2005 across the study region under RCP 4.5 (left) and RCP 8.5 (right) scenarios.

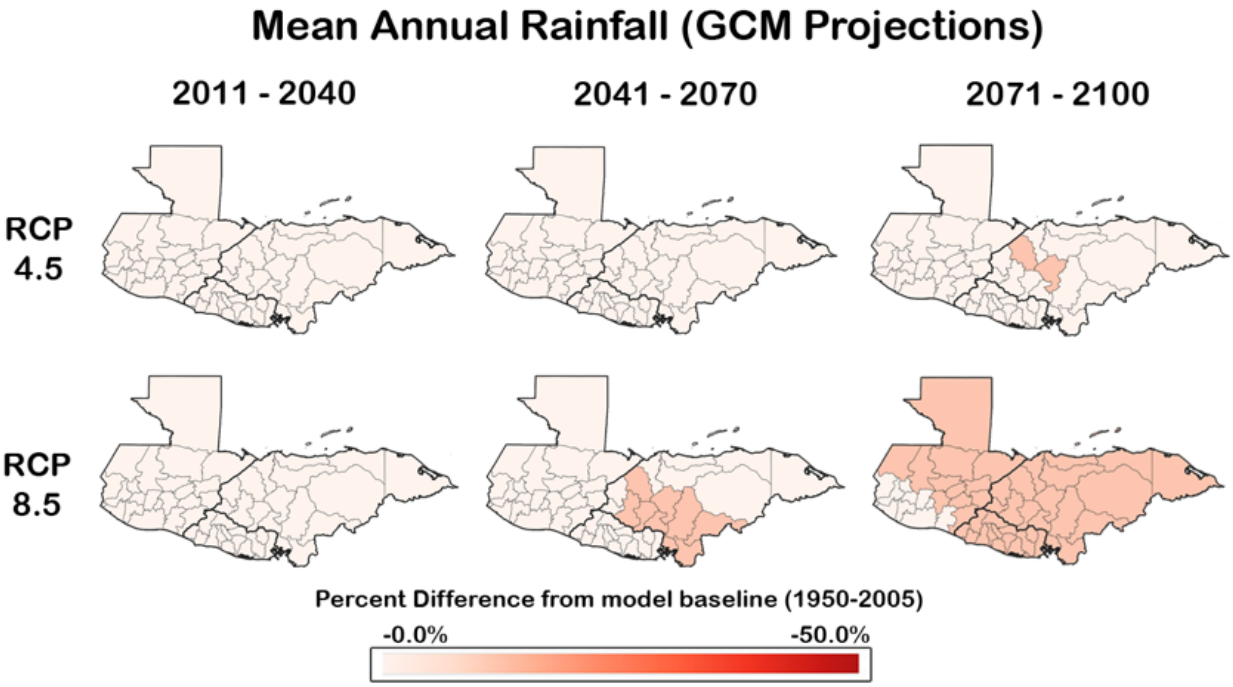

Supplemental Figure 10. GCM ensemble-average department-level changes in mean annual rainfall

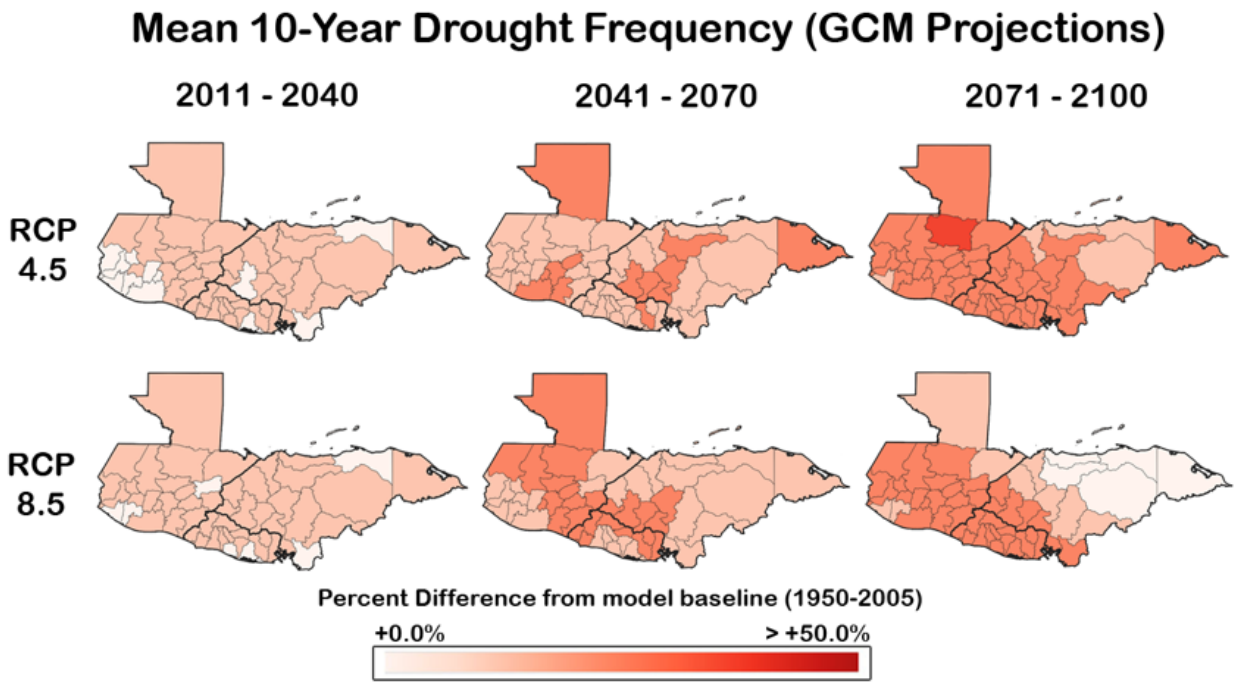

Supplemental Figure 11. GCM ensemble-average department-level changes in SPI-3 decadal drought frequency

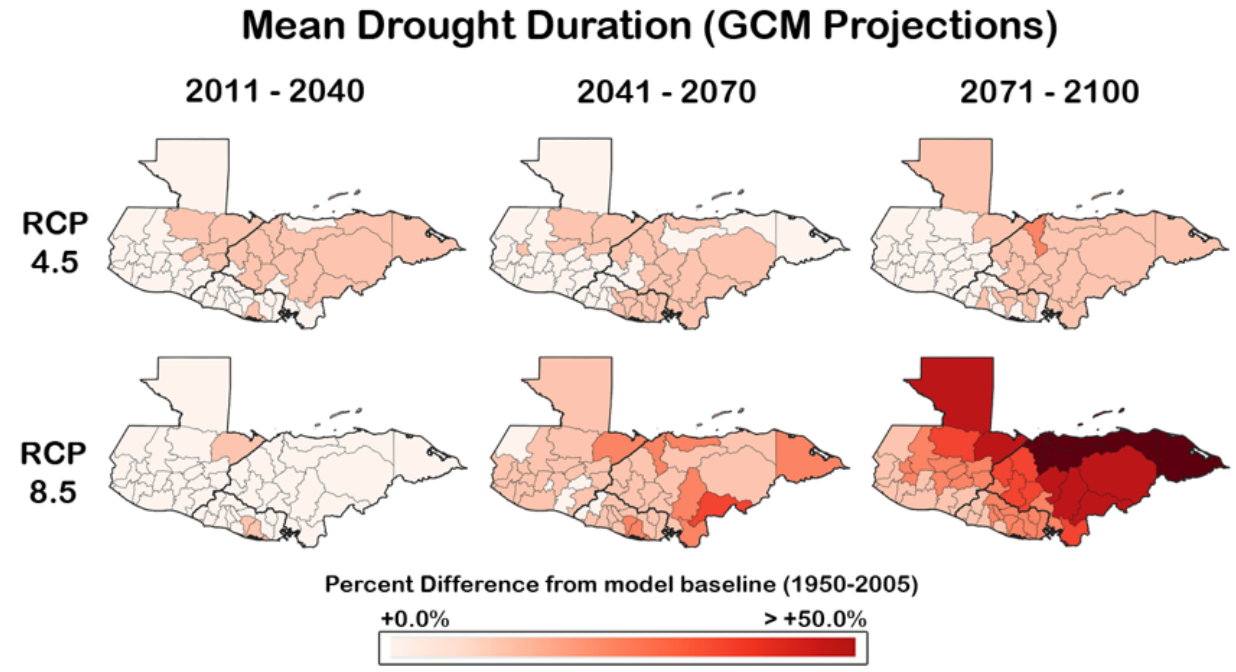

Supplemental Figure 12. GCM ensemble-average department-level changes in SPI-3 drought duration

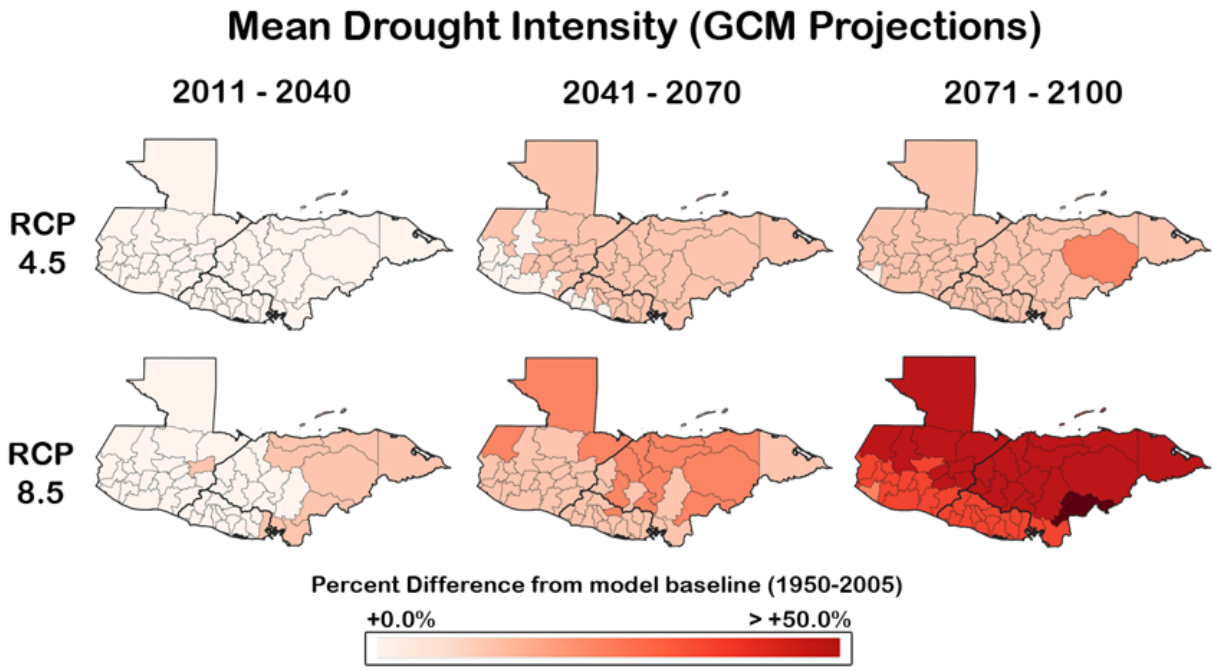

Supplemental Figure 13. GCM ensemble-average department-level changes in SPI-3 drought intensity

Supplemental Table 1. Percentage of Guatemalan rainfall stations and ERA-5 and GCM grid cells covering the entire study area that pass the Kolmogorov-Smirnov Test with 95% confidence (p = 0.05). The test was based on fits of monthly precipitation values to a 2-parameter Gamma Distribution and were performed at each station/cell for data from each calendar month at each rainfall station (n = 101) and each of the 1,796 grid cells in the gridded datasets for each calendar month. The GCM data test results from 1981-2018 represent averages from the historical and RCP 4.5 and historical and RCP 8.5 scenarios. GCM results from 1950-2005 are from the historical reference model runs. There is a nearly 100% KS-test pass rate for all datasets.

Period	SPI-scale	Months	Stations (n=101)	ERA-5	GCMs
1981 - 2018	3-month	All	99.50%	98.85%	99.18%
		May-Oct	100.00%	99.97%	99.99%
	12-month	All	100.00%	100.00%	100.00%
		May-Oct	100.00%	99.99%	100.00%
1950 - 2005	3-month	All	--	--	99.63%
		May-Oct	--	--	99.89%
	12-month	All	--	--	99.92%
		May-Oct	--	--	99.92%

Supplemental Table 2. Percent change values for the GCM ensemble-mean rainfall and drought metric projections relative to the 1950-2005 historical reference period.

GCM Ensemble-Mean Percentage (%) Changes from Average Historical (1950-2005) Values

			2011-2041		*2041-2070*		*2071-2100*	
Metric	**SPI Scale**	**Calendar Period**	**RCP 4.5**	**RCP 8.5**	**RCP 4.5**	**RCP 8.5**	**RCP 4.5**	**RCP 8.5**
Mean Annual Precipitation	N/A	Entire Year	-4.9	-3.2	-6.5	-8.7	-8.1	-14.1
		May-October	-5.1	-3.5	-7.0	-9.4	-8.5	-15.5
DROUGHT METRICS								
Mean Duration	SPI3	Entire Year	9.2	6.3	10.9	17.2	12.1	29.9
		May-October	8.9	6.3	9.7	14.4	10.7	22.5
	SPI12	Entire Year	25.8	18.3	52.8	83.9	68.0	324.0
		May-October	25.9	20.1	51.8	81.5	64.9	311.7
Mean Intensity	SPI3	Entire Year	6.5	8.8	12.1	19.1	16.6	41.5
		May-October	8.2	12.2	14.5	23.1	20.9	50.7
	SPI12	Entire Year	12.6	17.4	26.5	34.6	26.6	73.2
		May-October	11.6	15.2	25.3	35.1	26.6	75.3
10-year Mean Frequency	SPI3	Entire Year	12.0	13.1	17.7	18.9	23.7	21.2
		May-October	23.0	24.6	35.3	39.5	41.6	51.7
	SPI12	Entire Year	13.9	18.6	5.0	-2.6	6.0	-23.2
		May-October	15.1	17.9	6.6	-0.6	9.2	-22.2
Mean Annual Intensity-Weighted Drought Duration	SPI3	Entire Year	34.4	33.8	56.7	81.1	68.9	152.1
		May-October	50.3	54.0	84.8	121.5	103.9	229.7
	SPI12	Entire Year	54.0	50.2	91.5	127.0	108.3	237.9
		May-October	56.7	51.7	96.1	135.2	115.8	253.6

1.2 - Analysis of International and Internal Migration in Guatemala - Predicting Observed Movement Using Sociodemographic, Physical and Climatic Metrics

This section represents ongoing work that links the drought modeling and projections presented above (Ch. 1.1) to migration from and within Guatemala. The bulk of this work was presented at a symposium on migration and climate change hosted at La Universidad del Valle de Guatemala (UVG) in collaboration with Denver University and Columbia University in Guatemala City, Guatemala on January 23, 2023: "Simposio - Migración en América Central: Diálogo de Conocimientos Con la Participación de Expertos Locales e Internacionales Junto a las voces de la Comunidad Migrante." (symposium details provided as Supplemental Figure 1).

Background

Central American migration, especially the emigration north of people seeking opportunity in the United States, is a topic that receives much media, political and international attention. It is estimated that between the 2018 and 2021 fiscal years, roughly 377,000 migrants per year left Guatemala, El Salvador and Honduras, the vast majority headed to the United States, on average, with fiscal years 2019 and 2021 witnessing some 651,000 and 521,000 out-migrants, respectively. These migrants often are fleeing violence, political instability, lack of economic opportunity or natural disasters (Meyer, 2022), although the journey that many of them make northward is itself also extremely dangerous, with some 7,000 in-transit migrant deaths recorded in the Americas alone since 2014, though that figure is likely a gross underestimate (United Nations, 2022). How to manage these mass migrant flows has taken center stage in public debate and is one of the most divisive topics in the political landscape of the United States.

However, despite the inordinate amount of public attention, media and political energy spent on spotlighting, debating and speculating as to the main push and pull factors surrounding this issue, there is surprisingly little robust, academic investigation that quantitatively links observed migration flows to these potential factors in a definitive manner. Furthermore, as extreme climatic events are becoming more severe and potentially more commonplace, including in Central America, journalistic and political discussions have increasingly pointed to climatic shocks and stressors as being a significant driver in the migrant trends from the region in recent years (Lustgarten, 2020; Steffens, 2018). Specifically, the large 'migrant caravans' observed in 2017-2018 from Central America coincided with a severe, multi-year drought across the region from 2016-2019, compelling many to causally attribute that extreme climate event to the subsequent U.S.-bound migrant flows (Milman et al., 2018; Gustin and Henninger, 2019). Indeed, the U.S. White House even issued executive orders and accompanying reports that highlight climate change as a 'root cause' of migration from Central America and underscored the need for a multi-pronged approach to tackle the issue, primarily consisting of international aid funding in the hopes of bolstering economic conditions of these sending countries (U.S. National Security Council, 2021).

To support this speculative climate-migration attribution in the press and political fora, there have been a number of research studies that have explored the links between past climate stress,

projected future climate change and migration in the Americas, though they have been sparse and oftentimes not based on empirical observations. Oftentimes they instead are founded on coarse assumptions about theorized socioeconomic outcomes and behavior under scenarios of future climatic change (Rigaud et al., 2018). Given the importance of the debate around this topic and its international policy implications, more studies are needed that robustly identify the potential causal influence of different social, political, economic and physio-climatic factors on observed migration flows. However, the main barrier to such studies to date has largely been the lack of availability and/or analytical exploration of accurate and comprehensive empirical datasets of human movement within and from Central America at a fine-scale spatial and temporal resolution.

While the study presented here does not represent a casual identification effort, it does identify and delve into a rich empirical dataset on international and internal human movement - the 2018 Guatemalan national census, serving as a helpful quantitative inquiry of a rich and underexplored, yet highly relevant dataset. This work highlights migration data reported in the national census, which provides individual and household level records of international emigration and within-country movement dating as far back as 2002. The dataset and exploration shown here is not without its limitations, but it represents a promising first step into engaging empirical migration datasets explicitly, while much of the discussion and debate on the issue is limited to speculation, assumptions and qualitative inferences.

Though not a causal identification exercise, this work builds models that attempt to explain the observed variance in census-reported international emigration from, and internal migration within Guatemala using a collection of sociodemographic, physical and climatic covariates. I find that the majority (~55%) of the variance in international emigration reported at the household level between 2002 and 2018 can be explained in this manner, with both sociodemographic and drought stress-related variables emerging as significant predictors. Net trends in internal (i.e. inter-municipal) migration proved harder to robustly predict using the same approach, with roughly only a quarter of observed variance explained with these variables, though many of the same predictors emerged as significant as in the international emigration model. Continuing work with these, and similar, data is crucial to informing the ongoing public and policy debates in this space and will likely be central to my ongoing research work moving forward.

Data

The primary dataset used in this study is the 2018 Guatemala national census, which represents the most contemporary census conducted the country (as of Jan 2023) and the first such comprehensive sociodemographic survey since the country's prior census, released in 2002. The 2018 census contains detailed survey results at the individual (IND), household (HH) and residential building (RES) levels (equivalent to households in most cases), which comprise the three primary data tables provided in the digital dataset obtained from the census webpage, accessed in October 2022 and publicly available for download at https://www.censopoblacion.gt/descarga. These tables contain survey responses for a multitude of different demographic and socioeconomic indicators at relatively fine spatial-resolutions,

including a number of migration-related responses that inform patterns of both international and internal movement in recent years. The size and content of survey responses contained in the IND, HH and RES datasets are detailed in **Table 1**. In all three tables, the parent administrative units (*ADM-1 (departamento), n=22; ADM-2 (municipio), n=340*) are provided, as well as a binary flag for an urban/rural distinction.

Table 1. Composition of 2018 Guatemala national census survey data products. Variables used to construct migration-related model outcome variables are in bold.

Table	Surveyed Units (n)	Survey topics	Unique questions (n)
Individuals (IND)	*14,901,286*	age, gender, education, family hierarchy, country of birth and year arrived (if born abroad), ***municipio* of birth** (in Guatemala), ***municipio* of residence in 2013**, ethnicity, language skills, literacy, disabilities, access to technology (*phone, computer, internet*), employment, marital/family status	76
Households (HH)	*3,275,931*	property ownership/tenure, familial hierarchy/dynamics, access to basic utilities, possession of certain amenities *(radio, TV, refrigerator, car etc.),* size/room count, receipt of remittances, **international emigration** *(count, age, gender, departure year)*	30
Residence* (RES)	*3,943,431*	residence type, construction materials, occupation status	5

*HHs are nested within RESs (the vast majority as equal 1:1 units), with 75,275 RESs (~1.9%) containing multiple HHs. However 763,836 (~19%) of RESs are classified as unoccupied and therefore not reflected in the HH or IND surveys, hence the higher total RES *n*, compared to HH.

For the construction of average climate and climatic stress variables, gridded historical climate data was obtained from the hourly ERA5-Land Reanalysis dataset, which is provided at a 0.1° x 0.1° spatial resolution (~10 km at the equator), for the period of 1990-2018 (Muñoz Sabater, 2019). A number of climate variables were constructed from these grids, aggregated from hourly levels to annual averages for certain sub-periods of analysis, according to the migration outcome variable being modeled (Table 2). For exposure to high temperatures, annual degree-day totals above 25° C were calculated, following the methods described in Carleton (2017), in addition to using mean annual temperatures. For exposure to drought stress, standardized precipitation-evapotranspiration indices (SPEI) at a 12-month scale (Vicente-Serrano et al., 2010), using the ERA5-Land 'total evaporation' values for potential evapotranspiration values, which is consistent with their documentation[1]. Originally, multiple (6, 12, 24 month) scales of SPEI values were analyzed, but in order to clearly identify potential correlational signals

1 ERA5-Land dataset documentation: https://confluence.ecmwf.int/display/CKB/ERA5-Land%3A+data+documentation

between outcomes and droughts, it was decided to solely include one cumulative drought metric to avoid including multiple, highly-correlated metrics of similar nature. The 12-month scale was selected as a representative, intermediate-scale option. These SPEI values were computed by fitting historical precipitation values from 1970-2021 to a Pearson type III distribution (Ukkola et al., 2018). From them, an integrated measure of cumulative drought stress, equivalent to the annual, intensity-weighted total drought duration (AIWD) metric detailed in Depsky and Pons (2021) (Sec. 1.1) was calculated and utilized.

Table 2. Gridded historical climate variables obtained and constructed for Guatemala from the ERA5-Land Reanalysis dataset.

Climate Variable (1990-2018)	**ID**
Average surface temperature *(2m above land-surface)*	TEMP
Average annual precipitation totals	PPT
Annual degree-days above 25° C	DD25
Annual, intensity-weighted total drought duration, 12-month scale	AIWD12

Additionally, physical metrics of elevation and slope of terrain were evaluated and used as physical covariates in the predictive models constructed, obtained from the HydroSHEDS 15-second (~500 meter resolution) conditioned digital elevation model (DEM) (Lehner et al., 2008). Cultivated land was also obtained for use as a covariate, and also for robustness checks when constructing population- and agricultural area-weighted climate metrics in place of the default unweighted (i.e. area-averaged) aggregates. High-resolution agricultural areas throughout Guatemala were obtained from WorldCover 2020 (Zanaga et al., 2022) and aggregated to 1km resolution up from the native 10m resolution to harmonize its resolution with that of the LandScan 2020 population density grids (Rose et al., 2019), the gridded population layer utilized population-weighted robustness checks.

Methods

Model Construction and Migration Outcome Variables

While there are a number of potential avenues for statistical modeling, potentially including causal inference, the initial exploration of the Guatemalan census dataset conducted here utilizes simple, linear predictive modeling to attempt to explain observed variance in census migration variables. A total of five different outcome variables were produced from the international emigration and inter-municipality (from respondent's birth or from 2013) questions reported in the census (Table 1). Of these observed international and internal migration outcomes, two were selected for more in-depth analysis, while the remainder were cursorily tested and could be the subject of continued modeling efforts in the future. All models constructed were done so in a strictly predictive, or correlational, framework only and are detailed in Table 3, with the two outcomes of focus listed first.

Table 3. Migration outcome variables constructed from census responses for modeling analysis. All outcome variables are expressed in percentage (%) units of parent municipality census population totals in 2018. Models 1 and 2 are the focus of the following sections.

Model ID	Outcome variable (census table)	Migrant (n)	Spatial unit of model	Modeling Approach
1	**Total number of international emigrants from 2002-2018** ***(HH)***	**301,069**	**Municipality (MUNI)**	**Ordinary Least Squares (OLS)**
2	**Net internal migration between municipalities from 2013-2018** ***(IND)***	**319,669**	**MUNI**	**OLS**
3	Total net internal migration between municipalities over lifetime of respondents *(IND)*	2,442,802	MUNI	OLS
4	Total number of international emigrants in 2018 alone *(HH)*	23,637	MUNI	OLS
5	Total number of international emigrants from 2016-2018 *(HH)*	75,480	MUNI	OLS

Independent Covariates

Independent covariates, or predictor variables, were constructed from selected census survey responses to represent sociodemographic and economic characteristics of respondent individuals or households. Of the 111 unique questions recorded in the census in the IND, HH and RES tables, a total of 36 were constructed and used in the models described in Table 3. Many of these represent simplifications of multi-class responses into binary (yes/no) variables, and then converted to a fraction of their parent spatial unit (e.g. municipality) totals. For example, questions pertaining to individuals' self-identified ethnicity in the IND table were simplified from dozens of different ethnic groups responses to a simple binary indicator as to whether an individual is part of any indigenous and/or afro-descendent ethnic group, considered to be amongst the most marginalized and historically persecuted social classes in the country (Lopez-Carr et al., 2017). The full set of these census-derived sociodemographic covariates used in Models 1-5, as well as the physical and climate covariates, are detailed in Table 4 below.

Table 4. Full set of sociodemographic/economic (census-derived), physical and climatic predictor covariates utilized in the predictive migration modeling (models 1-5) analysis. Variables are identified by their class (SOC = sociodemographic, PHYS = physical, CLIM = climatic).

Covariates (n = 42)	Census source	Class

	table	
Age, years of formal education, urban resident, employed, member of indigenous or afro-descendent ethnic group, physically or mentally disabled, received only primary school education or lower, can read/write, can read/write Spanish, can read/write English, (log) population density *(n = 11)*	IND	SOC
HH occupied by owner, owner is woman, head of family is woman, access to water within HH, connected toilet, exclusive sanitation/drainage service, access to electricity, radio, TV, stove, cable, refrigerator, water tank, washing machine, internet access, hot water, motorcycle, car, exclusive kitchen, gas or electric energy for cooking, receipt of remittances from family members abroad (*remittances only used in Models 2 and 3*) *(n = 21)*	HH	SOC
is a formal/incorporated housing structure, roofing made of durable material, dirt floor *(n = 3)*	RES	SOC
Elevation, Slope of Terrain (%), Fraction of land under cultivation *(n = 3)*	--	PHYS
TEMP, PPT, DD25, AIWD12 *(n = 4)*	--	CLIM

Models 1-5 were all constructed using the full set of above covariates using the municipality (MUNI) as the spatial unit of analysis (*n = 340* nation-wide, Figure 1), which required aggregating the outcome variable and all predictors to the level of the parent municipality. Continuous variables (e.g. age, years of education) were averaged across MUNIs, while binary variables (e.g. employed, has electricity, etc.) are represented as fractions of MUNI totals for the relevant source table, such that IND-based census covariates are expressed as fractions of their parent populations, fraction of households for HH-based census variables and fraction of residences for RES-based census variables. For PHYS variables, elevation and slope of terrain were averaged across the land area of each parent MUNI, expressed in units of meters and % gradient, respectively. Cultivated land area is expressed as a fraction of total MUNI area. All four climate covariates were averaged across each MUNI extent using a uniform, area-weighted approach, though they were also computed using population (LandScan) and cultivated-area (WorldCover) weighting schemes for model robustness checks.

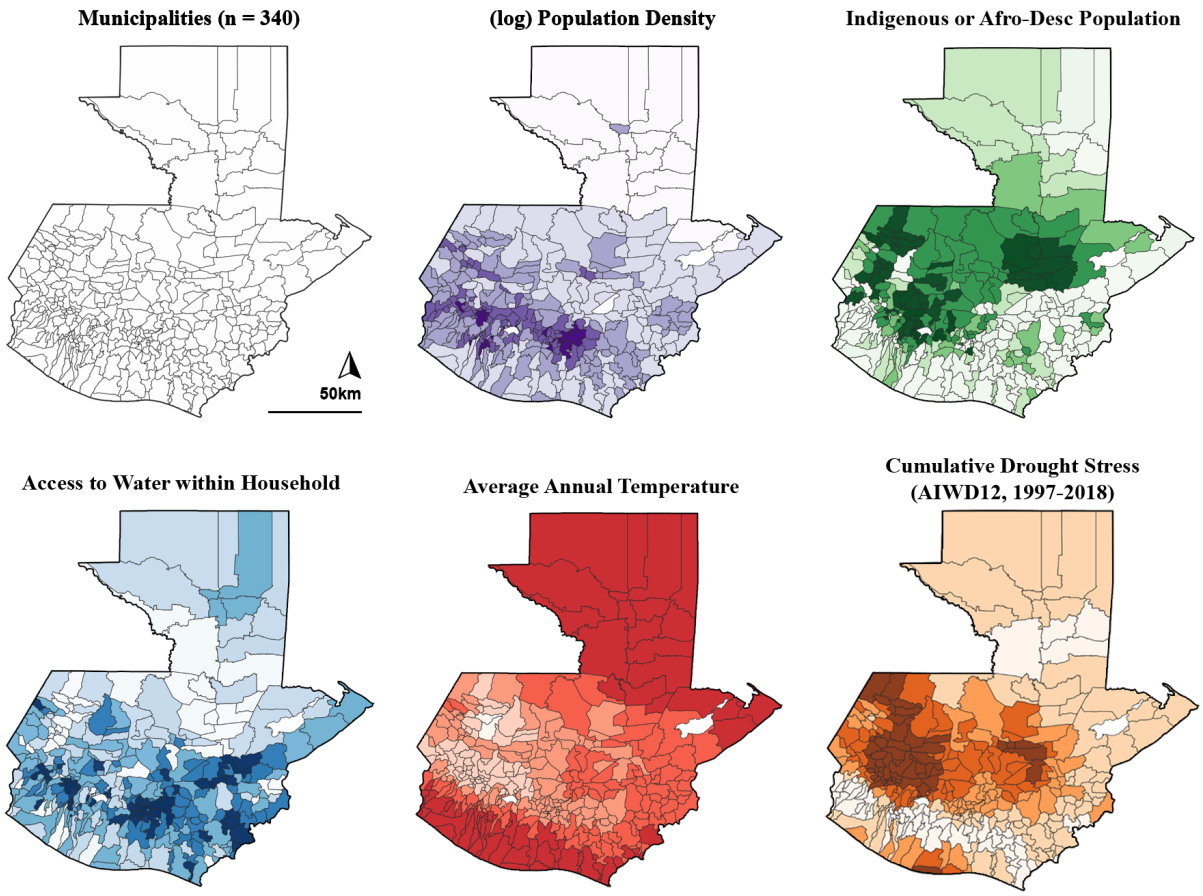

Figure 1. (*upper-left*) Municipality boundaries of Guatemala, the spatial unit of modeling for all OLS models (1-5), along with five examples of covariates constructed and aggregated to the municipal level, all color scales represent standardized ($\mu = 0, \sigma = 1$) min-to-max value ranges.

Modeling Approach

All models were carried out using an ordinary least squares (OLS) predictive linear modeling approach, such that the statistical significance of correlations between migration outcomes and covariates might be identified, but such that causal inference cannot be confidently identified. Additionally, given the high-level of multicollinearity between many of the covariates utilized (Figure S2), these modeling approaches facilitate modeling a relatively large number of independent variables in a predictive framework, then cross-validating the models to assess the extent to which observed variation in the outcome variable(s) of focus can be confidently explained with this given set of predictors.

Models were fitted to the entire set of 340 MUNIs in order to obtain estimates for each covariate's coefficient and levels of significance. To assess model performance, cross-validation was performed by splitting MUNIs randomly into 50/50% train/test subsets, fitting models on the training subset and subsequently testing that model's performance on the omitted test subset. Test R^2 (i.e. fraction of outcome variance explained on the test set) was used as the primary metric of performance, as per standard OLS machine learning practice (Gareth et al., 2013). All outcome and predictor variables were standardized ($\mu = 0, \sigma = 1$) to facilitate interpretability of coefficient estimates between covariates.

All climate CLIM variables were averaged across the given modeling period in question, along with 5 years of prior lag time for any given period, to represent average climatic conditions experienced during the period of observed migration and for a significant period prior to capture potential time-lagged influence of exposure to climatic variables on migration. Therefore, Model 1, which represents international emigration observed between 2002-2018, contains CLIM covariates averaged across the period of 1997-2018. Model 2 (internal migration from 2013-2018) contains CLIM variables averaged from 2008-2018, while Model 3 (emigration reported in 2018 alone) has CLIM variables for 2013-2018, and so forth.

Results and Discussion

Model results and discussion are presented here primarily for Models 1 and 2, as they represent the best representations of the international and internal migration survey responses in the 2018 national census. Results and discussion for Models 3-5 are mentioned in brief, but are largely framed in terms of their potential for future analysis.

Model 1 - Municipal International Emigration from 2002-2018

An OLS model to predict municipality-scale variation in reported international emigration, totaling 301,069 migrants, during the entire 2002-2018 period in the 2018 Guatemalan census was constructed using all covariates listed in Table 4. This outcome variable was expressed in terms of the fraction of the census-reported total population in 2018 for each municipality, displayed in Figure 2.

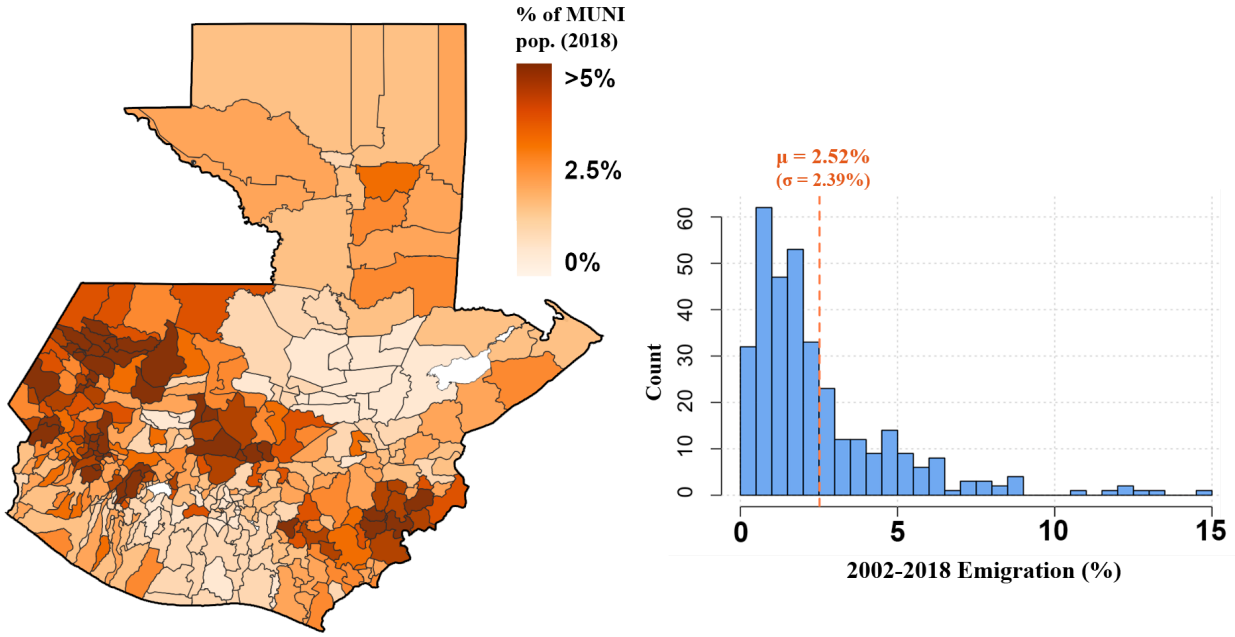

Figure 2. International emigration reported by households in the 2018 census between 2002-2018, aggregated to parent municipalities, and used as the outcome variable in Model 1. Units are expressed as percentages of census-reported population totals.

In explaining the municipality-scale emigration rates between 2002 and 2018 shown in Figure 2, our OLS model (Model 1) was able to explain more than half of the observed variance, with an average test set (half of MUNIs) R^2 of 0.55, averaged across 30 cross-validation (CV) iterations, each with a different random train/test split (50/50%). Average R^2 of the training subset was 0.75 and 0.70 when fit on the entire MUNI set (Figure 3), which suggests that some model over-fitting occurring, such that its performance on training data over-estimates the true predictive power (i.e. test set performance) when applied to municipalities omitted from the fitting process (Figure 4).

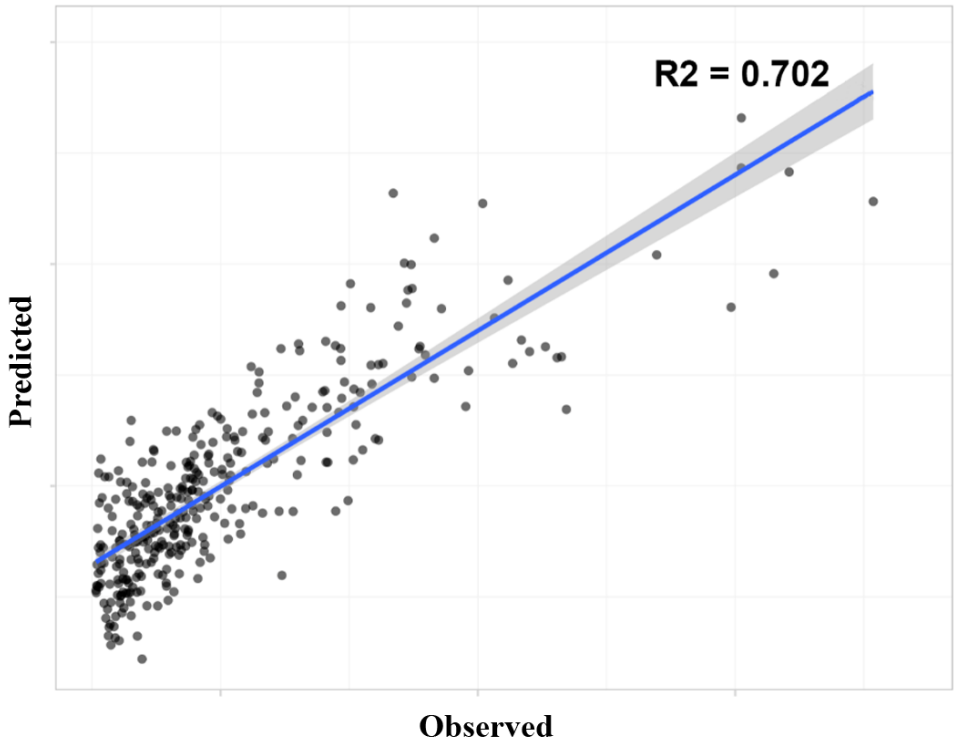

Figure 3. The OLS fit of Model 1 on the entire MUNI set (*n = 340*), yielding an R^2 of 0.70, though it is subject to over-fitting, as shown in Figure 4.

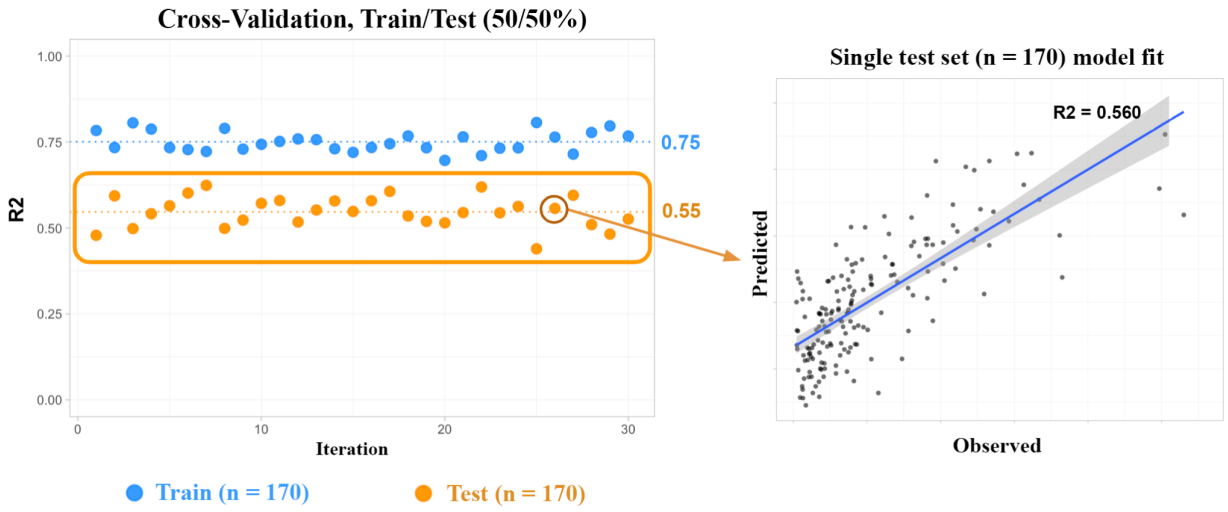

Figure 4. (*left*) Cross-validation iteration (30x) results for Model 1 using a 50/50% train/test splitting scheme for municipalities. Average training set R^2 is 0.75, while average test set R^2 is 0.55. (*right*) Predicted versus observed model values for the test set of municipalities in a single CV iteration.

Table 5 details which covariates exhibited the most statistically-significant predictive power for explaining international emigration from 2002-2018, filtered by those with a p-value < 0.05 in the model trained on the full dataset, sorted by coefficient magnitude. Since all variables were standardized, coefficients are expressed in units of standard deviations from the mean.

Table 5. Model 1 (OLS) results and coefficient estimates for all statistically-significant ($p < 0.05$) covariates, sorted by magnitude of coefficient. Units are in standard deviations from the mean, reflecting standardized variables ($\mu = 0$, $\sigma = 1$). Coefficient values greater than zero indicate positive relationships between a given covariate, all others constant, and international emigration rates from 2002-2018.

Variable (*census source table*)	**Coef. (β)**	**Std. Error**	**t-value**	**Pr(>|t|)**
years of education (IND)	-0.706	0.337	-2.096	0.037
female head of household (HH)	0.507	0.063	7.998	< 0.001***
gas or electric cooking (HH)	-0.427	0.112	-3.806	< 0.001***
female home-owner (HH)	-0.382	0.080	-4.784	< 0.001***
occupied by owner (HH)	0.316	0.067	4.690	< 0.001***
has motorcycle (HH)	0.268	0.073	3.673	< 0.001***
dirt floor of residence (RES)	-0.263	0.092	-2.846	0.005**
cumulative drought stress, AIWD12	0.200	0.073	2.726	0.007**
employed (IND)	-0.188	0.062	-3.026	0.003**
disability (IND)	0.176	0.048	3.621	< 0.001***
indigenous or afro-desc. ethnicity (IND)	0.142	0.072	1.985	0.048

Residual Std. Error	0.582		***Significance Levels***	
Multiple R^2	0.702		< 0.001	***
Adjusted R^2	0.660		0.001 - 0.01	**
F-statistic:	16.7		0.01 - 0.05	*
Deg. Freedom (model)	42			
Deg. Freedom (resid.)	298			
Model p-value	< 2.20E-16			

These results highlight a number of interesting trends and also raise some compelling questions for further analysis. It is important to acknowledge the multicollinearity between covariates (Fig. S2), the fact that the modeling framework is not causal but strictly predictive/correlational, as well as the likelihood that many important variables are unobserved (though potentially correlated with some predictors here). Bearing these caveats in mind, Model 1 results suggest that years of education, all other variables constant, is the strongest predictor of international emigration, with fewer years of formal schooling correlated with higher rates of international emigration (β = -0.71), such that for every standard deviation (s.d.) in years of additional education (equivalent to 1.2 years), there is a decrease of 0.71 s.d. of international emigration (i.e. -1.7% of municipal population). Other statistically-significant predictors that are negatively associated with emigration are i) access to gas or electric cooking fuel, ii) female home-ownership, iii) households with dirt floors, and iv) employment. Meanwhile, positively-associated predictors include i) female heads of households, ii) owner-occupied households, iii) possession of motorcycles, iv) cumulative exposure to drought stress from 1997-2018, v) personal disabilities and vi) being a member of an indigenous and/or afro-descendent ethnic group.

Some of these outcomes appear somewhat counter-intuitive, or in conflict with one another, such as the conflicting signs of coefficient estimates for female household ownership (-) versus female heads of household (+). Additionally, it seems possible that poverty can serve as a push-factor for migration, and many of these covariates serve as proxies for poverty (e.g. access to gas/electric stoves, owning a motorcycle, having a dirt-floored home, being employed). However, many of these poverty proxies also have conflicting coefficient signs. There are a number of possible reasons for these seemingly inconsistent results. First, the fact that there are so many similar, highly-collinear variables (Figure S2) makes interpretation of their coefficients difficult, due to the fact that their magnitudes represent the change in outcome variable per unit change in a given covariate, all other covariates held constant. Therefore, given that so many variables, especially proxies for poverty, are highly correlated, it is difficult to interpret these coefficients with clarity without first removing all other significantly-correlated variables. Ideally, the census would have reported a measure of poverty as a single variable, such as annual household income, but such a metric was not provided.

However, given that this exercise sought to investigate to what extent emigration rates at the municipal level could be predicted from the census and other physical/climatic variables, it still performs fairly well. The issue of multicollinearity and associated barriers to interpretability of covariate coefficients is mostly an issue with the census variables, which exhibit the highest level

of cross-correlation and redundancy (Figure S2). The physical and climate covariates, for example, exhibit less redundant multicollinearity across multiple covariates and therefore may be interpreted with slightly more confidence. From the perspective of identifying links between climate stress and out-migration, it is compelling that there is a statistically significant relationship between cumulative drought exposure from 1997-2018 and rates of emigration (β = 0.20), which suggest that every increase in 1 s.d. in exposure to drought stress as defined by AIWD12 predicts roughly an additional half-percent (0.48%, or 0.2 s.d.) of a given municipality's (2018) population having emigrated internationally between 2002 and 2018.

It is also worth noting that Model 1 omits the census variable regarding whether or not a given household receives remittances from a family member living abroad, as this is theoretically contingent (i.e. endogenous) on having had a family member emigrate in the past, including in the time period in question (2002-2018). However, I was curious as to how much better Model 1 would perform were that variable to be included and when including it, the model performance drastically increased, with a mean training set R2 of 0.91 and test set of 0.86, which at least provides some validation and internal consistency of survey responses with respect to international emigration. Were there to be a weak, or absent, relationship between the remittance survey responses and those indicating having sent family members abroad in the past, it would raise concerns about survey question responses more broadly. Cross-validation results and test set performance of this modified Model 1 are displayed in Figure S3.

Model 2 - Inter-Municipal Net Internal Migration from 2013-2018

The OLS model constructed to explain census reported net migration between municipalities from 2013 to 2018, representing 319,669 internal migrants, was constructed and analyzed in the same manner as that of Model 1. The only difference in covariates being that the household remittances-received variable was included here, as it did not pose an endogeneity concern for this outcome variable. This variable is expressed as a percentage of reported population totals in 2018 for each municipality is shown in Figure 5. Given that the national net sum of internal migrants is zero, the average municipal percentage change is roughly zero, although we can see significant net increases in the municipalities peripheral to the capital city, while the capital municipality (Guatemala) itself exhibits a net decrease. This suggests a pattern of peri-urban growth, or sprawl, while the density within the city center seems to be declining.

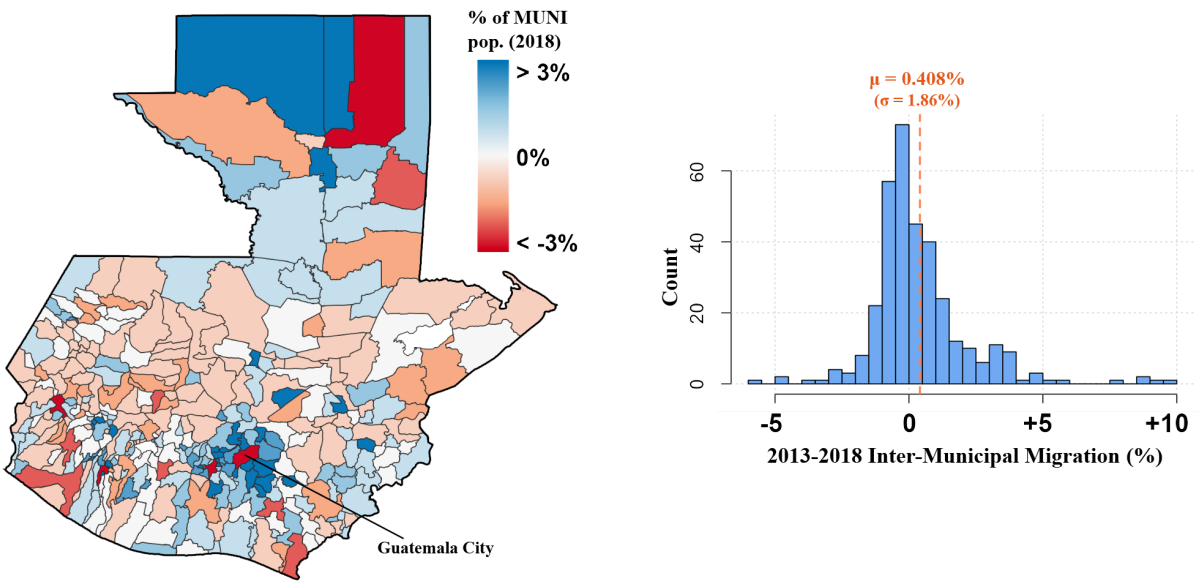

Figure 5. Net internal migration reported by individuals in the 2018 census between 2013-2018, aggregated to parent municipalities, and used as the outcome variable in Model 2. Units are expressed as percentages of census-reported population totals.

Overall, the explanatory power of Model 2 compared to Model 1 was markedly lower, suggesting that predicting variance in net internal migration between municipalities is more difficult using only this set of census-based, physical and climatic covariates. The R^2 of Model 2 when fit to the full municipality set was 0.46 (Fig. 6), but when performing the same cross-validation procedure as with Model 1, declines to 0.24 averaged across test sets (Figure 7), revealing an even more substantial over-fitting problem in Model 2 compared to Model 1.

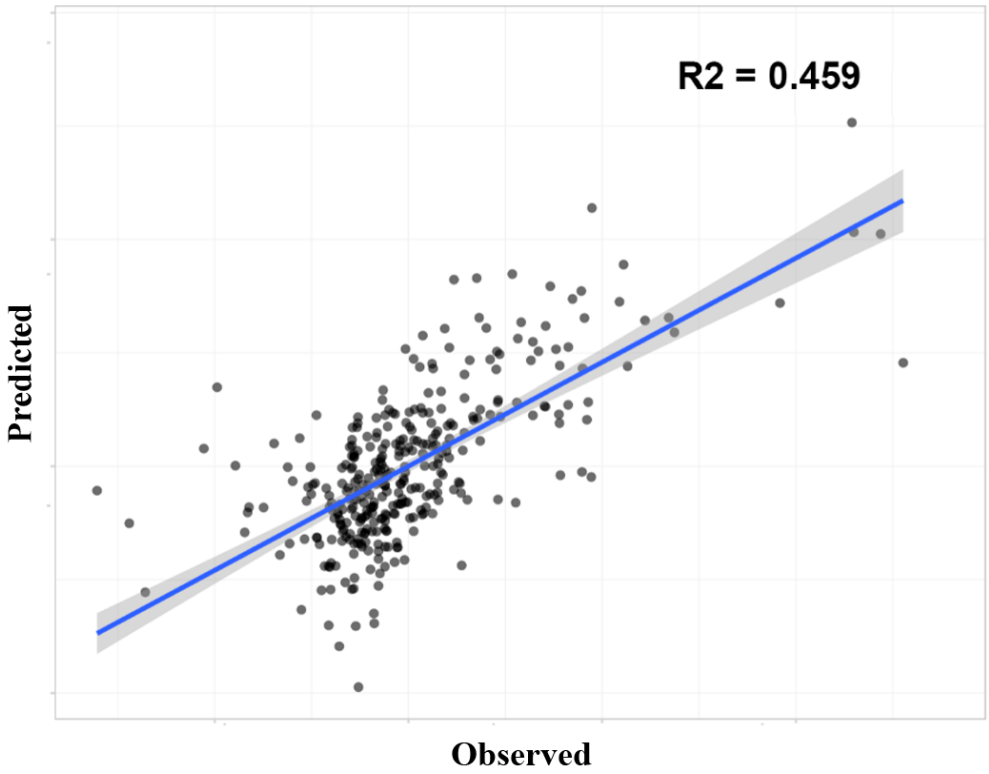

Figure 6. The OLS fit of Model 2 on the entire MUNI set (*n = 340*), yielding an R^2 of 0.46, though it is subject to substantial over-fitting, as shown in Figure 6.

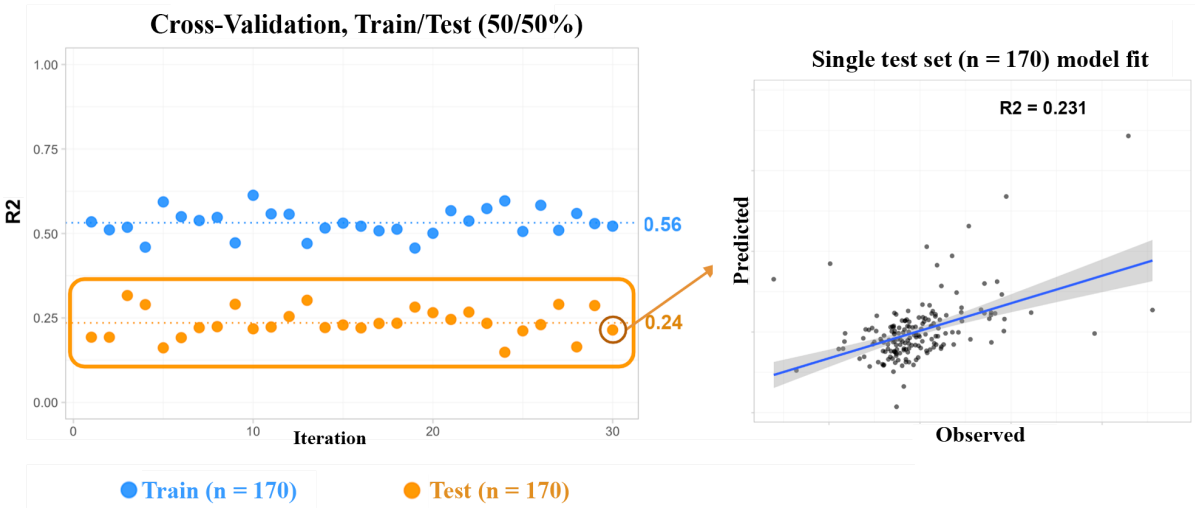

Figure 7. (*left*) Cross-validation iteration (30x) results for Model 2 using a 50/50% train/test splitting scheme for municipalities. Average training set R^2 is 0.56, while average test R^2 drops to 0.24. (*right*) Predicted versus observed model values for the test set of municipalities in a single CV iteration.

Table 6 details which covariates exhibited the most statistically-significant predictive power for explaining net, inter-municipal migration from 2013-2018, filtered by those with a p-value < 0.05 in the model trained on the full dataset and sorted by coefficient magnitude. Since all

variables were standardized, coefficients are expressed in units of standard deviations from the mean.

Table 6. Model 2 (OLS) results and coefficient estimates for all statistically-significant ($p < 0.05$) covariates, sorted by magnitude of coefficient. Units are in standard deviations from the mean, reflecting standardized variables ($\mu = 0, \sigma = 1$). Coefficient values greater than zero indicate positive relationships between a given covariate, all others constant, and inter-municipal migration rates from 2013-2018.

Variable (census source table)	**Coef. (β)**	**Std. Error**	**t-value**	**Pr(>|t|)**
years of education (IND) †	-1.025	0.452	-2.267	0.024*
primary school or lower education only (IND)	-0.859	0.348	-2.466	0.014*
age (IND)	-0.571	0.119	-4.813	< 0.001***
formal residence structure (RES)	0.531	0.157	3.393	0.001**
gas or electric cooking (HH) †	0.446	0.156	2.866	0.004**
can read/write English (IND)	0.432	0.089	4.837	< 0.001***
durable roofing material (RES)	-0.417	0.142	-2.925	0.004**
receives remittances from abroad (HH)	0.260	0.082	3.156	0.002**
female home-owner (HH) †	0.255	0.111	2.303	0.022*
female head of household (HH) †	-0.252	0.096	-2.620	0.009**
employed (IND) †	0.213	0.085	2.503	0.013*
annual average precipitation	-0.142	0.072	-1.974	0.049*
Residual Std. Error	0.583		***Significance Levels***	
Multiple R^2	0.459		< 0.001	***
Adjusted R^2	0.380		0.001 - 0.01	**
F-statistic:	5.86		0.01 - 0.05	*
Deg. Freedom (model)	43			
Deg. Freedom (resid.)	297			
Model p-value	< 2.20E-16			

† Covariate is also a statistically-significant ($p > 0.05$) predictor in Model 1

Due to the lower explanatory power of Model 2, it is difficult to interpret the model as a whole. However, observing which covariates emerged as significant predictors is still worth noting. Interestingly, years of education had the largest-magnitude coefficient, as in Model 1, suggesting that education is indeed an important predictor of human movement in Guatemala, be it abroad or internally. However, the outcome variable in Model 2 represents a net gain of residents at the municipal level, which reflects movement towards a place, rather than movement away from it. Every additional 1.2 years (1 s.d.) of formal schooling predicts a decrease in the outcome variable here, in this case a -1.03 s.d. (-1.91%) decline in net internal migration at the municipal level. However, while this relationship in Model 1 implied that more schooling corresponded to a

decreased likelihood of emigrating abroad, in Model 2 it can entail some combination of i) higher education being associated with a higher likelihood that someone will be inclined to change municipalities (i.e. higher outflow) and/or ii) places with higher education are less attractive receiving communities for internal migrants moving from another location (i.e. lower inflow). Alternative models in the future could in theory be constructed to look solely at immigration versus emigration, rather than net flows in order to disentangle these relationships more definitively.

Overall, five of the twelve statistically-significant covariates in Model 2 were also significant for Model 1, which were i) years of education, ii) gas or electric energy for cooking, iii) female head of household, iv) female ownership of household and v) employment. Interestingly all of these variables, except for years of education, exhibit reversed coefficient sign directions, as compared to Model 1, which makes intuitive sense, given that the outcome variables between the two models can be interpreted as potentially opposite measures. However, it is still possible that a municipality with a high net rate of internal migration (i.e. more incoming than outgoing migrants) can still have a large number of out-migrants. Again, we see the female household head and owner variables as being significant in Model 2, and again with opposing signs, implying that there is potentially an important gender element at play here, or that these measures are correlated with some other unobserved factors of importance. The fact that, conditional on there being a high proportion of women as heads of households in a given municipality, the presence also of a high proportion of women home-owners yields an opposing effect on the outcome is difficult to interpret and warrants further exploration.

For both Models 1 and 2, robustness checks using (LandScan 2020) population-weighted and (WorldCover 2020) cultivated land-weighted CLIM variables in place of the unweighted value (i.e. uniform, area-weighted) and there was negligible impact on the models' performance and coefficient estimates.

Models 3-5

The remaining models described in Table 3 were constructed but only briefly and without in-depth analysis. However, they could represent the topic of future efforts on this research front. A brief rationale for each model and potential next steps is provided here.

Model 3 is similar to Model 2, in that it explores net internal migration, with the difference being that its outcome represents internal movement at any point during respondents' lifetimes. This outcome represents the largest total sample size of reported migrants of all of the outcome variables assessed, totaling 2,442,802 lifetime internal migrants, or 16.4% of the national population tabulated in 2018. However, given the fact that the periods of respondents' lives are inherently different between individuals, and my desire to explore the potential predictive power of climatic variables over a uniform time period on observed migration outcomes, made it less sensible to focus on this outcome variable. In its current construction, Model 3's CLIM variables are averaged from 1997-2018, the same as Model 1. However, it could be helpful to re-construct Model 3 at the individual level, rather than municipality, perhaps in a logit/propensity framework that predicts the likelihood that any given individual will have made an inter-municipality move at some point in their lifetime.

Models 4 and 5 represent similar iterations of Model 1 by utilizing the international emigration responses provided in the survey. However, given general concerns about the accuracy and potential undercounting of household census responses regarding emigration of members abroad up to 16 years prior, I thought it prudent to construct models that only utilize emigration reported for recent years, with just 2018 represented in Model 4, and 2016-2018 in Model 5. However, this entailed sacrificing sample size of reported emigrants, whereby Model 1 represented a total of 301,069 reported international migrants, only 23,637 were reported in 2018 (Model 4) and 75,480 from 2016-2018 (Model 5).

Table 6. Performance (R^2) metrics of Models 3, 4 and 5 when fitted to the full set of municipalities, and also test set R^2 averaged across 30 iterations of 50/50% train/test cross-validation splits.

ID	Model	R^2 (all)	R^2 (test)
3	Inter-municipal migration over respondent lifetimes	0.438	0.204
4	International emigration in 2018 alone	0.590	0.400
5	International emigration from 2016 to 2018	0.593	0.403

Conclusions

Overall, the results of this study show that it is possible to model census-reported, municipal-level rates of international out-migration from Guatemala between 2002 and 2018 (Model 1) with fairly high explanatory power (~55% of variance explained on test data), using other reported sociodemographic census metrics and a handful of physical and climatic variables. Notably, education (-), female household heads (+), female household owners (-), home ownership (+), access to resources like gas/electric cooking (-), motorcycles (+), housing materials (i.e. dirt flooring) (-), employment (-), proportion of population with disabilities (+) and indigenous/Afro-descendent ethnicity (+) all emerged as significant predictors of emigration. Also, exposure to cumulative drought stress between 1997 and 2018 also exhibited statistically significant predictive power (+), with higher levels of exposure to drought stress corresponding to higher levels of international out-migration. However, many of the covariates employed here are highly collinear with one-another, and many likely serve as similar indicators of poverty, which means interpreting their sign and magnitudes should be done with caution.

Modeling inter-municipal migration between 2013 and 2018 proved more difficult (Model 2), with only 24% of observed variance explained on test set model data. However, some significant predictors emerged that were also seen in Model 1, namely education (-), access to gas/electric cooking (+), female head of household (-), female owner of house (+), and employment (+). Additionally, age (-), formal housing structure (+), English literacy (+), durable roofing materials (-), receipt of remittances (+), and mean annual precipitation (-) as significant predictors. However, as with Model 1, these may or may not reflect the true influencing (i.e. causal) factors behind these migrations patterns.

Limitations and Next Steps

Given the high number of covariates utilized from the census, one priority moving forward is to find comprehensive data on poverty rates and/or household-level estimates of annual income to

represent economic resources more directly. Along these lines, the models presented here could also be simplified by assessing the relative variable importance of each difference census-reported metric, many of which are highly collinear. This could potentially be done using other machine learning techniques, such as ridge regression or lasso, which apply penalty terms for each additional covariate and thereby converge on the subset of variables which contribute the most explanatory power for the outcome, reducing model over-fitting. This would also improve interpretability of the model and of statistically significant predictors that emerge. Similarly, alternative machine learning modeling methods could be tested to see if higher levels of predictive power could be achieved (e.g. lasso, ridge, random forests etc.), although with the fairly small sample size of municipalities ($n = 340$) this may not be successful.

Additionally, despite the fact that the 2018 national census represents an impressive survey of nearly the entire population of the country, there are still known limitations regarding its quality and completeness. Specifically, with respect to the migration-related responses, it is suspected that the total number of international migrants are likely under-estimated. In order to perform a comparison of these reported emigrant numbers to similar observations made in other reporting contexts, I obtained a daily record of (undocumented) migrant-apprehensions made by the United States Customs and Border Patrol (CBP) from 1999 to 2019 along the U.S. southwest border, which details of the home-country (or sub-national administrative unit) of each detainee, totaling 13,826,801 individual apprehensions, 678,345 of which were reportedly of Guatemalan migrants between 2002 and 2018, more than double the number of census-reported international emigrants during the same period.

However, the CBP data, by nature, represent apprehensions of migrants that are undocumented and often result in deportation. Data on how many of these apprehensions resulted in deportation to their home-countries is not known. Given that the Guatemalan census data on international emigrants is meant to reflect just migrants that have left and not returned, this higher CBP figure does not definitively entail a systematic undercounting in emigration values reported in the Guatemalan census, although conversations with local partners seem to suggest that undercounting it is likely still the case. More analysis could be done with this dataset and will likely be the subject of continued work, potentially in partnership with the UN International Office on Migration (IOM) in Guatemala.

Finally, constructing models in a framework to identify causal influence of certain factors on international and/or internal migration rates would represent a desirable evolution of this analysis and will be further explored moving forward.

References

Carleton, T. A. (2017). Crop-damaging temperatures increase suicide rates in India. Proceedings of the National Academy of Sciences of the United States of America, 114(33), 8746–8751. https://doi.org/10.1073/pnas.1701354114

Depsky, N., and Pons, D. (2021). Meteorological droughts are projected to worsen in Central America's dry corridor throughout the 21st century. Environmental Research Letters, 16(1). https://doi.org/10.1088/1748-9326/abc5e2

Gareth, J., Daniela, W., Trevor, H. and Robert, T., An introduction to statistical learning: with applications in R. Springer, 2013.

Gustin, G., Henninger, M., 2019. Central America's choice: Pray for rain or migrate - Ravaged by drought, farmers in rural Honduras and Guatemala live on the edge of hunger. Inside Climate News, NBC News.

Lehner, B., Verdin, K., Jarvis, A. (2008). New global hydrography derived from spaceborne elevation data. Eos, Transactions, American Geophysical Union, 89(10): 93–94. https://doi.org/10.1029/2008eo100001

Lopez-Carr, D., Martinez, A., Bilsborrow, R.E. and Whitmore, T.M., 2017. GEOGRAPHICAL AND INDIVIDUAL DETERMINANTS OF RURAL OUT MIGRATION TO A TROPICAL FOREST PROTECTED AREA: THE MAYA BIOSPHERE RESERVE, GUATEMALA. European Journal of Geography, 8(2).

Lustgarten, A., 2020. The Great Climate Migration. The New York Times Magazine.

Meyer, P., 2022. Central American Migration: Root Causes and U.S. Policy. Congressional Research Service.

Milman, O., Holden, E., Agren, D., 2018. The unseen driver behind the migrant caravan: climate change. The Guardian.

Muñoz Sabater, J., (2019): ERA5-Land hourly data from 1981 to present. Copernicus Climate Change Service (C3S) Climate Data Store (CDS). (Accessed on Oct 12, 2022), 10.24381/cds.e2161bac

Rigaud, K. K., de Sherbinin, A., Jones, B., Bergmann, J., Clement, V., Ober, K., … Midgley, A. (2018). Groundswell. Retrieved from https://openknowledge.worldbank.org/handle/10986/29461

Rose A.N., McKee J.J., Sims K.M., Bright E.A., Reith A.E., Urban M.L., 2020. LandScan 2019.

Steffens, G., 2018. Changing climate forces desperate Guatemalans to migrate. National Geographic.

Ukkola, A.M., Pitman, A.J., De Kauwe, M.G., Abramowitz, G., Herger, N., Evans, J.P. and Decker, M., 2018. Evaluating CMIP5 model agreement for multiple drought metrics. Journal of Hydrometeorology, 19(6), pp.969-988.

United Nations, 2022. More than 50,000 migrants 'die in search of a better life'. UN News.

United States National Security Council (White House), 2022. US Strategy for Addressing the Root Causes of Migration in Central America.

Vicente-Serrano, S.M., Beguería, S. and López-Moreno, J.I., 2010. A multiscalar drought index sensitive to global warming: the standardized precipitation evapotranspiration index. Journal of climate, 23(7), pp.1696-1718.

Zanaga, D., Van De Kerchove, R., Daems, D., De Keersmaecker, W., Brockmann, C., Kirches, G., Wevers, J., Cartus, O., Santoro, M., Fritz, S. and Lesiv, M., 2022. ESA WorldCover 10 m 2021 v200.

Supplemental Figures

Figure S1. Event flier and agenda for migration symposium in Guatemala City, Guatemala on January 23, 2023 where the above study was initially presented.

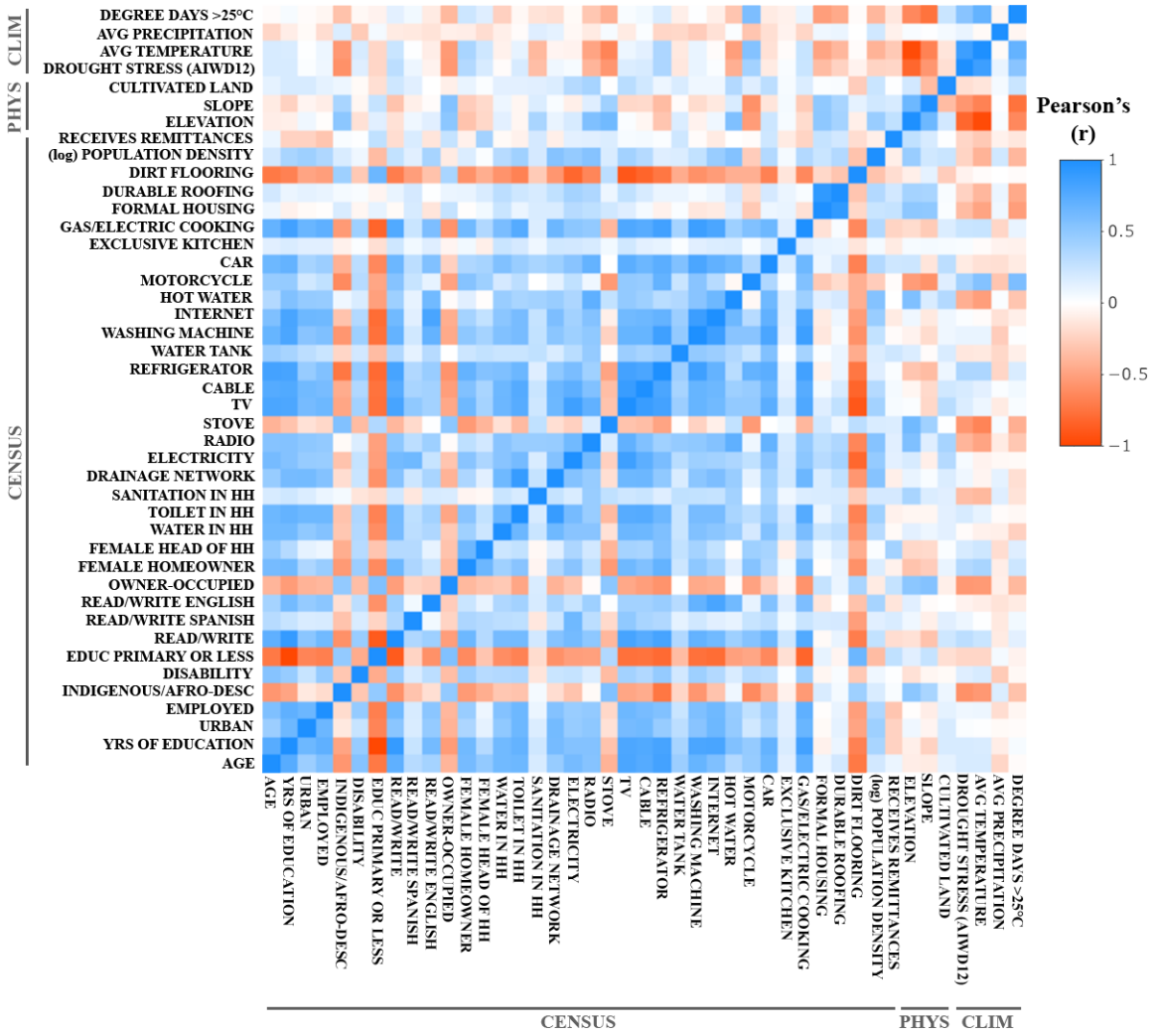

Figure S2. Cross-Correlation matrix of all 43 covariates used in Models 1-5. Strong multicollinearity across multiple variables can be seen, as well as many variables of similar cross-correlation profiles to all other covariates, especially in the census variable group.

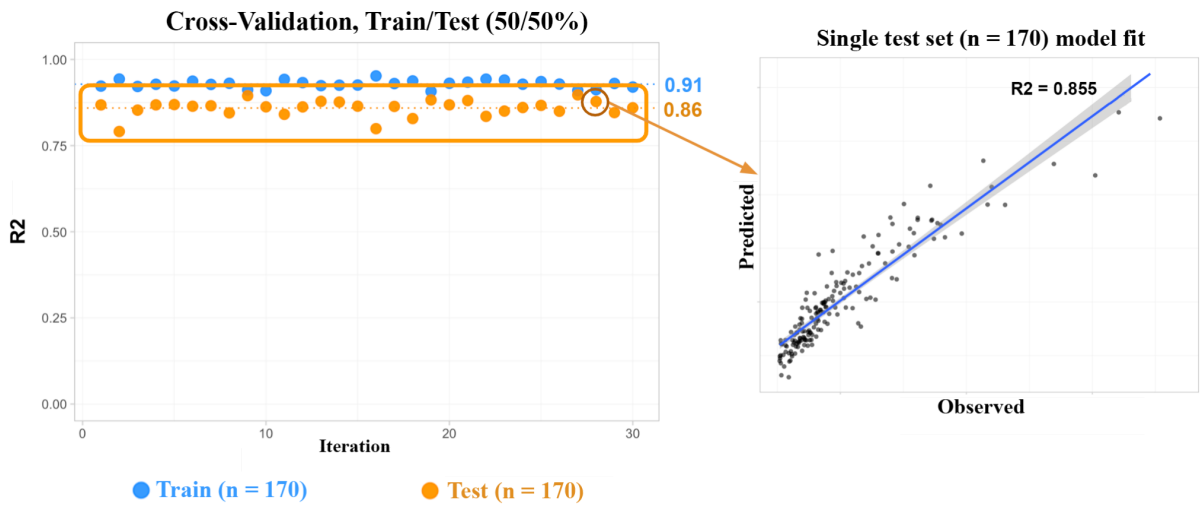

Figure S3. (*left*) Cross-validation iteration (30x) results for Model 1 with the household remittances covariate included, using a 50/50% train/test splitting scheme for municipalities. Average training set R^2 is 0.91, with an average test set R^2 is 0.86. (*right*) Predicted versus observed model values for the test set of municipalities in a single CV iteration.

Chapter 2 - The United States*:* Synthesizing existing evidence between climate, equity and displacement, advancing high-resolution population mapping techniques in California and assessing recovery and out-migration in Puerto Rico following Hurricane Maria.

2.1 - Climate and Displacement in the United States - A Review of the Literature

This section is adapted from (Cash et al., 2020). The project was conceptualized by Karen Chapple and Anna Cash, with the bulk of the literature review and summarization performed by Shazia Manji, Honora Montano and Melisa Krnjaic. I performed additional literature review, summarization of previously-reviewed material and wrote the vast majority of the final report text. Shazia Manji also authored a substantial portion of the 'Question 2' section text. Final document edits, layout and minor additional text contributions were carried out by Renee Roy Elias, Karen Chapple and Anna Cash. Note: the listed order of authors in the final published report was done alphabetically, not in terms of relative authorship and contribution. The published report can be found at https://www.sparcchub.org/wp-content/uploads/2020/04/Climate-and-Displacement-Lit-Review-6.19.2020.pdf

Introduction

Centuries of burning fossil fuels and emitting greenhouse gases into the Earth's atmosphere have indelibly altered the course of our planet's global climate system. There is broad scientific consensus that our shared future is one of higher average temperatures, rising sea levels and more frequent and severe climatic shocks. Many of these trends have already begun to emerge across the globe, forcing people either to adapt in place or to leave their homes in search of stability elsewhere. These impacts can be acute or insidious and, in some cases, afflict socioeconomically disadvantaged communities disproportionately. Therefore, understanding the complex interplay between the changing climate and our social, political, and economic institutions is imperative to develop the robust, adaptive policies needed to make our societies more resilient in the face of this change.

One widespread consequence of worsening climate conditions is the displacement of people from their homes and communities. Displacement of this kind can occur as the direct result of a climate shock – such as a major storm, fire, or flood – that physically destroys or damages property and infrastructure, or more gradually as a response to worsening climate stressors. These can include, for example, nuisance flooding and extreme heat, which can introduce or exacerbate economic hardships among people living in areas vulnerable to climate hazards. The

rising costs of utility bills, insurance premiums, or housing prices – resulting from housing stock shortages, changing preferences due to climate change, or increased property risks – may also lead to displacement. Furthermore, efforts to reduce greenhouse gas (GHG) emissions and prepare for climate change's worsening impacts, such as improvements in public and active transportation, urban greening, and energy efficiency measures, can have unintended consequences for the communities in which they are implemented. These essential climate mitigation and adaptation strategies may also be increasing the amenity values of these neighborhoods, namely by raising property values and housing costs, and thereby contributing to the indirect displacement of residents vulnerable to rising costs.

This literature review explores the role of climate change as a driver of displacement, bringing together several bodies of literature to elucidate the various mechanisms by which climate change is creating or increasing displacement pressures. The influence of climate on displacement varies greatly across countries, regions, and communities; this review focuses primarily on the relationship between climate change and displacement in the United States. It is meant to serve as a resource for both researchers and practitioners seeking to better understand climate and displacement, and as such we also highlight throughout the report equitable policy strategies that achieve climate goals while safeguarding vulnerable populations.

Guiding Questions

Specifically, this review is guided by the following three questions:

1. How are climate shocks and stressors related to displacement?
2. What are the unintended consequences of climate mitigation and adaptation (M/A) strategies, such as generating rising housing costs and associated displacement pressures?
3. How can current anti-displacement strategies better consider and protect vulnerable communities against climate hazards?

Results of our review related to Question 1 reveal that climate-driven shocks – which we define as major storms and wildfires – primarily drive direct displacement of people due to their immediate and physically hazardous nature. In contrast, climate stressors – which we define as extreme heat, droughts, nuisance flooding, and sea-level rise – act primarily as agents of displacement via more indirect pressures, such as adverse health effects and increases in cost of living. Living costs increase either via heightened utility and/or insurance costs in places experiencing these stressors, or because of rising housing costs in places with lower climate risks as they become relatively more attractive. However, we recognize that our definitions of climate shocks and stressors are somewhat fluid, and that many shocks and stressors exacerbate and occur simultaneously. There are many instances in which "shocks" serve as indirect drivers of displacement, such as is the case with the displacement of socioeconomically disadvantaged residents due to neighborhood change that occurs in the wake of a major storm. Similarly, there are instances in which "stressors" may serve to directly displace residents, as has been the case due to damages from sea-level rise and nuisance flooding. There are also significant inequities in exposure and vulnerability to these shocks and stressors, and in the ability to recover from them, with low-income, non-white communities and renters being disproportionately impacted.

Our exploration of the unintended consequences of climate mitigation and adaptation strategies (Question 2) shows that several commonly used policy strategies aimed at reducing GHG emissions and increasing resilience at the local level can potentially accelerate processes of gentrification and displacement of low-income residents in certain neighborhoods, under certain conditions. This is due to the fact that many of these investments – such as transit-oriented development, increased park and green space, infill development, and brownfield development – can result in higher property values in surrounding communities. Much of the literature reviewed for this section focuses on the impact of climate M/A policies on property and housing values, without explicitly naming or measuring displacement or gentrification. Therefore, the discussion presented in this section is at times predicated on the assumption that higher housing prices commonly contribute to the displacement of economically vulnerable residents.

The field of literature that considers how anti-displacement strategies can better protect vulnerable communities against the impacts of climate change (Question 3) was the sparsest among our three guiding questions; still, we highlight some valuable insights from this small body of literature. Namely, a large portion of the nation's affordable housing stock has been constructed in high-risk areas like floodplains, fire-prone areas, and zones of storm surge. Additional construction of such housing continues in these areas due to cheap land prices, with many of the planning procedures not paying proper consideration to worsening natural risks from climate change. Poor construction quality of such housing also contributes to their vulnerability to climate hazards. While affordable housing as well as other anti-displacement policies have the potential to mitigate the threats of climate change, they must be implemented in a community-engaged and research-informed manner.

Methods

This review includes literature published from the 1970s onward; the vast majority of papers and articles reviewed were written after the year 2000 as studies and reporting on climate change began to accelerate. The geographic scope of this review is primarily limited to the United States, with some international literature provided for additional context when necessary. We focus on the U.S. context for two reasons: 1) our intended audience includes researchers, policymakers, and practitioners who are addressing issues of climate and displacement primarily in the U.S., and we know that many parts of the world experience climate change and displacement in ways that may not be generalizable to the U.S., and 2) there is a sufficient wealth of U.S.-focused literature focused on climate and displacement to address our three guiding questions.

Literature reviewed for this study consisted of peer-reviewed academic papers, gray literature – such as reports, white papers, and working papers published outside of academic journals – and relevant, reputable journalistic sources. Peer-reviewed publications were generally given preference for inclusion so as to rely on the most rigorous research where possible; however, we found it vital to also include gray literature and other media reports because they offer timely and valuable insight into contemporary issues and provide information and commentary discussed by non-academic community members. For some of the issues explored – such as newer climate mitigation and adaptation strategies (Question 2) and the vulnerabilities of anti-displacement

strategies to climate change (Question 3) – the academic body of literature is nascent, therefore warranting a broader utilization of gray literature and media.

For Question 1, we paired search terms relevant to climate shocks and stressors – such as "sea level rise," "hurricanes," "wildfires," "drought," and "nuisance flooding" – with displacement-relevant terms – such as "displacement," "property values," "housing affordability," and "gentrification" – in order to identify literature that discussed the intersection of these two topics. We define gentrification as a process of neighborhood change that includes economic change in a historically disinvested neighborhood – by means of real estate investment and new higher-income residents moving in – as well as demographic change in terms of income levels, educational attainment, and the racial make-up of residents (Chapple and Zuk, 2015). Additionally, we reviewed recent academic studies that describe the growing scientific consensus on climate shocks and stressors, both in terms of historical patterns and future projections. This was done to contextualize the magnitude and scope of these hazards before discussing their influence on displacement. Overall, we identified and reviewed 233 relevant sources, the majority of which are academic papers.

For Question 2, we identified literature by pairing a range of land use, transportation, and energy-related search terms – such as "parks," "transit-oriented development," "rooftop solar," and "bike infrastructure" – with the same displacement-related search terms used in Question 1. Where necessary and/or relevant, we then filtered research by the most recent date, study area (with preference given to U.S.-based studies), and perceived relevance. By this method, we reviewed 133 sources, with some M/A strategies covered more thoroughly than others. Question 3, which explores the vulnerabilities of anti-displacement strategies to climate change, had the sparsest available literature of our three guiding questions, as few have studied the nexus of these topics in depth. However, there is a small and growing literature documenting the vulnerability of affordable housing to climate impacts, such as storms and flooding. For this question, we identified literature by pairing anti-displacement search terms – such as "affordable housing," "inclusionary zoning," and "rent control" – with climate hazard terms such as "flooding," "fires," and "storms" – to identify relevant sources. Our search yielded comparatively fewer results than Questions 1 or 2, and the majority of publications reviewed were gray or journalistic sources. A total of 18 sources were reviewed for this question. A full breakdown of search terms used can be found in Appendix A, and a breakdown of source types by guiding question can be found in Appendix B.

Question 1 - Climate Shocks, Stressors, and Displacement

Climate hazards often serve as direct or indirect drivers of displacement, though the ways in which they do so can be complex. This analysis was therefore segmented into a study of climate "shocks" and climate "stressors." Shocks are defined as climate-related events that present immediate, acute physical danger and can cause large-scale displacement of people in a matter of minutes or hours. In contrast, stressors are defined as pressures whose physical impacts are borne incrementally and over an extended period of time (months, years). For our consideration of climate "shocks," we identified two classes of shocks: i) major storms, and, ii) wildfires. For climate "stressors," we consider: i) sea-level rise (SLR) and associated tidal flooding, ii) extreme heat, and, iii) drought.

The literature regarding these hazards and their impacts is summarized below. However, we acknowledge that many of these climate hazards often occur in tandem, exacerbating one another, so we therefore highlight these intersections when relevant. Each hazard also results in distinct displacement pressures, so we discuss each separately. These pressures are characterized along a continuum of direct versus indirect drivers of displacement. Examples of direct displacement drivers caused by a given climate hazard may be the damage or destruction of one's home or property, or a threat to an individual's safety. Indirect drivers of displacement may be increased costs of living, perhaps associated with rising insurance premiums, utility bills, housing prices ushered in by neighborhood change after a climate shock, or housing cost increases in neighborhoods where stressors and shocks are less of a risk.

Climate Shock: Storms and Severe Weather

Climate Context

In many regions of the world, the patterns of storms and extreme weather are influenced by anthropogenic (human-caused) climate change and may worsen in the coming years. The climatic shocks discussed in this section include tropical cyclones (hurricanes and typhoons), floods, tornadoes and thunderstorms, and atmospheric rivers. Though recent occurrences and trends in severe weather are partly due to random, natural variability in the atmospheric system irrespective of a shifting climate, a number of historical trends and future projections can be confidently linked to human-influenced climate change and are listed below.

Hurricanes: Average intensity (i.e. maximum wind speeds, precipitation rates, storm surge levels) of hurricanes will very likely increase globally throughout the 21st century (Knutson et al., 2015; Walsh et al., 2015). Frequency of very intense hurricanes (e.g. category 4–5 hurricanes) will also likely increase globally, though global changes in frequency of all hurricane classes remains unclear (Christensen et al., 2013). Rates of intensification and duration of hurricanes may also increase under continued, increased ocean-warming (Kossin et al., 2017). These trends primarily threaten U.S. residents living in Caribbean areas such as Puerto Rico and along the Gulf and East coasts.

Tornadoes and Thunderstorms: The season for tornadoes and severe thunderstorms in the U.S. appears to be lengthening, though the average total number of storm days each year has decreased in recent years (Kossin et al., 2017). However, the number of distinct tornadoes on days in which they do occur appears to be increasing sharply (Elsner et al., 2015). Model projections predict that the frequency and intensity of severe thunderstorm environments across the U.S. will likely increase in coming decades, namely in the Midwest and southern Great Plains regions during spring months (Diffenbaugh et al., 2013; Kossin et al., 2017).

Atmospheric Rivers: These streams of tropical, atmospheric moisture that transport huge amounts of rainfall to (primarily) the West Coast of the U.S. are projected to increase in both frequency and intensity in the future as part of the changing global climate (Gao et al., 2015; Warner et al., 2015). However, the increase in these severe events does not necessarily translate to an increase in mean annual precipitation totals projected for western states (Kossin et al., 2017).

Floods: The fact that both high-intensity hurricanes and atmospheric rivers are projected to increase in frequency and magnitude means that flooding that accompanies these events will likely worsen in regions of impact. Similarly, the fairly confident conclusion that heavy rainfall events will increase across the country means that flooding risk will likely increase in many regions, a trend corroborated by observed increases in flood frequency and annual peak streamflows throughout the central U.S. and Mississippi River Valley in recent decades (Mallakpour and Villarini, 2015; McCabe et al., 2014; Wehner et al., 2017).

Inequities in Vulnerability

A large body of literature focuses on how various types of social vulnerability intersect with storms and displacement. In many regions, low-income or otherwise socially vulnerable communities are more likely to live in areas of higher risk to natural hazards than other residents, due to a legacy of segregation, siting of subsidized housing, and lower housing costs in higher risk areas. These disparities are often most pronounced in rapidly growing urban areas, such as Houston, Texas, or the greater Sacramento, California, area, where sprawl into high-risk areas, such as floodplains, has occurred due to the shortage of available land and housing closer to the city center (Burby et al., 2001; Godschalk, 1999; Paterson, 1998). One study of Austin, Texas, revealed that the proportion of low-income residents living in floodplains increased dramatically between 1990 and 2000 due to low property prices in those areas (Lee and Jung, 2014). Non-white, low-income, less educated residents in Houston also made up the bulk of the population in areas most impacted by flooding during Hurricane Harvey in 2017, partly due to a legacy of discriminatory housing policies precluding such residents from obtaining housing in more desirable and resilient neighborhoods, as well as under-investment in flood mitigation in these neighborhoods (Deaton, 2017; Greater Houston Flood Mitigation Consortium, 2019; Krause and Reeves, 2017). During Hurricane Katrina in 2005, low-income, black residents were the most likely to experience flooding, with renters and unemployed populations also disproportionately impacted (Frey and Singer, 2006; Graif, 2006).

These disparities are enabled and reinforced by the siting of public housing projects in high-risk floodplains. Roughly 8–9% of all subsidized or public housing projects are located in 100-year or 500-year floodplains, often due to the availability of cheap land and in conjunction with the Department of Housing and Urban Development's lack of a comprehensive flood risk policy (Mervosh, 2019; Peri et al., 2017; Rosoff and Yager, 2017). While flood risk has not historically been a part of Fair Housing conversations, these location decisions broadly fit a pattern of public housing being sited in areas of relatively less opportunity (Rabe Thomas, 2019; Rothstein, 2017). Moreover, flood maps maintained by FEMA, which inform the agency's National Flood Insurance Program, have been shown to be outdated or inaccurate in many instances and do not account for future trends resultant from a changing climate, such as sea-level rise, fueling a cycle of over-development, and under-insurance of communities located within floodplains (Bruggers, 2018; Rosoff and Yager, 2017; Scata, 2019; Wing, 2018). One study estimates that after accounting for updated flood frequencies and housing development in high risk areas, the population exposed to severe flooding in the U.S. is roughly triple that of previous, official estimates (Wing et al., 2018).

There is also differential vulnerability to climate hazards depending on the quality of housing stock. Low-income, non-white renters have been shown to be most likely to occupy older,

substandard housing built to lower building codes with less maintenance, increasing the risk of structural collapse, damage, or bodily harm in the event of a disaster (Burby et al., 2003; Fussell 2015; Krause and Reeves, 2017; Rosenbaum, 1996). Hurricane Maria in 2017 in Puerto Rico, for example, inflicted significantly more damage on low-income, often informally built housing structures as compared to those in more affluent areas built with stronger materials and under stricter building codes (Viglucci, 2018). One study found that living in low-quality housing, especially mobile home units, was one of the strongest predictors of tornado-related fatalities (2,587 deaths from 1980 to 2019) in the U.S (Lim et al., 2017; NOAA - NWS, 2019).

Many socially vulnerable communities also tend to be located closer to facilities containing hazardous materials, which may escape containment in times of storms and floods, potentially exposing nearby residents to dangerous contaminants (Bullard et al., 2008; Burby et al., 2003; Crowder and Downey, 2010; Krause and Reeves, 2017). Nearly 75% of the 82 Superfund sites (federally managed pollution remediation sites) that were located in counties impacted by Hurricane Harvey are in low-income and/or communities of color, a number of which experienced containment breaches during the storm, leading to concerns about toxic waste spreading into homes and neighborhoods (Baptiste, 2017). Additionally, disparities in evacuation rates and abilities have been observed across different communities in past storms. Specifically, renter, single-parent, low-income, and non-white households have exhibited slower, and lower overall rates of evacuation during major hurricanes, partly because they are closer to congested city centers and their residents have less access to personal vehicles (Cutter and Emrich, 2006; Van Zandt et al., 2012).

Driving Displacement and Inequities in Recovery

Major storm and flooding events often directly displace hundreds of thousands of people from their homes every year in the United States. For example, the 10 hurricanes of the Atlantic hurricane season of 2017 resulted in more than 3,300 deaths, nearly $300 billion in damage (the costliest season on record), and several million evacuees, damaging or destroying over a million homes, primarily in Puerto Rico during Hurricane Maria, and southeast Texas during Hurricane Harvey (NOAA, 2018). Early that same year, a number of consecutive atmospheric river storms struck California, resulting in the flooding of numerous communities, over $2 billion in damage and contributing to the partial failure of the Oroville Dam's main spillway, causing the evacuation of nearly 200,000 people. While many evacuees were able to return home relatively quickly, there were many who could not due to the loss of their homes or property and were thus permanently displaced.

The inequities in vulnerability discussed in the previous section put certain communities at higher risk of being displaced following disasters. Following Hurricane Katrina, which triggered the evacuation of some 1.7 million people, it has been shown that black residents were slower to return to New Orleans than white residents and were more likely to remain permanently displaced (Frey et al., 2007; Fussell et al., 2010; Graif, 2016). This was partly due to the fact that black residents were more likely to have been living in older homes located in high-risk flood zones, incurring greater property damage as a result. Additionally, limited social infrastructure for vulnerable residents to return in the context of privatized recovery efforts also played a role (Adams et al., 2009; Klein, 2007). A year after the hurricane, many residents were still unable to return home, though the differences between different races were stark; the white population at

this time was at 64% of pre-storm levels, while the black population of the city was at a mere 43% of pre-storm levels, failing to fully recover in subsequent years (Frey et al., 2007; Groen and Povlika, 2010). Similarly, the share of low-income and less-educated residents declined following the storm, with residents who had been living in subsidized rental units 70% less likely to be in their homes following Katrina than those living in market-rate units (Fussell and Harris, 2014).

Rental units also tend to be reconstructed more slowly or not at all compared to owner-occupied homes and high-value units (Fussell, 2015; Peacock et al., 2014; Zhang and Peacock, 2009). As seen in New Orleans following Hurricane Katrina, the damage-induced shortage in housing stock following disasters often causes a sharp increase in prices and can play a role in long-term neighborhood change or gentrification (Fussell et al., 2010; Peacock et al., 2014). Market-rate housing prices in New Orleans spiked by more than 40% in the months following the disaster and continued to rise in many neighborhoods (Levine et al., 2007; Opdyke, 2005). Following Hurricane Harvey, Houston has experienced similarly high rental prices due to increased demand from displaced tenants and reduced supply, as well as substantial losses for lower-income homeowners that could not afford to repair their homes, repay mortgage loans, or pay for short-term housing (Dickerson, 2017).

Additionally, choices made about redevelopment can accelerate neighborhood change. In New Orleans, for example, four large public housing developments that had sustained damages were redeveloped by the city into mixed-income units, contributing to a decline in the number of residents of public housing from roughly 5,000 pre-Katrina to just 1,900 following the storm (Fussell, 2015; Mitchell et al., 2011; Mueller et al., 2011). Not only were many residents not able to return, but some public housing demolition was viewed by residents as paving the way for accelerated gentrification, for example in the Treme neighborhood (Crutcher, 2010). Indeed, subsidized housing demolition can play a role in indirect displacement, gentrification, and demographic change (Goetz, 2011); when neighborhoods do gentrify around subsidized housing projects, the preservation of these projects can help ensure more diversity and access to opportunity in gentrifying neighborhoods (Dastrup and Ellen, 2016).

The structure and administration of federal recovery assistance programs, such as the Federal Emergency Management Agency (FEMA), have also been shown to exacerbate inequalities following some disasters. FEMA is the main source of reconstruction funding for households, but there is significant variation in coverage across geographies and socioeconomic status (Peacock et al., 2014). Government emergency assistance programs are primarily designed to restore wealth, and therefore primarily benefit homeowners, particularly those with more valuable properties (Comerio, 1997; Fussell and Harris, 2014; Hersher and Benincasa, 2019; Kamel, 2012; Mueller et al., 2011; Vigdor, 2008; Zhang and Peacock, 2009). Following Hurricane Katrina, low-income households and households of color were more likely to report insurance payments that were inadequate to meet repair and recovery needs, in part because of inadequate federal insurance coverage in low-income communities, especially communities of color (Peacock et al., 2014). Following Hurricane Harvey, white and upper-income residents were more likely to receive assistance from FEMA than black residents, even though the latter reported greater property damage (Hamel et al., 2017). The receipt of federal funds is also often slow and delayed, leaving at-risk and displaced households discouraged and waiting for crucially

needed funds (Blakely, 2008; Bubenik, 2018; Dickerson, 2017; Morris, 2018; Olshansky et al., 2008). One report from 2019 examined the financial impacts faced by homeowners following recent natural disasters and found racial inequities in credit score declines for homeowners hit by disasters, with communities of color experiencing a much larger decline on average than majority-white communities (Ratcliffe et al., 2019). Additionally, increases in mortgage delinquency and foreclosures for homeowners who have experienced natural disasters are more common than for those who have not, which can make sources of credit more difficult or expensive to obtain in the future.

Policy Highlights

Addressing the combined threats of storms and displacement is a complex undertaking for local, state, and federal agencies. The proposals to address storm and flood risk in the first place include updating federal flood maps, limiting development in high-risk areas, and strengthening protective infrastructure (Wing et al., 2018). Using social vulnerability maps to inform emergency mapping and recovery planning can help improve community resilience because socially vulnerable communities tend to be among the most impacted by disasters (Van Zandt et al., 2012).

In the aftermath of storms, then, Zhang and Peacock (2009) suggest that state and local governments impose moratoria on foreclosures and insurance cancellations during times of emergency, provide incentives to encourage the rebuilding of low-income and rental properties, reuse abandoned properties, and work with land bank programs to stabilize housing prices following disasters. In Houston, there are some examples of such efforts, including dedication of public land to affordable housing and strengthening community land trusts. Additionally, equitable recovery efforts in Houston aim to address unclear or “tangled title” issues complicating recovery funding access for low-income homeowners, as well as to provide increased access to recovery dollars for renters, and to improve housing quality for older apartments (Miller and Goodman, 2019). Calls for equitable recovery post-Hurricane Irma in Florida in 2017 include direct assistance to displaced tenants, replacement of mobile homes with high-quality, safe homes, and analysis of racial disparities in funding (Community Justice Project, 2018). Also, a rapid rehousing model out of Houston called Rapido – in which builders use pre-assembled temporary housing cores that can quickly expand to house more families – is getting attention. The backbone of this temporary-to-permanent model is the pre-planning efforts that cities and counties must undertake in advance of disasters to make permitting, funding, and implementation of effective disaster housing relief possible. (Binkovitz, 2016).

Local disaster recovery relief distribution programs should not only be analyzed, but also reformed to ensure an equitable apportionment of federal aid to victims after storms. This would help prevent instances like the lopsided assistance seen following Hurricane Harvey, in which wealthy, white, politically vocal residents received dramatically more aid than more heavily impacted disadvantaged communities of color (Capps, 2018).

Climate Shock: Wildfires

Climate Context

Decreasing summer precipitation, rising temperatures, increased lightning strikes, drier land and earlier spring snowmelt are all contributing to a lengthening and intensification of the fire season in the western U.S. (Holden et al., 2018; Romps et al., 2014; Westerling et al., 2006). Though this region has historically been prone to large-scale wildfires, especially during the summer and fall months, there has been a significant increase since the mid-1980s in the frequency and size of blazes from the Rocky Mountains westward (Higuera et al., 2015; Running, 2006; Westerling et al., 2016). In California, 15 of the state's 20 largest and most destructive fires have occurred since the year 2000 (CAL-FIRE 2019). Population growth throughout the region has contributed to an increase in human-induced wildfires over this time period (Byrant and Westerling, 2014). However, the principal increase in wildfires observed in recent decades has been due to an uptick of natural, lightning-induced fires.

Decades of forest management that focused on fire suppression rather than allowing periodic burns resulted in an overabundance of brush and vegetation, which has created conditions conducive to particularly destructive fires (Moore et al., 1999; Stephens et al., 2013; Westerling, 2016). These fuel-rich conditions, combined with higher temperatures that desiccate the landscape and increase the frequency of lightning strikes, have resulted in the significant surge in fires observed in recent years. (Wehner et al., 2017; Romps et al., 2014). One study showed that human-caused changes to the climate were likely responsible for much of the increased aridity in forests since the early 1970s and a doubling of burned forest area since the mid-1980s (Abatzoglou and Williams, 2016). Therefore, wildfires from both human and natural causes are fueled by changing physical and climate conditions and are projected to worsen in the coming decades, especially for western states, including Alaska (Flannigan et al., 2009; Westerling et al., 2011; Westerling et al., 2016; Young et al., 2016).

Inequities in Vulnerability

Given current trajectories of climate conditions and human development in the western U.S., it is estimated that residential wildfire risk will increase by a factor of three to four by the middle of this century, even under scenarios of global reduction of GHG emissions (Bryant and Westerling, 2008). Residential areas most at risk are those in the "wildland-urban interface" (WUI), populated zones among or adjacent to wildland vegetation (Berger and Susskind, 2018). The extent of the WUI in the U.S. has increased dramatically in recent years, due to the construction of some 12 million new homes between 1990 and 2010 in these areas, and WUI housing is estimated to be the most rapidly growing type of land-use in the conterminous U.S. (Radeloff et al., 2018). In California, it is estimated that some 11 million people, roughly a quarter of the state's population, live in areas of high-wildfire risk (California Wildfire Strike Force, 2019; NAIC, 2019). There are numerous reasons for this rapid expansion of development in WUI areas, but a major driving factor cited by California's governor, Gavin Newsom, is the housing affordability crisis throughout the state and many major cities in the broader region (California Wildfire Strike Force, 2019). The lack of affordable housing supply in the state's urban centers has driven many people to more affordable housing zones, many of which are located on the fringe of towns and urban centers, often in high-risk, WUI areas (California Wildfire Strike Force, 2019; Kasler, 2019; NAIC, 2019; Peterman et al., 2019; Thompson, 2019).

Exposure to wildfires is not limited to a single demographic or community type, though there have been a number of studies highlighting disparate patterns of fire risk across income and other

factors of social vulnerability in certain regions. One 2003 study estimated that a third of residents in WUI areas across the western U.S. struggled to cover the costs of basic needs, let alone additional costs of investing in fire mitigation projects and home renovations (Lynn, 2003). In the case of the devastating 2018 Camp Fire in Butte County, California, which claimed the lives of 85 people and forced over 50,000 people to evacuate, 14% of the affected residents were living below the poverty line and a quarter of them were reliant on Medicare or Medicaid for health insurance (Squires, 2018). Two analyses of the southeastern U.S. found that in six states there were numerous areas where high wildfire risk was correlated with high social vulnerability, as defined by poverty rates, race, level of education, and housing tenure, and that these communities lacked access to fire mitigation programs (Gaither et al., 2011; Poudyal et al., 2012). A similar study of the Pacific Northwest found that poor households disproportionately occupied high-risk zones and had less fire response capabilities compared to more affluent regions (Lynn and Gerlitz, 2006). In California's Tuolumne County, where some 80% of housing units are in high or extreme-risk areas, 40% of the population is older than 60, meaning there is a disproportionate exposure of elderly residents to wildfire throughout the county, a pattern shared by a number of neighboring foothill counties (Shuman, 2019). While patterns of disproportionate vulnerability across income levels, age or other demographic characteristics are not universal across the country, due to the diversity of income classes and community types occupying WUI zones such patterns are important to consider at the community-scale in order to identify potentially vulnerable sub-groups.

Driving Displacement and Inequities in Recovery

Catastrophic wildfires have resulted in the direct displacement of hundreds of thousands of people, many of them permanently. In the latter half of 2018, alone, there were an estimated 350,000 people displaced in California due to evacuation orders and destruction of their homes. These fire refugees found themselves in overcrowded shelters ill-equipped to house and supply the influx of people (Sellers, 2018). Multiple disease outbreaks were documented in such shelters and many people resorted to sleeping in their cars or outside, despite poor air quality and subsequent rainstorms (Squires, 2018; Wootson, 2018). Due to the extent of destruction and the prohibitive costs of rebuilding, many have been unable to return home, instead left to search for housing in a state with a chronic housing shortage and affordability crisis. As a result, many families have been left marginally housed, meaning, for example, they stay in a series of motels, paying up to ten times what they had paid in monthly rent before the fire, and ultimately looking to neighboring counties or states for available housing; many evacuees remain homeless, and several can be found in homeless encampments in the Bay Area's major cities, such as Oakland (Fuller and Haner, 2019; Sellers, 2018).

Many individuals who lost their homes to wildfires in previous years have remained homeless due not only to the lack of affordable housing but also to inadequate recovery assistance (Fuller and Haner, 2019; Mockrin et al., 2015). Relying on federal assistance to rebuild and recover has proven to be a slow and complex process for many, and the mechanisms for paying liabilities for utility-caused fires, such as the Tubbs and Camp Fires in California, have been shown to be insufficient and unsustainable for both recipients, ratepayers, and shareholders (Mockrin et al., 2015; Peterman et al., 2019). Newly constructed homes are often also subject to more stringent regulations requiring them to be made of fire-resistant materials, which can add to the cost of reconstruction and discourage some displaced homeowners from rebuilding altogether (Passy,

2018). Recovery for renters following fires is particularly difficult. The majority of renters nationwide lack renter's insurance, preventing them from receiving compensation for belongings lost in fires. Even those with insurance are left without support to find a new home due to the fact that most renter insurance plans do not provide relocation support in the event of a natural disaster (Marcus and Verma, 2017).

Even if they don't lose their homes and are not permanently displaced, those who live in a high-risk area may still face indirect displacement, due either to increased home insurance premiums or to the decrease in available housing stock in areas recently impacted by fire. Insurance payouts from the 2017 and 2018 California wildfire seasons amounted to some $26 billion, causing many insurance companies to eliminate high-risk properties from their portfolios and/or increase premiums on those they retain (Makaula, 2019; The Allstate Corp., 2018). Many residents in high-risk zones of western states have reported having their policies abruptly canceled, while others report facing instant rate increases of 200–500%, resulting in monthly premiums as high as $5,000–$7,000 (Makaula, 2019; Quinton, 2019; Smith, 2016; Shuman, 2019). For states like Montana and Idaho, where more than a quarter of all available housing stock is located in high-risk fire zones, the resulting high cost of home insurance alone has precluded many from being able to afford a home and has pressured others to relocate (Kasler, 2019). According to California's Department of Insurance, average rates in WUI zones are 50% higher than in the remainder of the state (Peterman et al., 2019). Not only are insurance rates in high-risk zones becoming dramatically more expensive, but in many cases, insurance is virtually impossible to obtain, as more companies decline to insure properties deemed too risky (Shuman, 2019; Thompson, 2019). This results in many residents resorting to unregulated "surplus" insurance plans or plans offered through state agencies, such as California's Fair Access to Insurance Requirements Plan, which tend to provide minimal coverage at very high cost (Peterman et al., 2019; Smith, 2016). Major utility-caused wildfires – such as the Tubbs and Camp Fires – have resulted in lawsuits, sinking utility stock prices, and mandatory fire mitigation investments. The costs of capital improvements to utility infrastructure then gets passed on to customers in the form of increased utility rates, which can be an additional, indirect cause of displacement for residents already facing high housing and insurance costs (Peterman et al., 2019).

In summary, growing fire risk due to climate change and increasing insurance and utility rates have converged with pre-existing shortages in affordable housing to create a unique landscape of direct and indirect displacement pressures, especially in western states, in a trend that is projected to worsen in decades to come.

Policy Highlights

A number of local, state and federal-level policy solutions have been proposed in recent years in an attempt to mitigate fire risk, improve post-fire recovery processes, and stabilize insurance rate hikes for homeowners. In December 2019, California imposed a one-year moratorium prohibiting insurance companies from dropping customers in fire-affected areas in order to prevent further financial burdens for victims, though critics cite the need for a longer-term, comprehensive solution (Serna, 2019). Many such policies are outlined in a report by the California Governor's Strike Force on Wildfires and Climate Change. These include recommendations to deprioritize new development in extreme fire risk areas and prioritize the

development of infill lots and overall housing production across the state, especially in low-risk urban areas. The report also proposes increasingly stringent wildland building codes and promises to provide a list of low-cost retrofits that homeowners can implement in order to improve the safety of their homes against fires. It also suggests improvements to local policies, such as fire risk assessments and evacuation plans. Additionally, the report recommends that the state's Department of Insurance begin to analyze trends in rate hikes in fire-prone areas to assess the increased burden being placed on residents – important information needed to curb displacement (CA Wildfire Strike Force, 2019). Other suggestions of climate-smart fire policies include implementing state-level policies requiring increased defensible space surrounding homes and encouraging more local Volunteer Organizations Active in Disasters (VOADs) in order to help rural communities access aid for post-fire recovery (Bryant and Westerling, 2014; Edgeley, 2017). Finally, in California, the Governor's declaration of a State of Emergency following wildfires in fall 2019 required landlords to justify any rent increase above 10 percent (California Office of the Attorney General). Since then, state legislation has passed capping rents for many rental units across the state. Following wildfires, this kind of renter protection may make the difference in whether people in low-income households are able to return.

Climate Stressor: Sea-Level Rise and Nuisance Flooding

Climate Context

Globally, it has been estimated that average sea-levels rose by roughly 7–8 inches from 1900 to present, with an additional rise of 12–98 inches (1.0–8.2 ft) in store by 2100 (Sweet et al., 2017). The exact amount of SLR is dependent on both global greenhouse gas (GHG) emissions and rates of ice-melt from places like Greenland and Antarctica, a process shown to be accelerating faster than previously thought (Dangendorf et al., 2017; Kopp et al., 2017; Kulp and Strauss, 2019). Rising sea levels and increased tidal flooding impact coastal communities throughout the U.S. and can act both as a direct and indirect driver of displacement. SLR is classified here as a climate stressor because, while it does exacerbate coastal surges of seawater during major storms, the underlying processes driving it are gradual and continuous and its (non-storm) effects are generally not life-threatening. Its physical impacts include the damage and destruction of homes and property, damage to important infrastructure such as roads and freeways, and the disruption of emergency operations.

One consequence of SLR in the U.S. is the increased frequency and extent of tidal flooding, also referred to as "nuisance," or "sunny day," flooding in coastal areas, which will only continue to worsen in coming decades. These events result from cyclical tidal patterns throughout the year and, depending on the geography and infrastructure of a given coastal community, can inundate and damage roads, beaches and walkways, homes and property. Between 1960 and 2010, the average number of tidal flooding days occurring each year in cities like Charleston, Annapolis and Baltimore has increased dramatically – up to 9 times the historical average in some places – costing tens of millions of dollars in damages and impacted economic activity (Sweet et al., 2014). Additionally, there is new research suggesting that the spatial extent of future SLR and its impact on coastal communities may be far greater than previously anticipated, estimating that globally, the number of people living in areas today that will be within high-tide zones by 2100 is about 190 million, roughly tripling previous estimates (Kulp and Strauss, 2019). SLR not only

impacts coastal cities via tidal flooding but also leads to the intrusion of saltwater into freshwater supplies that currently serve critical drinking water and ecological needs in some regions, such as South Florida and California (Curtis and Schneider, 2011; Lund et al., 2010; Noss et al., 2011; SFRCCC, 2015).

Inequities in Vulnerability

In the U.S., coastal counties make up roughly 40% of the country's population and in many of these counties tidal flooding and SLR have disproportionately impacted low-income and communities of color (Kusnetz, 2018; Morris, 2018; NOAA - OCM, 2019). In Atlantic City, New Jersey, working class communities in low-lying coastal areas have been some of the most impacted from nuisance flooding in recent years. However, the bulk of local municipal and federal protection efforts has been on constructing barriers along the downtown corridor and in front of wealthy, oceanfront neighborhoods (Upton, 2017). Many critics argue that such adaptation is guided by a desire to mitigate economic damages, but does not adequately address issues of social vulnerability and equity (Heberger et al., 2009; Martinich et al., 2013; Upton, 2017). One study found that in ten California counties throughout the San Francisco Bay Area and North Coast, populations vulnerable to SLR were disproportionately made up of people of color (Heberger et al., 2009). A similar analysis of the U.S. found that in many areas, socially vulnerable communities, as defined primarily by wealth and race, are disparately exposed to flooding by rising sea levels and less likely to be protected, a trend that is especially pronounced in the Gulf Coast region (Martinich et al., 2013).

Generally speaking, the resources needed to combat the effects of SLR are less available to lower-income communities and socially vulnerable groups. The amount of financial resources needed to build or upgrade seawalls and barriers, retrofit homes and buildings, make repairs following flooding, and ultimately to relocate, can be out of reach for many less-wealthy residents and communities (Curtis and Schneider, 2011). Political buy-in required to organize attention around these efforts and garner external funding and support can also be difficult to attain in vulnerable communities already lacking political voice (Hardy et al., 2017). In general, recovering from flooding events and SLR-related damage is much harder for lower-income residents, given the fact that many assistance and recovery programs are designed to restore wealth, which tends to favor residents with higher-value assets to begin with (Elliott and Howell, 2017; Howell and Elliott, 2018; Pais and Elliott, 2008). One study found that low-income homeowners whose wealth rests largely within their home values are unlikely to recover from the economic losses incurred if their homes are destroyed by flooding (Sarmiento and Miller, 2006).

Driving Displacement

The influence that sea-level rise has on the displacement of people in the United States is complex and will likely have related impacts that ripple throughout the country. SLR displaces people both directly, by inundating their homes and communities, as well as indirectly, by decreasing viable housing supply, increasing home insurance rates, diminishing regional economic opportunities and, in some cases, impacting local groundwater supplies. In Florida, where tidal flooding has already become commonplace in many cities, Curtis and Schneider (2011) estimate that upwards of 9.9 million people will be at risk of direct displacement by 2030. An additional 10 million people are likely to face flooding and potential direct displacement

from SLR-related impacts in California, South Carolina, and New Jersey combined (Curtis and Schneider, 2011). However, despite these increasing risks, housing growth rates in many high-risk flood zones in coastal states are accelerating. In New Jersey, there were nearly 3.5 times as many homes built in high-risk flood zones as in low-risk areas in the state from 2010 to 2016 (Climate Central and Zillow, 2018). While coastal communities will bear the direct impacts of these hazards, the resultant redistribution of population from these communities has the potential to impact states across the country as they are tasked with receiving and integrating those fleeing the threat of inundation (Hauer, 2017; Keenan, 2018).

As with many climate stressors (as opposed to shocks), some displacement pressures that burden residents from SLR can be diffuse and indirect. For example, SLR and nuisance flooding can increase insurance rates. In New Jersey, many residents received letters from the Federal Emergency Management Agency (FEMA) that their flood insurance rates would be increased by 5–18% annually due to risks from SLR; this itself can create significant displacement pressure for residents (Upton, 2017). Moftakhari et al. (2017) find that the cumulative cost of frequent nuisance flooding in Miami may exceed the cost of extreme but infrequent storm events. In another study on flooding in Miami, McAlpine and Porter (2018) estimate that, between 2005 and 2016, properties projected to be flooded by 2032 had already collectively lost over $465 million in market value. Overall, the housing market saw a decrease in almost $16 billion of home values along the eastern and Gulf coasts of the U.S. from 2005 to 2017 and industry leaders are explicitly expressing concern regarding displacement from SLR (Freddie Mac, 2016; McAlpine and Porter, 2019). While lower property values can translate to lower housing prices and therefore potentially offset economic displacement pressures faced from increased insurance prices, they can also result in "trapped populations" – those who cannot afford to sell their devalued homes for a loss, even if they are being compelled to do so by climate hazards (Freddie Mac, 2016; Upton, 2017). Lower prices in high-risk zones will also exacerbate disparate exposure of low-income residents to climate impacts, as they may be pushed to these areas due to affordability pressures.

In some areas, neighborhood change ushered in by the occurrence and perceived fear of future SLR has resulted in the displacement of long-time residents. Many long-time residents, whose families were originally excluded from desirable, beachfront neighborhoods due to racist, redlining policies, are now finding themselves evicted or priced out of their homes with few affordable housing options nearby (Campo-Flores and Kusisto, 2019; Green, 2019). One recent study showed that in Miami-Dade County, Florida, a region highly vulnerable to SLR, higher elevation properties have been appreciating in price faster than those at lower elevations, fueling regional "climate gentrification" in some neighborhoods (Keenan et al., 2018). Little Haiti is one such Miami neighborhood. Historically home to low-income and minority communities, it is becoming increasingly sought after by wealthy home buyers and developers due to its higher elevation (Green, 2019). This trend has resulted in housing price increases in Little Haiti that are double that of the city average as well as waves of evictions that have displaced residents and local businesses (Campo-Flores and Kusisto, 2019; Green, 2018; Green, 2019). This is one of many examples of communities that are experiencing climate-influenced gentrification across the country, a trend that is likely to increase as climate hazards intensify. In Seattle's Duwamish Valley, the Duwamish River Cleanup Coalition sees a cycle of SLR inundating the industrial area and then leading to infrastructure and public health investments that raise property values and

represent displacement pressures on long-term residents; as is described in the following section, this leads the Coalition to simultaneously focus on protecting the environment, empowering community, and promoting place-keeping (Lopez, 2019).

Policy Highlights

Given the complex nature of sea-level rise and its effects on the direct and indirect displacement of people in coastal communities, identifying and implementing effective policies can be a challenge. First and foremost, local, state, and federal agencies must acknowledge and assess the intersections of SLR, displacement and the shortage of affordable housing, and then craft responses accordingly. The city of Miami is attempting to do this, adopting a resolution last year to explicitly research climate change-driven gentrification in areas such as Little Haiti and to investigate methods to prevent displacement (City of Miami, 2018). This is in addition to $100 million allocated to affordable housing as part of the city's climate resilience-oriented Miami Forever Bond and adoption of inclusionary zoning policies to encourage denser development with more affordable units (City of Miami, 2019; Flechas and Harris, 2018). However, local advocacy groups such as the Family Action Network Movement, Catalyst Miami and the Community Justice Project are urging for more comprehensive solutions to the climate-driven displacement crisis in the city, such as community-driven development and climate resiliency planning, public land banking, revolving loan funds, improving the climate resilience of affordable housing, investing in green jobs and nurturing local, 'circular' economies (Adrien and Page, 2019; Bastien, 2019; Boyd, 2019; Duffrin, 2019). One example of collaborative, community-driven planning to improve coastal climate resilience while preventing displacement is Seattle's recent Duwamish Valley Action Plan, which details plans for improving green infrastructure, public health, increasing affordable housing and counteracting displacement. This includes economic development, such as hiring locally on city projects and providing funding for a coalition of residents to become affordable housing developers, particularly in the South Park neighborhood, which is "ground zero" for SLR in Seattle (City of Seattle, 2018; Duffrin, 2019; Lopez, 2019).

Climate Stressor: Extreme Heat

Climate Context

As average annual temperatures increase globally from year to year, extreme heat becomes more commonplace in many regions of the world and can drive displacement by increasing utility costs, necessitating building upgrades that spur evictions, and creating adverse health impacts for vulnerable community members. Heat waves and daily extreme temperatures are becoming more intense and more frequent in many communities and the effect of urban heat islands more pronounced (Vose et al., 2017). By the middle of this century, scholars estimate that mean temperatures of extreme heat waves (those that occur on average once per decade and last 5 days or longer) in the U.S. will increase by nearly 11°F, with the potential for even higher increases in the country's northern regions (Sun et al., 2015). However, in terms of total number of extreme heat days per year, the Southeast and Southwest will be the hottest in the country (Sun et al., 2015). By late century, high temperatures that currently only occur every 20 years, on average, will likely occur every year. Similarly, 1-in-20-year minimum temperatures will likely cease to occur (Wuebbles et al., 2014). In the same timeframe, the average number of days exceeding

100°F nationwide will likely double, and those above 105°F will quadruple (Dahl et al., 2019). Even assuming no future population growth, the number of people in the United States who will be exposed to 30 or more days each year with a heat index of 105°F or higher will likely increase from below one million people currently to over 90 million by the year 2050, and to 180 million by 2100 (Dahl et al., 2019).

Inequities in Vulnerability and Driving Displacement

Across the United States, high temperatures have been shown to have unevenly distributed impacts, with sick, elderly, low-income, non-white, homeless and other historically marginalized people most affected (Harlan et al., 2006; Reid et al., 2009). Heat waves and chronically high temperatures can present deadly health risks by increasing rates of heart attacks, heat strokes, and other cardiovascular and respiratory mortality (Curriero et al., 2002; Medina-Ramón et al., 2006). In 1995, more than 700 people were killed during a heat wave in Chicago, many of whom were isolated, elderly, African-American residents living in apartments without air conditioning (Klinenberg, 1999). In 2006, a severe heat wave in California's Central Valley killed at least 146 people, the majority of whom were members of Latinx farm laborer communities facing high levels of heat exposure while working outdoors (Knowlton et al., 2009; Mera et al., 2015). One study estimates that an increase of 5°F in average annual temperatures, which corresponds to a low-to-moderate GHG emissions scenario by the end of this century, could result in nearly 2,000 additional heat-related deaths nationwide each summer (Bobb et al., 2014).

Staying cool during heat waves and increasingly long and hot summers is vitally important, but can be difficult, expensive, or impossible for many, especially in disadvantaged communities. One study in New York City revealed that some 30% of residents in the city's most impoverished neighborhoods did not have air conditioning in their homes, compared to only 1% of those in the wealthiest neighborhoods (Ito et al., 2018). Another study of New York City found that poverty and access to air conditioning were strong predictors of heat-related mortality among seniors (Rosenthal et al., 2014). Racial inequities in access to air conditioning and resultant disproportionality of heat-related deaths have also been well-documented across the U.S. (Fletcher et al., 2012; Harlan, 2006; Jesdale, 2013; Mitchell, 2014; O'Neill et al., 2005; Rosenthal et al., 2014). For example, an analysis of Chicago, Detroit, Minneapolis and Pittsburgh found that air conditioning prevalence in black households was less than half of what it was in white households, and that deaths among black residents were more strongly associated with heat waves as compared to white residents (O'Neill et al., 2005).

While households without pre-existing AC units experience increased pressure to purchase cooling units, numerous household surveys cite cost pressures as a common reason for going without. Increased cooling needs during heat waves and summer months result in higher expenditures on electricity for powering AC, fans and other methods of cooling. The increased financial burden of additional cooling-related expenditures can be substantial for many households, especially for renters and low-income residents (Cook et al., 2008; Hernandez and Bird, 2010). Tenants already struggling to pay rent and other bills are often forced to decide between buying food or paying for electricity (Bhattacharaya et al., 2003; Evens, 2017; Harrison and Popke, 2011; Hernandez and Bird, 2010). An energy spending analysis for all U.S. households from 2001 to 2012 found that while households with annual incomes of $50,000 or greater spend on average 3% of their income on electricity, households making less than $10,000

annually spend about 33% of their incomes just to keep the lights on (ACCCE, 2013). This disproportionate burden is due not only to differences in incomes but also in housing quality and cooling efficiency, with houses and rental units in low-income and non-white areas tending to be older, poorly insulated and subject to neglect from landlords (Bednar, 2016; Boardman, 2013; Evans, 2004).

For many of these households, missed or delayed utility payments can exacerbate existing cycles of debt via late fees, power shut-offs, and additional charges for reconnection (Evens, 2017; Halpern-Meekin et al., 2015; Hernandez and Bird, 2010). In a number of recent instances, power shut-offs have even resulted in the deaths of a number of elderly residents who had their electricity cut in months when extreme heat waves afflicted their communities (Dahl et al., 2019). Currently, only 9 states have high temperature-based power cutoff restrictions (Dahl et al., 2019). Limited evidence also suggests that increased energy burdens may drive displacement by increasing the likelihood of evictions for renters. One recent study found that, with all other factors held constant, there was a strong causal relationship between an increased monthly electric utility bill and the probability of receiving an eviction notice (Finnigan and Meagher, 2016). Building upgrades and retrofits, while needed to lessen the energy burden on renters, may create additional vulnerabilities for low-income renters if the cost of capital improvements is passed on to tenants in the form of increased rent (Hernandez and Phillips, 2015).

Many low-income communities and communities of color are also subject to urban heat island effects – the phenomena by which urban areas experience higher temperatures than surrounding rural areas. In some cases, temperature differences between urban centers and surrounding areas can exceed 5°F during the hottest part of the day and by up to 20°F in the early evening (Akbari, 2005; Richards and Bradshaw, 2017). Neighborhoods within cities that generally experience the worst heat island effects are commonly low-income, non-white renter communities that have experienced decades of disinvestment and are densely developed and paved, while being devoid of shade and vegetation (Gronlund, 2014; Harlan, 2006; Jenerette, 2007; Jesdale, 2013; Mitchell, 2014; White-Newsome, 2009). A study of over 100 cities around the country found that neighborhoods that were formerly "redlined" by the Home Owners' Loan Corporation – meaning that they were designated as hazardous areas for real estate investment based primarily on their racial makeup – have on average higher land surface temperatures than non-redlined areas, in some areas by as much as 7 degrees Celsius. (Hoffman et al., 2020; Rothstein, 2017).

Though evidence has not shown extreme heat to directly displace communities in the same way that acute climate shocks do, extreme heat may drive indirect forms of displacement, principally by increasing energy-related costs – and in some cases the likelihood of evictions – for low-income households. Higher temperatures and increasingly severe and frequent heat waves may also shift market preferences for people overall. Numerous studies have shown that Americans will opt to pay more to avoid excess heat than excess cold, though not all residents can afford to be selective about where they live (Albouy et al., 2016; Fan et al., 2012; Fan et al., 2016). Given that many of the nation's hottest regions (e.g. Southern California) are also areas of major population growth, it is difficult to say if heat-related environmental preferences are, or will be, reflected in the housing market (Albouy et al., 2016). Those who would like to move because of the dangers or discomforts of high heat but cannot afford to do so may constitute "trapped populations" similar to those discussed in the case of sea-level rise.

Policy Highlights

While there have been many policy prescriptions aimed at reducing energy burdens and safeguarding against utility shut offs in the past, many of them have fallen short. The Low Income Home Energy Assistance Program (LIHEAP), for example, which provides utility bill assistance, is only utilized by a small percentage of households that qualify, largely due to uncoordinated outreach and implementation (Colton, 2014; Hernandez and Bird, 2010). Advocates have asserted that a more coordinated, regional approach focusing on energy conservation, energy literacy, and utility rate affordability would be the most effective (Hernandez and Bird, 2010). Increasing the availability of free or subsidized weatherization programs to improve housing efficiency, especially of low-income and rental units, is important, albeit with safeguards to ensure existing tenants are not evicted in the process (Hernandez and Bird, 2010). Tax credits, rebates and low-interest loans can also be employed to help lessen upfront costs for homeowners who would like to improve their homes' cooling efficiency (Bednar, 2016).

Outreach programs explaining the dangers of heat-related illnesses and how to stay cool during heat waves, along with heat-based utility shutoff restrictions should be implemented nationwide (Dahl et al., 2019; O'Neill et al., 2005). California took an important step in this direction in 2017 when Gov. Jerry Brown signed SB 598 into law, which placed additional restrictions on utility shut-offs aimed at protecting vulnerable residents (TURN, 2017). Urban greening projects, such as Los Angeles' goal of planting 90,000 new trees by 2021 as part of its L.A. Green New Deal plan, can have substantial benefits in terms of reducing urban heat island effects and are widely supported among residents (Byrne et al., 2016; The City of Los Angeles, 2019).

Climate Stressor: Drought

Climate Context

Many regions of the world – particularly rural agricultural areas – depend upon regular patterns of rainfall, soil moisture and streamflows in order to grow crops, nourish livestock, and maintain the livelihoods of farming communities. Disruptions to these cycles, such as the occurrence of an extended drought, can induce shortages of food and potable water, fuel regional conflicts, and drive displacement among afflicted communities (Antwi-Agyei et al., 2012; Gleick, 2014; Hannah et al., 2017; Henry et al., 2004; Kelley et al., 2015; Tucker et al., 2010).

Generally speaking, the scientific prognosis regarding trends in rainfall and drought patterns for a given region is less certain than it is regarding temperature. There is, however, fairly high certainty that many dry, subtropical regions (e.g. southern Mexico, Central America, portions of Sub-Saharan Africa, India etc.) will likely experience a higher frequency of droughts by the end of the 21st century due to human-induced climate change and reduced precipitation (IPCC, 2014).This includes regions in the U.S. such as Hawaii, Puerto Rico, the U.S. Virgin Islands, and the U.S.-affiliated Pacific islands, where droughts are projected to increase in both frequency and severity in the coming decades (Gould et al., 2018; Keener et al., 2018). For the contiguous U.S., definitive trends in precipitation are less clear, though changing climate conditions are expected to influence and exacerbate drought conditions in some regions (Wehner et al., 2017). Warmer temperatures will dry the soils of farmlands and decrease the amount of rainfall falling as snow,

which is of critical importance to water systems, particularly in western states dependent on mountain snowpack in winter for water supply throughout the year (Knowles et al., 2006; Mao et al., 2015; Seager et al., 2015; Stewart et al., 2005).

Even if annual precipitation totals do not decline, the earlier melting of snow and reduced snowpack may contribute to hydrologic drought (lack of adequate streamflow) during summer and fall months. (Hidalgo et al., 2009; Pierce et al., 2008). Some studies suggest that the southwestern and south-central regions of the U.S. will likely experience significant rainfall deficits in the spring and summer months, respectively, due to human-induced climate change (Easterling et al., 2017; Ryu and Hayhoe, 2017). Additionally, there have been a number of studies that suggest that major droughts, such as the one in California from 2011 to 2015, are at least partially attributable to human influence on the climate and may be more likely to occur in the future (Angélil et al., 2017; Diffenbaugh et al., 2015; Knutson et al., 2014; Swain et al., 2014).

Inequities in Vulnerability and Driving Displacement

Rainfed agricultural communities in developing nations are particularly vulnerable, and residents often must seek employment in nearby urban centers or neighboring countries during times of drought (Adger et al., 2015; Iglesias et al., 2009; Nawrotzki et al., 2015; Richards and Bradshaw, 2017; Warner, 2009). Globally, millions of people have been documented in recent decades as migrating out of high-risk drought zones, primarily in Africa and South-Central Asia (Richards and Bradshaw, 2017). Within the U.S, however, large-scale irrigation systems, federal subsidies and food imports decrease the vulnerability of agricultural communities and consumers to droughts, as compared to more climate-sensitive, rainfed-farming communities abroad. Therefore, fewer farming communities in the U.S. are forced to abandon their communities due directly to shortages of available food or potable water during a given drought. However, drought can act as a driver of indirect displacement in the U.S, especially for farm laborers seeking consistent employment or for farmers experiencing chronic loss of income during multi-year drought events (Howitt et al., 2015; Lang, 2015). The distinction between “direct” and “indirect” displacement becomes slightly blurred in some of these cases, since droughts themselves do not bring acute, life-threatening climatic hazards. However, those fleeing droughts are often doing so as a direct result of lost employment and ensuing food insecurity, exemplifying how “direct” and “indirect” displacement exist along a continuum (as opposed to a binary classification).

Periods of drought in the U.S. do commonly have disproportionate impacts on certain communities, particularly farm laborer populations, often composed of predominantly low-income, Latinx immigrants. Employment opportunities and income can fluctuate dramatically for these workers depending on the level of productivity for a given agricultural season. At the height of the 2011–2015 California drought, curtailed farm-water deliveries, fallowed croplands and diminished agricultural production meant poverty rates among the farm laborer community throughout California’s Central Valley soared (Lang, 2015). Many California farm laborers were forced into marginal living situations or were driven from their communities in search of work. The small city of Mendota, CA, which has a majority farm-laborer population, saw many of its residents living in shanty towns and makeshift structures. The result was an exodus of many of these residents from the city in search of work elsewhere, such as the

neighboring states of Oregon and Washington (Lang, 2015). While many perceive farm labor to be an inherently mobile and temporary occupation, this has been less true in recent years. The USDA estimated in its 2017 Census of Agriculture that over 80% of farmworkers were not migrants, but rather settled and working at locations within 75 miles of their homes (USDA-ERS, 2020). Therefore, drought-induced migration for these workers is often a costly, major disruption.

Impacts of drought on farmers themselves can also be drastic during times of drought. In 2015 alone, direct agricultural economic losses in California were estimated at about $1.8 billion, with a total economic impact statewide of over $2.7 billion (Howitt et al., 2015). There are few studies that specifically link the stresses of drought with the displacement of farmers within the U.S., but such events undoubtedly increase the debt burden and economic hardships of those affected and likely have diffuse effects in the decision-making process of smaller landholders and younger generations on whether to continue farming. One study does predict a net out-migration of nearly 4% of the adults living in rural counties throughout the country's Corn Belt by 2050 due to drought and other climate-related impacts on the region's crop yields, with even higher predicted values of out-migration by 2100 (Feng et al., 2012).

Drought also has the potential to continue to fuel displacement of people from other countries into the United States. While it remains difficult to confidently identify causal links between specific drought events and subsequent influxes of migrants into the U.S., there is a growing consensus that dry spells and droughts play an important role in the economic decision-making processes of members of vulnerable communities abroad, including the decision whether to emigrate. A recent study by the Inter-American Development Bank and the United Nations World Food Programme concluded that a major drought brought on by El Niño conditions in 2014 throughout Central America's Northern Triangle region (Guatemala, El Salvador, Honduras) caused a "significant increase in irregular migration to the United States" from 2014 to 2016 (IDB et al., 2017). A number of other studies and articles have also cited drought as being a major influencing factor for emigration from Central America to the United States in recent years, a trend that could potentially worsen if drought conditions grow more intense and more frequent, as predicted (Arévalo et al., 2015; IOM et al., 2016; IPCC, 2014; Steffans, 2018).

Policy Spotlight

An effective way to prevent drought-driven displacement among vulnerable communities, such as farm laborers, is to invest in alternative employment opportunities and skills-building programs that allow these workers to supplement their income locally during years of low agricultural production, or allow them to switch sectors altogether. One example is the program offered by the non-profit Proteus Inc. in Fresno, CA – a city in the heart of California's agricultural region – that provides training courses in solar panel design and installation, as well as truck driving (Hecht, 2015). Many current, former and displaced farmworkers have taken advantage of these programs, which are funded in part by the U.S. Department of Labor and the California Employment Development Program, to find new supplemental and full-time careers in more stable industries, including those oriented toward a green energy transition (Hecht, 2015). Programs like these can serve as a blueprint for other agricultural regions throughout the country facing instability due to droughts and climate change.

Question 2 - Unintended Consequences of Mitigation and Adaptation Strategies

Responding to the changing climate requires reducing greenhouse gas emissions (mitigation) as well as planning and preparing for its worsening impacts (adaptation), such as rising sea-levels, heat waves, droughts, fires, storms, and floods. Local and state actors have proposed or implemented a wide variety of climate change mitigation and adaptation (M/A) strategies, including land use, transportation and clean energy policies. These essential actions can, however, have unintended consequences for the communities in which they are applied, namely by raising property and housing values, and thereby contributing to the indirect displacement of vulnerable residents. This section presents findings from the literature on climate M/A measures, including urban greening, transit-oriented development, renewable energy and emissions trading policies, and their potential impacts on housing affordability, displacement, inequality and neighborhood change. Understanding negative impacts that may arise from such strategies can help policymakers weave necessary safeguards into these policies and even potentially leverage "green" investments to address not just climate goals, but those of housing affordability and displacement as well.

It is important to note that many of the policy strategies discussed, such as urban greening initiatives and transit-oriented development, are existing planning concepts that are not inherently climate-related. However, the climate change M/A benefits of such projects have made them common components of local and state climate plans. Unfortunately, there are many gaps in existing research. Much of the literature pertaining to the impacts of climate change M/A policies focuses on the impact of such measures on property and housing values, without directly discussing displacement or gentrification. While increasing property and housing prices may be precursors to displacement in certain cases, few studies explicitly make this connection explicit. Therefore, the discussion here of the ways in which climate M/A policies can act as a driver for indirect displacement and neighborhood change is largely based on this potential connection between higher housing prices and the displacement of economically vulnerable residents, rather than actual evidence of displacement.

In this section we focus primarily on urban greening, transportation, and energy-related adaptation and mitigation measures. Land use densification strategies – such as infill development, upzoning, and urban growth boundaries – may also help reduce greenhouse gas emissions by reducing vehicle miles traveled, and create climate change adaptation benefits through denser development (Cohen, 2018). Our initial review suggests that evidence is mixed on the extent to which these strategies contribute to displacement (Angotti and Morse, 2017; Been et al., 2018; Freemark, 2019; Haninger et al., 2017; Lang and Cavanagh, 2018; Mast, 2019; Nelson et al., 2002; Pough, 2018; Zuk and Chapple, 2016), suggesting a need for further research. There is a stronger body of evidence on urban greening initiatives to support climate mitigation and adaptation efforts, and their role in "green gentrification" if not implemented equitably. As a result, our review focuses primarily on urban greening, rather than densification, as a land use strategy for climate resilience.

Urban Greening

Strategies broadly categorized as urban greening consist of investments such as constructing parks and green space, planting trees and encouraging the use of community gardens and urban agriculture. From a mitigation and adaptation perspective, these initiatives help remove atmospheric carbon, cool urban heat islands, provide locally sourced food, and help manage stormwater runoff. However, we highlight research below that shows that urban greening often increases nearby property and housing prices, which can drive indirect displacement of low-income residents. Therefore, these strategies and investments, important as they are, should be implemented with concern to potential inequitable spillover effects that they may have on surrounding communities.

Parks and Green Space

Parks, open space, and green space refer to land that is undeveloped and reserved for the purposes of formal and informal sport and recreation, preservation of natural environments, provision of green space, and/or urban stormwater management. Parks and open space are generally found to increase property values of surrounding homes, with proximity to parks and park type playing some role in the degree of influence on price. Many of the studies showing this relationship also reveal that proximity to parks has the greatest impact on prices and that there is an observable distance-decay function between parks and homes, meaning that the impact of park proximity on home prices diminishes as the distance between them increases (Bolitzer and Netusil, 2000; Cho et al., 2011a, Conway et al., 2010; Lutzenhiser and Netusil, 2001; Miller, 2001; Nicholls, 2002). In general, evidence shows that passive-use parks (i.e. walking paths, trees, open fields etc.) result in higher premiums in home values than parks serving active recreation users (i.e. basketball, softball, tennis courts) (Crompton, 2005; Crompton, 2001; Hendon et al., 1967; More et al., 1988; Sainsbury, 1964). Findings are mixed regarding the role of park size on surrounding property values, with some studies showing that larger parks are associated with higher values (Lutzenhiser and Netusil, 2001; Miller, 2001), while others find smaller parks reflected in higher home values (Treg, 2010; Miller, 2001). Other factors, such as the relative abundance of park space, nearby home lot-sizes, and surrounding home types may influence the impact that parks have on surrounding property values (Cho et al., 2011b, Dehring and Dunse, 2006; Jim and Chen, 2010; Miller, 2001; Nicholls, 2002).

A smaller body of literature examines the role of parks in facilitating “green gentrification” specifically. A recent paper by Rigolon and Nemeth (2019) tests whether proximity to downtown cores, size, and function of new parks predict future gentrification of surrounding census tracts in 10 major U.S. cities. Their findings show that park type, particularly new greenway parks with walking/biking paths, and park proximity to downtown cores are strong predictors of gentrification, while park size is not. Their results support the findings of other studies focused on gentrification impacts of greenways in the U.S., which found that housing units near new greenway parks, such as the “BeltLine” in Atlanta, the “606” in Chicago, and the “High Line” in New York City, experienced higher price appreciation than those further away, a trend that is particularly pronounced for single family homes in low-income neighborhoods (Immergluck, 2009; Immergluck and Balan, 2018; Loughran, 2014; Rigolon and Nemeth, 2018; Smith et al., 2016).This contributes to declining affordability and potentially untenable property tax increases for low-income homeowners living in close proximity to new greenway projects, and may indirectly drive displacement for such residents.

It is worth noting that urban greening projects not only have the potential to usher in indirect displacement, but in some cases can lead to direct displacement. For example, in Atlanta, a water drainage tunnel built for the 1996 Olympics terminated in the neighborhood of Peoplestown south of downtown, and caused flooding that worsened following heavy rains in 2006 and 2012.The city is using eminent domain on several houses in the neighborhood to construct a park and pond as mitigation measures and residents have pushed back against these measures and the redevelopment as a vehicle for gentrification (Albright, 2017).

Street Trees

Street trees are planted in cities on public or private rights-of-way, forming part of urban tree canopies and urban forests. Trees remove carbon dioxide from the atmosphere (mitigation) and provide shade and cooling that lessens the intensity of urban heat island effects (adaptation) (LA's Green New Deal, 2019). In general, the presence of street trees is found to increase property values (Anderson and Cordell, 1988; Dombrow et al., 2000; Donavan and Butry, 2010; Donavan and Butry, 2011; Heckert and Mennis, 2012; Morales, 1980; Orland et al., 1992; Pandit et al., 2013; Theriault et al., 2002; Wachter and Wong, 2008). However, impacts on home values may vary depending on tree type, size, and location on public or private property, as well as household composition and stated preference for wooded areas (Donavan and Butry, 2011; Orland et al., 1992; Pandit et al., 2013; Theriault et al., 2002).

Urban Agriculture and Community Farms and Gardens

Community farms and gardens are defined as any piece of land farmed or gardened by a group of people utilizing either shared or individual plots on public or private land, often at schools, institutions, or the grounds of residential developments. They provide climate change mitigation benefits primarily by providing a local, alternative food source, which does not have the embedded greenhouse gas emissions associated with the transportation of store-bought food (Dubbeling and de Zeeuw, 2011; McClintock, 2010). While there is a limited amount of literature on the topic, existing studies and media coverage consistently show that community farms and gardens increase property values (Fisher, 1992; Guitart et al., 2012; Raver, 1993; Voicu and Been, 2008). Research also highlights how urban farms and gardens can be vital community spaces that materially support low-income residents as a form of community development, and serve as sites of political and community engagement (Aptekar, 2015; Marche, 2015; Martinez, 2010; McClintock, 2014; Ruelas et al., 2011).

Transportation

Cities and states utilize numerous transportation strategies in attempts to reduce dependence upon car travel and associated greenhouse gas emissions by expanding and improving modes of public transportation and infrastructure that promote walking, cycling, or rolling from one place to another. We reviewed literature on transit-oriented development, heavy and light passenger rail, bus rapid transit, pedestrian and bicycle infrastructure, and complete streets strategies (transportation policies and designs that enable streets to be safe and efficient for all people, regardless of transportation mode).

Transit-Oriented Development

Transit-oriented development (TOD) integrates a mix of residential, office, and commercial

development into a walkable neighborhood that is within half a mile of access to public transportation, such as a light-rail station or bus stop. This form of development is often proposed in conjunction with upzoning in these areas to allow for higher housing density as part of efforts to reduce vehicle miles traveled as well as increase housing supply. Studies of TOD find that areas adjacent to transit stops often experience enhanced commercial activity with the introduction of shops, restaurants, and other businesses that attract commuters and non-commuters alike, and that proximity to public transit and faster commute times often leads to higher home values and rents, resulting in gentrification and sometimes displacement as well (Bluestone et al., 2008; Chapple and Loukaitou-Sideris, 2019; Wardrip, 2011; Duncan, 2008; Hess and Almeida, 2007; Diaz, 1999). However, being immediately adjacent to transit hubs has been shown to cause decreases in property values due to heightened noise, congestion, pollution, and traffic (Cervero, 2006; Kilpatrick et al., 2007).

Passenger Rail

Passenger railways constitute public transit that operates on fixed rail lines and includes both heavy rail (elevated and/or separated from streets and traffic) and light rail (streetcars and other rail systems that may share roads, streetlights, and traffic with cars) systems. Findings are mixed as to whether rail station areas are more likely to experience gentrification and displacement than areas without a transit stop. Some studies find that new rail and transit developments often result in higher prices for nearby homes and with them the prospect of "transit-induced gentrification" (Chapple et al., 2017; Dawkins, 2016). One such study in Los Angeles found that both new heavy and light rail stations contributed to an uptick in nearby housing prices and gentrification, though the effects of new heavy rail stations were slightly higher than that of new light rail stations (Brown, 2015). In contrast, Boarnet et al. (2017) examined new rail station-induced displacement in Los Angeles and found mixed results. Move-out rates surrounding Gold Line stations increased for all income groups, with the greatest effect observed among higher-income households; however, surrounding Red and Purple Line stations, an increase in out-migration was only observed among the lowest-income households (Boarnet et al., 2017).

Equitable transit-oriented development (ETOD) has become an important pillar of anti-displacement strategies overall. One study of the Washington, D.C., Metro rail system and surrounding housing impacts suggests that implementing housing subsidies via supply-side mechanisms like Low-Income Housing Tax Credit housing, Section 8 Project-Based Rental Assistance, or Community Development Block Grants specifically in transit zones can serve as effective ways of creating low-income housing near transit (Dawkins and Moeckel, 2016). Acting to acquire land for affordable housing production before a transit investment is announced and land values go up is another strategy to promote neighborhood affordability. For example, TriMet, a transit agency in Portland, acquired and banked land adjacent to a light rail expansion, and then dedicated it to subsidized housing development, leveraging transit money and federal funds (Zuk and Carlton, 2015). The $24 million Denver Regional Transit-Oriented Development Fund makes similar kinds of strategic acquisitions. Other strategies include transit-based affordable housing production incentives, such as the Los Angeles Gold and Blue Line TOD Ordinance, which allows a density bonus of up to 50 percent in certain transit neighborhoods along the Gold and Blue lines if at least one-third of the new units are for low-income households or half of the units are reserved for qualifying senior citizens.

Bus Rapid Transit
Bus Rapid Transit (BRT) is defined as a bus transit service that operates on surface streets but in its own dedicated lanes. Adoption of BRT systems in the U.S. is still relatively nascent, though given the construction speed and cost advantages it holds over rail systems, it is beginning to become more widespread nationally. However, much of the literature to date focuses on other countries and generally offers mixed evidence regarding BRT's impact on surrounding land and property values. A number of studies find that BRT has little or no impact on property values (Cervero and Duncan, 2002; Knight and Trygg, 1977; Rodríguez and Targa, 2004), while others find that it leads to significant increases in property values and rents of surrounding residential areas (Brown, 2014; Bocarejo et al., 2013; Muñoz-Raskin, 2010; Perk and Catalá, 2009).

Pedestrian Infrastructure and Walkability
Expanding and improving pedestrian infrastructure entails constructing a network of paths and sidewalks that make walkable commutes viable. Studies consistently and universally find that residential properties located in walkable areas are associated with higher property values (Bliesner et al., 2010; Cortright, 2009; Leinberger, 2013; Leinberger and Alfonzo, 2012; Pivo and Fisher, 2009; Sohn et al., 2012; Washington, 2013). However, these findings are correlative and do not represent robust evidence of a causal link between walkability and increased values.

Bike Infrastructure
Expanding and improving bicycle infrastructure means ensuring that a network of pathways and lanes is in place to enable cycling and similar forms of mobility. The majority of studies examining bike infrastructure find that proximity to bike infrastructure tends to be associated with higher property values and serves as a specific selling point for sellers and a desired amenity for buyers (Asabere and Huffman, 2009; City of Vancouver, 1999; Greer, 2000; Lagerway and Punochar, 1987; Li and Joh, 2017; Lindsey, 2004; Macy and Macdonald, 1995; Miller, 1992; Moore, 1992; Racca and Dhanju, 2006; Welch et al., 2016). Given disparate investment in bicycle facilities in relatively privileged areas, bike infrastructure has frequently been a flashpoint in gentrification disputes (Chavis et al., 2018; Flanagan et al., 2016; Hoffman, 2013). Despite many studies finding positive or neutral impact from the presence of cycling infrastructure, a number of additional studies have found bike facilities to be negatively associated with property values (Lindsey, 2004; Netusil, 2005; Woolley, 2018). Given the wide variety of bicycle infrastructure types studied, from greenway trails to bike lane improvements, it is difficult to draw firm conclusions as to the likely effects of bike infrastructure investments on surrounding property values.

Complete Streets
Complete streets are a transportation, policy, and design approach that requires streets to be planned, designed, operated, and maintained to enable safe and efficient mobility access for all users, regardless of transportation mode. There is a relative lack of research specifically addressing the effect of complete streets on housing prices and/or displacement. However, one San Francisco study found that the city's complete streets yielded increased property values (Yu et al., 2018), while an analysis of complete streets in cities throughout New York and New Jersey found no statistically significant relationship between complete streets and property values (Vandegrift and Zanoni, 2018). More research is needed to fully understand the impact of complete streets on surrounding communities, though many of its individual components, such

as bike and transit-oriented infrastructure, do have relatively more, albeit oftentimes mixed, evidence.

Energy

We reviewed literature on both energy efficiency measures and renewable energy technology in order to assess how such investments can influence housing prices and potentially contribute to gentrification and displacement. Buildings are major energy consumers, so improving their energy efficiency significantly helps reduce overall greenhouse gas emissions and other pollutants and can also be effective in lowering household energy costs. Investing in renewable energy sources such as solar and wind at the individual building or neighborhood scale is also an important step toward reducing emissions. Renewable energy can also have adaptation benefits. Given the more distributed and modular nature of renewables, they are less prone to large-scale failure during storms and other disasters.

Energy Efficiency

Residential energy efficiency can include a wide variety of energy-saving measures that reduce energy use from lighting, heating and cooling, water use, and appliances. Research done to date overwhelmingly supports the finding that, regardless of geography or climate, the value of a property increases with the addition of energy efficiency measures (Alberini, 2013; Brounen and Kok, 2011; Dinan and Miranowski, 1989; Hyland et al., 2013; Jafari et al., 2017; Nevin and Watson, 1998; Pride et al., 2018; Schweitzer and Tonn, 2002; Ugarte, 2016). One national study found that energy efficient homes increased value by roughly 4–10%, though in cold states, such as Alaska, this was as high as 16% (Nevin and Watson, 1998). The impact of these increased housing values on the displacement of low-income residents is complex. This is due to the fact that while improved energy efficiency can make housing less affordable, it also serves to lower utility bills and burdens for renters and homeowners, thereby reducing the risk of utility shut-offs or eviction (Schweitzer and Tonn, 2002).

Wind Energy

Wind energy refers to the process of harnessing energy from passing currents of air and converting it to electricity. Research on the impact of wind turbines on property values yields mixed results, with the majority of U.S. studies finding that neither the announcement of planned wind farms nor their installation had appreciable impact on nearby property values (Atkinson-Palombo and Hoen, 2014; Carter, 2011; Hoen et al., 2011; Laposa and Mueller, 2010; Rakitan, 2017; Sims et al., 2008; Sterzinger et al., 2003). However, a number of non-U.S. studies found that wind turbines negatively impact property values (Dröes and Koster, 2016; Gibbons, 2015; Heintzelman and Tuttle, 2012; Jensen et al., 2014; Sunak and Madlener, 2012; Sunak and Madlener, 2016; Sunak and Madlener, 2017).

Solar Energy

Solar photovoltaic systems absorb and convert energy from the sun into electricity. Various types of solar generation exist, from small-scale rooftop solar panels and medium-sized community solar gardens, up to large, utility-scale solar plants. Research examining the intersection of solar panels and property values is fairly new, though three different studies and literature reviews suggest a positive relationship between property values and associated rooftop solar installations (Brinkley and Leach, 2018; Dastrup, et al., 2012; Mandell and Wilhelmsson, 2011). These

studies found that rooftop solar increased property values for homes on which they were installed, that new homes were more likely than older ones to increase in price with solar installations and that price impacts were related to neighborhood composition and the relative abundance of solar on surrounding homes.

Emissions Trading Schemes (Cap and Trade)
Some recent research has focused on the social and environmental equity impacts of large-scale climate mitigation efforts, such as regional cap and trade programs for the market-based trading of greenhouse gas emissions credits. Examples include California's cap and trade system (known as AB-32) implemented in 2006. Though there is no research suggesting that these programs have direct impacts on displacement, they may have inequitable health consequences for some disadvantaged communities by concentrating emissions and air pollutants in certain areas (Cushing et al., 2018; Shonkoff et al., 2009). Though these findings have been the subject of debate (Farber, 2012; Walch, 2018), California has pledged to reinvest a portion of its revenues from this program into disadvantaged communities statewide in an effort to address environmental injustices more broadly. Large-scale climate change mitigation policies like these are desperately needed at the national and global levels, but should nevertheless be implemented equitably. For example, Transformative Climate Communities (TCC), one of the programs that leverages cap-and-trade dollars toward improving wellbeing in disadvantaged communities, requires that investments be paired with place-based Displacement Avoidance Plans.

Question 3 - Vulnerability of Anti-Displacement Strategies to Climate Change

Anti-displacement strategies are broadly defined as public policies and investments aimed at preventing the displacement of vulnerable residents in a given community. In the context of the U.S., these strategies most commonly consist of regulations that are geared toward providing support to low-income residents facing increasing housing and other living costs so that they may be able to remain in their home communities. Examples of such anti-displacement strategies include the provision of publicly owned or subsidized affordable housing, inclusionary zoning and other affordability-oriented densification approaches, community land trusts, local employment programs, rent stabilization ordinances and eviction protections, utility payment assistance programs, and nutritional assistance programs, to name a few (see Cash and Zuk, 2019 for inventory of anti-displacement strategies). However, anti-displacement strategies also include disaster relief and recovery assistance programs that are specifically aimed at alleviating post-disaster burdens and thus decreasing the risk of permanent displacement of impacted residents. While not all of these anti-displacement strategies are directly vulnerable to a changing climate, they are all challenged by the economic and displacement impacts of climate change, pointing to a need for a thoughtful climate lens on their implementation.

Some strategies, however, are explicitly vulnerable to physical climate hazards, such as subsidized housing developments, which are often constructed with non-resilient materials and often located in high-risk areas, like floodplains or fire zones. Only a small number of states are attempting to build publicly subsidized housing with climate-resilient materials due to higher costs, though these extra costs have been steadily decreasing in recent years (Duffrin, 2019). Investing the extra dollars for climate-resilient materials is likely to pay for itself, especially in

highly climate-vulnerable regions, such as along the coast or in tornado-prone areas (housing construction quality has been shown to be one of the biggest predictors of tornado-caused deaths) (Duffrin, 2019; Lim et al., 2017). Poor construction of government-owned or subsidized housing is one of the reasons that low-income communities are disproportionately affected by climate impacts. Investment in more climate-resilient construction can reduce vulnerability to floods and storms (Martin et al., 2013; Ross, 2013).

Nearly a half million government-subsidized homes – roughly 9% of the nation's total – are located in floodplains, with many more located in areas at high risk of storm-related damage (Hammett and Worzala, 2018; Rosoff and Yager, 2017). However, these floodplains delineated by FEMA are largely out of date and do not account for worsening climate risks such as rising sea levels, more frequent extreme storms, and heavy rainfall, likely causing underestimates in the calculations of flood-vulnerable housing (Mervosh, 2019; Rosoff and Yager, 2017). One study of Florida housing funded by federal Low Income Housing Tax Credits (LIHTC) – the country's largest source of funding for affordable, multifamily housing – found that roughly 70% of these developments were located in coastal counties, and roughly a third of this housing stock statewide would likely be damaged or destroyed by a Category 5 hurricane. Some Florida counties stood to lose almost 100% of their LIHTC housing stock in such an event, including in areas where overall damage to other structures was relatively low (Hammett and Worzala, 2018; Uhlmann, 2018). Though many existing affordable housing projects were constructed before concerns regarding climate change were as prevalent as they are today, the new construction of affordable housing across the country has continued in high-risk areas in recent years, largely due to the low prices of climate-vulnerable lands (Hammett and Worzala, 2018; Mervosh, 2019; Uhlmann, 2018). In Florida, over two-thirds of new LIHTC housing stock was constructed in zones vulnerable to storm surges from 2004 to 2010 (Worzala and Hammett, 2017). Environmental justice advocates point out racial and socioeconomic inequities caused by high-risk, affordable housing developments, citing the legacy racist redlining practices as likely having contributed to the placement of earlier low-income housing projects in flood zones (Mervosh, 2019).

Some argue that the affordable housing crisis warrants the rapid construction of cheaply constructed housing units, even if they are located in high-risk zones, because abandoning existing developments in these zones without replacing them will worsen housing shortages and affordability (Duffrin, 2019; Mervosh, 2019). However, construction of new projects without proper regard for climate threats can end up exacerbating the displacement of low-income residents if these developments are destroyed by a storm, flood, or fire. Many residents displaced from government-subsidized housing are provided with interim housing vouchers to be used in the private housing market, but research shows that voucher holders are often discriminated against by landlords (Cunningham et al., 2018). After government-subsidized housing projects are damaged or destroyed, reconstruction efforts can be slow or incomplete, and homes are often simply rebuilt in the same high-risk zones as before (Cusick, 2018; Mervosh, 2019; Mock, 2019). This is partly due to the unique regulatory structure surrounding public housing projects. For example, FEMA relief for damaged LIHTC housing projects is limited to Small Business Administration grants, which makes rehabilitation efforts more debt-laden in comparison to restoration efforts of non-subsidized housing (Hammett and Worzala, 2018). Additionally, the tight operating budgets and restrictions against rent increases in LIHTC and other publicly

subsidized housing projects makes weatherizing and improving climate-resiliency financially difficult, resulting in the neglect of badly needed upgrades (Yager, 2015). However, for developments located in extreme-risk areas, investing in such upgrades may never be cost-effective due to the likelihood of destruction. The priority for such communities should be on relocation and reconstruction in safer areas (Duffrin, 2019).

Many policies have been proposed to improve the climate vulnerability of affordable housing projects. These include obvious measures like prohibiting the building of new developments in high-risk zones, as well as involving community stakeholders in the planning and pre-construction phases of new affordable housing projects (Giambrone, 2019; Worzala and Hammett, 2017). It is critical to assess geographic climate risks using up-to-date scientific information and analysis; such assessments should guide all housing development decisions, including affordable/public housing (Hammett and Worzala, 2018). Expanding the overall share and availability of affordable housing (perhaps by expanding LIHTC or disaster recovery community development block grants) may help address the affordable housing shortage following disasters (Ross, 2013). Protective infrastructure, such as dams, levees, barriers, grading, and landscaping should be maintained and constructed when necessary to protect existing affordable housing developments in high-risk zones (Ross, 2013; Uhlmann, 2019). Protective upgrades of housing units, via weatherization or replacement of poor construction materials, should be implemented without raising prices on tenants (Ross, 2013). One innovative example of developing green affordable housing is PUSH Buffalo's "Green Development Zones," where $60 million has been invested in green affordable housing, green infrastructure, and stormwater management in zones specifically designated for green development and green jobs creation (Ghirmatzion, 2019). Climate-vulnerable residents living in extreme risk zones could potentially qualify for housing vouchers, allowing them to relocate to safer areas while local governments move or reconstruct high-risk housing projects (Mervosh, 2019).

Another anti-displacement strategy, community land trusts (CLTs), is rapidly gaining momentum as a way to safeguard affordable housing in neighborhoods experiencing rapid increases in housing prices. By preserving community ownership of land and providing affordable housing within these areas, CLTs can serve as a useful tool in combating both affordable housing shortages and climate vulnerability. Though CLTs located in high-risk zones, such as flood plains, will accordingly be vulnerable to the effects of climate change, they more likely can serve to improve community resilience to climate change by allowing communities to return and rebuild without facing the climate-driven gentrification that may follow major storms or other shocks. The Caño Martín Peña CLT in Puerto Rico has allowed residents to return and recover from climate disasters, such as Hurricane Maria, more quickly and reliably than surrounding areas (Leon, 2019). Additionally, many CLTs incorporate a mission of sustainable land stewardship, which can have both climate mitigation and adaptation benefits (Land Trust Alliance, 2020).

Conclusion

Climate shocks and stressors exacerbate patterns of displacement. Some climate M/A strategies result, albeit unintentionally, in higher property values. Some existing anti-displacement

strategies are themselves vulnerable to climate stresses, while others have unrealized potential to mitigate climate hazards.

There are vast inequities in vulnerability to climate shocks and stressors between different socioeconomic and racial groups, especially related to exposure to these hazards and the ability to recover from them. These shocks and stressors also drive displacement, with shocks like storms, floods and fires responsible for both directly and indirectly displacing residents, while stressors like sea level rise, extreme heat and drought more strongly drive indirect displacement. Without proactive policy measures to improve climate resilience and address inequities in vulnerability, climate-driven displacement is likely to worsen as climate hazards become more frequent and intense.

Several commonly used policy strategies aimed at reducing greenhouse gas emissions and improving climate resilience at a local level can potentially have the unintended effects of accelerating gentrification and displacement of low-income residents in certain neighborhoods. This is due to the fact that many of these investments, such as transit-oriented development, parks and greenways, and rooftop solar can result in higher property values in surrounding communities. While many of these M/A strategies are essential parts of the fight to address climate change, they should be implemented with proper attention paid to the potential for the unintended, inequitable impacts they might have.

Finally, a large portion of the nation's affordable housing stock has been constructed in high-risk areas like floodplains, fire-prone areas and zones of storm surge. Additional construction of such housing continues in these areas due to cheap land prices, with little planning for the natural risks from climate change. Poor construction quality of such housing also contributes to their vulnerability to climate hazards. Still, affordable housing as well as other anti-displacement policies may help to mitigate the threats of climate change, suggesting a potential path forward.

Acknowledgements

This report was funded by the Strong, Prosperous, and Resilient Communities Challenge (SPARCC); the views contained herein are those of the authors and do not necessarily reflect those of SPARCC. The Urban Displacement Project team would like to thank Naomi Cytron of the Federal Reserve Bank of San Francisco, Marissa Ramirez of the Natural Resources Defense Council, and Lara Hansen and Rachel Gregg of EcoAdapt for their guidance and feedback on this paper.

References

Abatzoglou, J.T. and Williams, A.P., 2016. Impact of anthropogenic climate change on wildfire across western US forests. Proceedings of the National Academy of Sciences, 113(42), pp.11770-11775.

Adams, V., Van Hattum, T. and English, D., 2009. Chronic disaster syndrome: Displacement, disaster capitalism, and the eviction of the poor from New Orleans. American ethnologist, 36(4), pp.615-636.

Adger, W.N., Arnell, N.W., Black, R., Dercon, S., Geddes, A. and Thomas, D.S., 2015. Focus on environmental risks and migration: causes and consequences. Environmental Research Letters, 10(6), p.060201.

Adrien, J., Page, R., 2019. 'Climate Gentrification in Little Haiti: Fighting climate-induced displacement through legal advocacy and economics' [PowerPoint presentation]. Community Justice Project and Earth Economics.

Akbari, H., 2005. Energy saving potentials and air quality benefits of urban heat island mitigation (No. LBNL-58285). Ernest Orlando Lawrence Berkeley National Laboratory, Berkeley, CA (US).

Alberini, A., Banfi, S. and Ramseier, C., 2013. Energy efficiency investments in the home: Swiss homeowners and expectations about future energy prices. The Energy Journal, 34(1).

Albouy, D., Graf, W., Kellogg, R. and Wolff, H., 2016. Climate amenities, climate change, and American quality of life. Journal of the Association of Environmental and Resource Economists, 3(1), pp.205-246.

Albright, C., 2017. Gentrification is sweeping through America. Here are the people fighting back. The Guardian.

American Coalition for Clean Coal Electricity (ACCCE), 2015. Energy Cost Impacts on American Families. American Coalition for Clean Coal Electricity (Report).

Anderson, L.M. and Cordell, H.K., 1988. Influence of trees on residential property values in Athens, Georgia (USA): A survey based on actual sales prices. Landscape and Urban Planning, 15(1-2), pp.153-164.

Angélil, O., Stone, D., Wehner, M., Paciorek, C.J., Krishnan, H. and Collins, W., 2017. An independent assessment of anthropogenic attribution statements for recent extreme temperature and rainfall events. Journal of Climate, 30(1), pp.5-16.

Angotti, T. and Morse, S. eds., 2017. Zoned Out!: Race, Displacement, and City Planning in New York City. Urban Research (UR).

Antwi-Agyei, P., Fraser, E.D., Dougill, A.J., Stringer, L.C. and Simelton, E., 2012. Mapping the vulnerability of crop production to drought in Ghana using rainfall, yield and socioeconomic data. Applied Geography, 32(2), pp.324-334.

Aptekar, S., 2015, March. Visions of public space: Reproducing and resisting social hierarchies in a community garden. Sociological Forum, 30(1), pp. 209-227.

Arévalo, M., Mazariegos, F., Portal, I., Salinas, R., Caravantes, L., Herrarte, G., Barrientos, C., 2015. Como un Factor de Migrácion Interna y Externa dentro de un Contexto de Violencia y Crimen en los Países del Triángulo Norte: Guatemala, Honduras y El Salvador. International Organization for Migration, United Nations World Food Programme.

Asabere, P.K. and Huffman, F.E., 2009. The relative impacts of trails and greenbelts on home price. The Journal of Real Estate Finance and Economics, 38(4), pp.408-419.

Atkinson-Palombo, C. and Hoen, B., 2014. Relationship between wind turbines and residential property values in Massachusetts. University of Connecticut.

Baptiste, N., 2017. When Texas' Most Toxic Sites Flooded These Are the Communities that Suffered Most. Mother Jones.

Bastien, M. 2019. Little Haiti is Fighting Climate Change. UC Berkeley - The Othering and Belonging Institute.

Bednar, D., 2016. The Intersection of Energy and Justice: Exploring the Spatial, Racial, and Socioeconomic Patterns of Residential Heating Affordability, Consumption and Efficiency in Wayne County, Michigan (Doctoral dissertation). University of Michigan.

Been, V., Ellen, I.G. and O'Regan, K., 2019. Supply skepticism: Housing supply and affordability. Housing Policy Debate, 29(1), pp.25-40.

Berger, A., Susskind, J., 2018. Cataloguing the Interface: Wildfire and Urban Development in California. MIT - Leventhal Center for Advanced Urbanism.

Bhattacharya, J., DeLeire, T., Haider, S. and Currie, J., 2003. Heat or eat? Cold-weather shocks and nutrition in poor American families. American Journal of Public Health, 93(7), pp.1149-1154.

Binkovitz, L., 2016. As slow disaster recoveries plague residents, some argue key to relief is 'precovery'. Kinder Institute for Urban Research Urban Edge Blog.

Blakely, E.J., 2008. The Elliot Richardson Lecture 2008: Ethics in Times of Crisis. Public Integrity, 10(4), pp.355-364.

Bliesner, J., Bouton, S. and Schultz, B., 2010. Walkable Neighborhoods: An Economic Development Strategy. AARP Livable Communities.

Bluestone, B., Stevenson, M.H. and Williams, R., 2008. The Urban Experience: Economics, Society, and Public Policy. Oxford University Press.

Boardman, B., 2013. Fixing Fuel Poverty: Challenges and Solutions. Routledge.

Boarnet, M.G., Bostic, R.W., Rodnyansky, S., Santiago-Bartolomei, R., Williams, D. and Prohofsky, A., 2017. Sustainability and Displacement: Assessing the Spatial Pattern of Residential Moves Near Rail Transit. UC Davis: National Center for Sustainable Transportation.

Bobb, J.F., Peng, R.D., Bell, M.L. and Dominici, F., 2014. Heat-related mortality and adaptation to heat in the United States. Environmental health perspectives, 122(8), pp.811-816.

Bocarejo, J.P., Portilla, I. and Pérez, M.A., 2013. Impact of Transmilenio on Density, Land Use, and Land Value in Bogotá. Research in Transportation Economics, 40(1), pp.78-86.

Bolitzer, B. and Netusil, N.R., 2000. The impact of open spaces on property values in Portland, Oregon. Journal of Environmental Management, 59(3), pp.185-193.

Boyd, R., 2019. Has Climate Gentrification Hit Miami? The City Plans to Find Out. The Natural Resources Defense Council - Southeast Dispatch (Article).

Brinkley, C. and Leach, A., 2019. Energy next door: A meta-analysis of energy infrastructure impact on housing value. Energy Research and Social Science, 50, pp.51-65.

Brounen, D. and Kok, N., 2011. On the economics of energy labels in the housing market. Journal of Environmental Economics and Management, 62(2), pp.166-179.

Brown, A., 2014. Neighborhood Change Along the Orange Line (Doctoral dissertation, University of California, Los Angeles).

Brown, A.E., 2015. Uneven Effects: The Mixed Story of Transit-Oriented Gentrification in Los Angeles. Critical Planning, 22(1).

Bruggers, J., 2018. FEMA Flood Maps Ignore Climate Change, and Homeowners Are Paying the Price. Inside Climate News.

Bryant, B. and Westerling, A., 2008. Potential effects of climate change on residential wildfire risk in California. California Energy Commission, PIER Energy Related Environmental Research Program CEC-500-2009-048-D.

Bryant, B.P. and Westerling, A.L., 2014. Scenarios for future wildfire risk in California: links between changing demography, land use, climate, and wildfire. Environmetrics, 25(6), pp.454-471.

Bubenik, T., 2018. As Post-Harvey Buyout Money Rolls In, Some Have Already Given Up On The Program. Houston Public Media.

Bullard, R.D., Mohai, P., Saha, R. and Wright, B., 2008. Toxic wastes and race at twenty: Why race still matters after all of these years. Environmental Law, 38, p.371.

Burby, R.J., Steinberg, L.J. and Basolo, V., 2003. The tenure trap: The vulnerability of renters to joint natural and technological disasters. Urban Affairs Review, 39(1), pp.32-58.

Byrne, J., Ambrey, C., Portanger, C., Lo, A., Matthews, T., Baker, D. and Davison, A., 2016. Could urban greening mitigate suburban thermal inequity? the role of residents' dispositions and household practices. Environmental Research Letters, 11(9), p.095014.

California Department of Forestry and Fire Protection, 2019. Top 20 Most Destructive California Wildfires. CAL-FIRE Media.

California Office of the Attorney General., FAQs on Price Gouging. State of California Department of Justice. Available at: https://oag.ca.gov/consumers/pricegougingduringdisasters

California Wildfire Strike Force, 2019. Wildfires and Climate Change: California's Energy Future. Governor Newsom's Strike Force (Report).

Campo-Flores, A., Kusisto, L., 2019. On Higher Ground, Miami's Little Haiti Is the New Darling of Developers. The Wall Street Journal.

Capps, K., 2018. Why Are These Tiny Towns Getting So Much Hurricane Harvey Aid? CityLab.

Carter, J., 2011. The effect of wind farms on residential property values in Lee County, Illinois, Preliminary Draft. Illinois State University.

Cash, A., Zuk, M., 2019. Investment Without Displacement: From Slogan to Strategy. Shelterforce.

Cervero, R. and Duncan, M., 2002. Transit's Added Value. At what point does locating near transit raise real estate values? Urban Land, 61(2), pp.77-87.

Cervero, R., 2006. Effects of light and commuter rail transit on land prices: Experiences in San Diego County. Journal of the Transportation Research Forum.

Chapple, K. and Loukaitou-Sideris, A., 2019. Transit-Oriented Displacement Or Community Dividends? Understanding the Effects of Smarter Growth on Communities. MIT Press.

Chapple, K., Waddell, P., Chatman, D., Zuk, M., Loukaitou-Sideris, A., Ong, P., Gorska, K., Pech, C. and Gonzalez, S.R., 2017. Developing a new methodology for analyzing potential displacement. University of California, Berkeley and University of California, Los Angeles.

Chapple, K., Zuk, M., 2015. Gentrification Explained. Urban Displacement Project. Available at: https://www.urbandisplacement.org/gentrification-explained.

Chavis, C., Barnes, P.J., Grasso, S., Bhuyan, I.A., Nickkar, A., 2018. Bicycle Justice or Just Bicycles? Analyzing Equity in Baltimore's Bike Share Program. Department of Transportation and Urban Infrastructure at Morgan State University.

Cho, S.H., Kim, S.G. and Roberts, R.K., 2011b. Values of environmental landscape amenities during the 2000–2006 real estate boom and subsequent 2008 recession. Journal of Environmental Planning and Management, 54(1), pp.71-91.

Cho, S.H., Lambert, D.M., Kim, S.G., Roberts, R.K. and Park, W.M., 2011a. Relationship between value of open space and distance from housing locations within a community. Journal of Geographical Systems, 13(4), pp.393-414.

Christensen, J.H., Kanikicharla, K.K., Aldrian, E., An, S.I., Cavalcanti, I.F.A., De Castro, M., Dong, W., Goswami, P., Hall, A., Kanyanga, J.K. and Kitoh, A., 2013. Climate phenomena and their relevance for future regional climate change. In Climate Change 2013 the Physical Science Basis: Working Group I Contribution to the Fifth Assessment Report of the Intergovernmental Panel on Climate Change (pp. 1217-1308). Cambridge University Press.

City of Vancouver, 1999. 1999 Bicycle Plan: Reviewing the Past, Planning the Future. City of Vancouver Engineering Services and Bike Vancouver.

Climate Central and Zillow, 2018. Ocean at the Door: New Homes and the Rising Sea. Climate Central and Zillow (Research Report).

Cohen, D.A., 2018. Climate Justice and the Right to the City. Penn: Current Research on Sustainable Urban Development. Philadelphia: University of Pennsylvania.

Colton, R., 2014. May Illinois 2013 Home Energy Affordability Gap. Available from. http://www.homeenergyaffordabilitygap.com.

Comerio, M.C., 1997. Housing issues after disasters. Journal of Contingencies and Crisis Management, 5(3), pp.166-178.

Community Justice Project, 2018. Demand an Equitable Recovery. Community Justice Project. Available at: http://communityjusticeproject.com/cdbg.

Conway, D., Li, C.Q., Wolch, J., Kahle, C. and Jerrett, M., 2010. A spatial autocorrelation approach for examining the effects of urban greenspace on residential property values. The Journal of Real Estate Finance and Economics, 41(2), pp.150-169.

Cook, J.T., Frank, D.A., Casey, P.H., Rose-Jacobs, R., Black, M.M., Chilton, M., Decuba, S.E., Appugliese, D., Coleman, S., Heeren, T. and Berkowitz, C., 2008. A brief indicator of household energy security: associations with food security, child health, and child development in US infants and toddlers. Pediatrics, 122(4), pp.e867-e875.

Cortright, J., 2009. Walking the walk: How walkability raises home values in US cities. CEOs for Cities.

Crompton, J.L., 2001. The impact of parks on property values: A review of the empirical evidence. Journal of Leisure Research, 33(1), pp.1-31.

Crompton, J.L., 2005. The impact of parks on property values: empirical evidence from the past two decades in the United States. Managing Leisure, 10(4), pp.203-218.

Crowder, K. and Downey, L., 2010. Inter-neighborhood migration, race, and environmental hazards: Modeling microlevel processes of environmental inequality. American Journal of Sociology, 115(4), pp.1110-1149.

Crutcher Jr, M.E., 2010. Tremé: Race and Place in a New Orleans Neighborhood (Vol. 5). University of Georgia Press.

Cunningham, M., Galvez, M., Aranda, C.L., Santos, R., Wissoker, D.A., Oneto, A.D., Pitingolo, R. and Crawford, J., 2018. A Pilot Study of Landlord Acceptance of Housing Choice Vouchers. US Department of Housing and Urban Development, Office of Policy Development and Research.

Curriero, F.C., Heiner, K.S., Samet, J.M., Zeger, S.L., Strug, L. and Patz, J.A., 2002. Temperature and mortality in 11 cities of the eastern United States. American Journal of Epidemiology, 155(1), pp.80-87.

Curtis, K.J. and Schneider, A., 2011. Understanding the demographic implications of climate change: estimates of localized population predictions under future scenarios of sea-level rise. Population and Environment, 33(1), pp.28-54.

Cushing, L., Blaustein-Rejto, D., Wander, M., Pastor, M., Sadd, J., Zhu, A. and Morello-Frosch, R., 2018. Carbon trading, co-pollutants, and environmental equity: Evidence from California's cap-and-trade program (2011–2015). PLoS Medicine, 15(7).

Cusick, D., 2018. We want the opportunity to rebuild out of the floodplain. ClimateWire.

Cutter, S.L. and Emrich, C.T., 2006. Moral hazard, social catastrophe: The changing face of vulnerability along the hurricane coasts. The Annals of the American Academy of Political and Social Science, 604(1), pp.102-112.

Dahl, K., Spanger-Siegfried, E., Licker, R., Caldas, A., Abatzoglou, J., Mailloux, N., Cleetus, R., Udvardy, S., Declet-Barreto, J., Worth, P., 2019. Killer Heat in the United States. The Union of Concerned Scientists (Report).

Dangendorf, S., Marcos, M., Wöppelmann, G., Conrad, C.P., Frederikse, T. and Riva, R., 2017. Reassessment of 20th century global mean sea level rise. Proceedings of the National Academy of Sciences, 114(23), pp.5946-5951.

Dastrup, S. and Ellen, I.G., 2016. Linking residents to opportunity: gentrification and public housing. Cityscape, 18(3), pp.87-108.

Dastrup, S.R., Zivin, J.G., Costa, D.L. and Kahn, M.E., 2012. Understanding the Solar Home price premium: Electricity generation and "Green" social status. European Economic Review, 56(5), pp.961-973.

Dawkins, C. and Moeckel, R., 2016. Transit-induced gentrification: Who will stay, and who will go? Housing Policy Debate, 26(4-5), pp.801-818.

Deaton, J., 2017. Hurricane Harvey Hit Low-Income communities hardest. Nexus Media News.

Dehring, C. and Dunse, N., 2006. Housing density and the effect of proximity to public open space in Aberdeen, Scotland. Real Estate Economics, 34(4), pp.553-566.

Diaz, R.B., 1999. Impacts of Rail Transit on Property Values. McLean, VA: Booz Allen and Hamilton Inc, (pp. 1-8).

Dickerson, A.M., 2017. Hurricane Harvey and the Houston Housing Market. Texas Law Review Online, 96, pp.102.

Diffenbaugh, N.S., Scherer, M. and Trapp, R.J., 2013. Robust increases in severe thunderstorm environments in response to greenhouse forcing. Proceedings of the National Academy of Sciences, 110(41), pp.16361-16366.

Diffenbaugh, N.S., Swain, D.L. and Touma, D., 2015. Anthropogenic warming has increased drought risk in California. Proceedings of the National Academy of Sciences, 112(13), pp.3931-3936.

Dinan, T.M. and Miranowski, J.A., 1989. Estimating the implicit price of energy efficiency improvements in the residential housing market: A hedonic approach. Journal of Urban Economics, 25(1), pp.52-67.

Dombrow, J., Rodriguez, M. and Sirmans, C.F., 2000. The market value of mature trees in single-family housing markets. Appraisal Journal, 68(1), pp.39-43.

Donovan, G.H. and Butry, D.T., 2010. Trees in the city: Valuing street trees in Portland, Oregon. Landscape and Urban Planning, 94(2), pp.77-83.

Donovan, G.H. and Butry, D.T., 2011. The effect of urban trees on the rental price of single-family homes in Portland, Oregon. Urban Forestry and Urban Greening, 10(3), pp.163-168.

Dröes, M.I. and Koster, H.R., 2016. Renewable energy and negative externalities: The effect of wind turbines on house prices. Journal of Urban Economics, 96, pp.121-141.

Dubbeling, M. and De Zeeuw, H., 2011. Urban Agriculture and Climate Change Adaptation: Ensuring Food Security Through Adaptation. In Resilient Cities (pp. 441-449). Springer, Dordrecht.

Duffrin, L., 2019. Three Approaches to Preventing Climate Displacement. Crosswalk Magazine.

Duncan, M., 2008. Comparing rail transit capitalization benefits for single-family and condominium units in San Diego, California. Transportation Research Record, 2067(1), pp.120-130.

Easterling, D.R., K.E. Kunkel, J.R. Arnold, T. Knutson, A.N. LeGrande, L.R. Leung, R.S. Vose, D.E. Waliser, and M.F. Wehner, 2017: Precipitation change in the United States. In: Climate Science Special Report: Fourth National Climate Assessment, Volume I [Wuebbles, D.J., D.W. Fahey, K.A. Hibbard, D.J. Dokken, B.C. Stewart, and T.K. Maycock (eds.)]. U.S. Global Change Research Program, Washington, DC, USA, pp. 207-230, doi: 10.7930/J0H993CC.

Edgeley, C.M. and Paveglio, T.B., 2017. Community recovery and assistance following large wildfires: The case of the Carlton Complex Fire. International Journal of Disaster Risk Reduction, 25, pp.137-146.

Elliott, J.R. and Howell, J., 2017. Beyond disasters: a longitudinal analysis of natural hazards' unequal impacts on residential instability. Social Forces, 95(3), pp.1181-1207.

Elsner, J.B., Elsner, S.C. and Jagger, T.H., 2015. The increasing efficiency of tornado days in the United States. Climate Dynamics, 45(3-4), pp.651-659.

Evans, G.W., 2004. The environment of childhood poverty. American Psychologist, 59(2), p.77.

Evens, A., Garascia, M. and Isaacson, M., 2017. Utilities and health: Energy efficiency as a common link. The Electricity Journal, 30(5), pp.10-14.

Fan, Q., Klaiber, H.A. and Fisher-Vanden, K., 2012. Climate change impacts on us migration and household location choice (No. 323-2016-11437). AgEcon Search.

Fan, Q., Klaiber, H.A. and Fisher-Vanden, K., 2016. Does extreme weather drive interregional brain drain in the US? Evidence from a sorting model. Land Economics, 92(2), pp.363-388.

Farber, D.A., 2012. Pollution markets and social equity: Analyzing the fairness of cap and trade. Ecology Law Quarterly.

Federal Home Loan Mortgage Corporation (Freddie Mac), 2016. Life's a Beach. Freddie Mac - Insight (Article).

Feng, S., Oppenheimer, M. and Schlenker, W., 2012. Climate change, crop yields, and internal migration in the United States (No. w17734). National Bureau of Economic Research.

Finnigan, R. and Meagher, K., 2016, March. Energy Costs and Housing-Related Deprivation in the United States. In 2016 Annual Meeting. PAA.

Finnigan, R. and Meagher, K.D., 2019. Past Due: Combinations of Utility and Housing Hardship in the United States. Sociological Perspectives, 62(1), pp.96-119.

Fisher, I., 1992. A blessing for gardens where green is so rare. New York Times.

Flanagan, E., Lachapelle, U. and El-Geneidy, A., 2016. Riding tandem: Does cycling infrastructure investment mirror gentrification and privilege in Portland, OR and Chicago, IL? Research in Transportation Economics, 60, pp.14-24.

Flannigan, M., Stocks, B., Turetsky, M. and Wotton, M., 2009. Impacts of climate change on fire activity and fire management in the circumboreal forest. Global Change Biology, 15(3), pp.549-560.

Flechas, J., Harris, A., 2018. What would Miami build with $58 million the city wants to borrow? Here's the list. The Miami Herald.

Fletcher, B.A., Lin, S., Fitzgerald, E.F. and Hwang, S.A., 2012. Association of summer temperatures with hospital admissions for renal diseases in New York State: a case-crossover study. American Journal of Epidemiology, 175(9), pp.907-916.

Freemark, Y., 2019. Upzoning Chicago: Impacts of a zoning reform on property values and housing construction. Urban Affairs Review, pp.1-32.

Frey, W.H. and Singer, A., 2006. Katrina and Rita impacts on gulf coast populations: First census findings. Washington: Brookings Institution, Metropolitan Policy Program.

Frey, W.H., Singer, A. and Park, D., 2007. Resettling New Orleans: The first full picture from the Census. Brookings Institution Metropolitan Policy Program.

Fuller, T., Haner, J., 2019. Among the World's Most Dire Places: This California Homeless Camp. The New York Times.

Fussell, E. and Harris, E., 2014. Homeownership and housing displacement after Hurricane Katrina among low-income African-American mothers in New Orleans. Social Science Quarterly, 95(4), pp.1086-1100.

Fussell, E., 2015. The long-term recovery of New Orleans' population after Hurricane Katrina. American Behavioral Scientist, 59(10), pp.1231-1245.

Fussell, E., Sastry, N. and VanLandingham, M., 2010. Race, socioeconomic status, and return migration to New Orleans after Hurricane Katrina. Population and Environment, 31(1-3), pp.20-42.

Gaither, C.J., Poudyal, N.C., Goodrick, S., Bowker, J.M., Malone, S. and Gan, J., 2011. Wildland fire risk and social vulnerability in the Southeastern United States: An exploratory spatial data analysis approach. Forest Policy and Economics, 13(1), pp.24-36.

Gao, Y., Lu, J., Leung, L.R., Yang, Q., Hagos, S. and Qian, Y., 2015. Dynamical and thermodynamical modulations on future changes of landfalling atmospheric rivers over western North America. Geophysical Research Letters, 42(17), pp.7179-7186.

Ghirmatzion, 2019. 'People United for Sustainable Housing: A Just Transition Story' [PowerPoint presentation]. People United for Sustainable Housing Buffalo.

Giambrone, A., 2019. Three-quarters of D.C. metro residents say they support laws to stop building in high-risk areas. Curbed - Washington D.C. (Article).

Gibbons, S., 2015. Gone with the wind: Valuing the visual impacts of wind turbines through house prices. Journal of Environmental Economics and Management, 72, pp.177-196.

Gleick, P.H., 2014. Water, drought, climate change, and conflict in Syria. Weather, Climate, and Society, 6(3), pp.331-340.

Godschalk, D., Beatley, T., Berke, P., Brower, D. and Kaiser, E.J., 1998. Natural Hazard Mitigation: Recasting Disaster Policy and Planning. Island Press.

Goetz, E., 2011. Gentrification in black and white: The racial impact of public housing demolition in American cities. Urban Studies, 48(8), pp.1581-1604.

Gould, W.A., E.L. Díaz, (co-leads), N.L. Álvarez-Berríos, F. Aponte-González, W. Archibald, J.H. Bowden, L. Carrubba, W. Crespo, S.J. Fain, G. González, A. Goulbourne, E. Harmsen, E. Holupchinski,

A.H. Khalyani, J. Kossin, A.J. Leinberger, V.I. Marrero-Santiago, O. Martínez-Sánchez, K. McGinley, P. Méndez-Lázaro, J. Morell, M.M. Oyola, I.K. Parés-Ramos, R. Pulwarty, W.V. Sweet, A. Terando, and S. Torres-González, 2018: U.S. Caribbean. In Impacts, Risks, and Adaptation in the United States: Fourth National Climate Assessment, Volume II [Reidmiller, D.R., C.W. Avery, D.R. Easterling, K.E. Kunkel, K.L.M. Lewis, T.K. Maycock, and B.C. Stewart (eds.)]. U.S. Global Change Research Program, Washington, DC, USA, pp. 809–871. doi: 10.7930/NCA4.2018.CH20

Graif, C., 2016. (Un) natural disaster: vulnerability, long-distance displacement, and the extended geography of neighborhood distress and attainment after Katrina. Population and Environment, 37(3), pp.288-318.

Greater Houston Flood Mitigation Consortium, 2019. Affordable Multi-Family Housing: Risks and Opportunities. Greater Houston Flood Mitigation Consortium, Houston.

Green, N., 2018. In Miami's Little Haiti, one of the largest waves of evictions is currently underway. Public Radio International (PRI).

Green, N., 2019. As Seas Rise, Miami's Black Communities Fear Displacement From The High Ground. WLRN - Miami.

Greer, D.L., 2000. Omaha recreational trails: their effect on property values and public safety. Recreation and Leisure Studies Program, University of Nebraska at Omaha.

Groen, J.A. and Polivka, A.E., 2010. Going home after Hurricane Katrina: Determinants of return migration and changes in affected areas. Demography, 47(4), pp.821-844.

Gronlund, C.J., 2014. Racial and socioeconomic disparities in heat-related health effects and their mechanisms: a review. Current Epidemiology Reports, 1(3), pp.165-173.

Guitart, D., Pickering, C. and Byrne, J., 2012. Past results and future directions in urban community gardens research. Urban Forestry and Urban Greening, 11(4), pp.364-373.

Halpern-Meekin, S., Edin, K., Tach, L. and Sykes, J., 2015. It's not like I'm poor: How working families make ends meet in a post-welfare world. Univ of California Press.

Hamel, L., Wu, B., Brodie, M., Sim, S.C. and Marks, E., 2017. An Early Assessment of Hurricane Harvey's Impact on Vulnerable Texans in the Gulf Coast Region: Their Voices and Priorities to Inform Rebuilding Efforts. Henry J. Kaiser Family Foundation.

Hammett, L., Worzala, E., 2018. The Devastating Impact of Storm Surge on Coastal Communities A Case Study on Florida's Low-Income Housing Tax Credit Projects. Real Estate Issues, Volume 42, Number 12.

Haninger, K., Ma, L. and Timmins, C., 2017. The value of brownfield remediation. Journal of the Association of Environmental and Resource Economists, 4(1), pp.197-241.

Hannah, L., Donatti, C.I., Harvey, C.A., Alfaro, E., Rodriguez, D.A., Bouroncle, C., Castellanos, E., Diaz, F., Fung, E., Hidalgo, H.G. and Imbach, P., 2017. Regional modeling of climate change impacts on smallholder agriculture and ecosystems in Central America. Climatic Change, 141(1), pp.29-45.

Hardy, R.D., Milligan, R.A. and Heynen, N., 2017. Racial coastal formation: The environmental injustice of colorblind adaptation planning for sea-level rise. Geoforum, 87, pp.62-72.

Harlan, S.L., Brazel, A.J., Prashad, L., Stefanov, W.L. and Larsen, L., 2006. Neighborhood microclimates and vulnerability to heat stress. Social Science and Medicine, 63(11), pp.2847-2863.

Harrison, C. and Popke, J., 2011. "Because you got to have heat": the networked assemblage of energy poverty in eastern North Carolina. Annals of the Association of American Geographers, 101(4), pp.949-961.

Hauer, M.E., 2017. Migration induced by sea-level rise could reshape the US population landscape. Nature Climate Change, 7(5), p.321.

Heberger, M., Cooley, H., Herrera, P., Gleick, P.H., Moore, E., 2009. The Impacts of Sea-Level Rise on the California Coast. The Pacific Institute.

Hecht, P., 2015. Vanishing water, fewer jobs, but still hope in the Central Valley. The Sacramento Bee.

Heckert, M. and Mennis, J., 2012. The economic impact of greening urban vacant land: a spatial difference-in-differences analysis. Environment and Planning A, 44(12), pp.3010-3027.

Heintzelman, M.D. and Tuttle, C.M., 2012. Values in the wind: a hedonic analysis of wind power facilities. Land Economics, 88(3), pp.571-588.

Hendon, W.S., Kitchen, J.W. and Pringle, B., 1967. The sociological and economic impact of urban parks in Dallas, Texas. Lubbock, TX, Tech University Press

Henry, S., Schoumaker, B. and Beauchemin, C., 2004. The impact of rainfall on the first out-migration: A multi-level event-history analysis in Burkina Faso. Population and Environment, 25(5), pp.423-460.

Hernández, D. and Bird, S., 2010. Energy burden and the need for integrated low-income housing and energy policy. Poverty and Public Policy, 2(4), pp.5-25.

Hernández, D. and Phillips, D., 2015. Benefit or burden? Perceptions of energy efficiency efforts among low-income housing residents in New York City. Energy Research and Social Science, 8, pp.52-59.

Hersher, R., Benincasa, R., 2019. How Federal Disaster Money Favors The Rich. National Public Radio.

Hess, D.B. and Almeida, T.M., 2007. Impact of proximity to light rail rapid transit on station-area property values in Buffalo, New York. Urban Studies, 44(5-6), pp.1041-1068.

Hidalgo, H.G., Das, T., Dettinger, M.D., Cayan, D.R., Pierce, D.W., Barnett, T.P., Bala, G., Mirin, A., Wood, A.W., Bonfils, C. and Santer, B.D., 2009. Detection and attribution of streamflow timing changes to climate change in the western United States. Journal of Climate, 22(13), pp.3838-3855.

Higuera, P.E., Abatzoglou, J.T., Littell, J.S. and Morgan, P., 2015. The changing strength and nature of fire-climate relationships in the northern Rocky Mountains, USA, 1902-2008. PloS One, 10(6), p.e0127563.

Hoen, B., Wiser, R., Cappers, P., Thayer, M. and Sethi, G., 2011. Wind energy facilities and residential properties: the effect of proximity and view on sales prices. Journal of Real Estate Research, 33(3), pp.279-316.

Hoffman, J.S., Shandas, V. and Pendleton, N., 2020. The Effects of Historical Housing Policies on Resident Exposure to Intra-Urban Heat: A Study of 108 US Urban Areas. Climate, 8(1), p.12.

Hoffmann, M.L., 2013. Our bikes in the middle of the street: community-building, racism and gentrification in urban bicycle advocacy (doctoral dissertation). University of Minnesota.

Holden, Z.A., Swanson, A., Luce, C.H., Jolly, W.M., Maneta, M., Oyler, J.W., Warren, D.A., Parsons, R. and Affleck, D., 2018. Decreasing fire season precipitation increased recent western US forest wildfire activity. Proceedings of the National Academy of Sciences, 115(36), pp. E8349-E8357.

Howell, J. and Elliott, J.R., 2018. As Disaster Costs Rise, So Does Inequality. Socius: Sociological Research for a Dynamic World, 4(1), pp.1-3.

Howitt, R., MacEwan, D., Medellín-Azuara, J., Lund, J. and Sumner, D., 2017. Economic analysis of the 2015 drought for California agriculture. UC Davis Center for Watershed Sciences.

Hyland, M., Lyons, R.C. and Lyons, S., 2013. The value of domestic building energy efficiency—evidence from Ireland. Energy Economics, 40, pp.943-952.

Iglesias, A., Moneo, M. and Quiroga, S., 2009. Methods for evaluating social vulnerability to drought. In Coping with drought risk in agriculture and water supply systems (pp. 153-159). Springer, Dordrecht.

Immergluck, D. and Balan, T., 2018. Sustainable for whom? Green urban development, environmental gentrification, and the Atlanta Beltline. Urban Geography, 39(4), pp.546-562.

Immergluck, D., 2009. Large redevelopment initiatives, housing values and gentrification: the case of the Atlanta Beltline. Urban Studies, 46(8), pp.1723-1745.

Inter-American Development Bank (IDB), International Fund for Agricultural Development, International Organization for Migration and Organization of American States, United Nations World Food Programme, 2017. Food Security and Emigration: Why people flee and the impact on family members left behind in El Salvador, Guatemala, and Honduras. Inter-American Development Bank, International Fund for Agricultural Development, International Organization for Migration and Organization of American States, United Nations World Food Programme.

Internal Displacement Monitoring Centre (IDMC), 2019. Global Report on Internal Displacement 2019. Internal Displacement Monitoring Centre (Report).

International Organization for Migration (IOM), London School of Economics and Political Science, Organization of American States, United Nations World Food Programme, 2016. Hunger Without Borders, The hidden links between Food Insecurity, Violence and Migration in the Northern Triangle of Central America. International Organization for Migration (IOM), London School of Economics and Political Science, Organization of American States, United Nations World Food Programme.

IPCC, 2014: Climate Change 2014: Synthesis Report. Contribution of Working Groups I, II and III to the Fifth Assessment Report of the Intergovernmental Panel on Climate Change [Core Writing Team, R.K. Pachauri and L.A. Meyer (eds.)]. IPCC, Geneva, Switzerland, 151 pp.

Ito, K., Lane, K. and Olson, C., 2018. Equitable Access to Air Conditioning: A City Health Department's Perspective on Preventing Heat-related Deaths. Epidemiology, 29(6), pp.749-752.

Jafari, A., Valentin, V. and Berrens, R.P., 2017. Estimating the economic value of energy improvements in US residential housing. Journal of Construction Engineering and Management, 143(8), p.04017048.

Jenerette, G.D., Harlan, S.L., Brazel, A., Jones, N., Larsen, L. and Stefanov, W.L., 2007. Regional relationships between surface temperature, vegetation, and human settlement in a rapidly urbanizing ecosystem. Landscape Ecology, 22(3), pp.353-365.

Jensen, C.U., Panduro, T.E. and Lundhede, T.H., 2014. The vindication of Don Quixote: The impact of noise and visual pollution from wind turbines. Land Economics, 90(4), pp.668-682.

Jesdale, B.M., Morello-Frosch, R. and Cushing, L., 2013. The racial/ethnic distribution of heat risk–related land cover in relation to residential segregation. Environmental Health Perspectives, 121(7), pp.811-817.

Jim, C.Y. and Chen, W.Y., 2010. External effects of neighbourhood parks and landscape elements on high-rise residential value. Land Use Policy, 27(2), pp.662-670.

Kamel, N., 2012. Social marginalisation, federal assistance and repopulation patterns in the New Orleans metropolitan area following Hurricane Katrina. Urban Studies, 49(14), pp.3211-3231.

Kasler, D., Sabalow, R., Reese, P., 2019. 'Sticker shock' for California wildfire areas: Insurance rates doubled, policies dropped. The Sacramento Bee.

Keenan, J.M., Hill, T. and Gumber, A., 2018. Climate gentrification: from theory to empiricism in Miami-Dade County, Florida. Environmental Research Letters, 13(5), p.054001.

Keener, V., D. Helweg, S. Asam, S. Balwani, M. Burkett, C. Fletcher, T. Giambelluca, Z. Grecni, M. Nobrega-Olivera, J. Polovina, and G. Tribble, 2018: Hawai‘i and U.S.-Affiliated Pacific Islands. In Impacts, Risks, and Adaptation in the United States: Fourth National Climate Assessment, Volume II [Reidmiller, D.R., C.W. Avery, D.R. Easterling, K.E. Kunkel, K.L.M. Lewis, T.K. Maycock, and B.C. Stewart (eds.)]. U.S. Global Change Research Program, Washington, DC, USA, pp. 1242–1308. doi: 10.7930/NCA4.2018.CH27

Kelley, C.P., Mohtadi, S., Cane, M.A., Seager, R. and Kushnir, Y., 2015. Climate change in the Fertile Crescent and implications of the recent Syrian drought. Proceedings of the National Academy of Sciences, 112(11), pp.3241-3246.

Kilpatrick, J., Throupe, R., Carruthers, J. and Krause, A., 2007. The Impact of Transit Corridors on Residential Property Values. Journal of Real Estate Research, 29(3), pp.303-320.

Klein, N., 2007. The Shock Doctrine: The Rise of Disaster Capitalism. Macmillan.

Klinenberg, E., 1999. Denaturalizing disaster: A social autopsy of the 1995 Chicago heat wave. Theory and Society, 28(2), pp.239-295.

Knight, R.L. and Trygg, L.L., 1977. Land use impacts of rapid transit: implications of recent experience. Final report (No. DOT-TPI-10-77-29). De Leuw, Cather and Co., San Francisco, CA (USA).

Knowles, N., Dettinger, M.D. and Cayan, D.R., 2006. Trends in snowfall versus rainfall in the western United States. Journal of Climate, 19(18), pp.4545-4559.

Knowlton, K., Rotkin-Ellman, M., King, G., Margolis, H.G., Smith, D., Solomon, G., Trent, R. and English, P., 2008. The 2006 California heat wave: impacts on hospitalizations and emergency department visits. Environmental Health Perspectives, 117(1), pp.61-67.

Knutson, T.R., Sirutis, J.J., Zhao, M., Tuleya, R.E., Bender, M., Vecchi, G.A., Villarini, G. and Chavas, D., 2015. Global projections of intense tropical cyclone activity for the late twenty-first century from dynamical downscaling of CMIP5/RCP4. 5 scenarios. Journal of Climate, 28(18), pp.7203-7224.

Knutson, T.R., Zeng, F. and Wittenberg, A.T., 2014. Seasonal and annual mean precipitation extremes occurring during 2013: A US focused analysis. Bulletin of the American Meteorological Society, 95(9), pp. S19-S23.

Kopp, R.E., DeConto, R.M., Bader, D.A., Hay, C.C., Horton, R.M., Kulp, S., Oppenheimer, M., Pollard, D. and Strauss, B.H., 2017. Evolving understanding of Antarctic ice-sheet physics and ambiguity in probabilistic sea-level projections. Earth's Future, 5(12), pp.1217-1233.

Kossin, J.P., T. Hall, T. Knutson, K.E. Kunkel, R.J. Trapp, D.E. Waliser, and M.F. Wehner, 2017: Extreme storms. In: Climate Science Special Report: Fourth National Climate Assessment, Volume I [Wuebbles, D.J., D.W. Fahey, K.A. Hibbard, D.J. Dokken, B.C. Stewart, and T.K. Maycock (eds.)]. U.S. Global Change Research Program, Washington, DC, USA, pp. 257-276, doi: 10.7930/J07S7KXX.

Krause, E. and Reeves, R.V., 2017. Hurricanes hit the poor the hardest. Social Mobility Memos (blog).

Kulp, S.A. and Strauss, B.H., 2019. New elevation data triple estimates of global vulnerability to sea-level rise and coastal flooding. Nature Communications, 10(1), pp.1-12.

Kusnetz, N., 2018. Norfolk Wants to Remake Itself as Sea Level Rises, but Who Will Be Left Behind? Inside Climate News.

L.A.'s Green New Deal: Sustainable City Plan, 2019. Office of Los Angeles Mayor Eric Garcetti. Available at https://plan.lamayor.org/sites/default/files/pLAn_2019_final.pdf.

Lagerway, P. and Punochar, B., 1988. Evaluation of the Burke-Gilman Trail’s effect on property values and crime. Transportation Research Record, 1168, pp.57-59.

Land Trust Alliance, 2020. Jefferson Land Trust's Conservation Plan and Forward-Facing Forestry. Land Trust Alliance - Case Studies.

Lang, C. and Cavanagh, P., 2018. Incomplete Information and Adverse Impacts of Environmental Cleanup. Land Economics, 94(3), pp.386-404.

Lang, M., 2015. Without water, work or homes: Farm laborers displaced by drought. San Francisco Chronicle.

Laposa, S. and Mueller, A., 2010. Wind farm announcements and rural home prices: Maxwell ranch and rural Northern Colorado. Journal of Sustainable Real Estate, 2(1), pp.383-402.

Lee, D. and Jung, J., 2014. The growth of low-income population in floodplains: A case study of Austin, TX. KSCE Journal of Civil Engineering, 18(2), pp.683-693.

Leinberger, C.B. and Alfonzo, M., 2012. Walk this way: The economic promise of walkable places in metropolitan Washington, DC (p. 22). Washington, DC: Brookings Institution.

Leinberger, C.B. and Austin, M., 2013. The WalkUP Wake-Up Call: Atlanta. Atlanta, GA: The George Washington University School of Business.

Leon, H., 2019. Community Land Trusts in the Age of Climate Change. Shelterforce.

Levine, J.N., Esnard, A.M. and Sapat, A., 2007. Population displacement and housing dilemmas due to catastrophic disasters. Journal of Planning Literature, 22(1), pp.3-15.

Li, W. and Joh, K., 2017. Exploring the synergistic economic benefit of enhancing neighbourhood bikeability and public transit accessibility based on real estate sale transactions. Urban Studies, 54(15), pp.3480-3499.

Lim, J., Loveridge, S., Shupp, R. and Skidmore, M., 2017. Double danger in the double wide: Dimensions of poverty, housing quality and tornado impacts. Regional Science and Urban Economics, 65, pp.1-15.

Lindsey, G., Man, J., Payton, S. and Dickson, K., 2004. Property Values, Recreation Values, and Urban Greenways. Journal of Park and Recreation Administration, 22(3).

Lopez, L., 2019. 'Our Duwamish Valley: We are still here' [PowerPoint presentation]. Duwamish River Cleanup Coalition.

Loughran, K., 2014. Parks for profit: The high line, growth machines, and the uneven development of urban public spaces. City and Community, 13(1), pp.49-68.

Lund, J., Hanak, E., Fleenor, W., Bennett, W. and Howitt, R., 2010. Comparing futures for the Sacramento-San Joaquin delta (Vol. 3). Univ of California Press.

Lutzenhiser, M. and Netusil, N.R., 2001. The effect of open spaces on a home's sale price. Contemporary Economic Policy, 19(3), pp.291-298.

Lynn, K. and Gerlitz, W., 2006. Mapping the relationship between wildfire and poverty. USDA Forest Service Proceedings RMRS-P-41.

Lynn, K., 2003. Wildfire and rural poverty: disastrous connections. Natural Hazards Observer.

Macy, S., Alexander, L., Macdonald, S.H. and Ford, C., 1995. The effect of greenways on property values and public safety. The Conservation Fund and Colorado State Parks State Trails Program, Colorado State Parks, State Trails Program

Makaula, W., 2019. Homeowner's insurance rates in wildfire-prone areas on rise. KCRA News.

Mallakpour, I. and Villarini, G., 2015. The changing nature of flooding across the central United States. Nature Climate Change, 5(3), p.250.

Mandell, S. and Wilhelmsson, M., 2011. Willingness to pay for sustainable housing. Journal of Housing Research, 20(1), pp.35-51.

Mao, Y., Nijssen, B. and Lettenmaier, D.P., 2015. Is climate change implicated in the 2013–2014 California drought? A hydrologic perspective. Geophysical Research Letters, 42(8), pp.2805-2813.

Marche, G., 2015. What can urban gardening really do about gentrification? A case-study of three San Francisco community gardens. European Journal of American Studies, 10(3).

Marcus, J., Verma, P., 2017. Disaster and displacement in the Bay Area. UC Berkeley Economics (Blog).

Martin, C., Campillo, G., Meirovich, H., Navarrete, J., 2013. Climate Change Mitigation and Adaptation through Publicly-Assisted Housing Theoretical Framework for the IDB's Regional Policy Dialogue on Climate Change. Inter-American Development Bank.

Martinez, M.J., 2010. Power at the Roots: Gentrification, Community Gardens, and the Puerto Ricans of the Lower East Side. Lexington Books.

Martinich, J., Neumann, J., Ludwig, L. and Jantarasami, L., 2013. Risks of sea level rise to disadvantaged communities in the United States. Mitigation and Adaptation Strategies for Global Change, 18(2), pp.169-185.

Mast, E., 2019. The effect of new market-rate housing construction on the low-income housing market. Upjohn Institute Working Paper 19-307, W.E. Upjohn Institute for Employment Research.

McAlpine, S.A. and Porter, J.R., 2018. Estimating Recent Local Impacts of Sea-Level Rise on Current Real-Estate Losses: A Housing Market Case Study in Miami-Dade, Florida. Population Research and Policy Review, 37(6), pp.871-895.

McAlpine, S.A. and Porter, J.R., 2019. Rising Seas Erode $15.8 Billion in Home Value from Maine to Mississippi. First Street Foundation (Report).

McCabe, G.J. and Wolock, D.M., 2014. Spatial and temporal patterns in conterminous United States streamflow characteristics. Geophysical Research Letters, 41(19), pp.6889-6897.

McClintock, N., 2010. Why Farm the City? Theorizing Urban Agriculture Through a Lens of Metabolic Rift. Cambridge Journal of Regions, Economy and Society, 3(2), pp.191-207.

McClintock, N., 2014. Radical, reformist, and garden-variety neoliberal: coming to terms with urban agriculture's contradictions. Local Environment, 19(2), pp.147-171.

Medina-Ramón, M., Zanobetti, A., Cavanagh, D.P. and Schwartz, J., 2006. Extreme temperatures and mortality: assessing effect modification by personal characteristics and specific cause of death in a multi-city case-only analysis. Environmental Health Perspectives, 114(9), pp.1331-1336.

Mera, R., Massey, N., Rupp, D.E., Mote, P., Allen, M. and Frumhoff, P.C., 2015. Climate change, climate justice and the application of probabilistic event attribution to summer heat extremes in the California Central Valley. Climatic Change, 133(3), pp.427-438.

Mervosh, S., 2019. Unsafe to Stay, Unable to Go: Half a Million Face Flooding Risk in Government Homes. The New York Times.

Miller, A., Goodman, J., 2019. Striving for Equity in Post-Disaster Housing. Planning Magazine.

Miller, A.R., 2001. Valuing open space: Land economics and neighborhood parks (Doctoral dissertation, Massachusetts Institute of Technology).

Miller, M., 1992. The Impact of the Brush Creek Trail on Property Values and Crime. Environmental Studies and Planning Senior Project, Sonoma State University, Santa Rosa, CA.

Mitchell, B.C. and Chakraborty, J., 2014. Urban heat and climate justice: a landscape of thermal inequity in Pinellas County, Florida. Geographical Review, 104(4), pp.459-480.

Mitchell, C.M., Esnard, A.M. and Sapat, A., 2011. Hurricane events, population displacement, and sheltering provision in the United States. Natural Hazards Review, 13(2), pp.150-161.

Mock, B., 2019. Why Flood Victims Blame Their City, Not the Climate. CityLab.

Mockrin, M.H., Stewart, S.I., Radeloff, V.C., Hammer, R.B. and Alexandre, P.M., 2015. Adapting to wildfire: rebuilding after home loss. Society and Natural Resources, 28(8), pp.839-856.

Moftakhari, H.R., AghaKouchak, A., Sanders, B.F. and Matthew, R.A., 2017. Cumulative hazard: The case of nuisance flooding. Earth's Future, 5(2), pp.214-223.

Moore, M.M., Wallace Covington, W. and Fulé, P.Z., 1999. Reference conditions and ecological restoration: a southwestern ponderosa pine perspective. Ecological Applications, 9(4), pp.1266-1277.

Moore, R.L., 1992. The impacts of rail-trails: A study of the users and property owners from three trails. Rivers, Trails and Conservation Assistance Program, National Park Service, Washington, D.C.

Morales, D.J., 1980. The contribution of trees to residential property value. Journal of Arboriculture, 6(11), pp.305-308.

More, T.A., Stevens, T. and Allen, P.G., 1988. Valuation of urban parks. Landscape and Urban Planning, 15(1-2), pp.139-152.

Morris, M., 2018. Oft-flooded neighborhood slowly disappears, buyout by reluctant buyout. Houston Chronicle.

Mueller, E.J., Bell, H., Chang, B.B. and Henneberger, J., 2011. Looking for home after Katrina: postdisaster housing policy and low-income survivors. Journal of Planning Education and Research, 31(3), pp.291-307.

Munoz-Raskin, R., 2010. Walking accessibility to bus rapid transit: Does it affect property values? The case of Bogotá, Colombia. Transport Policy, 17(2), pp.72-84.

National Association of Insurance Commissioners (NAIC), 2019. Wildfires. The Center for Insurance Policy and Research.

National Oceanic and Atmospheric Administration - National Weather Service (NOAA - NWS), 2019. Annual U.S. Killer Tornado Statistics. Storm Prediction Center.

National Oceanic and Atmospheric Administration - Office for Coastal Management (NOAA - OCM), 2019. Fast Facts - Economics and Demographics.

National Oceanic and Atmospheric Administration (NOAA), 2018. Costliest U.S. tropical cyclones tables updated. National Hurricane Center.

Nawrotzki, R.J., Hunter, L.M., Runfola, D.M. and Riosmena, F., 2015. Climate change as a migration driver from rural and urban Mexico. Environmental Research Letters, 10(11), p.114023.

Nelson, A.C., Pendall, R., Dawkins, C.J. and Knaap, G.J., 2002. The Link Between Growth Management and Housing Affordability: The Academic Evidence. Growth Management and Affordable Housing: Do They Conflict? 117, p.158.

Netusil, N.R., 2005. The effect of environmental zoning and amenities on property values: Portland, Oregon. Land Economics, 81(2), pp.227-246.

Nevin, R. and Watson, G., 1998. Evidence of rational market valuations for home energy efficiency. The Appraisal Journal, 4(66), pp.401-409

Nicholls, S., 2002. Does open space pay? Measuring the impacts of green spaces on property values and the property tax base. College Station, TX, Texas A&M University (Doctoral dissertation).

Noss, R.F., 2011. Between the devil and the deep blue sea: Florida's unenviable position with respect to sea level rise. Climatic Change, 107(1-2), pp.1-16.

O'Neill, M.S., Zanobetti, A. and Schwartz, J., 2005. Disparities by race in heat-related mortality in four US cities: the role of air conditioning prevalence. Journal of Urban Health, 82(2), pp.191-197.

Olshansky, R.B., Johnson, L.A., Horne, J. and Nee, B., 2008. Longer view: Planning for the rebuilding of New Orleans. Journal of the American Planning Association, 74(3), pp.273-287.

Opdyke, J.D. 2005. Baton Rouge real estate becomes hot property. The Wall Street Journal Online.

Orland, B., Vining, J. and Ebreo, A., 1992. The effect of street trees on perceived values of residential property. Environment and Behavior, 24(3), pp.298-325.

Pais, J.F. and Elliott, J.R., 2008. Places as recovery machines: Vulnerability and neighborhood change after major hurricanes. Social Forces, 86(4), pp.1415-1453.

Pandit, R., Polyakov, M., Tapsuwan, S. and Moran, T., 2013. The effect of street trees on property value in Perth, Western Australia. Landscape and Urban Planning, 110, pp.134-142.

Passy, J., 2018. California wildfire victims face new challenges finding housing. MarketWatch.

Paterson, R.G., 1998. The third sector: Evolving partnerships in hazard mitigation (pp. 203-230). Joseph Henry Press, Washington, DC Pg.

Peacock, W.G., Van Zandt, S., Zhang, Y. and Highfield, W.E., 2014. Inequities in long-term housing recovery after disasters. Journal of the American Planning Association, 80(4), pp.356-371.

Peri, C., Rosoff, S., Yager, J., 2017. Population in the U.S. Floodplains. NYU Furman Center (Data Brief).

Perk, V.A. and Catala, M., 2009. Land use impacts of bus rapid transit: effects of BRT station proximity on property values along the Pittsburgh Martin Luther King, Jr. East Busway. National Bus Rapid Transit Institute, Federal Transit Administration, and Department of Transportation.

Peterman, C., Jones, D., Kahn, M., Nava, P., Wara, M., 2019. Final Report of the Commission on Catastrophic Wildfire Cost and Recovery. California Governor's Office of Planning and Research (Report).

Pierce, D.W., Barnett, T.P., Hidalgo, H.G., Das, T., Bonfils, C., Santer, B.D., Bala, G., Dettinger, M.D., Cayan, D.R., Mirin, A. and Wood, A.W., 2008. Attribution of declining western US snowpack to human effects. Journal of Climate, 21(23), pp.6425-6444.

Pivo, G. and Fisher, J.D., 2011. The walkability premium in commercial real estate investments. Real Estate Economics, 39(2), pp.185-219.

Poudyal, N.C., Johnson-Gaither, C., Goodrick, S., Bowker, J.M. and Gan, J., 2012. Locating spatial variation in the association between wildland fire risk and social vulnerability across six southern states. Environmental Management, 49(3), pp.623-635.

Pough, B., 2018. Neighborhood Upzoning and Racial Displacement: A Potential Target for Disparate Impact Litigation. University of Pennsylvania Journal of Law and Social Change, 21, pp. 267-294.

Pride, D., Little, J. and Mueller-Stoffels, M., 2018. The value of residential energy efficiency in interior Alaska: A hedonic pricing analysis. Energy Policy, 123, pp.450-460.

Quinton, S., 2019. As Wildfire Risk Increases, Home Insurance Is Harder to Find. PEW - Stateline.

Rabe Thomas, J., 2019. Separated by Design: How Some of America's Richest Towns Fight Affordable Housing. The Connecticut Mirror.

Racca, D.P. and Dhanju, A., 2006. Project Report for Property Value/Desirability Effects of Bike Paths Adjacent to Residential Areas. Delaware Center for Transportation. The State of Delaware Department of Transportation. Newark.

Radeloff, V.C., Helmers, D.P., Kramer, H.A., Mockrin, M.H., Alexandre, P.M., Bar-Massada, A., Butsic, V., Hawbaker, T.J., Martinuzzi, S., Syphard, A.D. and Stewart, S.I., 2018. Rapid growth of the US wildland-urban interface raises wildfire risk. Proceedings of the National Academy of Sciences, 115(13), pp.3314-3319.

Rakitan, T.J., 2017. Essays in the economics of energy development and disamenities (Doctoral dissertation). Iowa State University.

Ratcliffe, C., Congdon, W.J., Stanczyk, A., Teles, D., Martín, C. and Kotapati, B., 2019. Insult to Injury: Natural Disasters and Residents' Financial Health. Urban Institute.

Raver, A., 1993. Is this city big enough for gardens and houses? New York Times.

Reid, C.E., O'Neill, M.S., Gronlund, C.J., Brines, S.J., Brown, D.G., Diez-Roux, A.V. and Schwartz, J., 2009. Mapping community determinants of heat vulnerability. Environmental Health Perspectives, 117(11), pp.1730-1736.

Richards, J.A. and Bradshaw, S., 2017. Uprooted by Climate Change: Responding to the growing risk of displacement. Oxfam.

Rigolon, A. and Németh, J., 2018. "We're not in the business of housing:" Environmental gentrification and the nonprofitization of green infrastructure projects. Cities, 81, pp.71-80.

Rigolon, A. and Németh, J., 2019. Green gentrification or 'just green enough': Do park location, size and function affect whether a place gentrifies or not? Urban Studies, 57(2), pp.402-420.

Rodríguez, D.A. and Targa, F., 2004. Value of Accessibility to Bogotá's Bus Rapid Transit System. Transport Reviews, 24(5), pp.587-610.

Romps, D.M., Seeley, J.T., Vollaro, D. and Molinari, J., 2014. Projected increase in lightning strikes in the United States due to global warming. Science, 346(6211), pp.851-854.

Rosenbaum, E., 1996. Racial/ethnic differences in home ownership and housing quality, 1991. Social Problems, 43(4), pp.403-426.

Rosenthal, J.K., Kinney, P.L. and Metzger, K.B., 2014. Intra-urban vulnerability to heat-related mortality in New York City, 1997–2006. Health and Place, 30, pp.45-60.

Rosoff, S., Yager, J., 2017. Housing in the U.S. Floodplains. New York University Furman Center (Data Brief).

Ross, T., 2013. A Disaster in the Making: Addressing the Vulnerability of Low-Income Communities to Extreme Weather. Center for American Progress.

Rothstein, R., 2017. The Color of Law: A Forgotten History of How Our Government Segregated America. Liveright Publishing.

Ruelas, V., Iverson, E., Kiekel, P. and Peters, A., 2012. The role of farmers' markets in two low income, urban communities. Journal of Community Health, 37(3), pp.554-562.

Running, S.W., 2006. Is global warming causing more, larger wildfires? Science, 313(5789), pp.927-928.

Ryu, J.H. and Hayhoe, K., 2017. Observed and CMIP5 modeled influence of large-scale circulation on summer precipitation and drought in the South-Central United States. Climate Dynamics, 49(11-12), pp.4293-4310.

Sainsbury, J.C., 1964. The impact of urban parks on surrounding residential areas: A case study. Seattle, WA. (Master's Thesis, University of Washington).

Sampson, N.R., Gronlund, C.J., Buxton, M.A., Catalano, L., White-Newsome, J.L., Conlon, K.C., O'Neill, M.S., McCormick, S. and Parker, E.A., 2013. Staying cool in a changing climate: Reaching vulnerable populations during heat events. Global Environmental Change, 23(2), pp.475-484.

Sarmiento, C. and Miller, T.E., 2006. Inequities in flood management protection outcomes (No. 379-2016-21673). AgEcon Search (Conference Paper).

Scata, J., 2019. The Uncertain Flood Zone. Shelterforce.

Schweitzer, M. and Tonn, B., 2002. Non-energy benefits from the weatherization assistance program: A summary of findings from the recent literature. Prepared for U.S. Department of Energy, Oak Ridge National Laboratory, Oak Ridge, TN, USA.

Seager, R., Hoerling, M., Schubert, S., Wang, H., Lyon, B., Kumar, A., Nakamura, J. and Henderson, N., 2015. Causes of the 2011–14 California drought. Journal of Climate, 28(18), pp.6997-7024.

Sellers, F.S., Wilson, S., Craig, T., 2018. With illness in shelters and hotels at capacity, wildfire evacuees desperately seek refuge. The Washington Post.

Serna, J., 2019. California bans insurers from dropping policies in fire-ravaged areas. The Los Angeles Times.

Sheridan, S.C., 2007. A survey of public perception and response to heat warnings across four North American cities: an evaluation of municipal effectiveness. International Journal of Biometeorology, 52(1), pp.3-15.

Shonkoff, S.B., Morello-Frosch, R., Pastor, M. and Sadd, J., 2009. Minding the climate gap: environmental health and equity implications of climate change mitigation policies in California. Environmental Justice, 2(4), pp.173-177.

Shonkoff, S.B., Morello-Frosch, R., Pastor, M. and Sadd, J., 2009. Minding the climate gap: environmental health and equity implications of climate change mitigation policies in California. Environmental Justice, 2(4), pp.173-177.

Shuman, M., 2019. Fire risk leaves Tuolumne County residents scrambling to find affordable insurance. Modesto Bee.

Sims, S., Dent, P. and Oskrochi, G.R., 2008. Modelling the impact of wind farms on house prices in the UK. International Journal of Strategic Property Management, 12(4), pp.251-269.

Smith, G., Duda, S., Lee, J.M. and Thompson, M., 2016. Measuring the impact of the 606: understanding how a large public investment impacted the surrounding housing market. Institute for Housing Studies at DePaul University, Chicago.

Smith, K., 2016. This is how a California wildfire can change your homeowner's insurance rate. Press Telegram, San Gabriel Valley Tribune.

Sohn, D.W., Moudon, A.V. and Lee, J., 2012. The economic value of walkable neighborhoods. Urban Design International, 17(2), pp.115-128.

Southeast Florida Regional Climate Change Compact (SFRCCC) - Sea Level Rise Work Group, 2015. Unified Sea Level Rise Projection - Southeast Florida. Southeast Florida Regional Climate Change Compact (Report).

Squires, L., 2018. California Wildfires: Mapping Social Vulnerability. Direct Relief.

Steffans, G., 2018. Changing climate forces desperate Guatemalans to migrate. National Geographic.

Stephens, S.L., Agee, J.K., Fule, P.Z., North, M.P., Romme, W.H., Swetnam, T.W. and Turner, M.G., 2013. Managing forests and fire in changing climates. Science, 342(6154), pp.41-42.

Sterzinger, G., Beck, F., and Kostiuk, D., 2003. The effect of wind development on local property values. Renewable Energy Policy Project.

Stewart, I.T., Cayan, D.R. and Dettinger, M.D., 2005. Changes toward earlier streamflow timing across western North America. Journal of Climate, 18(8), pp.1136-1155.

Sun, L., Kunkel, K.E., Stevens, L.E., Buddenberg, A., Dobson, J.G. and Easterling, D.R., 2015. Regional surface climate conditions in CMIP3 and CMIP5 for the United States: differences, similarities, and implications for the US national climate assessment. National Oceanographic and Atmospheric Administration - Technical Report NESDIS 144.

Sunak, Y. and Madlener, R., 2012. The impact of wind farms on property values: a geographically weighted hedonic pricing model. Institute for Future Energy Consumer Needs and Behavior.

Sunak, Y. and Madlener, R., 2016. The impact of wind farm visibility on property values: A spatial difference-in-differences analysis. Energy Economics, 55, pp.79-91.

Sunak, Y. and Madlener, R., 2017. The impact of wind farms on property values: A locally weighted hedonic pricing model. Papers in Regional Science, 96(2), pp.423-444.

Swain, D.L., Tsiang, M., Haugen, M., Singh, D., Charland, A., Rajaratnam, B. and Diffenbaugh, N.S., 2014. The extraordinary California drought of 2013/2014: Character, context, and the role of climate change. Bulletin of the American Meteorological Society, 95(9), pp. S3-S7.

Sweet, W.V., Park, J., Marra, J., Zervas, C., Gill, S., 2014. Sea level rise and nuisance flood frequency changes around the United States. US Department of Commerce, National Oceanic and Atmospheric Administration, National Ocean Service, Center for Operational Oceanographic Products and Services.

Sweet, W.V., R. Horton, R.E. Kopp, A.N. LeGrande, and A. Romanou, 2017: Sea level rise. In: Climate Science Special Report: Fourth National Climate Assessment, Volume I [Wuebbles, D.J., D.W. Fahey, K.A. Hibbard, D.J. Dokken, B.C. Stewart, and T.K. Maycock (eds.)]. U.S. Global Change Research Program, Washington, DC, USA, pp. 333-363, doi: 10.7930/J0VM49F2.

The Allstate Corporation, 2018. Allstate Announces Impact of California Wildfires. Allstate Newsroom.

The City of Los Angeles - Office of the Mayor, 2019. L.A.'s Green New Deal Sustainability Plan 2019 (Report). The City of Los Angeles.

The City of Miami, 2018. Miami, FL Resolution R-18-0501. The City of Miami - Sea Level Rise Committee.

The City of Miami, 2019. Miami Forever Bond. The City of Miami - Office of Capital Improvements.

The City of Seattle, 2018. Duwamish Valley Action Plan. The City of Seattle - Office of Sustainability and the Environment.

The Utility Reform Network (TURN), 2017. Governor Signs TURN Bill to Reduce Shutoffs. TURN (Article).

Thériault, M., Kestens, Y. and Des Rosiers, F., 2002. The impact of mature trees on house values and on residential location choices in Quebec City, in Meeting of the IEMSs Society Lugano, Switzerland. International Environmental Modelling and Software Society, pp. 478–483.

Thompson, D., 2019. California Struggles with Insurance Costs and Wildfire Risks. Wildland Firefighter.

Treg, C., 2010. A Multilevel Property Hedonic Approach to Valuing Parks and Open Space (Doctoral Dissertation, University of Vermont).

Tucker, C.M., Eakin, H. and Castellanos, E.J., 2010. Perceptions of risk and adaptation: coffee producers, market shocks, and extreme weather in Central America and Mexico. Global Environmental Change, 20(1), pp.23-32.

Ugarte, S., van der Ree, B., Voogt, M., Eichhammer, W., Ordoñez, J.A., Reuter, M., Schlomann, B., Lloret Gallego, P. and Villafafila Robles, R., 2016. Energy efficiency for low-income households. Directorate-General for Internal Policies, Policy Department A: Economic and Scientific Policy.

Uhlmann, R., 2018. Florida tax-credit housing is often in flood zones, study finds. Clemson University, School of Business - The Newsstand (News Article).

United States Department of Agriculture - Economic Research Service (USDA - ERS), 2020. Farm Labor. United States Department of Agriculture - Economic Research Service, Farm Economy.

Upton, J., 2017. The Injustice of Atlantic City's Floods. Climate Central (Report).

US EPA, 2019. Overview of EPA's Brownfields Program, United States Environmental Protection Agency. Available at: https://www.epa.gov/brownfields/overview-epas-brownfields-program (Accessed: 8 February 2020).

Van Zandt, S., Peacock, W.G., Henry, D.W., Grover, H., Highfield, W.E. and Brody, S.D., 2012. Mapping social vulnerability to enhance housing and neighborhood resilience. Housing Policy Debate, 22(1), pp.29-55.

Vandegrift, D. and Zanoni, N., 2018. An economic analysis of complete streets policies. Landscape and Urban Planning, 171, pp.88-97.

Vigdor, J., 2008. The economic aftermath of Hurricane Katrina. Journal of Economic Perspectives, 22(4), pp.135-54.

Viglucci, A., 2018. Half of Puerto Rico's housing was built illegally. Then came Hurricane Maria. Miami Herald.

Viglucci, A., 2018. Miami will start making developers provide affordable housing in some new towers. Miami Herald.

Voicu, I. and Been, V., 2008. The effect of community gardens on neighboring property values. Real Estate Economics, 36(2), pp.241-283.

Vose, R.S., D.R. Easterling, K.E. Kunkel, A.N. LeGrande, and M.F. Wehner, 2017: Temperature changes in the United States. In: Climate Science Special Report: Fourth National Climate Assessment, Volume I [Wuebbles, D.J., D.W. Fahey, K.A. Hibbard, D.J. Dokken, B.C. Stewart, and T.K. Maycock (eds.)]. U.S. Global Change Research Program, Washington, DC, USA, pp. 185-206, doi: 10.7930/J0N29V45.

Wachter, S.M. and Wong, G., 2008. What is a tree worth? Green-city strategies, signaling and housing prices. Real Estate Economics, 36(2), pp.213-239.

Walch, R.T., 2018. The Effect of California's Carbon Cap and Trade Program on Co-Pollutants and Environmental Justice: Evidence from the Electricity Sector. Department of Economics at University of Oregon.

Walsh, K.J., Camargo, S.J., Vecchi, G.A., Daloz, A.S., Elsner, J., Emanuel, K., Horn, M., Lim, Y.K., Roberts, M., Patricola, C. and Scoccimarro, E., 2015. Hurricanes and climate: the US CLIVAR working group on hurricanes. Bulletin of the American Meteorological Society, 96(6), pp.997-1017.

Wardrip, K., 2011. Public Transit's Impact on Housing Costs: A Review of the Literature. Insights from Housing Policy Research, Center for Housing Policy and National Housing Conference.

Warner, K., Ehrhart, C., Sherbinin, A.D., Adamo, S. and Chai-Onn, T., 2009. In search of shelter: Mapping the effects of climate change on human migration and displacement. The Center for International Earth Science Information Network (CIESIN) - Columbia University.

Warner, M.D., Mass, C.F. and Salathé Jr, E.P., 2015. Changes in winter atmospheric rivers along the North American west coast in CMIP5 climate models. Journal of Hydrometeorology, 16(1), pp.118-128.

Washington, E., 2013. Role of walkability in driving home values. Leadership and Management in Engineering, 13(3), pp.123-130.

Wehner, M.F., J.R. Arnold, T. Knutson, K.E. Kunkel, and A.N. LeGrande, 2017: Droughts, floods, and wildfires. In: Climate Science Special Report: Fourth National Climate Assessment, Volume I [Wuebbles, D.J., D.W. Fahey, K.A. Hibbard, D.J. Dokken, B.C. Stewart, and T.K. Maycock (eds.)]. U.S. Global Change Research Program, Washington, DC, USA, pp. 231-256, doi: 10.7930/J0CJ8BNN.

Welch, T.F., Gehrke, S.R. and Wang, F., 2016. Long-term impact of network access to bike facilities and public transit stations on housing sales prices in Portland, Oregon. Journal of Transport Geography, 54, pp.264-272.

Westerling, A.L., 2016. Increasing western US forest wildfire activity: sensitivity to changes in the timing of spring. Philosophical Transactions of the Royal Society B: Biological Sciences, 371(1696), p.20150178.

Westerling, A.L., Brown, T.J., Schoennagel, T., Swetnam, T.W., Turner, M.G. and Veblen, T.T., 2016. Climate and Wildfire in Western US Forests. Forest Conservation in the Anthropocene: Science, Policy, and Practice, pp.43-55.

Westerling, A.L., Bryant, B.P., Preisler, H.K., Holmes, T.P., Hidalgo, H.G., Das, T. and Shrestha, S.R., 2011. Climate change and growth scenarios for California wildfire. Climatic Change, 109(1), pp.445-463.

Westerling, A.L., Hidalgo, H.G., Cayan, D.R. and Swetnam, T.W., 2006. Warming and earlier spring increase western US forest wildfire activity. Science, 313(5789), pp.940-943.

White-Newsome, J., O'Neill, M.S., Gronlund, C., Sunbury, T.M., Brines, S.J., Parker, E., Brown, D.G., Rood, R.B. and Rivera, Z., 2009. Climate change, heat waves, and environmental justice: Advancing knowledge and action. Environmental Justice, 2(4), pp.197-205.

Wing, O.E., Bates, P.D., Smith, A.M., Sampson, C.C., Johnson, K.A., Fargione, J. and Morefield, P., 2018. Estimates of present and future flood risk in the conterminous United States. Environmental Research Letters, 13(3), p.034023.

Wing, O.E., Bates, P.D., Smith, A.M., Sampson, C.C., Johnson, K.A., Fargione, J. and Morefield, P., 2018. Estimates of present and future flood risk in the conterminous United States. Environmental Research Letters, 13(3), p.034023.

Woolley, B., 2018. The effect of bike lane infrastructure on urban housing markets (senior thesis). University of Richmond.

Wootson, C.R., 2018. The deadliest, most destructive wildfire in California’s history has finally been contained. The Washington Post.

Worzala, E. and Hammett, V.L., 2017. Post-disaster recovery for real estate development: An analysis of multi-family investment from the perspective of a low-income housing tax credit (LIHTC) project. In Routledge Companion to Real Estate Development (pp. 260-273). Routledge.

Wuebbles, D., Meehl, G., Hayhoe, K., Karl, T.R., Kunkel, K., Santer, B., Wehner, M., Colle, B., Fischer, E.M., Fu, R. and Goodman, A., 2014. CMIP5 climate model analyses: climate extremes in the United States. Bulletin of the American Meteorological Society, 95(4), pp.571-583.

Yager, J., 2015. Planning for Resilience: The Challenge of Floodproofing Multifamily Housing. New York University Furman Center (Report).

Young, A.M., Higuera, P.E., Duffy, P.A. and Hu, F.S., 2017. Climatic thresholds shape northern high-latitude fire regimes and imply vulnerability to future climate change. Ecography, 40(5), pp.606-617.

Yu, C.Y., Xu, M., Towne, S.D. and Iman, S., 2018. Assessing the economic benefits and resilience of complete streets in Orlando, FL: A natural experimental design approach. Journal of Transport and Health, 8, pp.169-178.

Zhang, Y. and Peacock, W.G., 2009. Planning for housing recovery? Lessons learned from Hurricane Andrew. Journal of the American Planning Association, 76(1), pp.5-24.

Zuk, M. and Carlton, I., 2015. Equitable Transit Oriented Development: Examining the progress and continued challenges of developing affordable housing in opportunity and transit-rich neighborhoods. Poverty and Race Research Action Council.

Zuk, M. and Chapple, K., 2016. Housing Production, Filtering and Displacement: Untangling the Relationships. Institute of Governmental Studies, University of California, Berkeley.

Zuk, M., Bierbaum, A.H., Chapple, K., Gorska, K. and Loukaitou-Sideris, A., 2018. Gentrification, displacement, and the role of public investment. Journal of Planning Literature, 33(1), pp.31-44.

APPENDIX A - Literature Review Search Terms

DISPLACEMENT	***CLIMATE HAZARD***	***MITIGATION and ADAPTATION***
Neighborhood change Housing affordability Housing price Housing mobility Property values Property appreciation Displacement Gentrification Dislocation Relocation Right to return Utility costs Evictions	Climate gentrification Climate displacement Climate migration Disaster recovery, reconstruction Rising sea level Nuisance flooding, tidal floods Extreme heat Heat wave Urban heat island Drought Storms, storm surge Extreme weather Hurricanes Typhoons Tropical storm Wildfire, forest fire Fire insurance Insurance redlining	Energy efficiency Renewable energy (solar, wind) Green building certification Urban growth controls Infill development Upzoning, densification Brownfield redevelopment Parks and open space Street trees Urban agriculture and gardens Stormwater management Transit-Oriented Development Bus Rapid Transit Fixed rail (heavy and light) Walking, walkability Pedestrian infrastructure Biking, bike infrastructure Complete streets EV charging infrastructure Zero-emission vehicles
ANTI-DISPLACEMENT	***VULNERABILITY***	

Affordable housing Inclusionary zoning Rent control Rent regulations Code enforcement Building codes Preservation, acquisition	Renter, owner Public housing Affordable housing Housing quality Segregation Income, low-income, poverty Race, racism, racial equity Environmental justice Toxics, toxic exposure Citizenship, immigration	

Appendix B - References Matrix

	QUESTION 1	*QUESTION 2*	*QUESTION 3*	*TOTAL**
ACADEMIC	145	104	3	**251**
GRAY	48	26	6	**79**
MEDIA	40	3	9	**50**
TOTAL	**233**	**133**	**18**	

***** Totals do not add up because a small number of sources were referenced in multiple sections.

2.2 - High-Resolution Gridded Estimates of Population Sociodemographics from the 2020 Census in California

This section is adapted from (Depsky et al., 2022). The project formulation, data analysis, majority of the text and all figures were prepared by myself, with advising, edits and portions of the text contributed by Dr. Lara Cushing and Dr. Rachel Morello-Frosch. The published version of this work can be found at https://doi.org/10.1371/journal.pone.0270746, with related Zenodo and GitHub repositories accessible at https://doi.org/10.5281/zenodo.5874927 and http://github.com/njdepsky/CA-POP, respectively. NOTE: two additional grids following the paper publication were produced to provide representations of the population identifying as 'American Indian or Alaska Native' and are detailed in the following chapter.

Abstract

This paper introduces a series of high resolution (100 meter) population grids for eight different demographic variables across the state of California using data from the 2020 census. These layers constitute the 'CA-POP' dataset, and were produced using dasymetric mapping methods to downscale population estimates from 2020 census block geographies using finescale residential tax parcel boundaries and Microsoft's remotely sensed building footprint vector layers as ancillary data. In qualitative comparisons to a number of existing gridded population products, CA-POP showed good concordance and offers a number of benefits, including more recent data vintage, higher resolution, more accurate building footprint data, and in some cases more sophisticated but parsimonious and transparent dasymetric mapping methodologies. The CA-POP grids are freely available as GeoTIFF rasters online at github.com/njdepsky/CA-POP, where statewide grids with units of people-per-pixel exist for total population, Hispanic/Latinx population of any race, and non-Hispanic populations for the following groups: American Indian/Alaska Native, Asian, Black/African-American, Native Hawaiian and other Pacific Islander, White, other race or multiracial (two or more races) and residents under 18 years old (i.e. minors). Total (Hispanic/Latinx or non-Hispanic/Latinx) populations of residents identifying as American Indian/Alaska Native alone and in any combination of other races (alone or multiple) are also provided.

Introduction

Understanding the spatial distribution of human populations is integral to civic and land use planning, public policy design and various fields of academic research. For example, many public health studies in the United States (U.S.) seek to quantify the number of people residing near a potential environmental health hazard (Clark et al., 2014; Cushing et al., 2015; Grineski et al., 2017; Morello and Jesdale, 2006). Similarly, environmental justice and equity oriented research often evaluates the degree to which people of color and other socially disadvantaged populations live in closer proximity to environmental contaminants or hazards (Cushing et al., 2018; Grineski et al., 2017; Morello-Frosch et al., 2001). However, the ability to estimate fine-scale spatial distributions of populations in many prior studies has been limited to the spatial granularity of population estimates that are made available by public enumerating agencies, such as the U.S. Census Bureau.

In the U.S., the most granular spatial units of enumeration are census blocks, available in each decennial year (i.e. 2000, 2010, 2020). In non-decennial years, the finest scale estimates are made at the block group level, which are more coarse than census blocks. In California (CA), for example, blocks have an average land area of roughly 0.8 km^2 (~200 acres) and a population of about 75 people each, while block groups are roughly twenty times larger, both in average area and population. Census blocks therefore provide population information at a high spatial resolution, although in more sparsely populated regions, their areal extents tend to be much larger, consisting of large open, unpopulated spaces. Without more precise information about the likely locations of population within these areas, researchers are often forced to assume that populations are uniformly distributed across the entire area of the given census spatial unit (Cushing et al., 2018; Mohai and Saha, 2006; Sadd et al., 2011). Such simplifying assumptions may have significant implications on study findings, especially for research in rural areas and concerned with precisely quantifying populations within an area smaller than local census block or block group areas, such as a specified buffer distance surrounding a polluting facility (Cushing et al., 2018; McKenzie et al., 2016; Pastor et al., 2001).

To address this issue, many techniques have been developed to disaggregate population estimates to finer scales. Broadly speaking, this field of population downscaling is a form of 'dasymetric' mapping, a methodology which dates back many decades (Leyk et al., 2019; Petrov, 2012; Wright, 1936). Eicher and Brewer (2001) formalized many of the techniques and terminology used in modern dasymetric mapping studies in their study to disaggregate population from the 1990 U.S. census from 159 different counties. They refer to the county boundaries where they have observed population estimates as their "source zones", then mask out areas likely to be unpopulated within each county based on higher resolution, ancillary land use datasets, with final populated area boundaries within each county deemed their "target zones". Many subsequent studies emulated the dasymetric mapping techniques detailed in this study, usually employing various land use datasets as their primary source of ancillary data to reapportion population within source zones (e.g., Mennis and Hultgren, 2006; Sleeter, 2004; Tapp, 2010). Some studies construct multi-class weighting schemes to reapportion population to target zones based on the characteristics of the land use type (e.g. high-density versus low-density residential) (Su et al., 2010; Zandbergen and Ignizio, 2010), and often integrate additional ancillary datasets, such as tax parcel data (Mesgar and Jalilvand, 2017; Mitsova et al., 2012), home address (Tapp, 2010; Zandbergen, 2011) and mobile phone data (Liu et al., 2018).

More recently, researchers have begun to employ more complex machine learning techniques to predict fine-scale population distributions within source zones, often using a wide array of ancillary datasets, such as road networks, nighttime lights, infrastructure and building footprint data, in addition to land use layers as covariates in the models (Bhaduri et al., 2007; Lloyd et al., 2019; 2017; Qiu et al., 2020; Stevens et al., 2015; Tiecke et al., 2017). These highly-modeled approaches can represent a significant improvement from simpler techniques, especially in regions of the world for which source zone population estimates from official census surveys are infrequent and/or only exist at very coarse spatial resolutions (Graetz et al., 2020; Palacios-Lopez et al., 2021; Reed et al., 2018; Stevens et al., 2020; Thomson et al., 2020). Leyk et al. (2019) provide a thorough review of dasymetric mapping methods employed in past studies, including these highly-modeled approaches, to construct large-scale (i.e. global, continental) grids of population.

In this paper, we introduce a new suite of publicly available population grids, known as 'CA-POP', for the State of California that were produced using dasymetric mapping methods. The grids represent values for eight different demographic variables from the 2020 U.S. Census and are provided at a pixel resolution of 100 meters. Census blocks from the 2020 census were utilized as source zones and high resolution residential tax parcel boundaries and remotely-sensed, individual building footprints were the ancillary datasets used to construct target zones of population within each block. A relatively simple, polygon binary method (Eicher and Brewer, 2001) of reapportioning population from the block level source zones to parcel and/or building level target zones was utilized. A qualitative comparison to a few of the more heavily modeled gridded products available in California (e.g. LandScan, WorldPop) revealed that CA-POP performs very well in differentiating between populated and unpopulated regions, comparatively. This suggests that in contexts where both source zone population estimates and ancillary datasets are available at high resolutions, simpler, easily replicable dasymetric mapping techniques can yield high quality grids without constructing more complex modeling algorithms. Additionally, at the time of writing, many of these large-scale gridded products have yet to be updated to incorporate 2020 U.S. census values, though they likely will in the future.

Producing high-resolution CA-POP grids for various demographic variables estimated in the 2020 census, including racial and ethnic subgroups, can serve as a resource for studies that seek to specifically evaluate these communities. A precursor to the 2020 CA-POP grids developed by the authors, based on 2017 American Community Survey block group and 2010 block source zones, were employed by Casey et al. (2021) to assess social inequalities in residential proximity to large methane-emitting sites and in Pace et al. (2022) to estimate racial/ethnic inequalities in estimated drinking water concentrations of arsenic, nitrate, and hexavalent chromium from community water systems and areas of potentially high domestic well prevalence, demonstrating the utility of CA-POP for environmental equity studies. As more socio-demographic variables are released by future U.S. Census Bureau's American Community Surveys from the U.S. Census Bureau, additional grids based on these block group-level values may be produced and uploaded to the public CA-POP repository (github.com/njdepsky/CA-POP).

Data and Methods

In conjunction with the estimates of census block populations from the 2020 U.S. Census, two sources of ancillary data were used that represented spatial units at a sub-block level of spatial granularity: i) residential tax parcel boundaries and ii) estimates of the individual footprint of every building throughout the state. Both of these ancillary data sources were used to identify areas within each census block likely to contain populated, residential areas, as opposed to vacant, commercial or other non-residential space.

Census Data

We utilized block level estimates of population collected during the 2020 U.S. Census – the highest spatial-resolution available from the U.S. Census Bureau – from the (P.L. 94-171) Redistricting Data Summary File (Harris, 2021). The tabular block-population data for the Summary File, as well as the shapefile of block boundaries were obtained from the U.S. Census

Bureau in November 2021 for the entire state of California (Manson, 2020). Specifically, data for the following variables were obtained: i) total population, ii) Hispanic/Latinx population of any race, iii) non-Hispanic/Latinx populations for all major racial subgroups available in the P.L. 94-171 file, iv) total (Hispanic/Latinx or non-Hispanic/Latinx) populations of residents identifying as American Indian/Alaska Native alone and in any combination of other races (alone or multiple), and v) population of minors (younger than 18 years old) (Table 1). We produced grids for all racial/ethnic subgroups made available thus far for uniform (single) race classifications, with respondents identifying as another race or as multiple races grouped into a grid for "other/multiracial" residents.

In choosing our racial/ethnic groupings, we sought to maximize the utility of CA-POP for research employing race as a proxy for experiences of racism-- particularly racism operating at institutional and structural levels-- to determine opportunities and risk factors at the neighborhood level. This is in keeping with the understanding of race as a social construct that has been used to systematically discriminate against and socioeconomically marginalize specific groups of people (Bailey et al., 2021; Braveman and Parker Dominguez, 2021). We chose groupings that are typical in the environmental justice literature and somewhat reflect shared forms of discrimination (Morello-Frosch, 2002). However, we recognize that forms of discrimination vary widely between racial and ethnic groups that we have grouped together (for example, different immigration policies for Mexicans and Cubans, who might both identify as "Hispanic" or "Latino/Latinx"). We were limited in our ability to create more fine-grained categories due to the availability of current data, and grids for additional racial categorizations provided in subsequent 2020 Census or American Community Survey tables (e.g., additional sub-categories for Hispanic/Latinx and Asian respondents) can be generated when these data are released.

Table 1. Sociodemographic variables used for final grids

2020 Census Block Level Population Totals Obtained (P.L. 94-171 Code)	**CA-POP Grid Name**
Grids created for each variable:	
Population (*P002001)*	TOTAL
Hispanic or Latinx (*P002002)*	HISP
Non-Hispanic or Latinx, White (*P002005)*	NHWHITE
Non-Hispanic or Latinx, Black or African American (*P002006)*	NHBLACK
Non-Hispanic or Latinx, American Indian and Alaska Native (*P002007)*	NHAMIND
American Indian and Alaska Native alone (Hispanic/Latinx and Not-Hispanic/Latinx) (P001005)	AMIND_ALONE
*American Indian and Alaska Native alone or in any combination of multiple races (Hispanic/Latinx and Not-Hispanic/Latinx)**	AMIND_COMBO
Non-Hispanic or Latino, Asian (*P002008)*	NHASIAN
Non-Hispanic or Latinx, Native Hawaiian and Other Pacific Islander (*P002009)*	NHHIPI
OTHER/MULTI grid is the combined sum of:	NHOTHERMULTI
Non-Hispanic or Latinx, Some Other Race alone (*P002010)* + Non-Hispanic or Latinx, Population of two or more races (*P002011)*	

MINORS grid (population < 18 years old) created from: Population of adults (*P003001) (subtracted from P002001)*	MINORS

*AMIND_COMBO is the sum of P001__ 005,012,016,020,021,022,027,031,032,033,037,038,039,043,044,045,048,049,050,054,055,056,058,059,060,062,064,065,066,068,069,071

Two additional grids were produced and displayed relative to those originally provided in the Depsky et al., 2022 publication and made available to better represent the populations of California residents that identify as American Indian and Alaska Native alone (n= ~630,000) (AMIND_ALONE) and as American Indian and Alaska Native alone or in any combination of other races (n= ~1.4 million) (AMIND_COMBO), for both Hispanic and Non-Hispanic ethnicities. Our previous estimates, as detailed in the published article, only represented Non-Hispanic residents that identified as American Indian and Alaska Native alone (n= ~156,000). This update now provides flexibility for users to represent the American Indian and Alaska Native population in one of three ways across the state. However, it should be noted that new AMIND_ALONE grid contains overlapping population with with the total Hispanic (HISP) grid and the new AMIND_COMBO grid overlaps with both the HISP and the Not-Hispanic other/multi (NHOTHERMULTI) grids. AMIND_ALONE is fully contained within AMIND_COMBO.

The official population enumerated in the 2020 Census for the entire state of California is 39,538,223 people across 519,723 census blocks, with a mean area of 0.79 km^2, or 195 acres. Estimates for each of the above values at the block-group level for the 2020 census were also obtained for use in an accuracy assessment of the dasymetric mapping method employed for total population. Block-groups are at a significantly coarser spatial resolution than blocks (~1:20), with a total count of 25,607 and mean area of 16.0 km^2, or 3950 acres.

Residential Parcel Data

We utilized boundaries for all tax parcels in California from LightBox-Digital Map Products (accessible at digmap.com/platform/smartparcels/), which contains 12,728,980 parcels classified by 278 different land use types. This dataset is used by the California Air Resources Board, among other state agencies, and updated quarterly. The data we utilized for this study was from the final quarter of 2018 and represents tax parcels that were assessed either in 2018 (55% of total) or 2017 (45%). Although the vintage of these parcel boundaries is not perfectly consistent with the 2020 census population estimates, obtaining ancillary data with uniform vintages is challenging and rarely done in a completely harmonized manner (Mennis and Hultgren, 2006; Qiu et al., 2020; Reed et al., 2018). Given the relative recency of this parcel data, it is still a valuable source of ancillary data for dasymetric mapping of 2020 census populations.

We identified a total of 30 of these 278 land use classes as residential for use as ancillary data in creating the population grids, 8,839,658 residential parcels represented roughly two-thirds of all parcels statewide, and covered 6.7% of the total area represented in the full parcel dataset. The full list of these residential land use classes is shown in Supplemental Table A1. The average residential parcel area is 3,500 m^2 (~38,000 ft^2, ~0.86 acres), approximately 220x smaller than the average census block, making these parcel boundaries valuable for downscaling population

estimates within blocks. The highest proportion of residential parcel types are 'SINGLE FAMILY RESIDENTIAL' (n = 7,255,233, 82.1%) and 'CONDOMINIUM (RESIDENTIAL)' (n = 330,047, 3.73%).

In terms of area, the most abundant land use types are 'SINGLE FAMILY RESIDENTIAL' (12,850 km^2, 41.5%) and 'RURAL RESIDENCE (AGRICULTURAL)' (12,000 km^2, 38.8%). The amount of populated residential area within each parcel varies greatly, especially between certain land use types, such as 'SINGLE FAMILY RESIDENTIAL' and 'RURAL RESIDENCE (AGRICULTURAL)'. For example, the former tends to be fairly small, encompassing a single house and surrounding lot area, while the latter often includes a farm residence as well as adjacent agricultural fields. Therefore, even within many residential parcel boundaries, there is a need to further distinguish populated versus unpopulated space, which we largely achieve here through the use of building footprint data.

Building Footprint Data

Further distinguishing between open space and populated areas within blocks and larger residential parcels was done using publicly-available, remotely-sensed building footprints produced by Microsoft for the entire country. The initial version of this dataset was released in 2018, though a second version was released earlier this year and was obtained in November of 2021 for use in this study. These building footprints were identified from publicly-available satellite imagery of the U.S. and employed a series of machine learning (deep neural net) classification algorithms to identify likely building rooftops, converting these footprints to a polygon shapefile for each state. More information on the production of this dataset can be found on its online source repository (github.com/microsoft/USBuildingFootprints). This dataset contains estimated footprints of 11,542,912 distinct buildings across California, with an average individual building area of 277 m^2 (~2980 ft^2, ~0.07 acres), or approximately 13x smaller than the average size of residential parcels, and ~2,850x smaller than the average census block area statewide. The approximate date range of the source satellite image used to create each building footprint is also provided, with 91.6% of all buildings delineated using imagery from 2018 or later.

Despite being the ancillary data source of highest spatial granularity, one inherent limitation of the building footprint data is that it is a single-class dataset, with no distinction between building types, making it difficult to identify which buildings are residential structures. Additionally, the classification algorithm used for building delineation is not perfect, with Microsoft reporting its accuracy in terms of precision and recall at 98.5% and 92.4%, respectively. Precision pertains to relative error rates of false positives (detecting a building where there is none), suggesting a false positive rate of 1.5%, while recall pertains to false negative error rates (failing to detect an existing building), suggesting a false negative rate of 7.6%. This rate of false negatives is not insignificant, and examples of such instances can be seen in Supplemental Figure A1. Given these limitations of the buildings footprint data, we opted to use entire parcel boundaries to represent populated areas in small residential plots to avoid completely relying on the building footprint data to identify populated structures within all residential parcels, described in further detail below. However, the relative performance of this building detection algorithm is still remarkable and the dataset allows for substantial spatial downscaling of likely residential zones,

especially in areas where fine-scale residential parcels are absent. Figure 1 presents examples of census block group boundaries and the ancillary datasets.

Figure 1. Examples of the three data sources used for the population grid creation process in urban (top row) and rural (bottom row) settings. The 2020 census blocks represent the source zones of population and the parcel and building footprint data the ancillary data comprising the target population zones.

Dasymetric Methods

Using the 2020 census blocks as source zones for population estimates across California, the residential parcel and individual building polygons were used to apportion population to smaller subregions within each block. Therefore, some combination of residential parcels and/or building boundaries served as the target zones for population within each census block, with this final vector layer of populated areas then converted to a 100m-resolution statewide grid. This approach could be classified as a form of 'polygon binary' dasymetric mapping, where vector polygon ancillary data sources are used to define populated versus unpopulated classifications within source zones, assuming population is homogeneously distributed amongst the populated target zones regions within each source zone. (Eicher and Brewer, 2001).

Other, more complex dasymetric mapping techniques that utilize multi-class information associated with ancillary data to assign population density weights to each land use region have been employed in past studies as well (Mennis and Hultgren, 2006; Mitsova et al., 2012; Su et al., 2010). In theory, a similar approach could have been employed with the residential parcel ancillary data used in this study, assigning relative population density weights for each of the 30 residential parcel types. However, coming up with appropriate weights for each parcel type is not straightforward, especially as many of the residential parcel classes are absent or rare in some counties compared to others. Also, many of the studies that apply multi-class weighting schemes

utilize population source zones and ancillary land use datasets at much coarser resolutions than the data sources we used (e.g. census tracts rather than blocks) (Eicher and Brewer, 2001; Huang et al., 2021; Mitsova et al., 2012). Accounting for likely variation in population densities between parcel types is less important with smaller source zones like those used in our study. In addition, residential parcels tended to be fairly homogenous within census blocks (i.e. a single block rarely contained both highrise apartments *and* single family homes or rural residences), reducing the need for a multi-class weighting scheme. Furthermore, given that the building footprint data lack classifications of structure type and the fact that both parcel and building boundaries were often both utilized to apportion population within a given census block, we opted to treat both ancillary data sources in a binary fashion.

Creation of the 100m x 100m statewide grids from the 2020 census population estimates was done for each census block, in a stepwise fashion as follows:

A) **Identified all "small" residential parcels to include as eventual target zones in each census block.**
"Small" residential parcels were defined as those with an area less than or equal to one acre (~4050 m^2). However, for five high-density residential classes ('APARTMENT HOUSE (100+ UNITS)', 'APARTMENT HOUSE (5+ UNITS)', 'APARTMENTS (GENERIC)', 'COOPERATIVE (RESIDENTIAL)', 'HIGHRISE APARTMENTS'), parcels of up to 10 acres (~40,500 m^2) were included in this "small" categorization. These thresholds were utilized to exclude parcels that contain large areas of open space in addition to residential structures. This was most commonly seen in RURAL RESIDENCE (AGRICULTURAL) parcels, which have a size (~18 acres) of roughly 40x that of average SINGLE FAMILY RESIDENTIAL parcels (~0.45 acres), on average, despite both types tending to encompass just one single family house. Therefore, parcel sizes for most residential parcel types were limited to 1-acre so that any open space contained within them would not exceed the size of a medium to large yard surrounding a single-family home (Supplemental Figure A2). This 1-acre threshold corresponds to roughly 40% of the area of a single 100 x 100m grid cell and therefore, any open yard space within these plots are likely to minimally impact the eventual gridded output. The 10-acre threshold utilized for the five high-density parcel types was selected after manual inspection of those parcel classes were determined to often occupy more area (i.e. a full city block) in urban zones without containing large amounts of unpopulated space.

These small residential parcels were selected as target zones amongst the ancillary data because most inaccuracies observed upon manual inspection of several hundred parcels were instances of large open spaces being assigned a residential use code, masked out here by selecting only small residential parcels. Given the somewhat common occurrence of false negatives in the building footprint dataset, we did not want to rely on these footprints alone to constrain populated area, though other gridded population efforts have employed such an approach, including the "constrained" WorldPop population grids (Lloyd et al., 2019) and those produced by Huang et al. (2021) for the CONUS region.

B) **Identified all building footprints within "large" residential parcels not included in step (A) and combined those footprints with the small residential polygon boundaries from (A) to produce the final target zones for populations within all**

census blocks containing some residential parcel area.
Building footprints within all "large" residential parcels were assumed to be residential and selected as target zones for population, which masked out open space in these large parcels but still included likely housing structures. These building polygon geometries were then merged with the small residential parcel polygons selected in step (A) to produce the final target zone extents for population apportionment within each census block. Therefore, the target zones within a single census block could consist of both small residential parcel boundaries as well as building footprints if both small and large residential parcels are present.

Given the fact that intersecting the census block, residential parcel and building footprint polygon geometries resulted in some small slivers or fragments of individual parcels or building footprints being assigned to certain blocks, a sliver-removal algorithm was employed to remove most of these instances and an upper population density limit of 1 person per 10 m^2 . This threshold value roughly corresponds to the top 99.9th percentile of observed population density in the original census block source zones and was employed to remove erroneous target zone geometries composed only of small sliver/fragment polygons. Steps (A) and (B) were applied to all census blocks that had some amount of residential parcel area.

C) **Identified all building footprints within census blocks with a non-zero population, but which contain no residential parcels, and set as target zones for those blocks.**
A small portion of the state's population resides in census blocks without residential parcels, largely in sparsely-populated regions. In these instances, the only ancillary data available was the building footprint data and population was uniformly apportioned across all building geometries in these cases. The main limitation inherent in this approach is that not all structures are residential, resulting in some likely over-apportionment of populations to non-residential structures, an issue that was largely avoided in step (B) by selecting only buildings within large residential parcels.

D) **Identified any remaining blocks that have a non-zero population but do not contain any residential parcels nor building footprints. We used the census block boundary as the target zone in this case, assuming uniform population distribution across these blocks.**
A tiny fraction of the state's estimated 2020 population are enumerated in census blocks with neither residential parcels nor detected building footprints. In these cases, the target zones were simply treated as equivalent to the source zones (census block boundaries) and populations were uniformly distributed throughout these areas.

The resultant target zone polygonal geometries produced in steps (A-D) were uniformly assigned population densities based on their parent source zone populations and then converted to 100m x 100m statewide raster grids, which contain values of people per pixel (Figure 2). Roughly 34.5 million people in this final grid (87.2% of the state population) fell within small residential parcels (Step A), 3.6 million (9.1%) resided in large residential parcels and therefore are represented by building footprints within those parcels (Step B), 1.3 million (3.4%) fell in blocks with no residential parcels identified and therefore uniformly represented across all building

footprints within these blocks, and for 128,000 people (0.3%) there existed neither residential parcel boundaries nor building footprints within their census blocks, resulting in a uniform distribution of those populations across their entire block areas (Figure 3). All geospatial operations were performed in a PostgreSQL (v13.3) programming environment using the PostGIS (v2.5) spatial database extension.

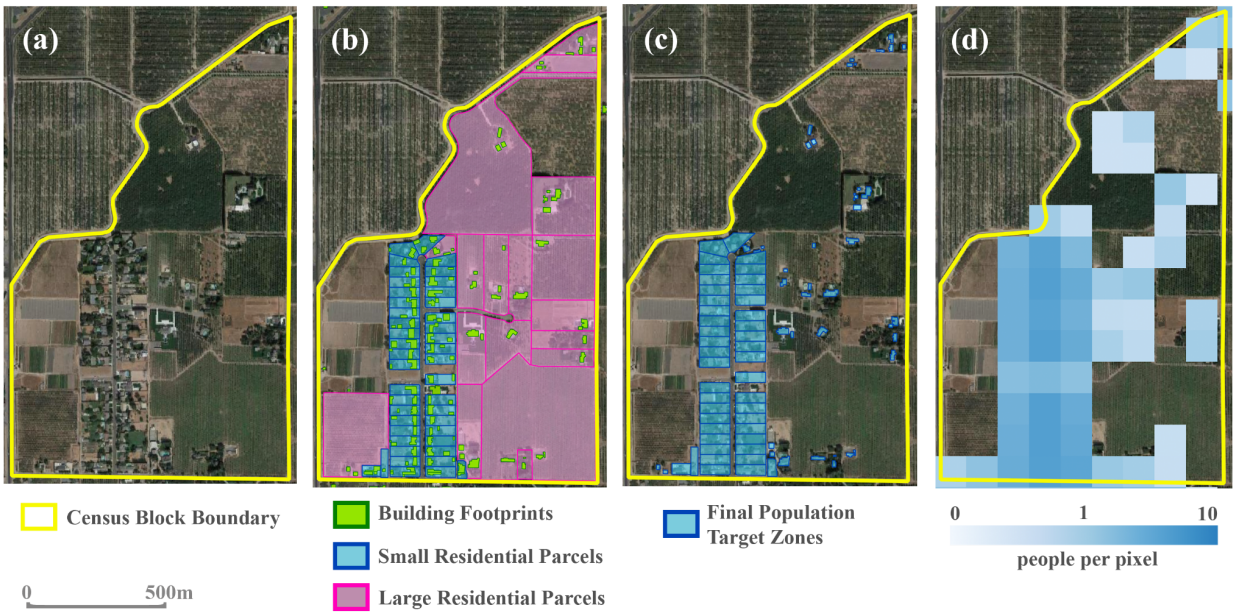

Figure 2. An example of the dasymetric mapping method applied to a single census block just north of Modesto, CA. Panel (a) shows the block boundary; (b) shows the ancillary residential parcel and building footprint boundaries; (c) shows the polygon boundaries used as the final target zones to assign the block's population values, retaining the small residential parcel polygons and building footprint polygons within large residential parcels; (d) shows the 100m-resolution grid produced from population apportioned to the final target zones.

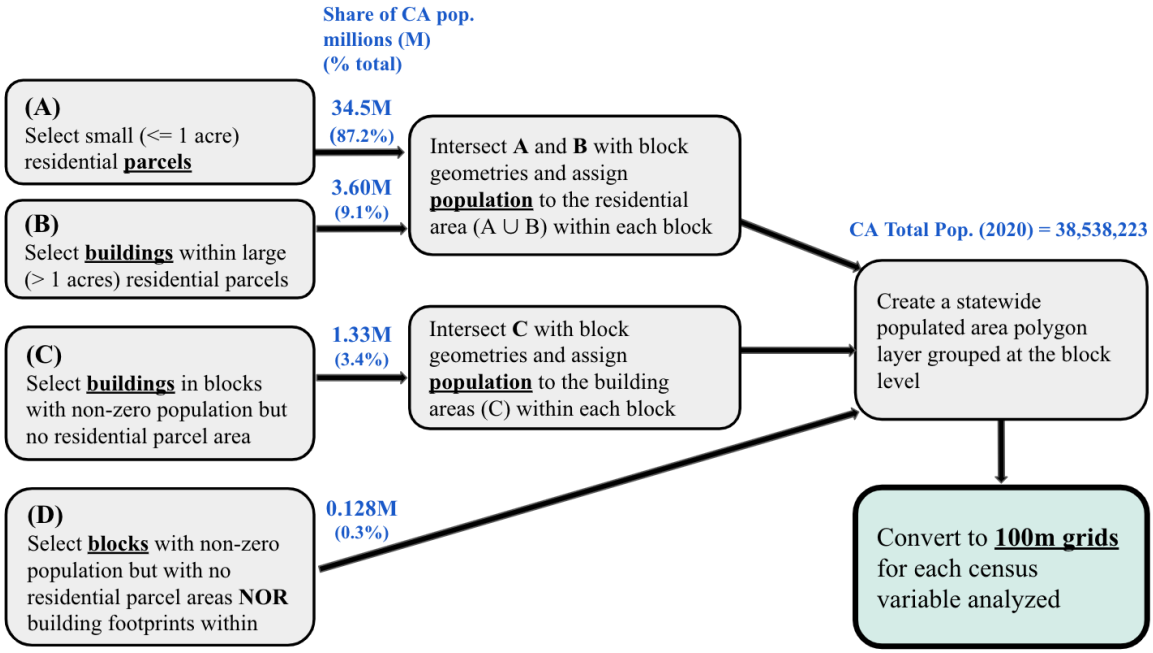

Figure 3. A workflow chart illustrating the process of identifying target zones from the residential parcel and building footprint ancillary datasets within each census block and producing the final statewide grids for each population variable considered.

Accuracy Assessment

Census blocks are the finest spatial unit of population estimation tabulated in the census, and therefore represent the highest resolution set of "ground-truthed" population estimates available to evaluate population estimation accuracy for different dasymetric modeling exercises. Given the fact that these block-level populations are used to constrain population totals in these grids, there is not an easy way to assess the relative accuracy of the dasymetric mapping approach aside from physically visiting the areas or manual inspection of the final product against recent satellite imagery and with contextual knowledge about likely populated areas. More highly modeled, machine learning based prediction models of population can perform accuracy assessments using a cross-validation process, whereby certain observed population constraints are withheld from the modeling process and errors at those omitted locations relative to observed values are measured (Gervasoni et al., 2019; Qiu et al., 2020). However, past applications of traditional dasymetric mapping techniques, like those employed in this study, have often evaluated accuracy of their techniques by producing population grids that are constrained by observed populations at a spatial unit that is coarser (e.g. block groups or tracts) than the finest unit available, then evaluating errors relative to observations at the finest spatial unit (blocks) (Huang et al., 2021; Mennis and Hultgren, 2006; Tapp, 2010).

We performed this type of accuracy assessment for our mapping technique by producing a statewide grid using 2020 population estimates at the block-group level (~20x larger than blocks) but using the same ancillary datasets and dasymetric mapping process described above. Block-level errors were then calculated by comparing values from this grid within each census block's census population value. These errors are not exactly analogous to those that may exist in the block-constrained grids that we ultimately produced, which are likely lower in magnitude due

to the finer resolution of the input data, but rather are meant to demonstrate the general utility of using residential parcel and building footprint data to downscale population estimates within census unit boundaries, and are presented in the following section.

Results

Statewide, 100-meter resolution raster grids were produced for each of the eight 2020 U.S. Census demographic variables listed in Table 1 for the entire state of California. Examples of these grids for four of these variables at different locations across the state are provided in Figure 4 and are publicly available online (see Data Availability).

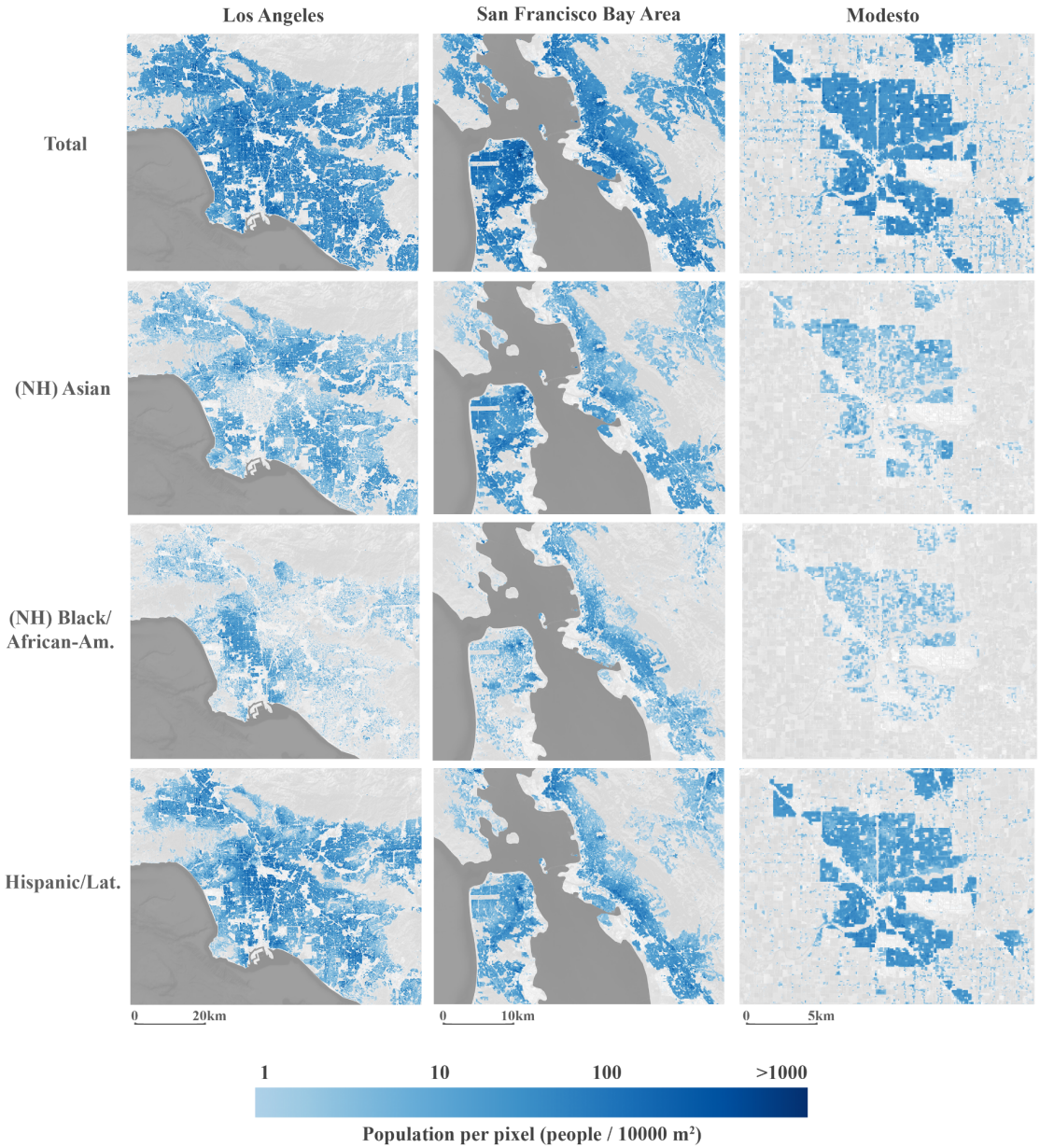

Figure 4. Examples of the final CA-POP grids for four demographic population variables at three different locations in California.

To assess the relative accuracy of these methods as compared to simply assuming uniform population distribution within blocks, the same population grid was created using block-groups as source zones and then compared to observed block level population values to assess the errors when using coarser source zones. The errors in each block-level estimate between the modeled (block group constrained grid) and observed (census block level data) were calculated and are summarized in terms of root mean-squared errors (RMSE) across all blocks and the squared Pearson correlation coefficient (R^2). The same procedure was carried out for a simple uniform, areal weighting technique, which estimates block level population values assuming a homogenous population distribution across the entire spatial area of each block group. Comparing these summary error values between the block group constrained dasymetric grid versus the simple uniform areal weighting technique demonstrates the improved accuracy of using these dasymetric mapping techniques, in terms of lower absolute error magnitudes (RMSE) and higher agreement of population distribution (R^2) at the block level when using these dasymetric techniques compared to uniform areal weighting (Table 2).

Table 2. Summary error statistics between the block group constrained dasymetric population grids and simple, uniform areal population estimation techniques.

Block Population Estimation Method	***RMSE (people)***	***R^2***
Block group-constrained, dasymetric population grid	67.57	0.77
Uniform, areal weighting of block group population	107.2	0.52

However, it is important to consider that these accuracy values only reflect the improved accuracy of the block group constrained grid compared to uniform areal weighting, and not the block constrained grid, which is how the final grids in this study were produced. By design, the block level errors of the block constrained grid are zero, and calculating an analogous set of accuracy measures would require ground truthed estimates of population at the sub-block target zones (i.e. residential parcels and buildings), which are not available. Therefore, the accuracy improvements as compared to uniform areal weighting shown in Table 2 are simply to demonstrate the value of utilizing the dasymetric mapping techniques in CA-POP generally, and do not reflect exact accuracy values of the final grids.

Comparison to Other Gridded Products

Four different, commonly-used gridded population products were evaluated against the CA-POP grids: i) Gridded Population of the World v4.11 (GPW), ii) WorldPop (100m, unconstrained) (WP_{UC}), iii) WorldPop (100m, constrained) (WP_C), and iv) LandScan (LS). At the time of writing, each of these products' population source zones were based on the 2010 census at the block level, with populations in later-year grids estimated via different growth forecasting assumptions to extrapolate 2010 values (Doxsey-Whitfield et al., 2015; Lloyd et al., 2019; Rose

et al., 2020). The latest GPW, WP_{UC} and WP_C population grids are for 2020 and LS for 2019, though presumably they will be updated to 2020 census block source zone populations in the near future.

This incongruity of population source zone vintage between these gridded products and CA-POP make direct comparisons of the grids challenging, and producing an earlier (i.e. 2010) version of CA-POP would be infeasible given the more recent vintage of its ancillary data. Additionally, once the census block source zone populations underpinning each of the other gridded products are updated to the 2020 census, block-level errors should in theory be zero and equal to those associated with the CA-POP grids. Given the fact that each of these grids utilize the highest resolution observed population estimates available, there is no straightforward way to estimate errors in their apportionment of population from source to target zones.

Therefore, we conducted a qualitative assessment of the advantages and disadvantages of CA-POP to these four products based on their underlying data, methods and final grid resolutions, as well as through a series of manual accuracy assessments using contemporary[2] satellite imagery in Google Earth. We also assessed the population grids produced for the CONUS region by Huang et al. (2021), which utilized an earlier version of the Microsoft building footprints as ancillary data.

The GPW product employs the simplest methodology of the grids evaluated, apportioning population from source zones (blocks) to grid pixels through a simple, uniform areal weighting technique, masking out some unpopulated zones, such as water bodies and is provided at a 1km resolution. WorldPop employs a much more complex approach based on constructing machine learning models using a wide suite of covariates, such as roads, land cover, nighttime lights, infrastructure, protected areas, among others to predict population distributions within source zones (Leyk et al., 2019; Lloyd et al., 2019). The WP_C grids represent the results of these predictive models, but with population constrained to building footprints as represented in a recent buildings dataset from Maxar/Ecopia (WorldPop.org, Lloyd et al., 2019). Both WorldPop datasets are provided at 1km and 100m grid resolutions. LandScan employs a “smart interpolation” approach to weight pixels by likelihood of containing population based on a large suite of ancillary data and apportioning populations accordingly, and is provided at a 1km resolution (Leyk et al., 2019; Rose et al., 2020).

Therefore, one advantage of CA-POP over the GPW and LS grids is its higher resolution (100m compared to 1km), made possible from the fine scale parcel and building footprint ancillary data utilized in its production. This allows for a more granular representation of population distributions, especially in sparsely populated regions (Figure 5). Also, the dasymetric mapping techniques used in CA-POP are a significant improvement over GPW’s simple, areal weighting techniques that assume uniform population distribution throughout census blocks.

[2] Satellite base imagery from 2020 and 2021

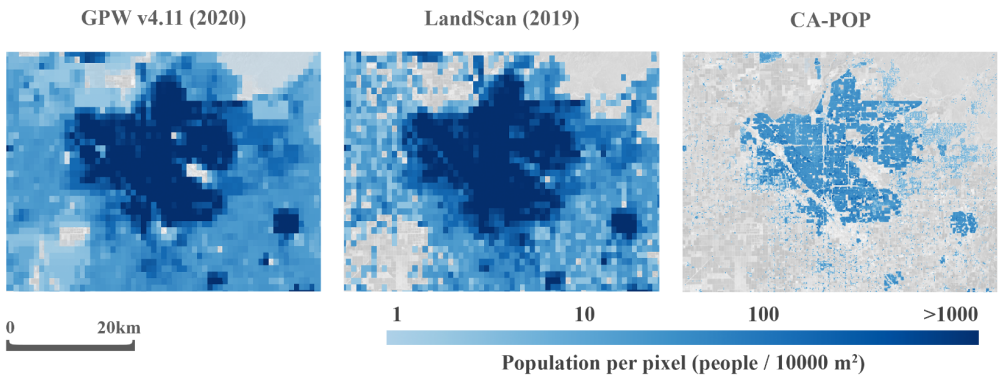

Figure 5. CA-POP compared to the GPW and LS 1km resolution datasets near Fresno, CA.

The CA-POP techniques are simpler than the more heavily modeled approaches used in LS and the WP grids, requiring fewer input datasets and are therefore more easily reproducible. The WP and LS products are particularly well-suited for predicting populations in regions of the world where official population estimates are sparse or more coarsely resolved compared to U.S. census blocks. However, given the high resolution of the population source zones and ancillary datasets used in CA-POP, it is not apparent that WP and LS approaches produce more accurate grids than CA-POP in a California context. In fact, the global Maxar/Ecopia building footprint dataset used to constrain the population apportionment extents in WP_C looks to poorly capture residential structures in many areas of California, especially in medium to low density settings, compared to the Microsoft building footprint data used in CA-POP (Figure 6). Conversely, the WP_{UC}, which utilizes nighttime lights and topography covariates in its predictive modeling algorithm seems to routinely assign population values to pixels based on the pattern of light scatter from street lights or topographic characteristics of the landscape, resulting in the allocation of low population densities across vast swaths of uninhabited space (Figure 6).

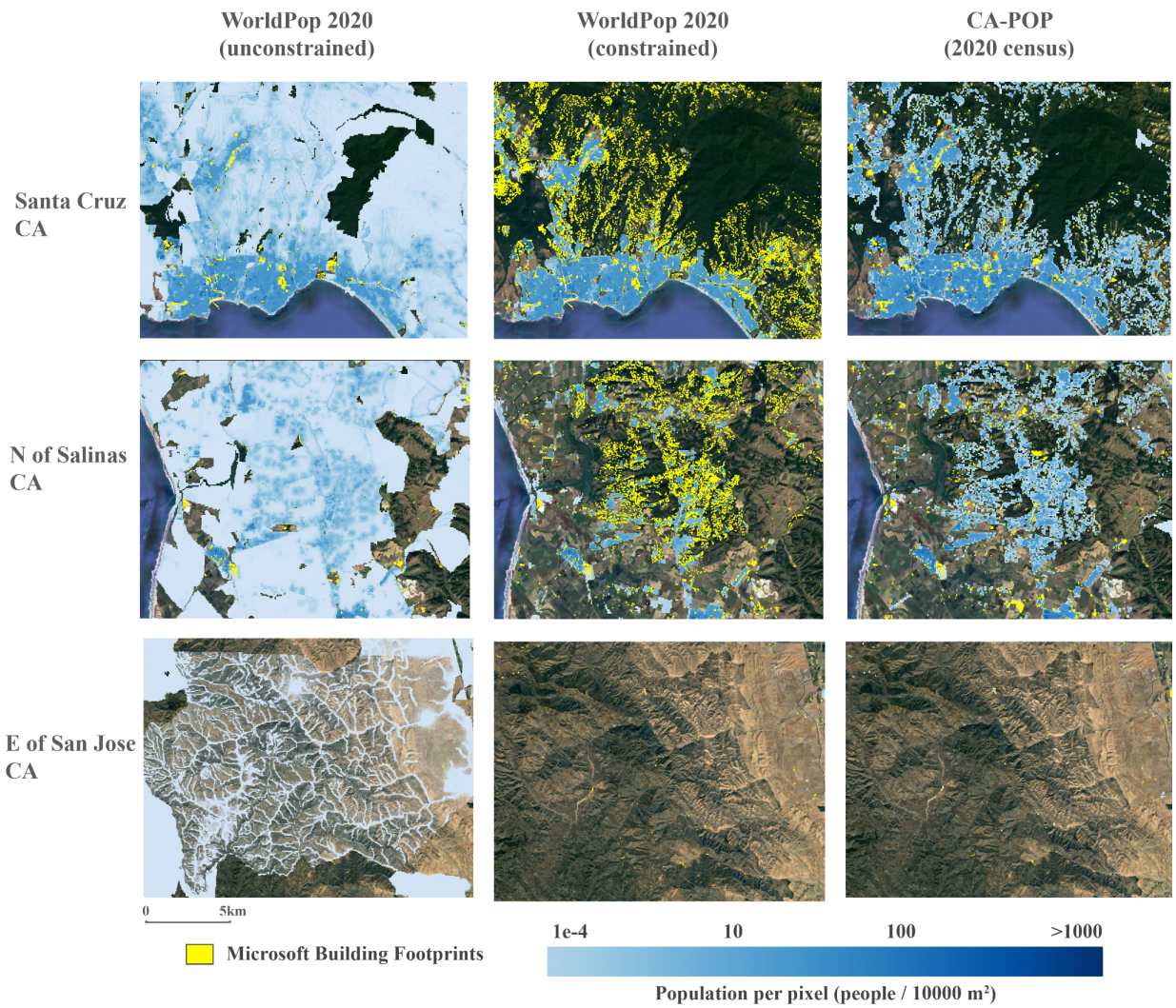

Figure 6. Comparison of CA-POP with the unconstrained and constrained WorldPop grids for three example locations in California. The first two rows represent populated areas and the third row represents largely unpopulated, open space. Over-apportionment of population across open space is seen in the unconstrained WorldPop grid and under-apportionment to buildings footprints detected by Microsoft (yellow area) in residential parcels is evident in the constrained WorldPop grid, as compared to CA-POP.

The CONUS level grids produced by Huang et al. (2021) represent the closest, previously published, methodological approach to CA-POP, apportioning population from census tract source zones to Microsoft building footprints (v1) that fall within residential areas identified in a national OpenStreetMap land use database. However, by assigning population solely to Microsoft building footprint boundaries, the approach is vulnerable to the building detection errors associated with that dataset, namely the occurrence of false negatives. Additionally, population values and source zones in the study correspond to 2017 American Community Survey census tracts, a much coarser geographic unit compared to census blocks.

Table 3. Description of gridded datasets assessed.

Product	Resolution	Population Apportionment Methods[3]	Gridded Variables
Gridded Population of the World v4.11 (GPW)	1km	Areal weighting assuming uniform population distribution using limited land use data (e.g. water bodies) to mask uninhabited areas	Population count Population density Population by age and sex (5-year age bins)
WorldPop (unconstrained) (WP_{UC})	100m	Random forest machine learning algorithm using a wide array of gridded and binary/categorical input covariates (e.g. topography, land cover, nighttime lights, local climate variables etc.)	Population count Population density Population by age and sex (5-year age bins)
WorldPop (constrained) (WP_C)	100m	Similar modeling approach and input datasets as WP_{UC} but with population limited to Maxar/Ecopia building footprint boundaries	Population count Population by age and sex (5-year age bins)
LandScan (LS)	1km	"Smart interpolation" modeling approach to weight pixels based on their likelihood of containing population using a large suite of ancillary datasets (e.g. topography, land cover, climate, infrastructure etc.)	Population count
Huang et al., 2021	100m	Assigns population to Microsoft building footprints (v1) that are masked to residential areas using OpenStreetMap land use data using census tracts as source zones	Population count
CA-POP	100m	Uses high resolution statewide tax parcel dataset from LightBox-DMP and Microsoft building footprints (v2) as ancillary datasets to apportion populations from 2020 census block source zones	Population count (total) Hispanic/Latinx population Non-Hispanic/Latinx population for six racial subgroups Population of minors (<18 y/o)

Though not centrally relevant to the comparison of these products to CA-POP, we also evaluated the accuracy of each of the latest GPW, WP_{UC}, WP_C and LS grids to the 2020 Census at the block level to understand which product most closely matches 'observed' 2020 values (Supplemental Table A2). Differences between each of these grids compared to 2020 census block populations are shown in Table 3. LS demonstrates the lowest statewide, absolute population estimate error compared to the 2020 census, though performs the worst of the four

[3] GPW, WPC, WPUC and LS datasets all currently use 2010 census blocks as their source zones, which will likely be updated to 2020 census blocks in subsequent grids

gridded products in terms of block level RMSE and correlation coefficient (R^2), possibly due to its large grid pixel area ($1km^2$) relative to the average census block area ($0.79km^2$) and the fact that it represents estimates for 2019, rather than 2020. The WorldPop products have the highest absolute error in terms of total population but most closely match block-level distributional population patterns observed in the 2020 census, demonstrated by the low RMSE and high R^2 values compared to the other products.

Discussion

Overall, the CA-POP grids look to perform well when compared against other available gridded population products (e.g. GPW, WorldPop, LandScan) in terms of its high resolution and ability to capture known residential areas in its population apportionment. Additionally, to our knowledge, CA-POP represents one of the first products to integrate 2020 census values into a set of gridded population products publicly available for use. CA-POP also contains additional demographic variables compared to many alternative products, which can be of use in many research applications concerned with specific demographic subgroups, such as environmental health, equity and justice oriented research. Gridded raster products allow for easier spatial analysis of values within a given zone of interest compared to vector polygon layers due to the relative ease of summing or averaging pixels within an area as opposed to intersecting multiple vector polygon layers and conducting some form of subsequent areal weighting within the zone of interest.

Limitations and Potential Improvements

Though CA-POP represents a fairly accurate and easily replicable method of gridding different census variables, there are a number of known limitations and improvements that could still be made. For one, the accuracy of the CA-POP grids relates to the certainty of the 2020 U.S. census values, which was unique for a number of reasons, including the COVID-19 pandemic, a potential citizenship question, natural disasters, and various operational changes to the census enumeration process that may have led to an undercount of particular groups, especially marginalized populations (Elliott, 2021). Recently, The Urban Institute approximated this possible bias by state and urban area through a process of statistically simulating the likely “true” census values, with their results suggesting that the 2020 census in California is biased low by roughly 345,097 people (-0.87%) (Elliott, 2021). Nationally, the study indicates that these undercounts are proportionally higher in certain population subgroups, such as Black and Hispanic communities and for young children (-2.45%, -2.17% -4.86%, respectively) (Elliott, 2021). Therefore, the CA-POP grids based on these census values should be interpreted with the knowledge that statewide totals are likely lower than true populations, especially in certain disadvantaged communities.

Other future improvements to CA-POP could include updating ancillary datasets as they are made available, such as residential tax parcel boundaries of a more recent vintage than 2017-2018, or more accurate building footprint data. Additional types of ancillary data could also be considered to further inform the apportionment of population to eventual target zones within census blocks, such as home address data (Tapp, 2010; Zandbergen, 2011) or mobile phone usage data (Liu et al., 2018). The ancillary building footprint data that is utilized can also be potentially further analyzed to infer additional information about likely building types based

on patterns and characteristics of building geometry and proximity to one another, analyses for which Jochem and Tatem (2021) constructed the R package *foot*.

Additionally, some form of multi-class weighting technique could be employed to apportion population between different residential parcel types, as is done in similar studies (Eicher and Brewer, 2001; Mitsova et al., 2012; Su et al., 2010). This would require estimating the different relative population density in each of the 30 residential parcel types and then distributing population within a single source zone according to those weights, rather than distributing population evenly across the target zones within each block. Also, additional demographic census variables to the eight initial CA-POP grids provided here are planned to be produced as they are released from the U.S. Census.

Conclusion

In this study, we present a set of high-resolution gridded population products using values from the 2020 U.S. Census for the entire state of California, known as 'CA-POP'. These grids were produced via dasymetric techniques, using census blocks as the population source zones, with population estimates from the 2020 census redistricting Summary File (P.L. 94-171), and leveraging two high-resolution ancillary datasets (residential parcel boundaries and building footprints), to reapportion the estimated population distributions at the sub-block scale. This downscaled population layer was then converted to 100 meter resolution statewide grids for eight population variables of interest provided by the 2020 census. These represent total population, Hispanic/Latinx population of any race, and non-Hispanic populations of: American Indian/Alaska Native, Asian, Black/African-American, Native Hawaiian and other Pacific Islander, White, other race or multiracial (two or more races), total (Hispanic/Latinx or non-Hispanic/Latinx) populations of residents identifying as American Indian/Alaska Native alone and in any combination of other races (alone or multiple) and residents under 18 years old (i.e. minors).

Data Availability

All CA-POP grids are publicly available at github.com/njdepsky/CA-POP and as an archive on Zenodo at https://zenodo.org/badge/latestdoi/434382697. The grids are provided as zipped GeoTIFF files and are projected in the following coordinate reference system (CRS): EPSG:3310 - NAD83 / California Albers - Projected, (units = meters). Future updates and additions to these grids will be provided at this location along with appropriate documentation.

Acknowledgements

This study was funded by the California Air Resources Board (# 18RD018- RM-F and NJD), the Strategic Growth Council (CCRP0022 - RM-F, NJD and LC) and U.S. Environmental Protection Agency (#84003901 LC, RM-F and ND)

References

Bailey, Z.D., Feldman, J.M., Bassett, M.T., 2021. How Structural Racism Works — Racist Policies as a Root Cause of U.S. Racial Health Inequities. N. Engl. J. Med. 384, 768–773. https://doi.org/10.1056/NEJMms2025396

Bhaduri, B., Bright, E., Coleman, P., Urban, M.L., 2007. LandScan USA: a high-resolution geospatial and temporal modeling approach for population distribution and dynamics. GeoJournal 69, 103–117. https://doi.org/10.1007/s10708-007-9105-9

Braveman, P., Parker Dominguez, T., 2021. Abandon "Race." Focus on Racism. Front. Public Health 9.

Casey, J.A., Cushing, L., Depsky, N., Morello-Frosch, R., 2021. Climate Justice and California's Methane Superemitters: Environmental Equity Assessment of Community Proximity and Exposure Intensity. Environ. Sci. Technol. 55, 14746–14757. https://doi.org/10.1021/acs.est.1c04328

Clark, L.P., Millet, D.B., Marshall, J.D., 2014. National Patterns in Environmental Injustice and Inequality: Outdoor NO2 Air Pollution in the United States. PLoS ONE 9, e94431. https://doi.org/10.1371/journal.pone.0094431

Cushing, L., Blaustein-Rejto, D., Wander, M., Pastor, M., Sadd, J., Zhu, A., Morello-Frosch, R., 2018. Carbon trading, co-pollutants, and environmental equity: Evidence from California's cap-and-trade program (2011–2015). PLOS Med. 15, e1002604. https://doi.org/10.1371/journal.pmed.1002604

Cushing, L., Faust, J., August, L.M., Cendak, R., Wieland, W., Alexeeff, G., 2015. Racial/Ethnic Disparities in Cumulative Environmental Health Impacts in California: Evidence From a Statewide Environmental Justice Screening Tool (CalEnviroScreen 1.1). Am. J. Public Health 105, 2341–2348. https://doi.org/10.2105/AJPH.2015.302643

Doxsey-Whitfield, E., MacManus, K., Adamo, S.B., Pistolesi, L., Squires, J., Borkovska, O., Baptista, S.R., 2015. Taking Advantage of the Improved Availability of Census Data: A First Look at the Gridded Population of the World, Version 4. Pap. Appl. Geogr. 1, 226–234. https://doi.org/10.1080/23754931.2015.1014272

Eicher, C.L., Brewer, C.A., 2001. Dasymetric Mapping and Areal Interpolation: Implementation and Evaluation. Cartogr. Geogr. Inf. Sci. 28, 125–138. https://doi.org/10.1559/152304001782173727

Elliott, Diana; Martin, Steven; Shakesprere, J., and Kelly, J. (2021). Simulating the 2020 Census, (November).

Gervasoni, L., Fenet, S., Perrier, R., Sturm, P., 2019. Convolutional neural networks for disaggregated population mapping using open data. Proc. - 2018 IEEE 5th Int. Conf. Data Sci. Adv. Anal., DSAA 2018 594–603. https://doi.org/10.1109/DSAA.2018.00076

Graetz, N., Ummel, K., Cohen, D.A., 2020. Small-Area Analyses Using Public American Community Survey Data: A Tree-Based Spatial Microsimulation Technique, SSRN Electronic Journal., https://doi.org/10.2139/ssrn.3574679

Grineski, S.E., Collins, T.W., Morales, D.X., 2017. Asian Americans and disproportionate exposure to carcinogenic hazardous air pollutants: A national study. Soc. Sci. Med. 185, 71–80. https://doi.org/10.1016/j.socscimed.2017.05.042

Harris, C., 2021. The 2020 Census.

Huang, X., Wang, C., Li, Z., Ning, H., 2021. A 100 m population grid in the CONUS by disaggregating census data with open-source Microsoft building footprints. Big Earth Data 5, 112–133. https://doi.org/10.1080/20964471.2020.1776200

Jochem, W.C., Tatem, A.J., 2021. Tools for mapping multi-scale settlement patterns of building footprints: An introduction to the R package foot. PLoS ONE 16, 1–19. https://doi.org/10.1371/journal.pone.0247535

Leyk, S., Gaughan, A.E., Adamo, S.B., De Sherbinin, A., Balk, D., Freire, S., Rose, A., Stevens, F.R., Blankespoor, B., Frye, C., Comenetz, J., Sorichetta, A., Macmanus, K., Pistolesi, L., Levy, M., Tatem, A.J., Pesaresi, M., 2019. The spatial allocation of population: a review of large-scale gridded population data products and their fitness for use. Earth Syst. Sci. Data 11, 1385–1409. https://doi.org/10.5194/essd-11-1385-2019

Liu, L., Peng, Z., Wu, H., Jiao, H., Yu, Y., 2018. Exploring urban spatial feature with dasymetric mapping based on mobile phone data and LUR-2SFCAe method. Sustain. Switz. 10, 1–15. https://doi.org/10.3390/su10072432

Lloyd, C.T., Chamberlain, H., Kerr, D., Yetman, G., Pistolesi, L., Stevens, F.R., Gaughan, A.E., Nieves, J.J., Hornby, G., MacManus, K., Sinha, P., Bondarenko, M., Sorichetta, A., Tatem, A.J., 2019. Global spatio-temporally harmonised datasets for producing high-resolution gridded population distribution datasets. Big Earth Data 3, 108–139. https://doi.org/10.1080/20964471.2019.1625151

Lloyd, C.T., Sorichetta, A., Tatem, A.J., 2017. High resolution global gridded data for use in population studies. Sci. Data 4, 170001. https://doi.org/10.1038/sdata.2017.1

Manson, S.M., 2020. IPUMS national historical geographic information system: version 15.0.

McKenzie, L.M., Allshouse, W.B., Burke, T., Blair, B.D., Adgate, J.L., 2016. Population Size, Growth, and Environmental Justice Near Oil and Gas Wells in Colorado. Environ. Sci. Technol. 50, 11471–11480. https://doi.org/10.1021/acs.est.6b04391

Mennis, J., Hultgren, T., 2006. Intelligent dasymetric mapping and its application to areal interpolation. Cartogr. Geogr. Inf. Sci. 33, 179–194. https://doi.org/10.1559/152304006779077309

Mesgar, M.A.A., Jalilvand, P., 2017. Vulnerability Analysis of the Urban Environments to Different Seismic Scenarios: Residential Buildings and Associated Population Distribution Modelling through Integrating Dasymetric Mapping Method and GIS. Procedia Eng. 198, 454–466. https://doi.org/10.1016/j.proeng.2017.07.100

Mitsova, D., Esnard, A.M., Li, Y., 2012. Using enhanced dasymetric mapping techniques to improve the spatial accuracy of sea level rise vulnerability assessments. J. Coast. Conserv. 16, 355–372. https://doi.org/10.1007/s11852-012-0206-3

Mohai, P., Saha, R., 2006. Reassessing racial and socioeconomic disparities in environmental justice research. Demography 43, 383–399. https://doi.org/10.1353/dem.2006.0017

Morello, -Frosch Rachel, Jesdale, B.M., 2006. Separate and Unequal: Residential Segregation and Estimated Cancer Risks Associated with Ambient Air Toxics in U.S. Metropolitan Areas. Environ. Health Perspect. 114, 386–393. https://doi.org/10.1289/ehp.8500

Morello-Frosch, R., 2002. The political economy of environmental discrimination. Env. Plann C Gov Policy 20, 477–496.

Morello-Frosch, R., Pastor, M., Sadd, J., 2001. Environmental Justice and Southern California's "Riskscape": The Distribution of Air Toxics Exposures and Health Risks among Diverse Communities. Urban Aff. Rev. 36, 551–578. https://doi.org/10.1177/10780870122184993

Pace, C., Balazs, C., Bangia, K., Depsky, N., Renteria, A., Morello-Frosch, R., Cushing, L.J., 2022. Inequities in Drinking Water Quality Among Domestic Well Communities and Community Water Systems, California, 2011–2019. Am. J. Public Health 112, 88–97.

Palacios-Lopez, D., Bachofer, F., Esch, T., Marconcini, M., Macmanus, K., Sorichetta, A., Zeidler, J., Dech, S., Tatem, A.J., Reinartz, P., 2021. High-resolution gridded population datasets: Exploring the capabilities of the world settlement footprint 2019 imperviousness layer for the african continent. Remote Sens. 13, 1–26. https://doi.org/10.3390/rs13061142

Pastor, M., Sadd, J., Hipp, J., 2001. Which Came First? Toxic Facilities, Minority Move-In, and Environmental Justice. J. Urban Aff. 23, 1–21. https://doi.org/10.1111/0735-2166.00072

Petrov, A., 2012. One hundred years of dasymetric mapping: Back to the origin. Cartogr. J. 49, 256–264. https://doi.org/10.1179/1743277412Y.0000000001

Qiu, G., Bao, Y., Yang, X., Wang, C., Ye, T., Stein, A., Jia, P., 2020. Local population mapping using a random forest model based on remote and social sensing data: A case study in Zhengzhou, China. Remote Sens. 12. https://doi.org/10.3390/rs12101618

Reed, F.J., Gaughan, A.E., Stevens, F.R., Yetman, G., Sorichetta, A., Tatem, A.J., 2018. Gridded population maps informed by different built settlement products. Data 3. https://doi.org/10.3390/data3030033

Rose, A.N., McKee, J.J., Sims, K.M., Bright, E.A., Reith, A.E., Urban, M.L., 2020. LandScan 2019.

Sadd, J.L., Pastor, M., Morello-Frosch, R., Scoggins, J., Jesdale, B., 2011. Playing It Safe: Assessing Cumulative Impact and Social Vulnerability through an Environmental Justice Screening Method in the South Coast Air Basin, California. Int. J. Environ. Res. Public. Health 8, 1441–1459. https://doi.org/10.3390/ijerph8051441

Sleeter, R., 2004. Dasymetric mapping techniques for the San Francisco Bay Region, California. Urban Reg. Inf. Syst. Assoc. Annu. Conf. Proc. 1–12.

Stevens, F.R., Gaughan, A.E., Linard, C., Tatem, A.J., 2015. Disaggregating Census Data for Population Mapping Using Random Forests with Remotely-Sensed and Ancillary Data. PLOS ONE 10, e0107042. https://doi.org/10.1371/journal.pone.0107042

Stevens, F.R., Gaughan, A.E., Nieves, J.J., King, A., Sorichetta, A., Linard, C., Tatem, A.J., 2020. Comparisons of two global built area land cover datasets in methods to disaggregate human population in eleven countries from the global South. Int. J. Digit. Earth 13, 78–100. https://doi.org/10.1080/17538947.2019.1633424

Su, M.D., Lin, M.C., Hsieh, H.I., Tsai, B.W., Lin, C.H., 2010. Multi-layer multi-class dasymetric mapping to estimate population distribution. Sci. Total Environ. 408, 4807–4816. https://doi.org/10.1016/j.scitotenv.2010.06.032

Tapp, A.F., 2010. Areal interpolation and dasymetric mapping methods using local ancillary data sources. Cartogr. Geogr. Inf. Sci. 37, 215–228. https://doi.org/10.1559/152304010792194976

Thomson, D.R., Rhoda, D.A., Tatem, A.J., Castro, M.C., 2020. Gridded population survey sampling: A systematic scoping review of the field and strategic research agenda. Int. J. Health Geogr. 19, 1–16. https://doi.org/10.1186/s12942-020-00230-4

Tiecke, T.G., Liu, X., Zhang, A., Gros, A., Li, N., Yetman, G., Kilic, T., Murray, S., Blankespoor, B., Prydz, E.B., Dang, H.-A.H., 2017. Mapping the World Population One Building at a Time. Mapp. World Popul. One Build. Time. https://doi.org/10.1596/33700

Wright, J.K., 1936. A method of mapping densities of population: With Cape Cod as an example. Geogr. Rev. 26, 103–110.

Zandbergen, P.A., 2011. Dasymetric Mapping Using High Resolution Address Point Datasets. Trans. GIS 15, 5–27. https://doi.org/10.1111/j.1467-9671.2011.01270.x

Zandbergen, P.A., Ignizio, D.A., 2010. Comparison of dasymetric mapping techniques for small-area population estimates. Cartogr. Geogr. Inf. Sci. 37, 199–214. https://doi.org/10.1559/152304010792194985

Supplemental Material

Table A1. Land use codes from tax parcel dataset identified as residential

Parcel Land Use Code	Parcel Count	Total Area [km2]	% Res. Area
APARTMENT HOUSE (100+ UNITS)	1724	16.17	0.05%
APARTMENT HOUSE (5+ UNITS)	112705	491.82	1.59%
APARTMENTS (GENERIC)	32154	92.30	0.30%
CLUSTER HOME (RESIDENTIAL)	51547	37.06	0.12%
COMM/OFC/RES MIXED USE	18307	57.81	0.19%
CONDOMINIUM (RESIDENTIAL)	330047	228.86	0.74%
COOPERATIVE (RESIDENTIAL)	184	0.87	0.00%
DORMITORY, GROUP QUARTERS (RESIDENTIAL)	86	3.57	0.01%
DUPLEX (2 UNITS, ANY COMBINATION)	236620	436.01	1.41%
FRATERNITY HOUSE, SORORITY HOUSE	263	3.10	0.01%
GARDEN APT, COURT APT (5+ UNITS)	275	0.83	0.00%
HIGHRISE APARTMENTS	20	0.08	0.00%
HOMES (RETIRED; HANDICAP, REST; CONVALESCENT; NURSING)	3959	34.73	0.11%
MANUFACTURED, MODULAR, PRE-FABRICATED HOMES	9252	96.33	0.31%
MISC RESIDENTIAL IMPROVEMENT	16837	689.14	2.22%
MOBILE HOME	140782	2185.87	7.06%
MOBILE HOME PARK, TRAILER PARK	5251	220.52	0.71%
MULTI-FAMILY DWELLINGS (GENERIC, ANY COMBINATION 2+)	72299	280.49	0.91%
PLANNED UNIT DEVELOPMENT (PUD) (RESIDENTIAL)	143406	130.58	0.42%
QUADRUPLEX (4 UNITS, ANY	63375	66.32	0.21%

COMBINATION)			
RESIDENTIAL (GENERAL) (SINGLE)	25325	717.73	2.32%
RESIDENTIAL COMMON AREA (CONDO/PUD/ETC.)	18792	118.42	0.38%
RESIDENTIAL INCOME (GENERAL) (MULTI-FAMILY)	18794	123.72	0.40%
RURAL RESIDENCE (AGRICULTURAL)	166093	12004.65	38.75%
SINGLE FAMILY RESIDENTIAL	7255233	12849.40	41.48%
STORES & APARTMENTS	1599	1.80	0.01%
TIMESHARE (RESIDENTIAL)	1218	2.23	0.01%
TOWNHOUSE (RESIDENTIAL)	44892	9.32	0.03%
TRIPLEX (3 UNITS, ANY COMBINATION)	60875	73.61	0.24%

Table A2. Comparison of Gridded Datasets to California 2020 Census Block Populations. RMSE and R^2 values are calculated by comparing the modeled versus 2020 census values for all blocks.

Gridded Product (based on 2010 census)	**Resolution**	**Statewide Absolute Error (people, % state total)**	**RMSE (people)**	**R^2**
GPW 2020	1km	+ 434,804 (1.10%)	112.8	0.48
WorldPop (unconstrained) 2020	100m	+ 1,730,616 (4.38%)	66.7	0.80
WorldPop (constrained) 2020	100m	+ 1,150,917 (2.91%)	61.0	0.83
LandScan 2019	1km	- 54,127 (-0.14%)	148.3	0.29

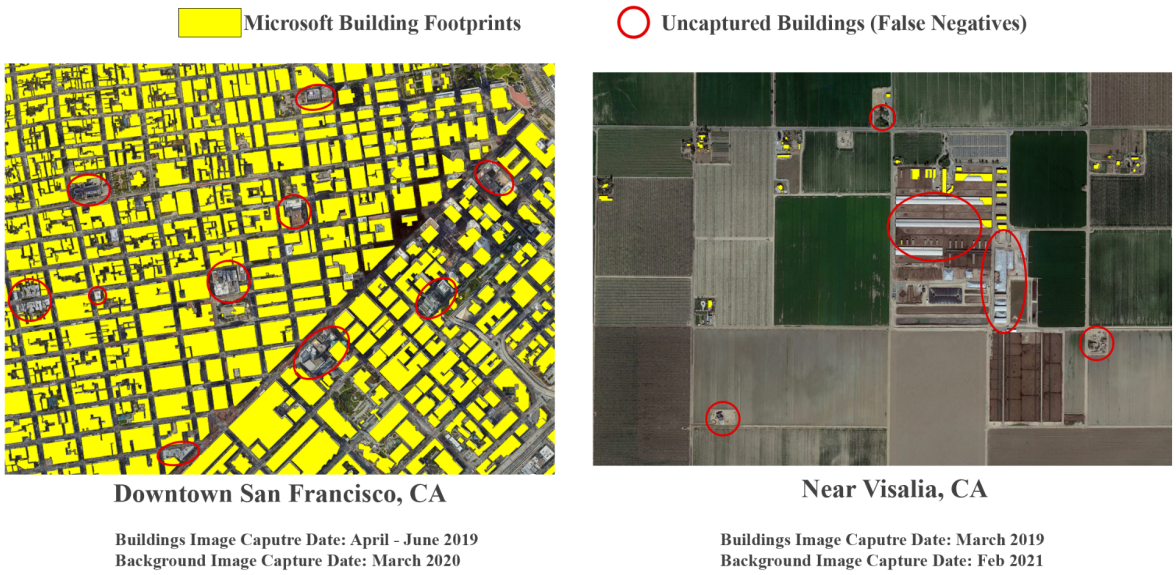

Supplemental Figure A1. False negatives in the Microsoft building footprint data in an urban and rural context. These locations were chosen based on the presence of false negatives and do not generally reflect the typical proportion of false negative instances around the state.

Supplemental Figure A2. Examples of 1-acre (~4050 km^2) residential parcels, which was used as the upper area threshold for low-density residential parcels.

2.3 - Power Loss and Re-electrification of Puerto Rico Following Hurricane Maria and Inter-Census Population Change

This section represents a remote sensing and machine learning investigation of outage patterns and inequities in recovery and population change between the 2010 and 2020 Decennial Censuses. The work was carried out solely by myself and has not yet been published.

Objective

The goal of this project is to investigate the effects of Hurricane Maria on Puerto Rico's electricity sector in the months and years following the storm. Of particular interest are the spatial and temporal patterns of power outages across the island. Using the patterns of outage duration and magnitude identified in this process, I also investigate the extent to which various physical, demographic and socioeconomic variables correlate with outage severity in the months immediately following Maria. Additionally, block group-level population changes between the 2010 and 2020 decennial U.S. censuses are assessed in an attempt to identify possible predictors of observed change using a suite of covariates that include physical and socioeconomic variables as well as the measure of outage and recovery from Maria evaluated in the first study objective.

Context

Hurricane Maria made landfall on the southeastern corner of Puerto Rico's main island on September 20, 2017 with category 4 intensity (on the Saffir-Simpson scale), with maximum speeds of roughly 155mph (Pasch et al., 2018). Over the following ~8 hours, it traversed the island from southeast to northwest, weakening as it traveled overland, eventually re-emerging over the Atlantic and continuing its path northward (Figure 1). The storm was the strongest to hit Puerto Rico in roughly 90 years, since a category 5 hurricane struck the island in 1928 (Pasch et al., 2018). Storm surges of seawater were greater than 5 feet above ground level in some parts of the island, causing flooding and destruction of shorelines and coastal communities.
Storm-associated rainfall totals reached up to 38 inches in some areas of Puerto Rico, causing record-high flows in many inland streams and resulting in mudslides and flooding across the island (Pasch et al., 2018).

Figure 1. Approximate path of Hurricane Maria over Puerto Rico (NOAA).

Estimates put the Hurricane Maria's death toll at just over 3,000, with the majority of these occurring in Puerto Rico and the remainder taking place in surrounding islands such as Dominica (Milken Inst. School of Public Health, 2018). Economic damages of the storm totaled more than $90 billion, making it Puerto Rico's most costly storm and the third-costliest Atlantic Hurricane on record, behind Hurricanes Katrina ($161bn) and Harvey ($125bn) (NOAA - Office for Coastal Management, 2019). The loss of electricity following Maria's devastation also constituted the longest blackout in US history (Pasch et al., 2018), with nearly the entire island without electricity and running water, which endured in some regions for many months. Backup generators and off-grid systems provided some emergency power for isolated facilities and locations but the entire power grid, operated by the Puerto Rican Electric Power Authority (PREPA), was offline for over a week following the storm (US Dept. of Energy, 2017). Service to its customers began to slowly recover beginning on September 29th, but full recovery took nearly a year in some communities (Robles, 2018). One month following the storm, fewer than 20% of PREPA's customers had power. Even after roughly seven months, though power had been restored to roughly 95% of the island, some 60,000 residents still remained without electricity (US Dept. of Energy, 2017). Delays in restoring power were reportedly worse in rural areas and in regions more proximate to the storm's passage (Mercy Corps - U.S., 2019; Román et al., 2019). This study seeks to both assess the power outages experienced across the island during the recovery period and to investigate the relationships between the severity of these outages and various physical, demographic and socioeconomic characteristics at a high spatial resolution.

Methods

The study area for this analysis was limited to Puerto Rico and did not encompass neighboring island nations also impacted by Hurricane Maria. The administrative boundary (level 0) for Puerto Rico was obtained from the Database for Global Administrative Areas (GADM) platform, version 3.6 (GADM, 2018), with more granular administrative boundaries obtained from the U.S. Census Bureau.

In order to evaluate the status of electrification on the island both before and after Hurricane Maria, satellite imagery of nighttime lights was collected and analyzed from the NASA/NOAA Suomi National Polar-Orbiting Partnership (Suomi-NPP) platform. Specifically, images from the Day-Night band (DNB) of the Visible Infrared Imaging Radiometer Suite (VIIRS) sensor aboard

this satellite were used to assess nighttime lights. Daily/nightly data from this platform are publicly available from January 19, 2012 to present day and were obtained from NASA's Level-1 and Atmosphere Archive and Distribution System - Distributed Data Archive Center (LAADS-DAAC) in November 2019 (NASA, 2019). The VNP46 collection of VIIRS DNB data was utilized, as recommended by the product's architects (Román et al., 2018). This collection contains global, nightly mosaics of VIIRS DNB data at a 500-meter pixel resolution and is downloadable for a specific temporal or spatial subset. The VNP46 data collection was announced in its public release documentation to contain two datasets, with the first, known as VNP46A1, being the raw, top-of-atmosphere (TOA) images collected by the VIIRS sensor, and the second, known as VNP46A2, being an improved version of the TOA data with corrections for interferences from clouds, lunar irradiance, seasonal variations in vegetation, bidirectional reflectance distribution function (BRDF) effects, other atmospheric interference effects, and temporal gap filling of missing data (Román et al., 2018) (Figure 2).

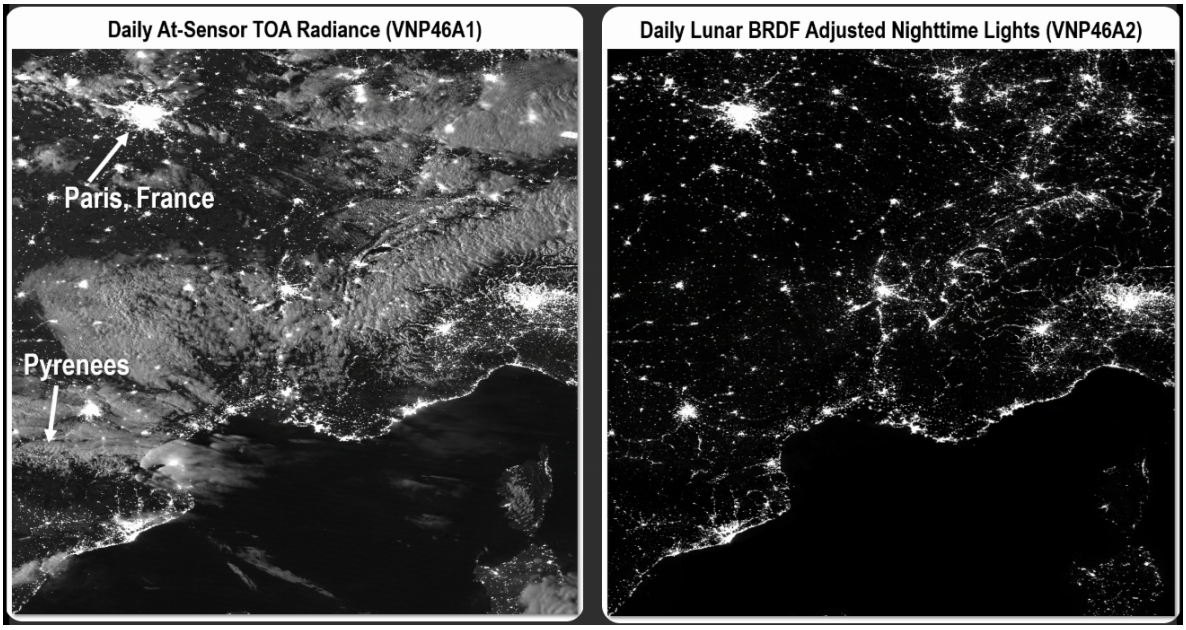

Figure 2. Comparison of VNP46A1 and VNP46A2 datasets (VNP46A2 is still not publicly available as of November 2019). *Image credit: NASA*

However, despite public announcement of both the VNP46A1 and VNP46A2 datasets in June 2018, only the raw, TOA VNP46A1 dataset is available for public use (as of November 2019). There is no official release date for the superior VNP46A2 product, though it was ascertained via personal exchange with NASA support staff that its release is imminent. Therefore, VNP46A1 imagery was utilized despite its known quality issues. For this study, nightly VNP46A1 images were obtained from January 1, 2015 - October 30, 2019, a total of 1,764 images. This study period was selected in order to have ample pre-storm data (>2 years) from which to construct pixel-wise averages of radiance before Maria and ample post-storm data (>2 years) to assess pixel-wise outages and electricity recovery trajectories.

Given the issues of this TOA dataset, some corrections needed to be applied, though it was not feasible in the scope of this project to fully apply all corrective algorithms detailed in the

construction of VNP46A2. Raw radiance values were used from the band in the dataset, which provides values of radiance in units of nW/cm2/sr. Clouds were then masked from each nightly image using data from a cloud quality flag band provided alongside each image. Pixels in this quality band are flagged as being clear, cloudy, having shadows, or containing cirrus clouds for varying degrees of certainty (medium, probably, confidently). For this analysis, only "confidently clear" pixels were retained, representing the most stringent cloud-masking approach and was done to minimize any possible interference from clouds.

The most significant source of variation in observed radiance values aside from changes in anthropogenic sources of light, fires or other natural occurrences (e.g. aurora borealis), are due to reflectance of moonlight on the Earth's surface, also known as lunar irradiance. The additional radiance due to moonlight is starkly seen in the VNP46A1 collection over the study area (Figure 3). The lunar cycle pertains to the changing lunar phase (i.e. new moon vs. full moon) and repeats every ~29.5 days. Therefore, in order to overcome this cyclical interference in radiance caused by the moon, a 30-day moving window average of DNB radiance values was computed to smooth these effects.

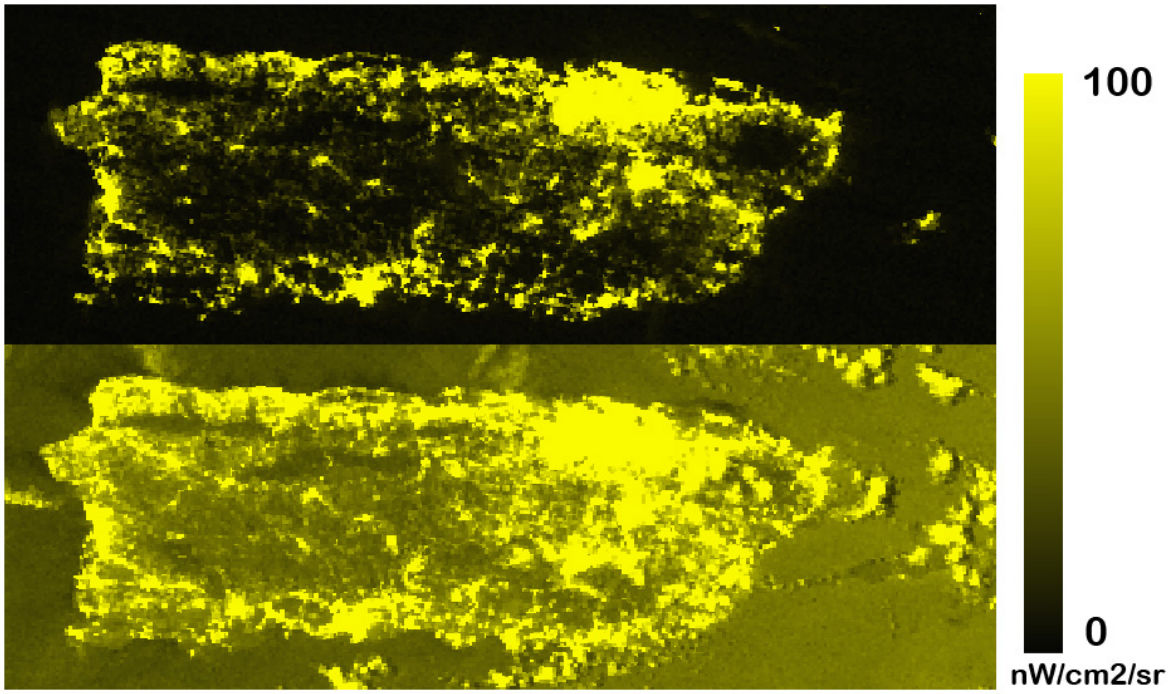

Figure 3. Comparison of two VNP46A1 images for different moon phases [01/28/17]: (*top*) Moon Illumination Fraction = 0.01 (New Moon), (*bottom*) [02/10/17]: Moon Illumination Fraction = 0.99 (Full Moon).

Originally, I explored the possibility of quantifying the interference of lunar irradiance on pixels within the study area by observing the variation of radiance values observed at pixels known to be uninhabited and far from anthropogenic sources of light. In theory, these control points could potentially provide a sense of the baseline level of noise in the nightly data observed at all pixels due to moonlight and other sensor-related effects. Using a 10-day moving average of the original

nightly DNB values, I attempted to build a predictive model of DNB radiance using just the moon phase and sensor information (lunar illuminance, phase angle, lunar/solar/sensor azimuth and zenith) provided as separate bands in the dataset. Using just these variables, I found that one could predict radiance at uninhabited pixels fairly well. Multivariate ordinary least-squares (OLS) models using log-radiance as the outcome variable at a few test control pixels explained ~73% of the variance observed at those locations using just lunar and sensor-related variables provided as extra bands to each image in the collection (Figure 4).

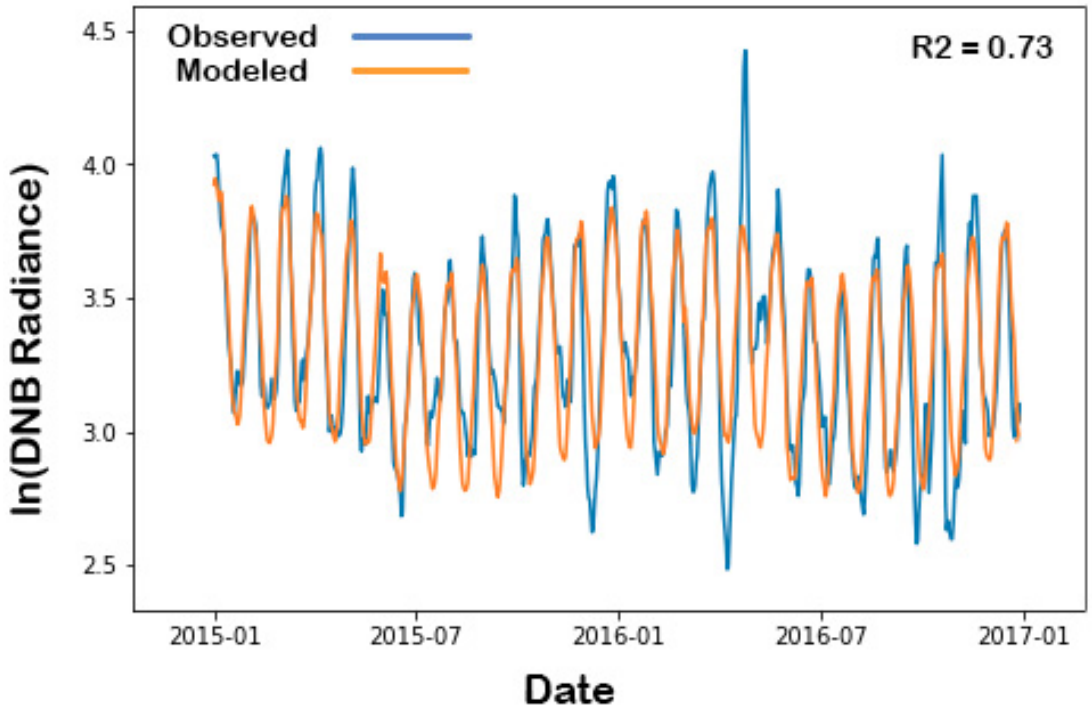

Figure 4. 10-day moving-average data for observed log-DNB Radiance values at an unpopulated pixel from 2015-2017 compared to predicted values from a multivariate OLS model using only moon phase (illumination fraction, phase angle, azimuth, zenith) and sensor information (angle, zenith, azimuth) as predictor variables.

However, given the complexity of trying to formalize this corrective approach for all pixels and the error introduced by it, I ultimately decided to simply use a centered, 30-day moving window-average time-series of log-radiance at each pixel.

Each nightly VIIRS image was masked to the boundary of Puerto Rico plus a buffer of 500m outward from its coastlines in order to ensure the capture of all pixels that intersect any part of its land area. A time-series of DNB-Radiance values were extracted for the 2015-2019 time period at each of the 500m-by-500m pixels within this area, a total of 46,647 pixels.

Figure 5. Zoomed-in view of the 500m meshgrid constructed across the island corresponding to VIIRS

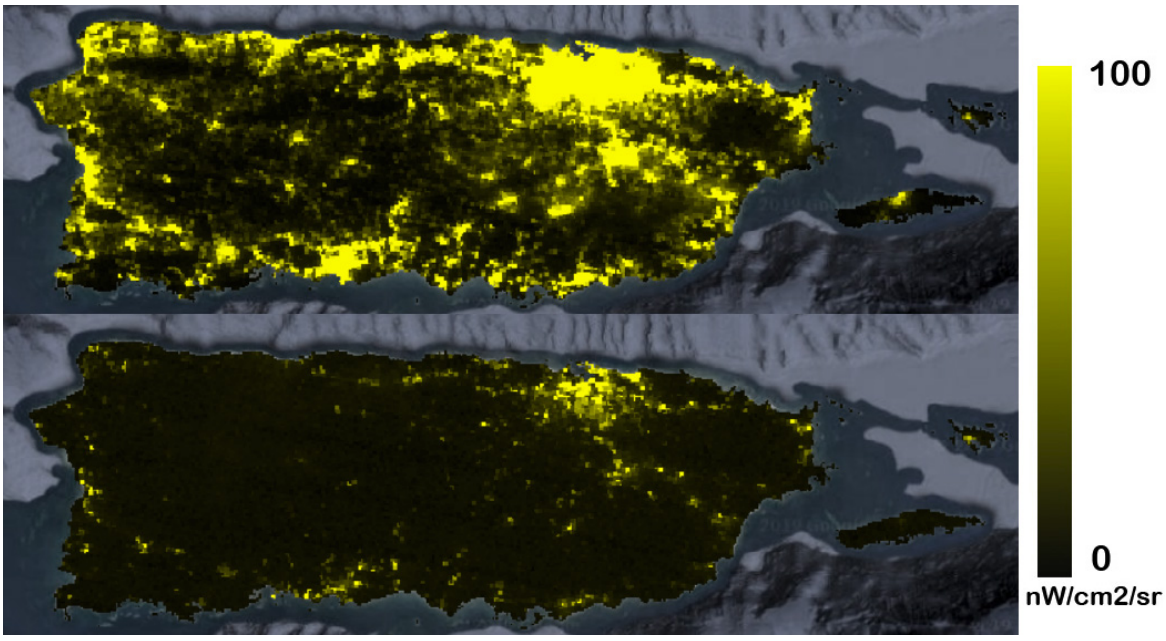

Figure 6. Examples of VIIRS images masked to Puerto Rico's boundary. (*top*) Pre-storm Radiance values on a clear night with a nearly new moon [07/24/17]. (*bottom*) Radiance values on a clear night five days after the storm made landfall, also with a nearly new moon [09/25/17].

Constructing the Power-Outage Outcome Variable

In order to assess the magnitude and duration of the electricity shortage at every location across the island, it was necessary to construct common metrics of relative power outage at each pixel using the time-series data extracted from the VIIRS imagery. Therefore, the pre-storm mean of log-radiances at each pixel location, averaged from January 1, 2015 to September 1, 2017. Given the potential prior impacts of Hurricane Irma on the island in early September 2017, including some scattered power outages, a date cutoff for calculating these "pre-storm" averages was set as Sept 1 in order to omit possible influence from Irma.

Using these mean values, radiance values at each pixel were assessed for the post-storm period, beginning on September 19, 2017, when the island began to experience significant effects of the storm, with landfall occurring the following day. For each day in the post-storm period, the fraction of the pre-storm mean and its 30-day moving-window averaged value were computed. Therefore, if a day in the post-storm period had a log-radiance value of 4.0 and its pre-storm mean was 5.0, its fraction-of-mean value for that day would be 0.8, or 80%. These daily fractions were then averaged over various different post-storm periods to produce a single, integrated measure of presumed power outage for each period that accounts for both the magnitude and duration of negative radiance anomalies following the storm. This was done for every pixel in the study period for post storm periods extending by 30-day intervals following the storm's onset, such as 09/19/17-10/20/17 (Maria + 30 days), 09/19/17-11/19/17 (Maria + 60), and so forth up to 750 days following the storm, or 09/19/17-10/10/19 (Maria + 750).

Given the fact that the bulk of the recovery and re-electrification process occurred within the first 7 months following the storm, the post-storm period for this study was defined as being from 09/19/17-4/18/18 (Maria + 210). This is when PREPA estimates of customers with restored power exceeded 95% and also looks to be when observed DNB radiance values appear to plateau in some of the communities known to be most delayed in recovery (Shermeyer, 2018). It should be noted that it took some residents months beyond this date to receive full power again (Robles 2018; Román et al., 2019). However, by late April 2018, most communities had some level of service, with incremental improvements to power supply occurring in subsequent months. This pattern is reflected in Figure 7, where an example time-series of a pixel within the town of Yabucoa, which was one of the communities first hit and last recovered, shows a period of outage and steady recovery lasting approximately 7 months, after which radiance levels plateau below the pre-storm mean, improving incrementally over the following 2 years.

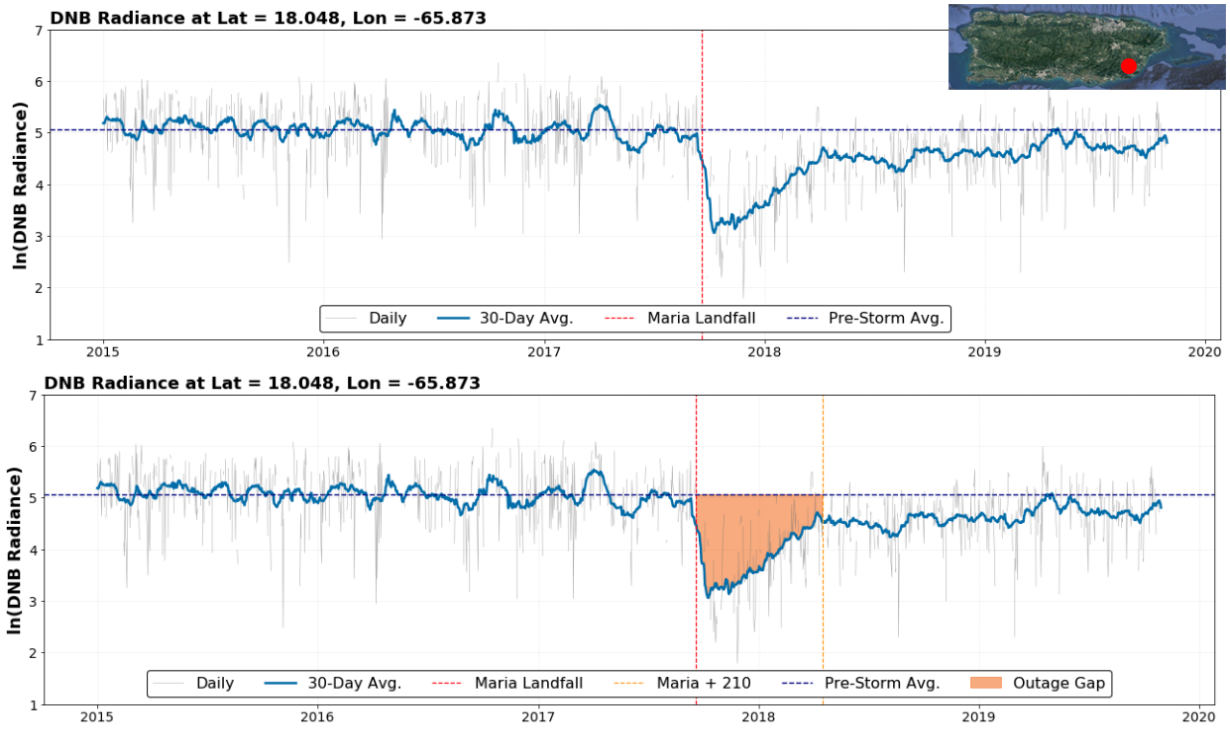

Figure 7. Example time-series of log-DNB-Radiance values at a location in the southwestern town of Yabucoa, one of the first communities hit by the storm. (*top*) Time-series showing daily and 30-day moving-window averaged values. (*bottom*) Same time-series with the post-storm period defined as Maria + 210 days, and the region in orange representing the relative gap below pre-storm mean radiance.

The relative, post-storm power outage at each grid cell, as defined by the mean daily fraction of pre-storm radiance in the 210 days following the storm, was calculated for each pixel and used as the outcome variable for the multivariate, OLS regression of post-storm outages in relation to various physical and socioeconomic covariates. It was assumed that this variable represents an acceptable measure of both the magnitude and duration of outages for the majority of the post-storm recovery period at each location.

Constructing the 2010-2020 Population Outcome Variable

I also evaluated to what extent the selected physical or socioeconomic covariates (detailed below), including the power-outage metric computed above, serve as significant predictors of population change at the block group-level between 2010 and 2020. Using the 2010 and 2020 decennial census population counts at the block-group level, I computed percentage change in totals. However, given that block-group boundaries are often updated between censuses and ACS years, 2010 and 2020 census block group population counts were approximated within the 2017 block group geometries in order to spatially harmonize the outcome variable in this modeling exercise with the ACS covariates. This was done using a populated area-weighted approach, whereby populated areas in 2010 and 2020 were estimated from WorldPop's 2010 and 2020 unconstrained population per pixel rasters (100m resolution), which represent fine-scale, global gridded models of populated area based on contemporary census estimates and

globally-available ancillary datasets (e.g. road density) in each of those years (Stevens et al., 2015; WorldPop 2016). A minimum population density threshold of 1 person per pixel was selected (equivalent to 100 people/km^2), with any pixel values below this assumed to be unpopulated space.

These populated-area polygons for 2010 and 2020 were then intersected with the 2017 census block group boundaries, and area-weighted to estimate the 2010 and 2020 population counts in each 2017 block group. A similar process was employed to area-weight ACS variables within VIIRS grid cells and is illustrated in more detail below. The percent change in block-group level populations considered in this predictive modeling exercise were limited to block groups with a minimum population of 100 people, as reported in the 2013-2017 ACS (2,519 of 2,552 block groups), and all percent change values were winsorized to the 99.5th percentile, to remove large outliers due to small population baselines and such that the range of possible values range from -100% to roughly +100% (99.5th percentile = +101.2%).

Physical Covariates

The physical, pixel-wise variables considered as potentially important in explaining this post-storm (Maria + 210) outage variable were i) mean elevation, ii) mean slope, iii) the distance (from pixel centroid) to the nearest major road or highway, iv) the distance from the storm's centerline path, and v) the distance to the approximate point of Maria's landfall on Puerto Rico's main island (Figure 8).

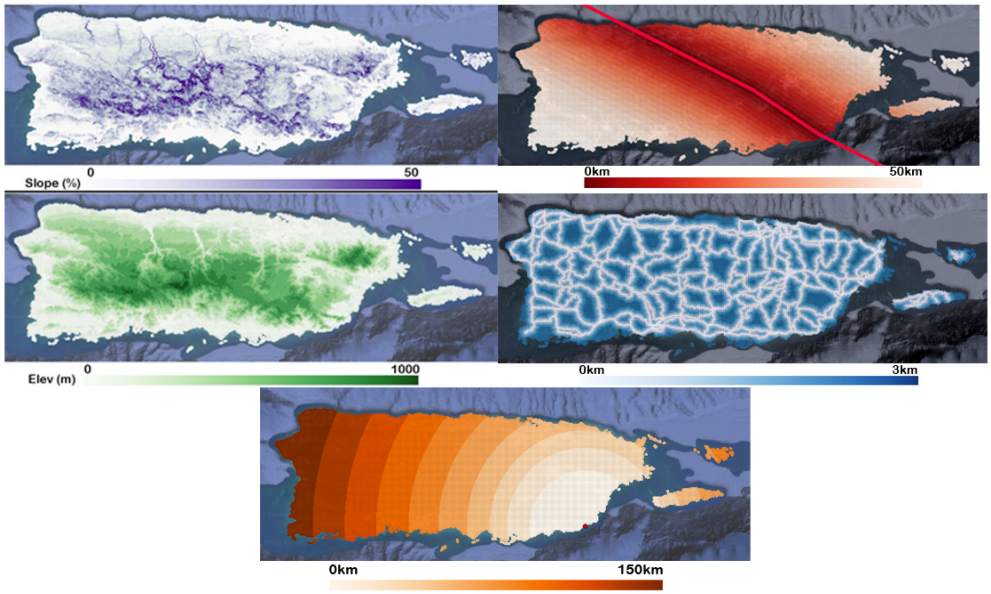

Figure 8. Physical Variables averaged to the 500-meter VIIRS pixel grid. (*top-left*) Slope, (*top-right*) distance to storm centerline path, (*middle-left*) elevation, (*middle-right*) distance to major roads, (*bottom*) distance to Maria's point of landfall.

Elevation was considered due to it being a potential measure both of inaccessibility as well as of increased exposure to high storm-winds. Given that most populated centers and emergency infrastructure are located at low elevations on the island, it was assumed that access to higher elevations by these services is potentially difficult. Additionally, NOAA reports state that many

higher elevations of the island likely experienced wind-speeds commensurate with category 5 storms, although there were no official measurements made at these elevations during the storm's passing (Pasch et al., 2018). A 100-meter resolution digital elevation model (DEM) used to calculate mean elevation within each pixel was obtained from a National Atlas of United States dataset made available on the Stanford Digital Repository (National Atlas of the United States, 2012).

Slope was also included as a measure of inaccessibility and a proxy for increased likelihood of destabilization events, such as mudslides/landslides, of which many were observed across the island. Average percent grades were derived from the same DEM used for elevation. Distances to the storm's path and its point of landfall were used as proxies for relative exposure to the storm's impacts, such as high winds, heavy rainfall and related flooding. Distance to storm-landfall was deemed an important distinct metric due to the fact that cyclone intensities typically diminish rapidly upon making landfall (Phillipson et al., 2021), such that a simple measure of distance to its centerline path alone does not serve as a sufficient proxy for exposure to storm-related hazards. Ideally, high-resolution maps of the storm's actual physical characteristics (wind, rainfall etc.) would be utilized and preferable to these proxy measures, though were not easily discovered in a thorough search of publicly-available models and datasets pertaining to Hurricane Maria. The approximate storm path used for this study was obtained from NOAA (2019), from which the point of landfall was estimated as well. Distance to major roads was included to represent another proxy of remoteness and inaccessibility for pixel locations across the island. A map of major roads was obtained from the National Atlas of the United States (National Atlas of the United States, 2014).

Demographic/Socioeconomic Covariates

All demographic and socioeconomic covariates used in both the storm outage and population change modeling analyses were derived from the 5-year American Community Survey (ACS) from 2013-2017 at the block-group level (*n=2,552*). For modeling the outage magnitudes from Maria, these estimates represent characteristics of block-group populations for the roughly five years leading up to the storm, averaged by grid cell. They were also used to represent average block group characteristics when using 2010 to 2020 census population change as the outcome variable, as they represent the median five year period between 2010 and 2020. The 5-year ACS dataset, as opposed to the 1-year or 3-year ACS dataset, due to it being the most accurate and finely spatially-resolved product, albeit spanning a longer survey period. 1-year and 3-year options are only available for populated areas of 20k or more residents (U.S. Census Bureau, 2021). The block-group level ACS variables used include measures of population distribution, race and ethnicity, income and other measures of livelihood and access to goods and services.

For modeling electricity outage and recovery, these ACS metric values were calculated for all 500m grid cells using the following process and illustrated in Figure 9:

1. Mask out unpopulated areas within 2017 census block group polygon geometries. This was done using WorldPop's 2017 unconstrained population per pixel raster. A minimum population density threshold of 1 person per pixel was set (equivalent to 100 people/km^2) with any pixel values below this assumed to be unpopulated space.
2. This populated area was then intersected with each 2017 block group boundary in order to obtain populated area-by-block group geometries.

3. The spatial layer obtained in Step 2 was then intersected with each 500m grid cell, yielding the populated area-by-block group present within each VIIRS grid cell. Using these intersected pieces of each block group's populated area, ACS measures were averaged within each grid cell using an area-weighted approach.

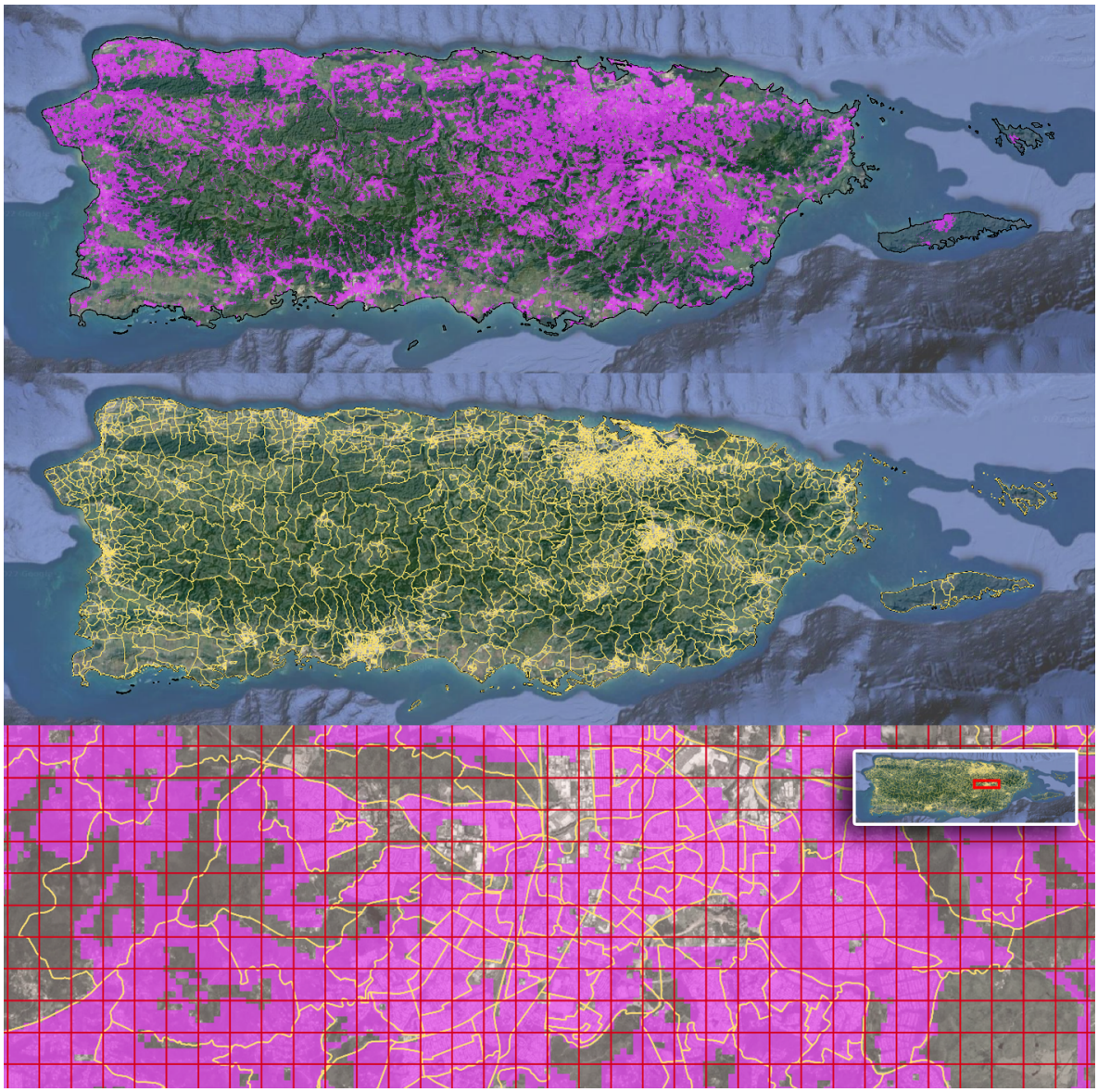

Figure 9. (*top*) Populated area (purple) derived from WorldPop's 2017 gridded population data of Puerto Rico (100m resolution) using a minimum population per pixel threshold of 1. (*middle*) Boundaries of Puerto Rican block groups for 2017 (U.S. Census Bureau TIGER/Line shapefile). (*bottom*) Example of populated area (purple), block group boundaries (yellow) and VIIRS grid cells (red) surrounding the city of Caguas.

Masking out unpopulated grid cells was important for the analysis because only those grid cells that exhibit a detectable level of radiance due to human activity were desired for analysis in the OLS regression model. Uninhabited or very sparsely-populated grid cells will have weak, if any,

difference between pre-storm and post-storm radiance values and will only add noise to the model. At the VIIRS grid cell level, a population threshold of 25 people per 500m pixel, which similarly translates to an approximate population density of 100 people/km^2 was used as the definition of "populated" or not. This thresholding approach succeeded in capturing roughly 95.3% of the total island population across 21,057 grid cells, with the remaining 4.7% dispersed across the remaining 25,590 sparsely populated (<100 ppl/km^2) grid cells.

A total of seventeen different ACS variables were assessed to evaluate if they served as significant predictors for both modeled outcomes: i) post-storm power outages (Maria + 210) and ii) 2010 to 2020 population change. These metrics represent a wide variety of measures for race, wealth and access to goods and services, many of which serve as indicators for underrepresented and/or socially vulnerable communities that have been seen to be disproportionately impacted by previous hurricanes in the U.S (Frey et al., 2007; Fussell, 2015; Graif, 2016). These data, as well as the 2017 boundary shapefile for the 2,552 block-groups in Puerto Rico, were downloaded from the IPUMS National Historical Geographic Information System (NHGIS) data portal[16], which collates and organizes public U.S. Census data for research use. Each of these variables, along with the other physical covariates utilized are detailed in Table 1.

Table 1. Socioeconomic (ACS) and Physical Covariates utilized in outage and population change models.

Variable	**Abbrev**	**Description [Units]**	**Data Source**
Population density	*ppl_km2*	Number of people per km2 [ppl/km2]	2013-2017 ACS
Avg age	*age_mean*	Average age for entire population [years]	2013-2017 ACS
Avg age of housing structure	*age_struct*	Average age of all housing structures, defined by roughly decadal age bins with a max age of 1939 or earlier (age in 2017 defined as 90 years) and ceiling of 2014 or later (age in 2017 defined as 1.5 years) [years]	2013-2017 ACS
Avg annual per capita income	*pcinc*	Per capita income in the past 12 months for entire population [2017 inflation-adjusted USD]	2013-2017 ACS
Avg travel time to work	*commute_avg*	Commuting time to work for workers 16 years and over who did not work at home [mins]	2013-2017 ACS
Avg number of years of education	*yeduc_mean*	Educational Attainment for the Population 25 Years and Over [years]	2013-2017 ACS
Male %	*male_pct*	Percent of male residents of any age [%]	2013-2017 ACS
All-white %	*allwht_pct*	Percent of self-identified white-only (hispanic non-hispanic, single race) residents [%]	2013-2017 ACS
All-black %	*allblk_pct*	Percent of self-identified black-only (hispanic non-hispanic, single race) residents [%]	2013-2017 ACS

Hispanic (all) %	*hisp_pct*	Percent of self-identified Hispanic or Latino residents (of any race) [%]	2013-2017 ACS
Heating from utility	*heat_util_pct*	Percent of occupied housing units whose heating is supplied by utility gas or any form of electricity [%]	2013-2017 ACS
Homeowner %	*howner_pct*	Percent of occupied housing units inhabited by the building owner (non-renters) [%]	2013-2017 ACS
Receives public assistance income %	*pub_asst_pct*	Percent of all households that receive some form of public assistance income in the past 12 months [%]	2013-2017 ACS
No healthcare %	*noHins_pct*	Percent of civilian noninstitutionalized population without some form of health insurance coverage [%]	2013-2017 ACS
Employment %	*empl_pct*	Percent of the population 16 years and older that is in the labor force [%]	2013-2017 ACS
Unmarried %	*single_pct*	Percent of population 15 years and over self-declared as never married, widowed or divorced [%]	2013-2017 ACS
Commute with auto %	*trans_work_auto_pct*	Percent of workers 16 years and over who utilize non-public car, truck or van to commute [%]	2013-2017 ACS
Avg elevation	*elev_mean*	Mean elevation [m]	National Atlas of the US
Avg slope	*slope_mean*	Mean slope, expressed as percent gradient [%]	National Atlas of the US
Distance to storm path	*dist2path*	Distance from the centroid of the given spatial unit (e.g. grid cell or block group) to Maria's centerline path [km]	NOAA
Distance to major road	*dist2rd*	Distance from the centroid of the given spatial unit to the nearest highway or major road [km]	National Atlas of the US
Distance to point of storm landfall	*dist2landfall*	Distance from the centroid of the given spatial unit to the point of Hurricane Maria's landfall on Puerto Rico's main island [km]	NOAA

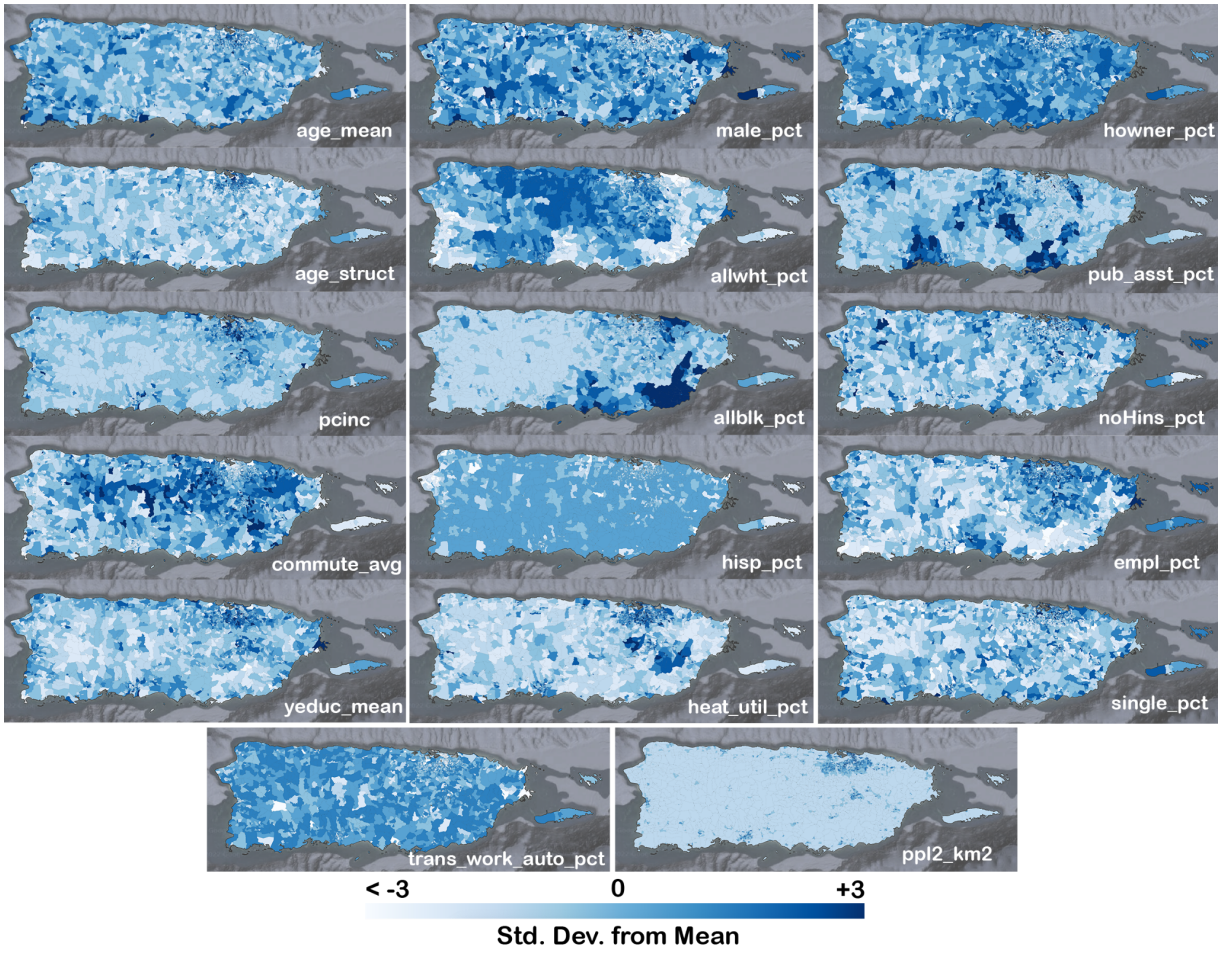

Figure 10. American Community Survey (2013-2017) block-group covariates assessed (standardized values, $\mu = 0$, $\sigma = 1$).

Modeling Approach

For both the post-storm power outage and recovery, as well as the 2010-2020 block group population change outcome variables, analysis was limited to correlational, predictive modeling methods, as opposed to causal identification. The goal of the predictive modeling analysis was to explore how much of the observed variance in each of these outcomes could be explored using two different machine learning methods i) OLS and ii) random forests, with the latter approach further detailed below. For the population change model, the Maria + 210 post-storm outage outcome variable was included as an additional independent covariate in order to assess any potential predictive power that post-Maria electricity outages may have with respect to overall population trends between 2010 and 2020.

Random Forests

In addition to simple OLS, the more complex, tree-based machine learning (ML) method known as ‘random forests’ (RF) was employed in an attempt to construct a model that exhibits higher predictive power, without suffering from overfitting. RF is a derivative of another tree-based ML method that utilizes aggregations of multiple trees, known as bagging, but with improvements to the manner in which these trees are constructed, such that they are more decorrelated from one

another compared to bagging, in turn increasing RF's predictive power (Gareth et al., 2013). RF can be used for quantitative, regression-tree applications, such as this one, or for qualitative classification-tree applications. The fundamental mechanism behind all tree-based methods is the practice of splitting the dataset into different subsets based on threshold values for a given covariate (e.g. all grid cells with a population density of greater/less than 1000 people/km^2), then fitting separate linear (i.e. regression) or classification models to each of these subsets. When multiple trees, each of which may contain multiple such splits, or 'branches', are employed, as in RF, their relative performance can complement one another to result in an aggregated multi-tree model with superior predictive power than simple OLS, or even a single regression tree-based method (Gareth et al., 2013).

When using the RF method to predict the Maria + 210 outage outcome variable, all 22 socioeconomic and physical covariates were utilized and a forest size of 50 trees was employed based on the relationship between tree-count and test-set MSE illustrated in Figure 11, which shows that increasing the number of trees utilized in the RF model dramatically decreases MSE for test subsets (30%) of the data for the first 10 to 20 trees, then with marginal MSE reduction leveling off around 0.20 for forest sizes of roughly 25 or greater. I therefore selected a forest size of 50 trees in order to fully capture the test-MSE reductions associated with the first ~20 trees and some of the additional marginal gains beyond 20, but without needlessly inflating the forest size and computing resources required to construct and test the model.

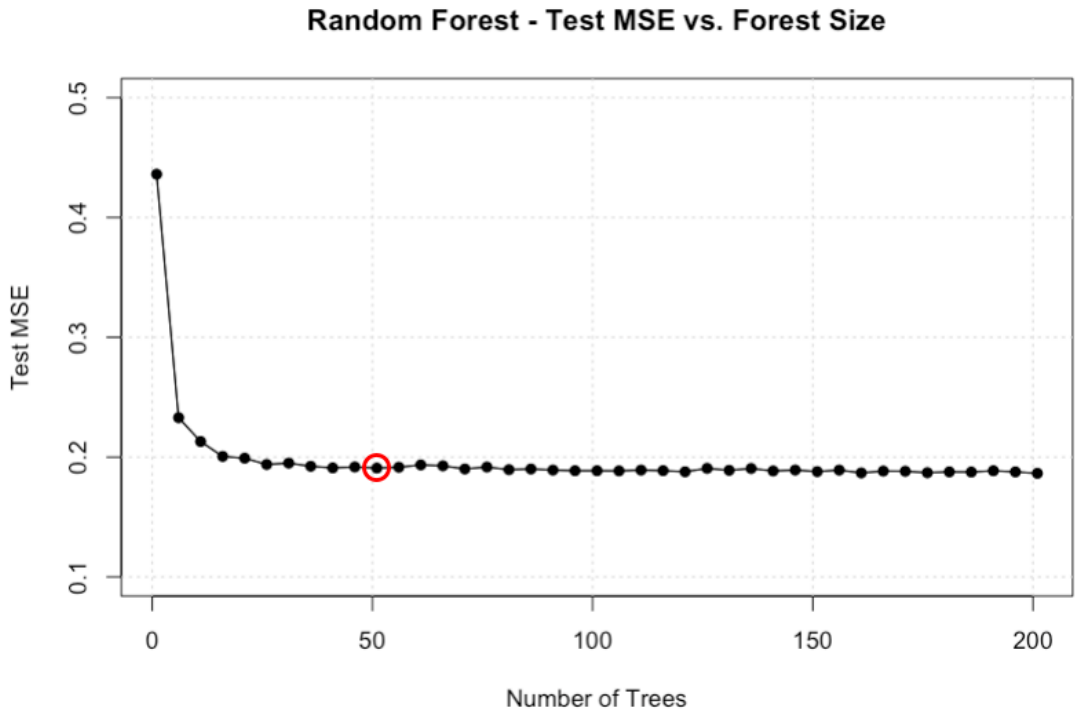

Figure 11. MSE for a 30% test subset of the data for different tree counts (i.e. forest size) in the RF outage model. Each point represents results from a single cross-validation iteration for the given forest size. A forest size of 50 trees was selected as it captures the vast majority of MSE reductions without needlessly inflating the tree count and associated computing requirements.

The same approach for determining forest size was used when applying RF to predict the block group-level percent population change outage outcome variable with all 22 socioeconomic variables, physical variables and the Maria + 210 outage variable. Ultimately, a forest size of 60 trees was selected based on the relationship between tree-count and test-set MSE illustrated in Supplemental Figure 1. For both the OLS and RF approaches, models were fit using the entire set of covariate observations and then randomly split into training and test subsets 30 different times in order to assess model accuracy on the test subset and identify potential model overfitting (Gareth et al., 2013). For all models, the outcome and predictor variables were standardized ($\mu = 0, \sigma = 1$) to allow for analogous interpretation of model coefficients.

Results

Outcome Variable 1 - Post-Maria Electricity Outage and Recovery

The resultant map of average outage level in the post-storm (Maria + 210) period for each 500m VIIRS pixel across the island shows post-storm cumulative outages to be clearly concentrated in the southeastern corner of the island and to more or less track the path of the storm, although there are also many other portions of the island that look to have endured significant outages as well. Overall, the southwestern corner of the island and southern central coast show relatively less outage compared to the remainder of the area. The island of Vieques on the eastern shore of mainland Puerto Rico looks to have suffered significant outage severity as well.

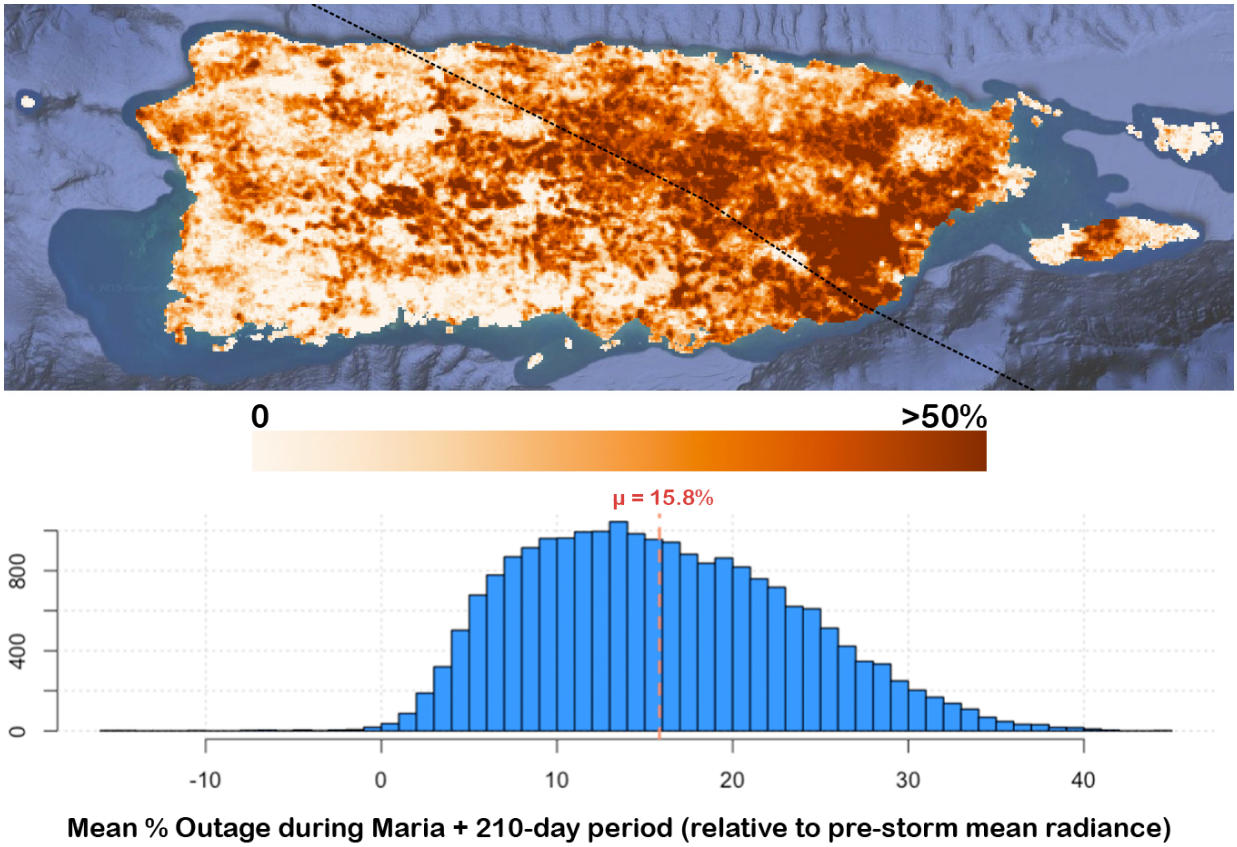

Figure 12. (*top*) Outage Severity Map, calculated as the mean daily percentage of pre-storm average radiance deficit in the post-storm (Maria + 210) period compared to mean pre-storm radiance. Used as the outcome variable for the OLS regression. Storm path shown as dashed line. (*bottom*) The distribution of outage values by 500m VIIRS grid cells, the mean outage value is 15.8%.

Ordinary Least Squares

The results of the OLS regression of this outage outcome variable compared to the physical and socioeconomic ACS variables assessed are shown below in Table 2. In summary, a simple, multivariate, linear model of these variables can explain the (slight) majority (~51%) of observed variance in our post-storm outage metric when fit to the full set of observations.

Table 2. OLS regression results for the post-storm power outage and recovery outcome variable (Maria + 210), ordered by magnitude of coefficient estimate. All covariates were standardized ($\mu = 0$, $\sigma = 1$).

Variable	Coef. (β) Estimate	Std. Error	t-value	Pr(>|t|)
dist2landfall	-0.469	0.0074	-63.20	< 0.001***
yeduc_mean	-0.151	0.0081	-18.62	< 0.001***
elev_mean	0.135	0.0065	20.86	< 0.001***
dist2path	-0.132	0.0071	-18.64	< 0.001***
pcinc	-0.120	0.0077	-15.54	< 0.001***
dist2rd	0.106	0.0051	20.83	< 0.001***

ppl_km2_2017	-0.093	0.0063	-14.73	< 0.001***
slope_mean	0.089	0.0060	14.75	< 0.001***
allwht_pct	-0.087	0.0075	-11.53	< 0.001***
allblk_pct	0.078	0.0075	10.32	< 0.001***
pub_asst_pct	-0.068	0.0054	-12.66	< 0.001***
hisp_pct	-0.064	0.0051	-12.46	< 0.001***
commute_avg	0.060	0.0055	10.93	< 0.001***
age_mean	0.047	0.0065	7.19	< 0.001***
single_pct	-0.034	0.0056	-6.04	< 0.001***
age_struct	0.026	0.0063	4.08	< 0.001***
heat_util_pct	-0.021	0.0058	-3.57	< 0.001***
trans_work_auto_pct	0.017	0.0052	3.30	< 0.001***
empl_pct	0.014	0.0068	2.12	0.034*
noHins_pct	-0.013	0.0051	-2.62	0.009**
howner_pct	-0.008	0.0058	-1.40	0.160
male_pct	0.005	0.0051	0.93	0.354
Residual Std. Error	0.6999		***Significance Levels***	
Multiple R^2	0.511		< 0.001	***
Adjusted R^2	0.510		0.001 - 0.01	**
F-statistic:	997.8		0.01 - 0.05	*
Deg. Freedom (model)	22		> 0.05	
Deg. Freedom (resid.)	21034			
Model p-value	< 2.20E-16			

The model results shown in Table 2 suggest that almost all included covariates represented significant predictors of the post-storm outage outcome variable, with only the percent of homeownership and percent male residents failing to achieve levels of significance of $p < 0.05$.

However, it's possible that this model suffers from overfitting and its reported predictive power may not persist when applied to a subset of test data omitted from model fitting. In order to assess this, cross-validation was performed by randomly splitting grid cells into training subset and test subsets, containing 70% and 30% of grid cells respectively. The OLS model was then fit to the training set, with the resultant variable coefficients used to predict the Maria + 210 outage outcome values for the grid cells in the test subset. This was done 30 times, with different random train-test splits in each iteration, with the coefficient of determination (R^2) evaluated for each iteration's test model performance. The R^2 values for each iteration's training and test subset are displayed in Figure 13.

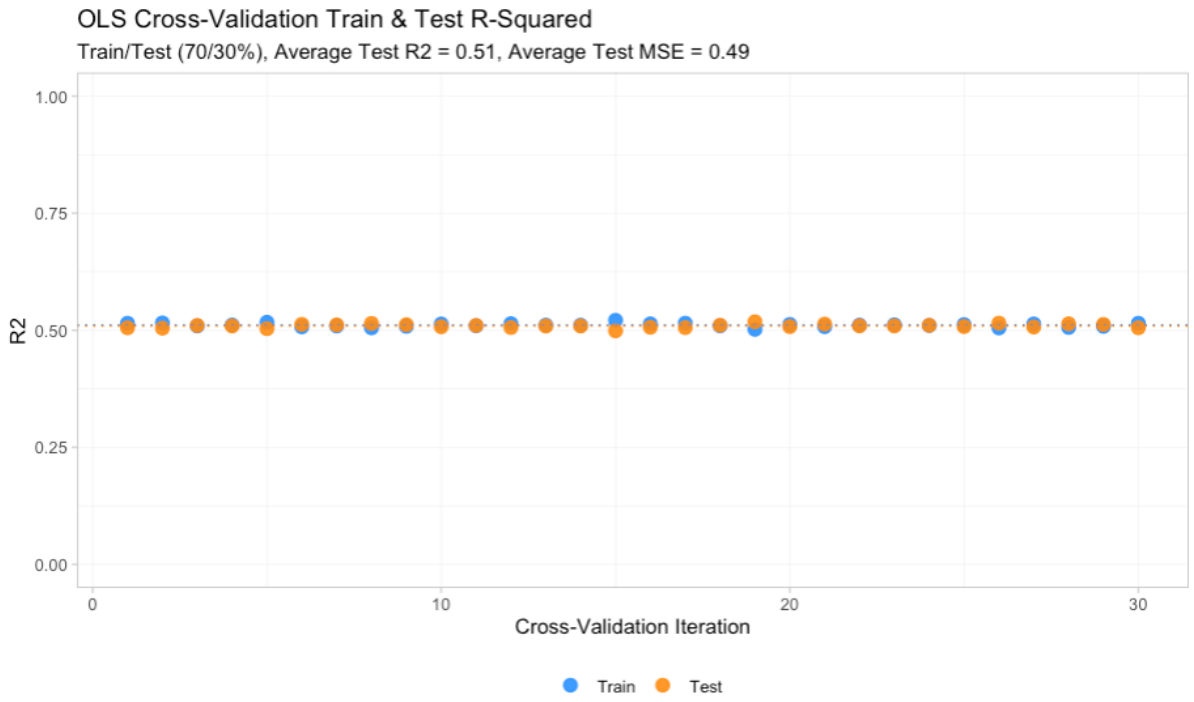

Figure 13. Performance of the post-storm outage OLS model for 30 iterations of cross-validation using 70/30% train/test splits, in terms of R^2.

From Figure 13, we can see that the model performance is highly robust to cross-validation, with performance on test subsets of grid cells achieving essentially equivalent performance to training subsets in terms of R^2 (mean training $R^2 = 0.511$, mean test $R^2 = 0.509$). This instills confidence that the model fit to the full dataset, detailed in Table 2 has valid predictive power for explaining just over half (51%) of the observed variance in the Maria + 210 outage and recovery outcome variable utilized here. Figure 14 demonstrates the scatter plot of predicted versus observed values for all grid cells using the OLS model trained on the full dataset.

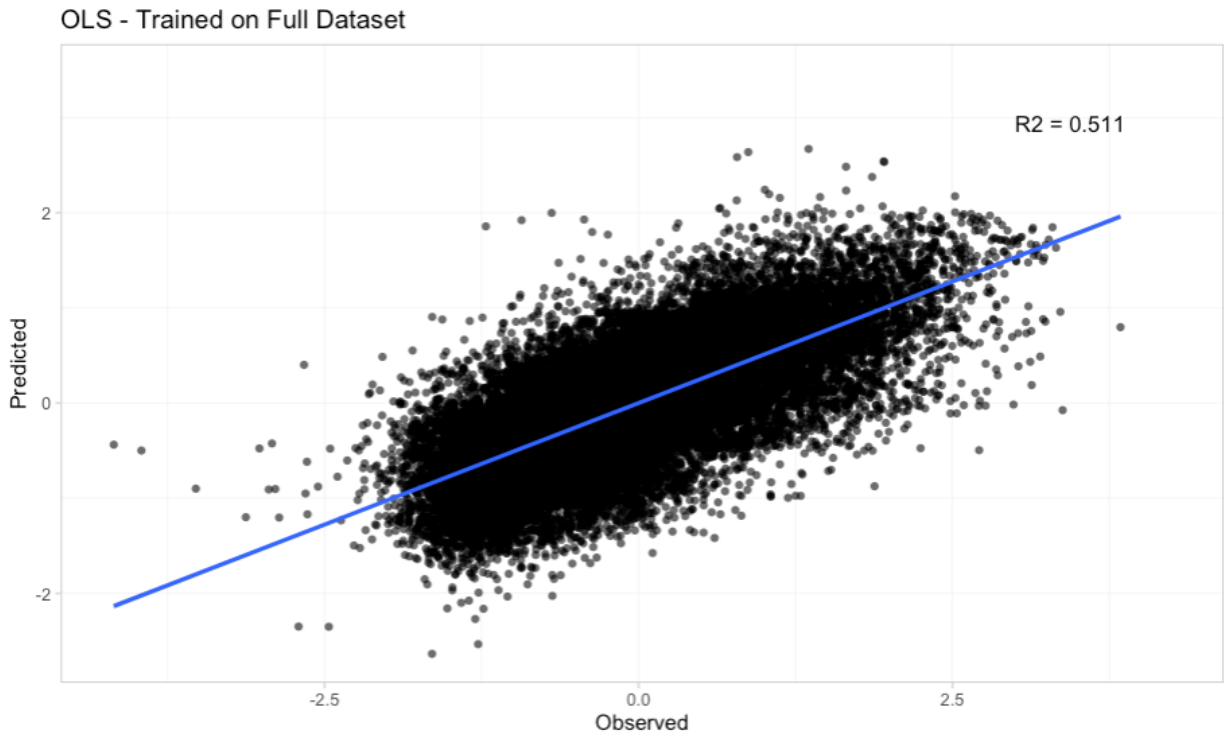

Figure 14. Scatter plot of predicted versus observed values for the Maria + 210 outage outcome variable for the OLS model trained on all grid cells (n=21,057).

Quadratic and cubic forms of all predictors, as well as log-transformed forms of the three distance metrics (landfall point, storm path, major roads) were also assessed in this modeling framework in an effort to identify non-linear relationships and potentially improve the model's predictive power. Inclusion of these additional covariates yielded slight improvements in model performance, with an $R^2 = 0.558$ when trained on the full dataset and a mean test $R^2 = 0.553$ when cross-validated using the same approach as above. However, these marginal gains in model performance came at the cost of more than tripling the number of covariates used, complicating its interpretability, and therefore additional terms are omitted from the final model form shown above and discussed in the following section.

Random Forests

When using the 50-tree RF method to predict the Maria + 210 outage outcome variable on all 22 socioeconomic and physical covariates, the resulting model achieved substantially higher performance relative to simple OLS, with an $R^2 = 0.829$ when trained on all ~21k grid cells. The same cross-validation process was employed, splitting the data into training and test subsets (70/30%) and running 30 iterations, which revealed a similar level of robustness to overfitting as with OLS, although with a much higher overall mean training and test R^2 (0.807 and 0.822, resp.), shown in Figure 15.

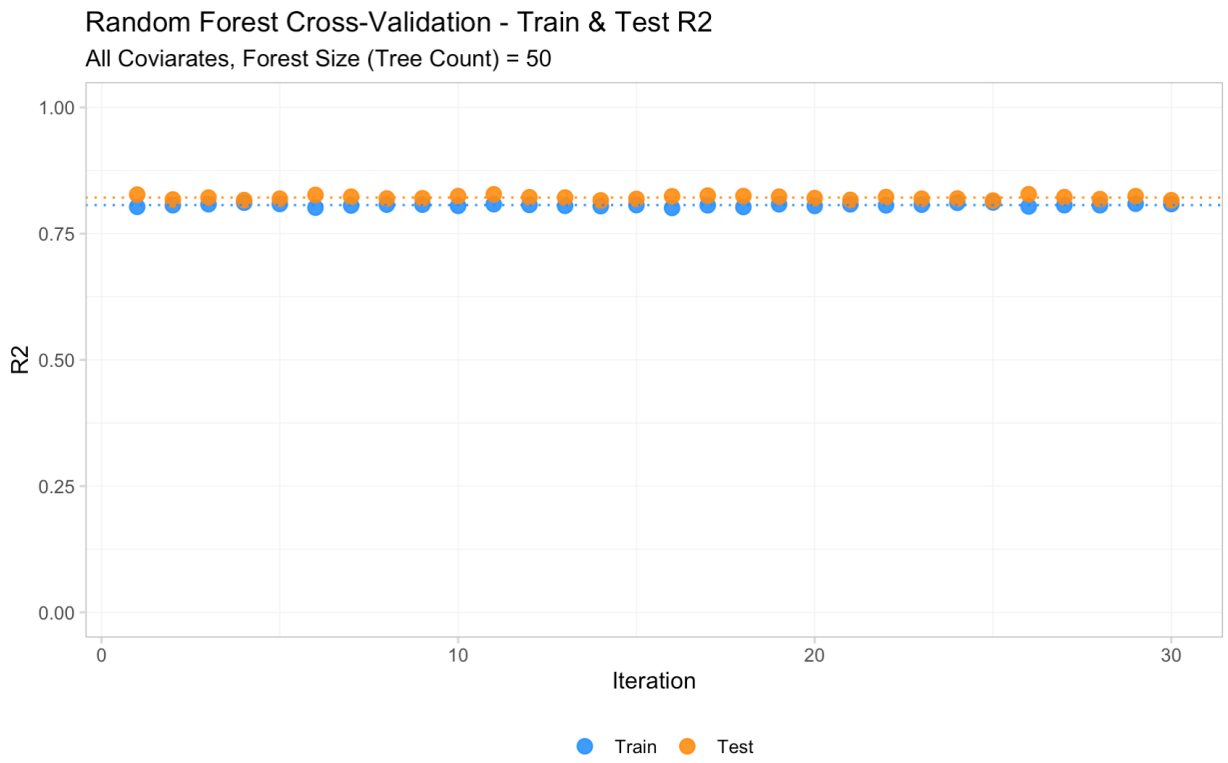

Figure 15. Performance of the post-storm outage RF model for 30 iterations of cross-validation using 70/30% train/test splits, in terms of R^2. Mean test $R^2 = 0.822$.

Overall, this encouraging result from using RF implies that nearly 83% of the observed variation in our Maria + 210 outage variable can be accurately predicted using our selected set of 17 socioeconomic and five physical variables alone, if the RF approach is utilized.

To interpret the significance of each covariate in predicting our outcome variable in the RF approach, there are not simple β-coefficient estimates, as in OLS, associated with each variable, making them less interpretable than simple linear models. However, the relative predictive power of each covariate in an RF model can be gleaned by evaluating how much a given metric of performance, such as MSE, changes when trees are split by a threshold value of that covariate, with higher levels of reduction in MSE following such splits indicating higher importances of that variable. For this RF model of Maria + 210 outages, the variable importance plot based on MSE is shown in Figure 16.

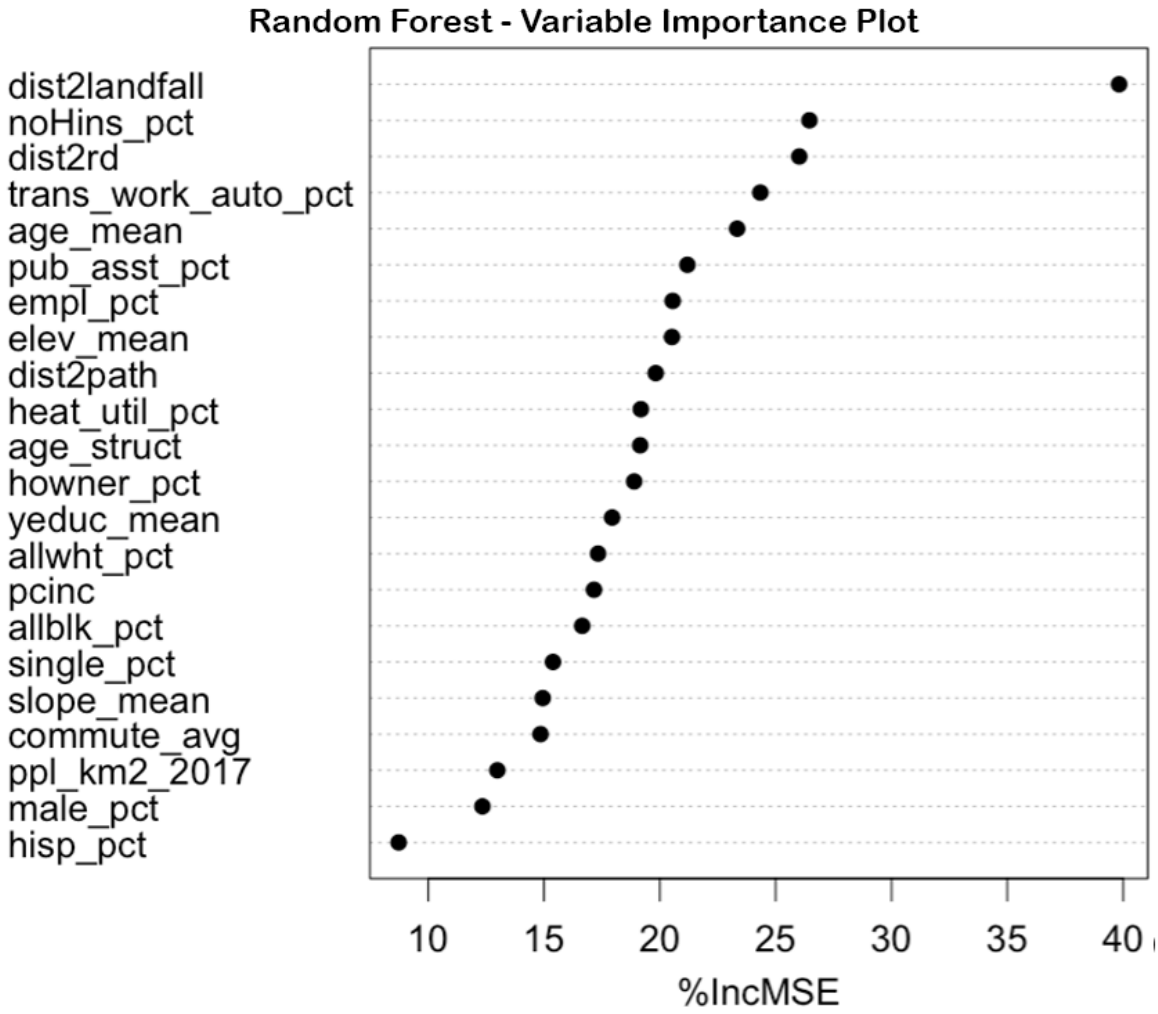

Figure 16. Variable importance plot for the Maria + 210 outage RF model, using percent changes in MSE as the metric of importance evaluation for each covariate. High values indicate high importance.

An RF model including all quadratic, cubic and log-transformed distance variables was also constructed, but similarly to OLS, only marginal increases in predictive power were achieved. Compared to the RF model trained on the original 22 covariates, which had an R^2=0.829, the mean test R^2 using the model trained on the expanded set of 69 covariates only improved to R^2=0.839. This indicates that the vast majority of predictive power for explaining Maria + 210 outages can be achieved through an RF approach trained using solely the original set of 22 covariates.

Outcome Variable 2 - Block Group Population Change from 2010-2020

Results of modeling the block group-level population reported between the 2010 and 2020 decennial censuses for all 2,519 block groups in Puerto Rico (with a population of at least 100 people or more during the 2013-2017 ACS) proved more difficult to obtain a model with strong predictive power without falling prey to overfitting. The decision was made to construct this model using block groups as the spatial unit of analysis since those are the native units for which populations were reported, and which correspond to the finest spatial unit reported in the 2013-2017 ACS. Population change was calculated at the 500m VIIRS grid pixel level via

area-weighted averaging of grid cells intersected with block groups, but resulted in overly-fine spatial units for which to estimate population changes, introducing substantial noise in the percent population change estimates. I therefore elected to design the model using block groups as the spatial unit of analysis. Figure 17 shows the population trend rates used as the outcome variable in this model.

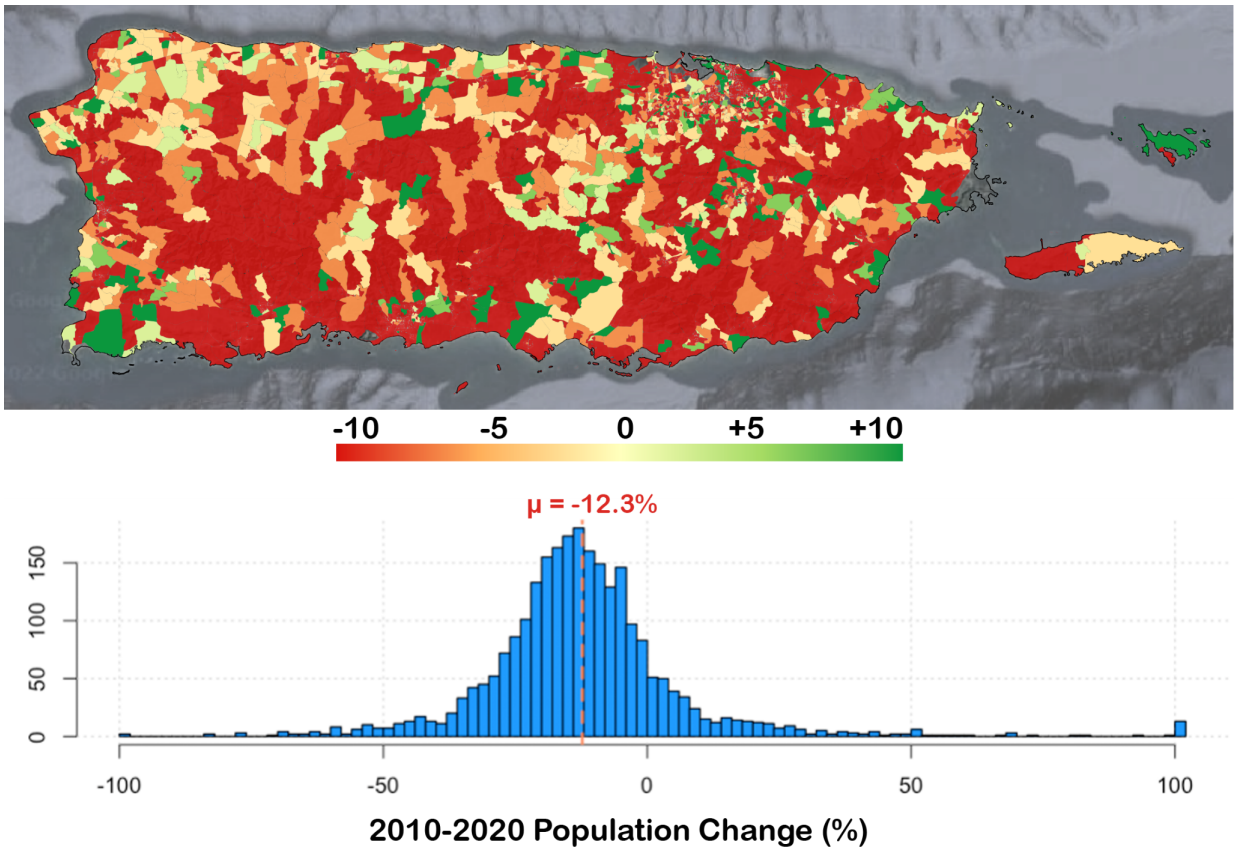

Figure 17. (*top*) Block group-level population changes, expressed as percent differences from the 2010 census, as compared to the 2020 census. Block groups with fewer than 100 residents reported in the 2013-2017 ACS (n = 33) were excluded, and percent change values were winsorized to the 99.5th percentile, which corresponds to ~+100%. (*bottom*) A histogram of the values, mean is equal to -12.3%.

Overall, the spatial pattern of block group population trends from 2010 to 2020 are not abundantly clear from Figure 17, with what appears to be somewhat opposing trends, even in seemingly similar, adjacent block groups. That said, the vast majority of low-density, rural block groups experienced large declines in population, and overall, the average block group experienced a 12.3% decline in population (439,915 people) between the 2010 and 2020 censuses, which is in line with a decades-long trend of population decline on the island, commonly attributed to lack of economic opportunity, worsening island-wide external debt burdens and exposure to natural hazards (Hinojosa et al., 2018).

Ordinary Least Squares

Results of the OLS regression modeling for block group percent population changes between 2010 and 2020 was done using all of the same 22 physical and socioeconomic ACS covariates as

the post-storm outage model, but now also including the Maria + 210 outage variable. Trained on the full dataset, the OLS model achieved a multiple R^2 of just 0.171, in other words, explaining just over 17% of the observed variance in 2010-2020 block group population trends (Table 3).

Table 3. OLS regression results for block group-level percent population change from 2010 to 2020, ordered by magnitude of coefficient estimate. All covariates were standardized ($\mu = 0$, $\sigma = 1$).

Variable	Coef. (β) Estimate	Std. Error	t-value	Pr(>|t|)
ppl_km2_2017	-0.204	0.026	-7.947	< 0.001***
age_struct	-0.173	0.026	-6.69E+00	< 0.001***
yeduc_mean	0.108	0.031	3.475	< 0.001***
pcinc	0.104	0.029	3.58	< 0.001***
howner_pct	-0.094	0.027	-3.538	< 0.001***
dist2path	-0.093	0.025	-3.701	< 0.001***
hisp_pct	-0.075	0.019	-3.879	< 0.001***
empl_pct	0.073	0.025	2.888	0.004**
age_mean	0.065	0.025	2.594	0.009**
outage_mag	-0.062	0.027	-2.301	0.021*
heat_util_pct	0.042	0.024	1.731	0.084
single_pct	-0.035	0.023	-1.525	0.127
noHins_pct	-0.023	0.021	-1.093	0.274
elev_mean	0.023	0.030	0.762	0.446
pub_asst_pct	0.020	0.021	0.988	0.323
allblk_pct	-0.020	0.026	-0.755	0.45
dist2landfall	0.015	0.028	0.523	0.601
male_pct	-0.014	0.019	-0.715	0.475
slope_mean	-0.013	0.031	-0.422	0.673
commute_avg	0.011	0.020	0.545	0.586
trans_work_auto_pct	0.010	0.022	0.432	0.666
allwht_pct	-0.009	0.027	-3.28E-01	0.743
dist2rd	0.000	0.019	-0.025	0.98
Residual Std. Error	0.9149		***Significance Levels***	
Multiple R^2	0.1707		< 0.001	***
Adjusted R^2	0.163		0.001 - 0.01	**
F-statistic:	22.33		0.01 - 0.05	*
Deg. Freedom (model)	23		> 0.05	

Deg. Freedom (resid.)	2496			
Model p-value	< 2.20E-16			

Evaluating the model's test-set performance and investigating whether it suffers from overfitting was done in the same manner as with the outage OLS model, by splitting the data 70/30% across train/test subsets and running 30 cross-validation iterations, shown in Figure 18. This resulted in a slightly wider spread between training (mean $R^2 = 0.183$) and test sets (mean $R^2 = 0.134$) as compared to the outage OLS model, which suggests that the model fit to the entire dataset here may be mildly overfit. Therefore, we can only say that this model can actually explain no more than 13.4% of observed variance, based on the test R2. A scatterplot of this model trained on the entire dataset is illustrated by Supplemental Figure 2.

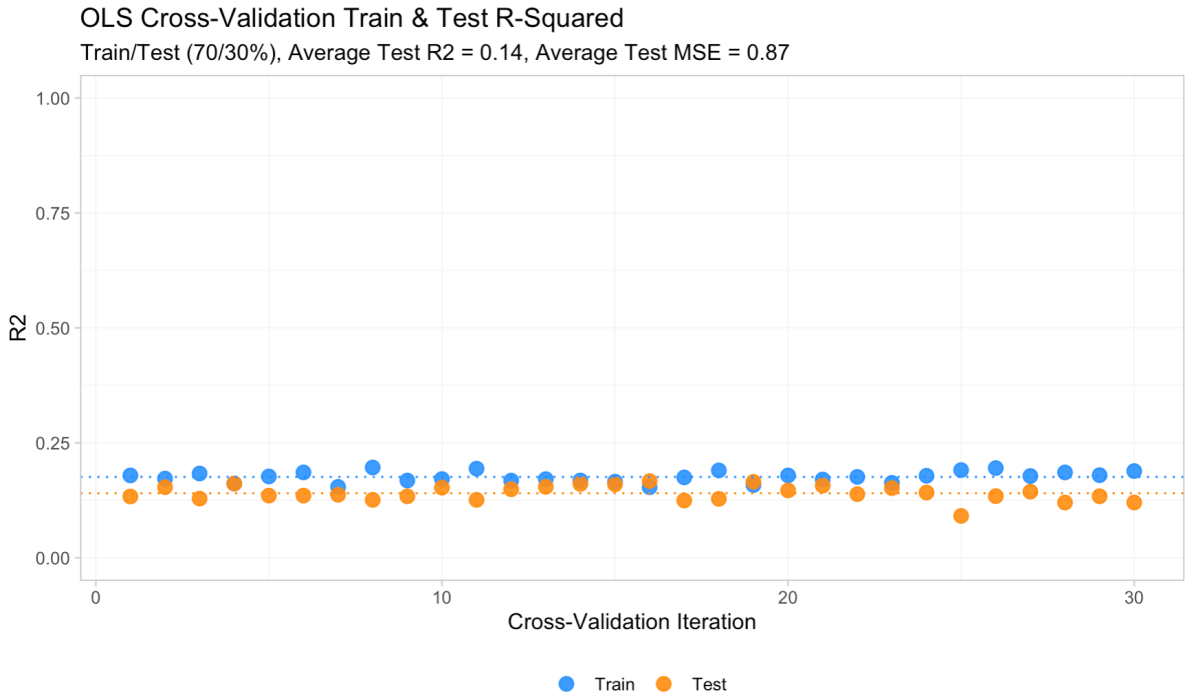

Figure 18. Performance of the percent population change OLS model for 30 iterations of cross-validation using 70/30% train/test splits, in terms of R^2.

Re-running the OLS analysis with all quadratic, cubic and log-transformed distance covariates very slightly improved the R^2 of the model trained on the entire dataset ($R^2 = 0.210$), but came at the cost of badly overfitting the model, with mean test R2 deteriorating to just 0.044. Therefore, this modeling approach was not pursued.

Random Forests

Using the same RF approach as with the outage outcome variable yielded essentially no improvements in predictive power of the model, unlike in the case of modeling outages. Applying the same 30-iteration cross-validation approach to assess test accuracy resulted in a mean test R^2 of just 0.151, which represents a very marginal improvement over the OLS test R^2 of 0.134. Therefore, no additional analysis of the RF model was conducted, though the train-test

R^2 and variable importance plots are shown in Supplemental Figures 3 and 4. Including quadratic, cubic and log-transformed distance variables did not improve the RF model performance, with mean test R^2 declining slightly to 0.144.

Discussion

Post-Maria Electricity Outage and Recovery

Based on the results of the OLS model for the post-storm outage outcome variable, which appears to explain roughly 51% of observed variance and is robust to cross-validation, it appears that strongest predictor of post-storm power outage patterns for the 7 months following the storm (Maria + 210) is the distance to the storm's point of landfall. Each standard deviation of increased proximity to the landfall point corresponds to a 0.47 standard deviation increase in the Maria + 210 outage variable experienced in a given grid cell (the negative coefficient for *dist2landfall* in Table 2 implies that increased distance from landfall decreases outage severity). A similar relationship was observed for the distance to storm path variable, which was the fourth-strongest predictor in the OLS model, with a coefficient of -0.132, implying that one standard deviation of increased proximity to the storm path corresponds with 0.132 standard deviations of increase in outage likelihood. These relationships make intuitive sense, as one would expect that closer proximity to the storm would result in higher exposure to hazardous winds, rain and potential flooding, and therefore result in more damage to homes and grid infrastructure, and in turn more severe post-storm outages. The higher magnitude of the *dist2landfall* variable compared to *dist2path* is noteworthy, as it highlights the importance of the decay in storm intensity following landfall, and suggests that simple proximity to its centerline path is not as important as proximity to its most intense point over land in predicting post-storm outage severity and duration.

In fact, all five physical variables were among the ten strongest predictors of outages, in terms of coefficient magnitudes, with elevation, distance to major roads and slope all showing positive correlations with outage (β = 0.135, 0.106 and 0.089, resp.), which implies that remoteness and less accessible/rugged terrain are correlated with more severe outages. This could be due to a number of factors, including the relative fragility of grid infrastructure in remote areas, difficulty in accessing and repairing this infrastructure and also potentially exposure to worse hazards, such as higher winds commonly experienced at higher elevations or erosion, landslides or debris flows more common in steeper terrain.

The other variables in the top ten predictors, in terms of coefficient magnitudes, included years of schooling (*yeduc_mean*), per capita income (*pcinc*), population density (*ppl_km2*), percent of White (*allwht_pct*) and Black (*allblk_pct*) residents (β = -0.151, -0.120, +0.093, -0.087, +0.078, resp.). Many of these variables are collinear (Figure 19) with one another, and this analysis does not engage in speculating causality; however, these coefficient values suggest that measures of relative privilege and opportunity, such as communities with higher levels of education, income, majority-White residents tend to be negatively associated with severe post-storm outages, while less dense communities with higher proportions of Black residents, all other factors being equal, tended to experience more severe outages.

When analyzing the results from the RF model on the Maria + 210 outage outcome, we again can see from Figure 16 that the *dist2landfall* variable serves as the most important predictor, resulting in the biggest decrease in test-set MSE when tree-splits within the model occur over that value. However, the relative order of importance of the remaining covariates in the RF model is not equivalently aligned with the order of β-coefficient estimates observed in OLS, with only four out of ten of the "most important" RF variables common to the top-ten list from OLS, all physical variables (*dist2landfall*, *dist2rd*, *elev_mean*, *dist2path*). The fact that these physical variables are present in the top ten variables for both OLS and RF indicates the importance of these metrics in predicting post-storm outages, and, by logical proxy, damaging hurricane impacts. The inconsistency in the order of importance for the remaining covariates between OLS and RF is likely due to the more complex and somewhat randomly-constructed nature of RF models, combined with the high level of multicollinearity between many covariates, as seen in Figure 19.

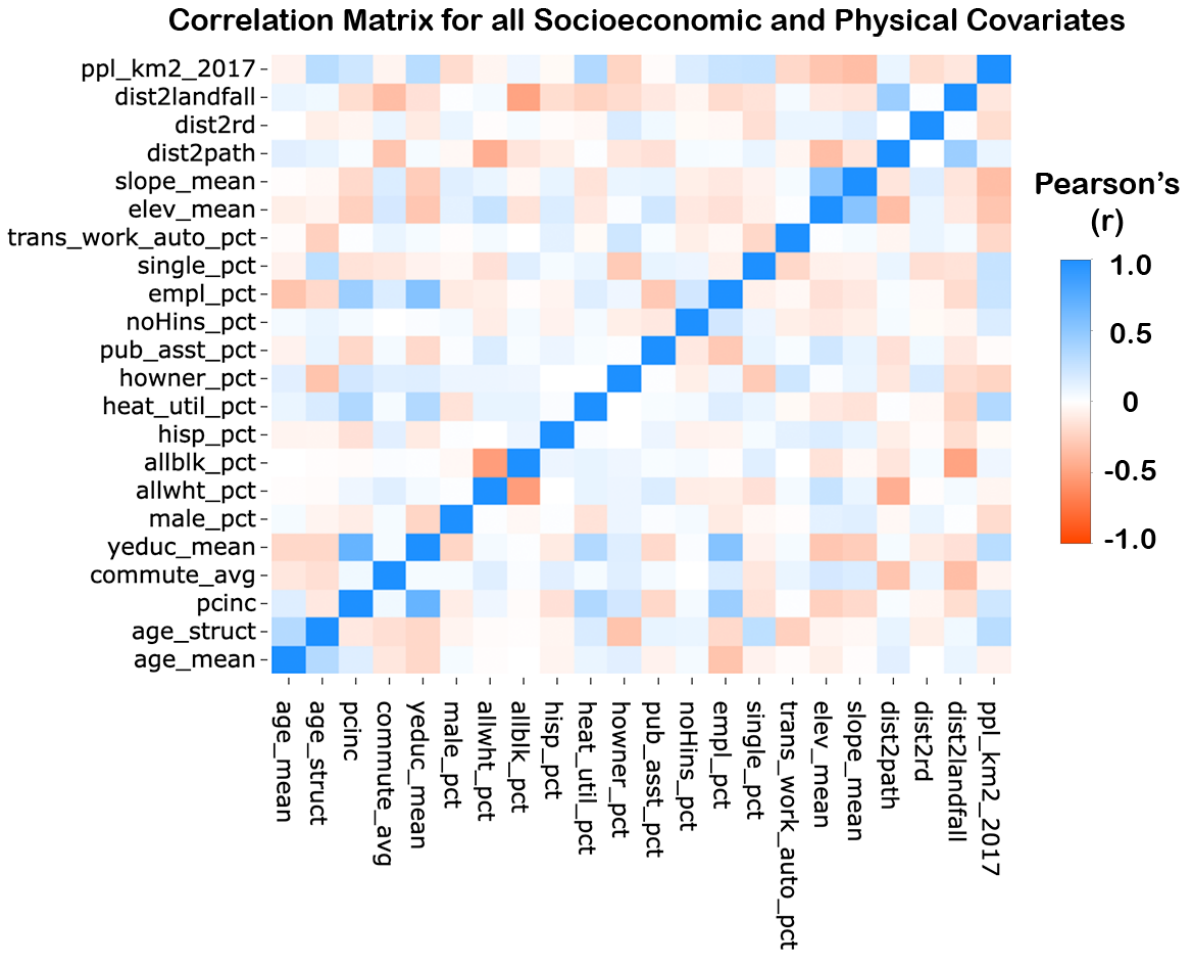

Figure 19. Cross-Correlation matrix of all 22 covariates used in the Maria + 210 outage OLS and RF models. Strong multicollinearity across multiple variables can be seen.

Block Group Population Change from 2010-2020

Though both the OLS and RF models yielded relatively low levels of model performance, evaluating which covariates emerged as the stronger predictors is still of interest. Looking at the top ten covariates in terms of beta-coefficient magnitudes in the OLS model, which also are the only covariates with levels of significance within $p < 0.05$, we see more socioeconomic metrics here, as compared to the outage model, which featured all five physical covariates in the top ten. Overall, the top five covariates suggest denser (*ppl_km2_2017,* β = -0.204), newly-built (*age_struct*, β = -0.173), more educated (*yeduc_mean*, β = 0.108), higher-income (*pcinc*, β = 0.104) areas with higher proportion of renters (*howner_pct*, β = -0.094) are positively correlated with population growth.

Conclusion

This analysis demonstrates that post-hurricane impacts on a region's electricity grid can be approximated at a fine spatial scale using publicly-available satellite imagery. In addition, the geospatial pattern of the magnitude and duration of post-storm blackouts and energy shortages can be predictively modeled through the use of different physical and socioeconomic covariates using different machine learning methods. In the case of post-Maria Puerto Rico, a simple OLS model explained more than half of the observed spatial variance in outages experienced by 500m grid cells across the island, with physical variables - namely the distance to the storm's point of landfall - serving as particularly important predictors, though other socioeconomic variables, such as average years of education obtained, income and racial composition bore sizable influence on the overall predictive power of this model. Using regression-tree random forests, a more sophisticated machine learning method, the nearly 83% of the observed outage variance was explained, without resulting in model overfitting, again with distance to landfall surfacing as the most influential covariate.

Attempts to model observed block group-level population trends between the 2010 and 2020 censuses across Puerto Rico proved more difficult. The same set of covariates were employed plus the outage variable used as the outcome variable in the first modeling exercise, such that any correlation between post-Maria outages and out-migration from 2010-home block groups could be potentially captured. However, the performance of this OLS model only explained a little more than 13% of observed variance in percent population trends, and the random forest approach only explained up to roughly 15%. That said, some tentative conclusions about the socioeconomic profile of block groups based on this, albeit weak, prediction models can still be drawn. Namely, it appears that denser, newer, more educated, richer areas experienced more population growth between 2010 and 2020, while the majority of the island experienced a population decline during that period of nearly 440,000 residents (~12%) over the course of the decade. This outcome confirms the complex nature of migration modeling, with many different important push and pull factors not captured in this modeling approach likely playing a large role in explaining population trends across block groups.

Therefore, a number of improvements could be made in iterations of this work to better capture such nuance. For one, exploring a mixed methods approach whereby emigrants and island residents provide qualitative insight as to influencing factors to migration decisions could help guide model design. Also, better understanding of potential census estimate bias should be

considered, especially with 2020 values, which reportedly contain substantial population undercounts in certain communities (Elliott, 2021). Better imagery datasets could be explored as well, which may decrease some of the noise in nighttime radiance caused by non-human factors, such as surface-reflected moonlight.

Supplemental Figures

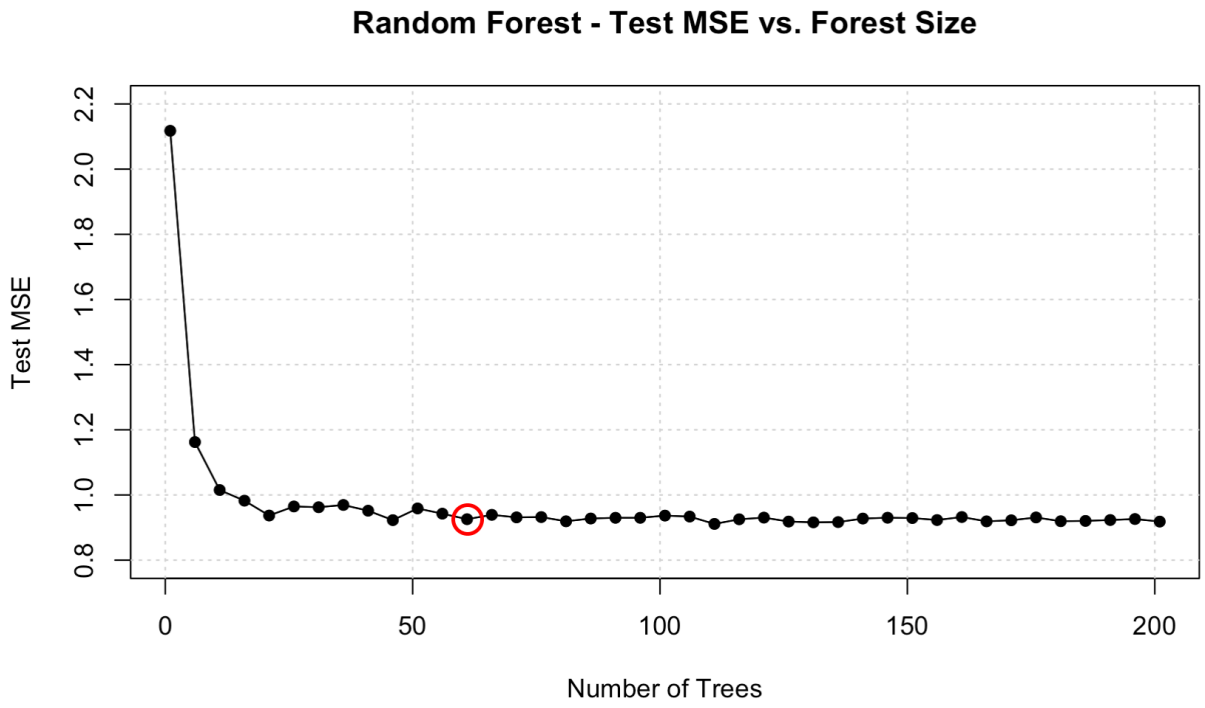

Supplemental Figure 1. MSE for a 30% test subset of the data for different tree counts (i.e. forest size) in the RF model of population change. Each point represents results from a single cross-validation iteration for the given forest size. A forest size of 60 trees was selected as it captures the vast majority of MSE reductions without needlessly inflating the tree count and associated computing requirements.

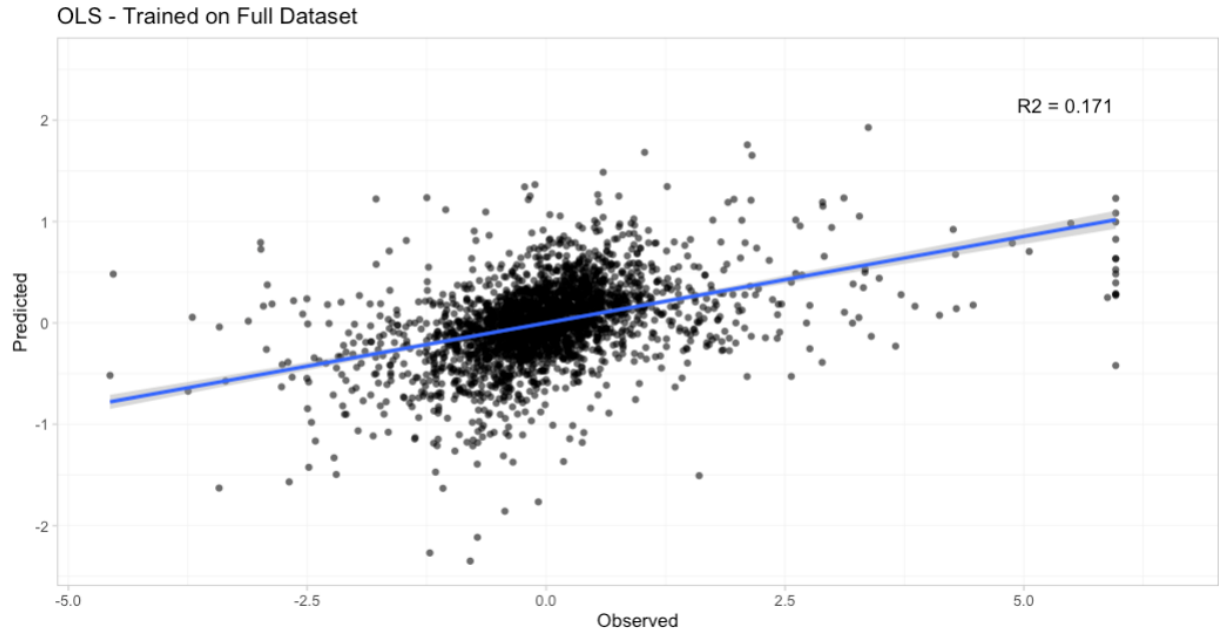

Supplemental Figure 2. Scatter plot of predicted versus observed values for the block group-level percent population change outcome variable for the OLS model trained on all block groups (n=2,519).

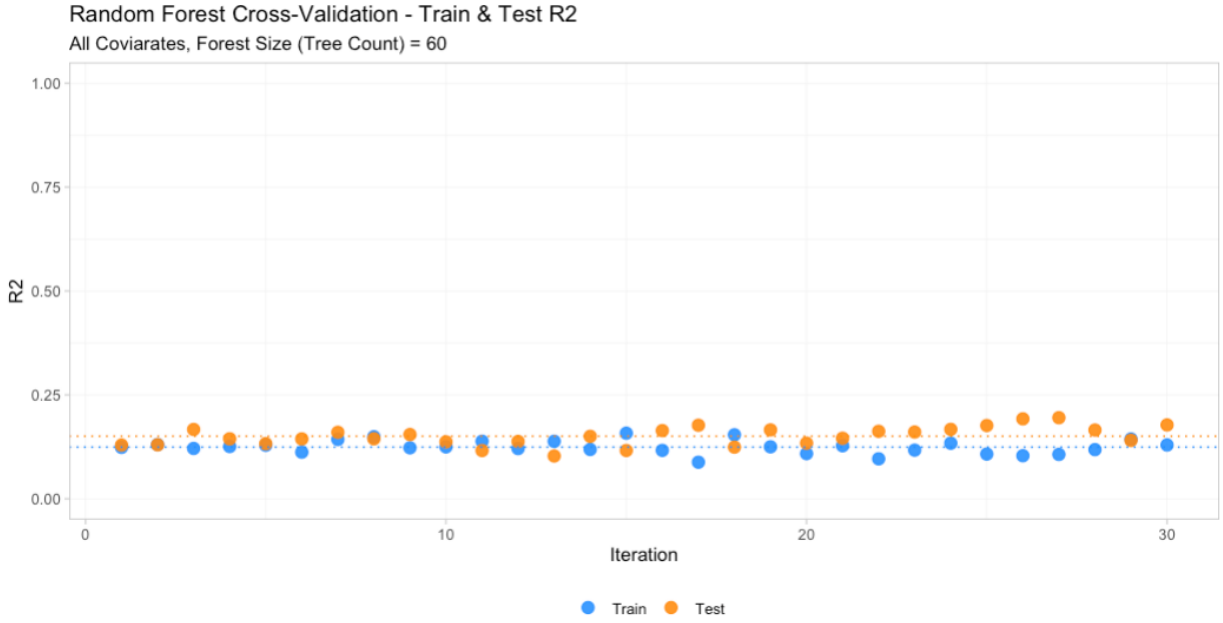

Supplemental Figure 3. Performance of the percent population change RF model for 30 iterations of cross-validation using 70/30% train/test splits, in terms of R^2. Mean test $R^2 = 0.151$.

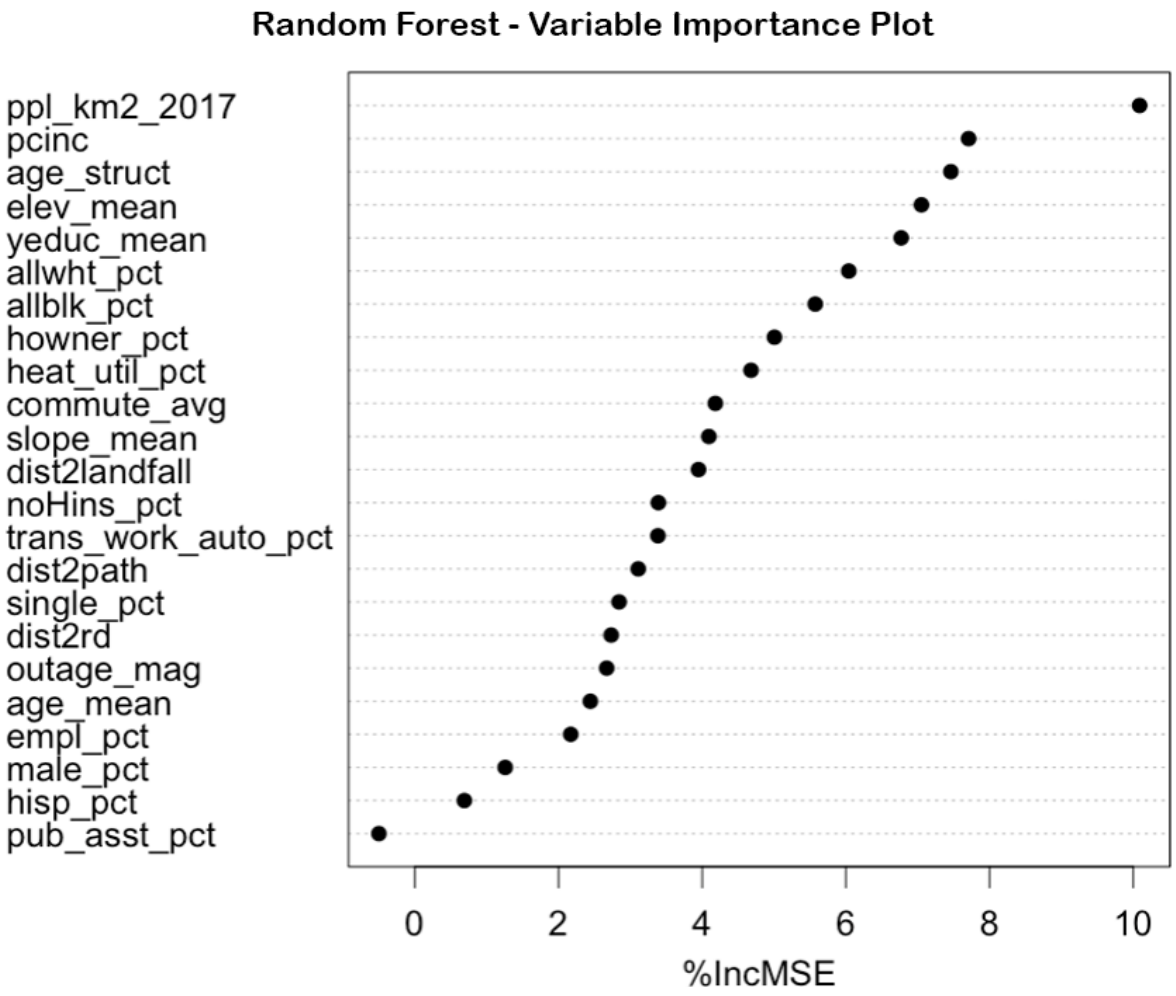

Supplemental Figure 4. Variable importance plot for the block group-level percent population change RF model, using percent changes in MSE as the metric of importance evaluation for each covariate. High values indicate high importance.

References

Database for Global Administrative Areas - Version 3.6. University of California, Davis, 2018.

Elliott, Diana; Martin, Steven; Shakesprere, J., and Kelly, J. (2021). Simulating the 2020 Census, (November).

Frey, William H., Audrey Singer, and David Park. “Resettling New Orleans: The first full picture from the Census. Brookings Institution Metropolitan Policy Program.”, 2007.

Fussell, Elizabeth. “The long-term recovery of New Orleans’ population after Hurricane Katrina.” American Behavioral Scientist 59, no. 10: 1231-1245, 2015.

Gareth, J., Daniela, W., Trevor, H. and Robert, T., An introduction to statistical learning: with applications in R. Springer, 2013.

Graif, Corina. “(Un) natural disaster: vulnerability, long-distance displacement, and the extended geography of neighborhood distress and attainment after Katrina.” Population and Environment 37, no. 3: 288-318, 2016.

Hinojosa, B. J., Meléndez, E., and Maria, C. (2018). Puerto Rican Exodus : One Year Since Hurricane Maria. *Center for Puerto Rican Studies, Hunter College, CUNY*, (September), 1–8.

Manson, Steven, Schroeder, J, Van Riper, D and Ruggles, S. IPUMS National Historical Geographic Information System: Version 14.0 [Database]. Minneapolis, MN: IPUMS. http://doi.org/10.18128/D050.V14.0, 2019.

Mercy Corps - United States, Quick facts: Hurricane Maria's effect on Puerto Rico, 2019.

Milken Institute School of Public Health, Ascertainment of the Estimated Excess Mortality from Hurricane María Puerto Rico. George Washington University, Milken Institute School of Public Health, 2018.

NASA Level-1 and Atmosphere Archive and Distribution System - Distributed Data Archive Center (LAADS-DAAC). URL: https://ladsweb.modaps.eosdis.nasa.gov/search/, 2019.

National Atlas of the United States. 100-Meter Resolution Elevation of Puerto Rico and the U.S. Virgin Islands, Albers projection. National Atlas of the United States. Available at: http://purl.stanford.edu/mb182my4891, 2012.

National Atlas of the United States, 1:1,000,000-Scale Major Roads of the United States. URL: http://nationalatlas.gov/atlas-ftp-global-map.html, 2014.

National Oceanic And Atmospheric Administration (NOAA) Office for Coastal Management - Hurricane Costs, Fast Facts. Last updated July 10, 2019.

National Oceanic And Atmospheric Administration (NOAA) - National Hurricane Center and Central Pacific Hurricane Center, NHC GIS Archive, Tropical Cyclone Best Track, 2019.

Pasch, R. J., Penny, A. B., and Berg, R., National Hurricane center tropical cyclone report: Hurricane Maria. TROPICAL CYCLONE REPORT AL152017, National Oceanic And Atmospheric Administration and the National Weather Service, 1-48, 2018.

Phillipson, L.M. and Toumi, R., A Physical Interpretation of Recent Tropical Cyclone Post-Landfall Decay. Geophysical Research Letters, 48(18), p.e2021GL094105, 2021.

Robles, F., Puerto Rico spent 11 months turning the power back on. They finally got to her. New York Times, 2018.

Román, Miguel O., Zhuosen Wang, Qingsong Sun, Virginia Kalb, Steven D. Miller, Andrew Molthan, Lori Schultz et al., "NASA's Black Marble nighttime lights product suite." Remote Sensing of Environment 210: 113-143, 2018.

Román, Miguel O., Eleanor C. Stokes, Ranjay Shrestha, Zhuosen Wang, Lori Schultz, Edil A. Sepúlveda Carlo, Qingsong Sun et al., "Satellite-based assessment of electricity restoration efforts in Puerto Rico after Hurricane Maria." PloS one 14, no. 6, 2019.

Shermeyer, J., Assessment of electrical and infrastructure recovery in Puerto Rico following hurricane Maria using a multisource time series of satellite imagery. In Earth Resources and Environmental Remote Sensing/GIS Applications IX (Vol. 10790, p. 1079010). International Society for Optics and Photonics, October 2018.

Stevens, F.R., Gaughan, A.E., Linard, C., Tatem, A.J.. Disaggregating Census Data for Population Mapping Using Random Forests with Remotely-Sensed and Ancillary Data. PLOS ONE 10, e0107042. https://doi.org/10.1371/journal.pone.0107042, 2015.

United States Department of Energy, Infrastructure Security and Energy Restoration, "Hurricanes Nate, Maria, Irma, and Harvey Situation Reports", Situation Report, 2017.

WorldPop (www.worldpop.org - School of Geography and Environmental Science, University of Southampton). Puerto Rico 100m Population. Alpha version 2010, 2015 and 2020 estimates of numbers of people per pixel (ppp) and people per hectare (pph), with national totals adjusted to match UN population division estimates (http://esa.un.org/wpp/) and remaining unadjusted, 2016.

Chapter 3 - Global Coastlines: Assessing impacts from projected 21st-century sea level rise and potential adaptation pathways

3.1 - DSCIM-Coastal v1.1: An Open-Source Modeling Platform for Global Impacts of Sea Level Rise

This section is adapted from (Depsky, Bolliger et al., 2022). Project formulation, discussion and contributions to the text was done by Solomon Hsiang, Michael Greenstone, Trevor Houser, Robert E. Kopp and Ian Bolliger. Data curation and analysis was primarily performed by myself, Ian Bolliger, Daniel Allen and Jun Ho Choi, with additional contributions from Ali Hamidi and Michael Delgado. The pyCIAM model source code and SLIIDERS input dataset construction was done by Ian Bolliger, myself, Daniel Allen and Jun Ho Choi. I served as the primary author of the final published manuscript, with major contributions from Ian Bolliger and Jun Ho Choi and minor contributions from the remainder of the authors listed. The published version of this work can be found at https://doi.org/10.5194/egusphere-2022-198.

Abstract

Sea level rise (SLR) may impose substantial economic costs to coastal communities worldwide, but characterizing its global impact remains challenging because SLR costs depend heavily on natural characteristics and human investments at each location—including topography, the spatial distribution of assets, and local adaptation decisions. To date, several impact models have been developed to estimate global costs of SLR, yet the limited availability of open-source and modular platforms that easily ingest up-to-date socioeconomic and physical data sources restricts the ability of existing systems to transparently incorporate new insights. In this paper, we present a modular, open-source platform designed to address this need, providing end-to-end transparency from global input data to a scalable least-cost optimization framework that estimates adaptation and net SLR costs for nearly 10,000 global coastline segments and administrative regions. Our approach accounts both for uncertainty in the magnitude of global mean sea level (GMSL) rise and spatial variability in local relative sea level rise. Using this platform, we evaluate costs across 230 possible socioeconomic and SLR trajectories in the 21st century. According to the latest Intergovernmental Panel on Climate Change Assessment Report (AR6), GMSL is likely to rise during the 21st-century by 0.40-0.69 meters if late-century warming reaches 2° C and by 0.58-0.91 m with 4° C of warming (Fox-Kemper et al., 2021). We estimate that for the likely costs of GMSL rise associated with 2° C, annual end-of-century costs will be between $110 billion and $530 billion, depending on socioeconomic pathways and assuming optimal adaptation. For the likely SLR associated with 4° C warming, these costs range from $200 billion to $750 billion. Under a low-likelihood, high-impact storyline that incorporates deeply uncertain physical processes like marine ice cliff instability, AR6 notes that GMSL rise in higher emissions scenarios could approach 2.0 m by 2100. Accordingly, we also model the impacts of 1.5 and 2.0 m GMSL rises by 2100; the associated annual cost estimates

range from $420 billion to $1.5 trillion by end-of-century under the same set of assumptions. Our modeling platform is publicly available in an effort to spur research collaboration and support decision-making, with segment-level physical and socioeconomic input characteristics provided at *https://doi.org/10.5281/zenodo.6449231*, source code for this dataset at *https://doi.org/10.5281/zenodo.6456115*, the modeling framework at *https://doi.org/10.5281/zenodo.6453099*, and model results at *https://doi.org/10.5281/zenodo.6014086*.

1 - Introduction

Global mean sea level (GMSL) is projected to increase between 0.40-0.69 m for 2° C of warming and 0.58-0.91 m for 4° C of warming by 2100, though accelerated ice-sheet instability could result in substantially higher values (approaching 2 m) by end-of-century (Fox-Kemper et al., 2021). Coastal communities and ecosystems will experience a variety of impacts, including more frequent tidal flooding, higher extreme sea levels (ESLs)[4], erosion, wetland degradation, salinization of soils and water reservoirs, and loss of land area to permanent inundation (Oppenheimer et al., 2019; R. Nicholls et al., 2006). The magnitude of relative sea level rise (RSLR) and associated impacts will vary by locality, depending upon global greenhouse gas (GHG) emissions (Fox-Kemper et al., 2021), ice sheet instabilities (DeConto et al., 2021; Bamber et al., 2019; Fox-Kemper et al., 2021), local atmosphere-ocean dynamics (Fox-Kemper et al., 2021), economic growth along coastlines (O'Neill et al., 2017; Neumann et al., 2015; Armstrong et al., 2016), and adaptation actions (Hinkel et al., 2018, 2014; Diaz, 2016; Lincke and Hinkel, 2021).

Despite advances in our understanding of GMSL, the global costs of these changes remain poorly constrained. A key obstacle to quantifying these global impacts is their strong dependence on the details of local conditions, such as topography, the spatial distribution of populations and assets, and local adaptation decisions. A challenge for modelers is the dual objectives of fully accounting for these various factors at the local granularity necessary for accurate representation while also scaling these calculations globally. Improvements in computation and data availability now make achieving these two objectives feasible, but it has remained challenging for existing custom-built systems to be regularly updated to reflect new insights or improvements to global data sets describing local conditions.

This paper presents what is to our knowledge the first fully open-source coastal modeling platform that (i) integrates up-to-date local data on socioeconomic and physical conditions along coastlines globally, (ii) projects the physical, socioeconomic and ecological impacts of SLR along coastlines and (iii) directly models the costs and benefits of both retreat and protection as potential adaptation strategies. The platform is fully coded in the open-source computer language Python (v3.9) and integrates recently released, satellite-augmented global data layers describing coastal elevations, local sea levels, and the distribution of population and physical capital with widely used socioeconomic datasets. These data layers are projected onto 9,568 unique coastal segments that span global coastlines. Each of these segments is then modeled as independently choosing across local, forward-looking adaptation strategies in an effort to minimize overall

[4] Terminology and acronyms for concepts related to sea level align with those recommended for contemporary use in Gregory et al. (2019).

losses, following the framework developed in (Diaz, 2016). Using this platform, we evaluated net costs across 230 possible socioeconomic and SLR trajectories in the 21st century to present here, though the tool is capable of accommodating tens to hundreds of thousands of future simulations in parallel if desired.

We estimate annual end-of-century costs associated with 2° C of warming (+0.40-0.69 m GMSL by 2100) to be between $110 billion and $530 billion, and for 4° C warming (+0.58-0.91 m) to range from $200 billion to $750 billion, depending on socioeconomic pathways and assuming optimal adaptation. Under a low-likelihood, high-impact storyline that incorporates deeply uncertain physical processes like marine ice cliff instability, where end-of-century GMSL rise reaches +1.5-2.0 m, the associated annual cost estimates range from $420 billion to $1.5 trillion.

All code used to aggregate and combine input data, as well as to estimate SLR impacts, is publicly available. This encourages further development by the coastal impacts research community and modularizes the modeling process to facilitate seamless incorporation of future improvements to input datasets and additional model components.

1.1 The Basic Architecture of Global Coastal Impact Models

Global coastal models that estimate impacts of SLR and ESLs seek to quantify the exposure of some variable(s) of concern, such as human population, capital assets, and coastal ecosystems, to these physical hazards. They generally report the magnitude of exposure to these hazards as their final output, and convert this exposure into some outcome of interest, such as economic losses (Hinkel et al., 2014; Diaz, 2016; Lincke and Hinkel, 2018). These models usually contain spatially explicit representations of physical coastline characteristics (e.g. coast lengths, elevation and land surface areas), exposure variables, and physical hazard variables.

To estimate future impacts, global coastal models must assume or model trajectories of pertinent physical and socioeconomic values over time. Most climate change-oriented impacts models assess multiple trajectories of GMSL and many account for local RSLR and associated ESLs, which commonly correspond to different GHG emissions pathways (Hinkel et al., 2014; Diaz, 2016; Lincke and Hinkel, 2018, 2021). They may also contain different future trajectories of human population and capital asset growth, such as those represented in the Shared Socioeconomic Pathways (SSPs) database (Riahi et al., 2017; Hinkel et al., 2014; Lincke and Hinkel, 2018, 2021; Tiggeloven et al., 2020).

The spatial and temporal resolution of model components can vary between studies and is sometimes limited by the resolution of available input datasets and/or by available computing resources. Additionally, many models also include some form of adaptive decision-making, such as allowing different coastal segments to construct protective coastal barriers (Hinkel et al., 2014; Diaz, 2016; Lincke and Hinkel, 2018, 2021; Tiggeloven et al., 2020) or retreating inland (Diaz, 2016; Lincke and Hinkel, 2021), usually guided by some form of local cost-benefit analysis.

1.2 Closely Related Efforts and Platform Genealogy

Several past studies employed global coastal impact models to estimate future damages from SLR and ESLs under various trajectories of global GHG emissions, socioeconomic scenarios, and adaptation pathways for thousands of sub-national coastline segments (Hinkel et al., 2014; Diaz, 2016; Lincke and Hinkel, 2018, 2021). Many of these studies used the Dynamic Interactive Vulnerability Assessment (DIVA) Coastal Database and modeling tool as their source of information for describing local coastlines. Originally developed by the Dynamic and Interactive Assessment of National, Regional and Global Vulnerability of Coastal Zones to Climate Change and Sea-Level Rise (DINAS-COAST) project (Vafeidis et al., 2008; Hinkel and Klein, 2009), the DIVA database partitions global coastlines into 12,148 segments and provides local physical attributes (e.g., inundation areas by elevation, extreme sea level heights, wetland areas, erosion characteristics) as well as socioeconomic characteristics (e.g. population densities, land use), allowing for more spatially disaggregated coastal impact analyses (Vafeidis et al., 2008; Hinkel and Klein, 2009). At the time of its initial release in 2008, DIVA represented a substantial improvement over previous global, coastal databases and impact studies, which were most commonly performed using data at much coarser spatial resolutions (Hoozemans et al., 1993; Yohe and Tol, 2002; R. J. Nicholls, 2004, 2002; Dronkers et al., 1990; Pardaens et al., 2011; Hinkel et al., 2013). Presently, however, the DINAS-COAST program is no longer funded, and the accessibility of the DIVA database has fluctuated. Recently, a landing page has been created for the DIVA model at http://diva.globalclimateforum.org, though as of early 2022 the corresponding dataset is only available via direct correspondence with its authors. The underlying code and input data used to construct the DIVA database is not publicly available, making it difficult to replicate prior studies' results and diagnose issues that have appeared in previous versions of the dataset (Sect. 1.5.1). In this work, we address these issues of accessibility and transparency by generating a publically-available global dataset of coastal socioeconomic metrics, updating all core data layers used to generate DIVA and releasing the data assimilation model used to aggregate these into the final data product. The full set of data updates are described in Sect. 1 below.

In a key early analysis, Hinkel et al. (2014) employed the DIVA database to model the combination of coastal flood damages and adaptation (specifically, protective levee construction) under twelve scenarios of future RSLR and socioeconomic projections for sub-national coastal zones. Sea level rise scenarios in this study were constructed from estimates of global thermal expansion and regional ocean dynamic sea level data corresponding to low-, medium-, and high-emissions Coupled Model Intercomparison Project Phase 5 (CMIP5) experiments (Taylor et al., 2012) (Representative Concentration Pathways 2.6, 4.5, and 8.5) in four Earth System Models (ESMs), combined with low, medium, and high land-ice scenarios. The study also evaluated two different digital elevation models (DEMs) for estimating population exposure in coastal floodplains to SLR and ESLs, the GLOBE DEM (Hastings and Dunbar, 1999), which was the original DEM used in DIVA (Hinkel and Klein, 2009), and the more recent Shuttle Radar Topography Mission (SRTM) DEM (Rodriguez et al., 2005). They found that their results were highly sensitive to the choice of DEM, which underscores the importance of updating global data layers used in coastal impact modeling as improved products are made available, which is one of the central aims of the work we present in this paper.

Expanding on the approach of Hinkel et al. (2014), Diaz (2016) developed the Coastal Impact and Adaptation Model (CIAM), a global modeling tool that estimated 21st century costs and

adaptation strategies for each DIVA segment. One core innovation presented in CIAM was that it allowed for each segment to choose between dike construction, as in Hinkel et al. (2014), and managed or reactive retreat. However, an obstacle to widespread usage of CIAM was its development in the commercial General Algebraic Modeling System (GAMS) closed-source platform. We build on the work by Diaz (2016), using the underlying decision-making framework of CIAM; however, we adapt, re-code, and optimize CIAM in the open-source Python computing language.

The architecture of CIAM was designed to capture key aspects of local adaptive decision-making that will likely be used by coastal communities worldwide. The objective of CIAM was to develop an optimization framework that could be applied locally, but generalized globally. To limit the computational challenge of solving stochastic dynamic programs for thousands of independent coastline segments, Diaz (2016) simplified the set of possible adaptation choices to a set of discrete decisions that are calibrated to local conditions. CIAM differentiated between six types of costs (i.e. “damages") due to RSLR and ESLs (Sect. 1.2): (a) the cost of permanent inundation of immobile capital or land, and ESL-related (b) damages to capital, (c) mortality, (d) expenditures on protection (i.e. infrastructure construction), (e) relocation costs, and (f) wetland loss. Possible protection actions include constructing levees at the 10, 100, 1000, and 10000-year ESL heights at each segment, and possible retreat actions include proactively vacating all land area under local mean sea level (MSL) or within the 10, 100, 1000, or 10000-year ESL floodplain. Simulations in CIAM are implemented using discrete time-steps, termed “adaptation planning periods” (40-50 years), during which each segment updates their retreat or protection height based on the maximum RSLR projected to occur within the period. CIAM also allows for modelers to select a “no planned adaptation” option that constrains retreat to be reactive, rather than forward-looking, such that the population and capital assets only choose to relocate inland once they are permanently inundated by rising sea levels. Diaz (2016) considered a single socioeconomic growth trajectory based on the 2012 United Nations World Population Prospects (UN DESA, 2012), Penn World Table version 7.0 (Heston et al., 2011) and the 2011 IMF World Economic Outlook (IMF, 2011) projections and uses DIVA’s older GLOBE DEM. The SLR trajectories used by Diaz (2016) were the 5th, 50th, and 95th percentiles of probabilistic RSLR projections from Kopp et al. (2014) for RCPs 2.6, 4.5, and 8.5, as well as a no-SLR baseline.

Here, we build on the approach of Diaz (2016), adapting and optimizing the decision-framework of CIAM to an entirely new set of global data inputs (i.e. replacing DIVA) and an open-source computer language. Given continued advancement in sea level rise modeling efforts and the improvement of global data inputs (e.g. coastal DEMs), it is essential that coastal impacts modeling platforms are able to integrate these updates. Additionally, we believe that these platforms should be developed in an open-source, transparent, and reproducible framework that will allow for increased collaboration and more rapid iteration amongst coastal impacts researchers, as has been done for modeling communities across numerous scientific disciplines (Krogh and Hippel, 2006). The platform we develop addresses these objectives by integrating the latest available physical, climate, and socioeconomic input data for an expanded suite of future SLR and economic growth trajectories in an updated and open-source version of the CIAM framework that, in addition to improved accessibility and transparency, results in greater resolution and substantially improved computational efficiency.

1.3 This Study: The Data-driven Spatial Climate Impact Model - Coastal Impacts

This modeling platform was developed as the sea level rise impacts module of the Data-driven Spatial Climate Impact Model (DSCIM) architecture (Rode et al., 2021), and is thus named DSCIM-Coastal. It is partitioned into two distinct components, each made available as open-source products: (i) the collection, harmonization, and aggregation of updated physical and socioeconomic input datasets by coastal segment, which is named the Sea Level Impacts Input Dataset by Elevation, Region, and Scenario, or SLIIDERS, and (ii) the modeling platform itself, called pyCIAM (short for "Python-based CIAM"). Both components have been developed in accordance with FAIR Guiding Principles for scientific data management (Wilkinson et al., 2016) that are intended to improve the Findability, Accessibility, Interoperability, and Reuse of scientific data.[5]

The SLIIDERS data set is conceptually similar to DIVA in that it contains a suite of variables defined across a collection of coastal segments designed for coastal impact modeling efforts. However, while DIVA is not publicly accessible, SLIIDERS and all of its components are available with open access licenses, thereby supporting transparency and replicability of coastal damage analyses for research communities around the globe.[6] In addition, the partition of global coastlines that defines separate coastal segments as units of analysis has been revamped in order to achieve greater balance in geographic coverage and reduce redundant computations. SLIIDERS also contains updated topographic, geographic, and socioeconomic input datasets, including refined coastal DEMs and socioeconomic growth trajectories.

pyCIAM is an open-source, computationally efficient and functional modeling platform for segment-level adaptation decision making that incorporates the following improvements to the original implementation of CIAM (Diaz, 2016): (i) updates to (and expansion of) all topographic, geographic and socioeconomic input data using SLIIDERS, and updated oceanographic inputs using a large suite of 23 SLR projections, (ii) improvements to model representation of different variables, such as population and capital asset distribution and storm damage calculations, (iii) availability as an open-source, self-contained Python package and input database, making the workflow easily accessible and modifiable for other researchers, and (iv) improved computational efficiency and scalability, enabling the application of CIAM to large, probabilistic ensembles of sea-level change.

---

[5] These data and modeling components abide by the FAIR criterion as specified by The Future of Research Communications and e-Scholarship (FORCE11). Specifically, they are i) Findable via unique and persistent identifiers, with these identifiers specified in component metadata and indexed in a searchable resource (Zenodo, Github); ii) Accessible in that they are retrievable via these identifiers and are open, free and universally implementable; iii) Interpretable through the use of a formal, accessible, shared and broadly applicable language/vocabulary (manuscript and metadata in standard English and code in Python) and the inclusion of appropriate references to other data where necessary (e.g. input data sources); and iv) Reusable by specifying accurate and relevant attributes, applying an accessible data usage license and complying with coastal modeling community standards of language and data/code provision (Force11.org).

[6] One of the input data sources used in generating SLIIDERS, CoastalDEM (Kulp and Strauss, 2019), is not freely available at the resolution employed in this study but is available for research use at a lower resolution.

The pyCIAM model is configured to utilize the SLIIDERS inputs and SLR projections presented here, but can easily be run using a modified set of inputs or SLR pathways, provided the data structure is consistent with this configuration. Similarly, the SLIIDERS product can be used independently from pyCIAM as inputs for other coastal analysis or as contextual information on coastal zones. It can also be recreated using alternate input sources as desired, as the scripts to generate the product are provided with it.

The following sections describe how SLIIDERS and pyCIAM are constructed, show example results of model outputs and diagnostics from 2005-2100 and compare to the results of Diaz (2016), and discuss current limitations to the model and input datasets, outlining planned improvements and future research priorities.

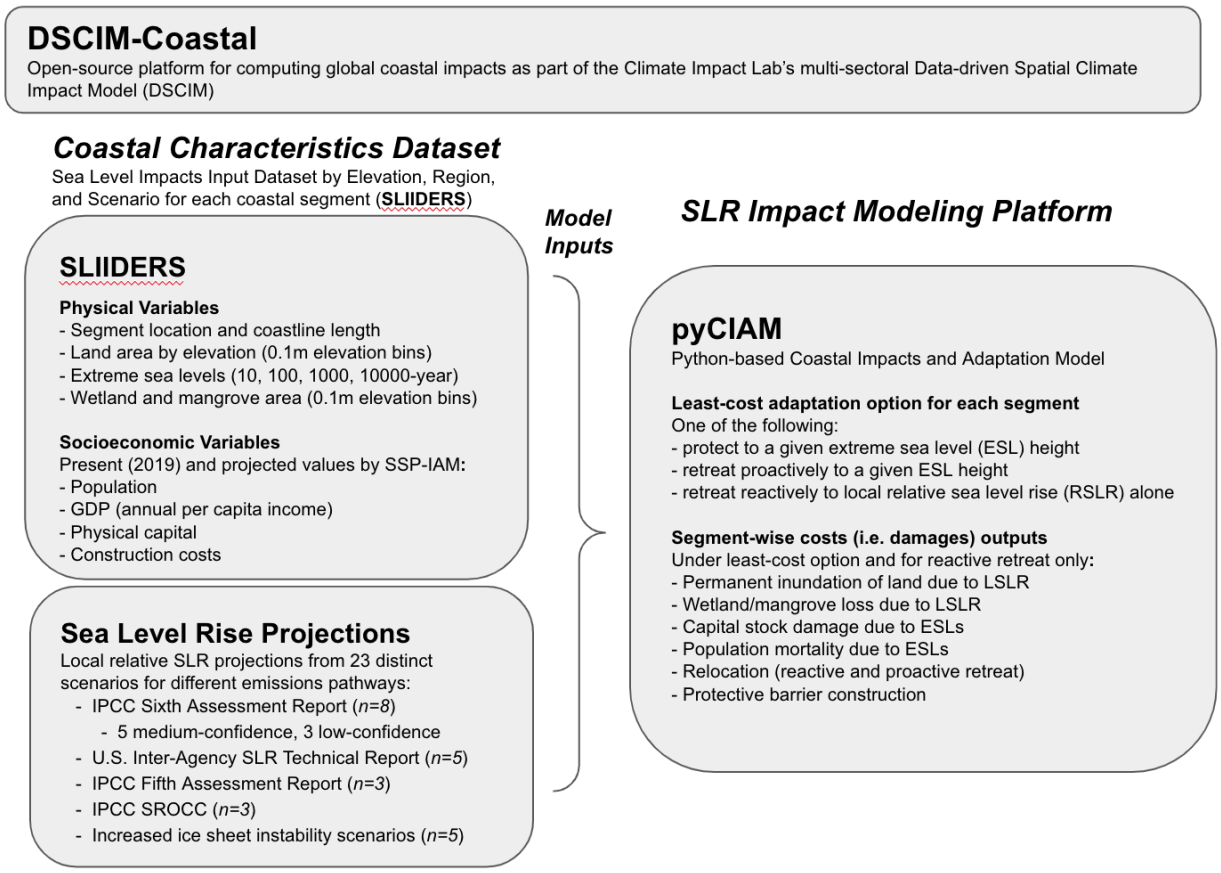

Figure 1. Components of the Coastal portion of the Data-driven Spatial Climate Impact Model (DSCIM-Coastal)

2 - Methods and Data

We constructed the Python Coastal Impacts and Adaptation Model (pyCIAM) by adapting the original code and structure of the Coastal Impacts and Adaptation Model (CIAM) (Diaz, 2016),

obtained from http://github.com/delavane/CIAM in June 2020, with changes subsequently made in three phases:

1. Porting the model from GAMS to a standalone Python module (creating *pyCIAM*)
2. Updating all model inputs with the *SLIIDERS* data and SLR projections, constituting newer, improved physical and socioeconomic datasets
3. Implementing changes to the model functionality itself for the purposes of:
   - Computational efficiency
   - Updating assumptions where new data provided previously unavailable insights
   - Aligning model implementation with the model description in Diaz (2016)
   - Reducing noise in numerical approximation algorithms

2.1 Model Structure

The aspects of CIAM as presented in (Diaz, 2016) that are maintained in pyCIAM include the segment-based structure of the model and the adaptation actions that each segment is permitted to take throughout the modeling period, comprised of the following options:

- *Reactive Retreat*: When a portion of land falls below MSL, all people and mobile capital are relocated to an unaffected, inland region away from the coast that is not in danger of future impacts from SLR or ESLs, and immobile capital is abandoned.
- *Protection*: Construction of a generic levee to protect the entire coastline segment. Available choices for protection height include the 10, 100, 1000, and 10,000-year return values of ESL. This height changes linearly with RSLR.
- *Proactive Retreat*: All people and mobile capital below a certain retreat height are assumed to be relocated to a safe, inland region, and immobile capital below that height is abandoned. The options for that retreat height level are discretized to the same values available for protection, with the addition of a "low retreat" option representing the maximum MSL projected during a "planning period" (10 years).

Note that, as described in Diaz (2016), each coastal segment may only choose one adaptation option, e.g. *retreat-1000*, for the entire model duration. While the height of the retreat level changes over time as the 1000-year ESL return value changes due to RSLR, the segment cannot, for example, choose retreat-100 for the first 40 years and then protect-10000.

The model is discretized into time steps (10 years in the original CIAM, annual in pyCIAM), during which all time evolving parameters are held constant. In addition, the segments use a configurable set of "planning periods" (40-50 years each period in CIAM, 10 years each in pyCIAM), which each correspond to a set of one or more timesteps. For each planning period, a single height is chosen for retreat or protection (assuming the segment does not select "reactive retreat") that represents the maximum height projected for the chosen ESL return value during the planning period.

2.2 Cost Calculation

Costs estimated by pyCIAM are categorized in the same manner as described in (Diaz, 2016) and are characterized as follows:

2.2.1 Inundation Costs

The value of land and immobile capital lost to inundation. In Diaz (2016), immobile capital was allowed to fully depreciate if the strategy chosen is proactive retreat, such that capital-related losses due to inundation are always 0. This was based on a theoretical argument that for a planned retreat, a rational social planner would cease the creation of new physical capital far enough in advance that all remaining capital would have fully depreciated by the time the retreat occurs (Yohe et al., 1995). However, this assumption has been critiqued in subsequent work (Lincke and Hinkel, 2021) due to its lack of empirical grounding. Furthermore, it ignores the welfare loss associated with not replacing depreciating assets in the years leading up to retreat. These new capital investments would have been made in the absence of SLR, and thus the lack of investment should be counted when assessing total SLR impacts. Therefore, pyCIAM alters CIAM's assumption of full depreciation, instead modeling immobile capital to experience no excess depreciation beyond the background rate implicitly included in the capital growth model used to generate SSP-aligned capital projections. This results in the full estimated value of capital being lost when abandoned or inundated, in line with the assumptions of Lincke and Hinkel (2021).

2.2.2 Retreat Costs

The costs of relocating population and mobile capital and of demolishing immobile capital. Following Diaz (2016), capital relocation costs are valued at 10% of total value, and immobile capital demolition costs are valued at 5%. In Diaz (2016), the intangible relocation cost is valued at one year of per capita income, which varies by country and over time and was an admittedly arbitrary assumption. We use a value of 8.8 times local income, for reasons described in Sect. 1.3.

2.2.3 Protection Costs

The construction and maintenance costs of building a protective levee, along with the value of lost land. As in Diaz (2016), maintenance costs are assumed to be 2% of the initial construction cost, and the value of lost land is calculated as the local land value (which varies over countries and years) times the length and width of the barrier, assuming a slope.

2.2.4 Wetlands Loss

The value of wetlands lost to either SLR or protection. As in Diaz (2016), wetlands are assumed to be able to partially absorb SLR up to 1 cm/year, with the degree of loss increasing

quadratically with the rate of SLR. Above the critical threshold of 1 cm year, all inundated wetlands are lost. In addition, all wetland area below a protective barrier is also assumed to be lost. More details on the calculation of wetland loss can be found in Equation 8 of the Diaz (2016) supplemental information.

2.2.5 Extreme Sea Level Capital Damage

The value of capital loss occurring due to ESL events, using a depth-damage relationship that takes the shape . The probability density function of ESL values at each segment location is represented as a Gumbel distribution, derived from Muis et al. (2016) in Diaz (2016) and from Muis et al. (2020) in pyCIAM. The product of this PDF and the estimated capital loss conditional on each ESL height in the distribution is integrated to obtain the annual expectation of ESL-driven capital loss per elevation slice, and these costs are summed over elevation to obtain the annual damages per segment (see Diaz (2016), Supplementary Material Section 2.1, Eqs 9-12). For computational efficiency, this set of discrete products, integrations, and sums is performed on a variety of example inputs prior to executing the actual CIAM model. In Diaz (2016), functions are fit to these outputs to relate ESL height to loss for different adaptation options, with unique coefficients for each segment.

$$D_{r,s,t} = (1 - \rho_{s,t}) C_{s,t} \left(\frac{\sigma_{0,r,s}}{1 + \sigma_{A,r,s} exp(\sigma_{B,r,s} H_{r,s,t})} \right) \quad (1)$$

$$D_{p,s,t} = (1 - \rho_{s,t}) C_{s,t} \left(\frac{\sigma_{0,p,s} + \sigma_{1,p,s} S_{s,t}}{1 + \sigma_{A,p,s} exp(\sigma_{B,p,s} H_{p,s,t})} \right) \quad (2)$$

where

$D_{r/p,s,t}$
is the ESL-driven expected capital loss conditional on retreat or protection to height r or p, respectively, for segment s in time step t,

$\rho_{s,t}$
is a country-level resilience factor (defined in Diaz (2016)),

$C_{s,t}$
is the capital density (in $ per km^2),

$H_{r/p,s,t}$

is the difference between the retreat or protection height and local mean sea level,

$S_{s,t}$

is the local mean sea level, and σ are the fitted coefficients.

However, this has two notable issues. First, this fixed functional form may not fully represent heterogeneous relationships between adaptation height, MSL, and damage across segments, due to differing elevational distributions of capital at each segment. Second, in Diaz (2016) the damages conditional on a given retreat standard (e.g. 1-in-10 year ESL height) are a function only of the difference between MSL and the retreat standard, not of the absolute MSL height. This cannot be true unless capital is homogeneously distributed over elevation. This assumption is at odds with reality and with the rest of the Diaz (2016) CIAM model, which assumes that the elevational distribution of capital follows that of land area.

In pyCIAM, we correct these issues by employing a multi-dimensional lookup table instead of these two functions. For each segment, we find the lowest and highest values of MSL (*S*) and of the difference between retreat/protection height and MSL (*H*) across all SLR scenarios we wish to simulate, all adaptation choices, and all timesteps. We then choose 100 equally spaced values between these bounds for each of the two variables. For both of the adaptation categories (retreat and protection), we now have 10,000 scenarios reflecting different combinations of and . We normalize capital stock so that it sums to one, yielding fractional capital stock in each elevation slice. The current implementation assumes that these ratios remain fixed over time. However, should one wish to model within-country migration due to considerations such as SSP-consistent coastal urbanization and migration flows (e.g. Jones and O'Neill (2016); Merkens et al. (2016)), such changes can be accommodated by updating the appropriate variables in the SLIIDERS input dataset. For each of the 20,000 scenarios, we calculate damages using a discrete double integral over ESL height and elevation slice. In the pyCIAM model, the equations for damage are thus:

$$D_{r/p,s,t} = (1 - \rho_{s,t}) K_{s,t} \gamma(H_{r/p,s,t}, S_{s,t}) \tag{3}$$

where

$D_{r/p,s,t}$

is the ESL-driven expected capital loss conditional on retreat or protection to height r or p, respectively, for segment s in time step t,

$\rho_{s,t}$

is a country-level resilience factor (defined in Diaz (2016)),

$K_{s,t}$

is the total value of capital stock in segment s at time t,

$H_{r/p,s,t}$

is the difference between the retreat or protection height and local mean sea level,

$S_{s,t}$

is the local mean sea level, and γ is the bilinear interpolation function across H and S, using the previously defined lookup table.

2.2.6 Extreme Sea Level Mortality

The expectation of annual costs of mortality occurring due to ESL events, where death equivalents are valued using a Value of a Statistical Life (VSL) framework, as employed in Diaz (2016), which assumes 1% mortality for all populations exposed to a given ESL, based on Jonkman and Vrijling (2008). This is modeled similarly to the ESL-driven capital loss, except that the 1% mortality assumption is used in place of the depth-damage function. In the implementation of Diaz (2016), both the mortality assumption and the depth-damage function appear to have been used in conjunction, although the text of the Diaz (2016) paper states that the depth-damage function should only be used in the estimation of capital stock damage, not mortality. We therefore corrected this discrepancy in our implementation of ESL-driven mortality estimates in pyCIAM.

2.2.7 Least Cost Optimization

For each planning period, every segment considers each of the possible adaptation options and assesses costs at each annual time step within the period. Like Diaz (2016), we maintain the assumption that these decision-making agents have perfect foresight of projected RSLR over this planning period; however, we reduce these periods from 40-50 years to 10 years (Sect. 1.7.2). The maximum heights of projected RSLR at each segment during a given planning period in turn influence the heights at which protect or retreat adaptation options are employed. For segments that just adapt via reactive retreat, the height of retreat would exactly match this projected RSLR, while segments employing 10, 100, 1000, 10000-year retreat or protect actions would consider the heights of these ESLs atop this projected RSLR baseline for that planning period. Once adaptation costs are calculated for all adaptation periods, we follow (Diaz, 2016) and calculate the NPV across the entire model duration for each adaptation option, and each segment chooses the least cost option.[7]

2.3 Estimating Non-market Costs of Relocation

Diaz (2016) portrays the costs associated with "optimal adaptation" and "reactive retreat only" scenarios as bounds on future costs. This is justified by the observation that coastal adaptation at present does not appear to be economically rational, such that populations do not relocate or protect themselves when it seems optimal to do so (McNamara et al., 2015; Armstrong et al., 2016; Haer et al., 2017; Bakkensen et al., 2018; Hinkel et al., 2018; Suckall et al., 2018). This observation could be explained by uncaptured non-market costs of relocation associated with, for example, non-pecuniary emotional consequences. Accounting for these impacts would indicate that the total welfare impact of forced relocation is greater than the market costs associated with simply abandoning immobile capital.

[7] In contrast to (Diaz, 2016), we include initial adaptation costs from the first planning period in this NPV calculation (Sect. *1.7.3*).

Though CIAM partially represents non-market costs associated with moving, the model does not re-create observed patterns of settlement when it is initialized and run under an optimal adaptation scenario. Instead, it results in an excess of instantaneous relocation, suggesting that these non-market costs may not be fully represented. Specifically, when the optimal adaptation scenario is run under the baseline parameterization in Diaz (2016) and with the assumption of no climate-driven sea level rise, we observe that $1.26T of capital and 33M people instantly relocate. Adjusting for population and capital growth over the century, this instant relocation represents 41% and 44% of the *cumulative* relocation realized by the end of the century under the median SLR scenario for RCP 4.5. This large amount of instantaneous relocation clearly conflicts with the observed distribution of people and capital and suggests that there may be larger costs of relocation than are realized in the parameterization of CIAM used in Diaz (2016).

Diaz (2016) assumed these non-market costs are equal in value to consumption of one year of local GDP per capita, based on this value falling between two alternative estimates: 0.5 years (obtained from the author's personal communication with Robert Mendelsohn) and 3.0 years, the value assumed in the FUND Integrated Assessment Model (Tol 1996). In a similar modeling framework, Lincke and Hinkel (2021) used the FUND value directly and further provided a literature review that finds empirical and theoretical estimates of total relocation costs varying between 2.3 and 9.5 years of average local income per capita. These empirical findings suggest that the factor of one used in Diaz (2016) may underestimate relocation costs.

To address this, we adopt an approach to calibrate these unobserved non-market costs of relocation against real world behavior. Our calibration approximates a "revealed preference" approach, in which the behavior of agents is thought to reveal information about their preferences and values that is not otherwise visible (other elements of DSCIM adopt related methods to estimate the undocumented costs of adaptation decisions in other sectors, e.g. see Carleton et al. (2020)). Intuitively, this strategy relies on the insight that if individuals found the benefits of moving to be larger than the combined market and non-market costs, they would relocate. We cannot observe the non-market costs, but we can estimate the benefits and the market costs. If we observe that individuals have not relocated but CIAM computes that the benefits outweigh the market costs even before considering SLR, then we can estimate a lower bound on the implied non-market costs (equal to the benefits minus the market costs) that must be present in order to prevent them from relocating and rationalize their observed behavior.

Our ability to constrain non-market costs using a revealed preference approach is constrained by our ability to accurately model benefits and market costs of relocation. There are inherent limitations in a global model (e.g. input data inaccuracies, preference heterogeneity) such that, at a segment-level, there will likely be some segments where benefits and/or market relocation costs are not measured exactly. Thus, we choose a relocation cost parameter by taking the exposure-weighted median value of segment-specific estimates of non-market costs.

To do this, we identify the total population and physical capital that would instantaneously relocate when the model is initialized in the absence of non-market relocation costs, assuming median estimates of RSLR in a no-climate change scenario (i.e., no change in GMSL, and RSLR associated only with land subsidence). For this simulation, we choose middle-of-the-road socioeconomic projections characterized by SSP2 and the International Institute for Applied Systems Analysis (IIASA) GDP growth model (Crespo Cuaresma, 2017). We then steadily increase the relocation cost parameter until 50% of that population and capital no longer

instantaneously relocates under the optimal adaptation scenario. This median approach balances the desire to capture the non-market costs causing observed non-relocation with the recognition that data and parameter limitations associated with a global model will inevitably cause some seemingly irrational discrepancy between modeled and observed behavior. Because this median occurs at different values for population and physical capital, we average the two values (6.7 and 10.9 years of local income, respectively) to obtain the 8.8 factor used in pyCIAM. Fig. 2 illustrates this calculation.

We note that this approach is facilitated by the resolution of the input data represented in SLIIDERS and of the model outputs provided by pyCIAM. The DIVA inputs used in Diaz (2016) assume that population and capital density are homogeneously distributed throughout each segment, and are non-varying by elevation. This could introduce substantial noise in the elevation distribution of the observed present-day state of these two variables and would prohibit the analysis described above. By leveraging global gridded datasets of population, capital, and elevation, SLIIDERS and pyCIAM capture heterogeneous density and better represent the true present-day elevation distribution of population and capital within each segment (Sects. 1.6.1, 1.6.3, and 1.5.3).

After updating the non-market cost parameter, we additionally follow the approach of (Lincke and Hinkel, 2021) and do not distinguish between the non-market costs of reactive and proactive retreat. (Diaz, 2016) assigns five times higher costs to reactive retreat, though there is no empirical basis reported for this additional cost. Thus, both proactive and reactive retreat in pyCIAM incur losses equivalent to 8.8 years of income, rather than one and five years, respectively, in (Diaz, 2016).

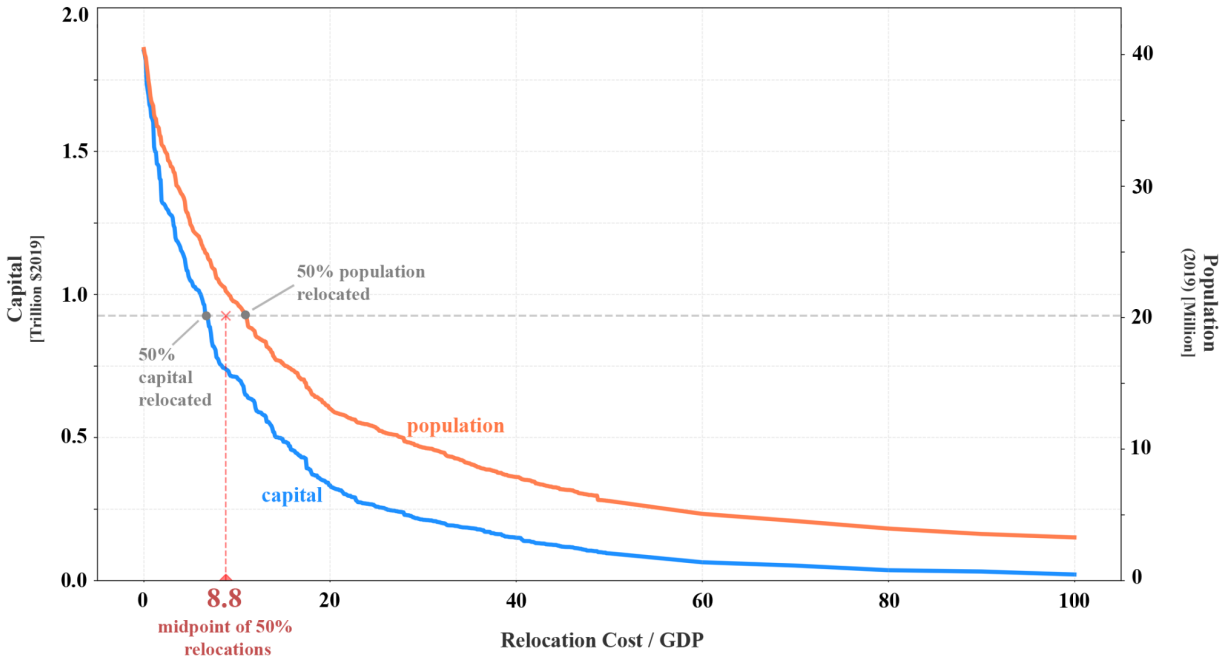

Figure 2. Estimation of the non-market relocation cost parameter through revealed preference. Curves show the magnitude of the population (orange) and physical capital(blue) that is instantaneously relocated

in the optimal adaptation scenario of pyCIAM, assuming SSP2-IIASA socioeconomic projections and median no-climate change RSLR, as a function of this parameter. The parameter is normalized by local GDP per capita. We identify the parameter values for which 50% of the population and capital instantaneously relocated under an assumption of zero non-market costs are no longer relocated, and average these two values to estimate the relocation parameter used in pyCIAM.

2.4 Porting CIAM from GAMS to Python

CIAM was constructed in the closed-source General Algebraic Modeling System (GAMS) language. However, the model does not require the dynamic programming capabilities offered by GAMS. Therefore, porting the model to Python, a commonly used, open-source programming language, offers greater flexibility, access, and efficiency without loss of functionality. Before adding additional resolution to the model, pyCIAM computed a global run of a single SLR trajectory in 15-20 seconds, compared to 6-8 hours for CIAM. To ensure that this first stage of changes did not introduce changes to model functionality, we ensured that this version of pyCIAM replicated the results from the CIAM (in GAMS) model obtained from its source repository before updating model inputs. This replication was largely confirmed, with only very minor deviations between the computed results and those reported in (Diaz, 2016). The observed deviations were also reflected in the outputs of the unaltered CIAM model we obtained, suggesting that the configuration of the publicly available CIAM model was likely slightly altered from that used in Diaz (2016) (Table 1).

Table 1. Comparison of select model results as reported in Diaz (2016) with those calculated from the original CIAM code in GAMS obtained from its online source repository and those calculated by pyCIAM after porting CIAM to Python and before any additional changes. Values reflect median relative sea level rise projections from Kopp et al. (2014) under a high emissions scenario (RCP 8.5). Model runs were conducted on an Apple MacBook Pro laptop with a 2.8 GHz Quad-Core Intel Core i7 processor and 16GB of RAM.

Billion USD ($2010)	**Diaz 2016 (paper results)**	**CIAM (GAMS)**	**pyCIAM**
Global NPV (2010-2100)	1700	1692.2	1692.2
U.S. NPV (2010-2100)	419	419.7	419.7
Australia NPV (2010-2100)	208	208.6	208.6
Brazil NPV (2010-2100)	98	97.5	97.5
China NPV (2010-2100)	87	87.0	87.0
Wetland Loss in 2100	80	79.3	79.3
Global Costs in 2100 (optimal adaptation)	270	282.1	282.1

Global Costs in 2100 (no adaptation)	2200	2251.5	2251.5
Calculation runtime		6-8 hours	15-20 seconds

2.5 Physical Model Inputs in SLIIDERS

2.5.1 Coastal Segments

To improve the traceability of data inputs and the efficiency of model optimization, we replaced the irregular DIVA coastal segments with segments based on the points at which ESLs are estimated in the Coastal Dataset for the Evaluation of Climate Impacts (CoDEC). This represents a roughly uniform, 50-km spacing of global coastline points (Muis et al., 2020). We made a number of slight alterations to the original CoDEC point set and used these points as midpoints of 50-km coastline segments (Sect. 4). The alterations ensured that (a) the coastline segments were nested by country boundaries, as the DIVA segments are, and (b) any extra points corresponding to offshore buoy gauges (used for validation in CoDEC) were removed. We also thinned European CoDEC points, originally provided at an extra fine 10km spacing, to 50km in order to have globally uniform spacing. We also manually added 19 segments for small island states or small slivers of national coastlines not represented in the original CoDEC point set (e.g. Anguilla, Tokelau, Jordan's small coastline, etc.). The final subset of CoDEC coastal points utilized in pyCIAM totaled 9,568. Natural Earth coastlines were used to make the point-to-segment conversion (1:10m resolution[8]). The coastline lengths of each segment, used to calculate the potential costs of building protective barriers, were derived from this final set of segments (Sect. 4.1).

The decision to replace the coastal segments was motivated by several reasons. First, in the version of DIVA (v1.5.5) used in Diaz (2016), we found that many of the coastal segment lengths in high latitude regions were substantially overestimated, likely due to a geographic projection error. This error looked to be corrected in versions of DIVA used in subsequent studies; however, we nevertheless wished to avoid dependence of pyCIAM on DIVA, with uncertainty surrounding its ongoing development support and dataset availability. Second, we found that DIVA contains a substantial over-representation of small, mostly unpopulated land masses in island regions within its set of 12,148 segments. For example, DIVA contains 1,316 individual segments for French Polynesia, constituting 10.8% of all global segments despite representing less than 0.004% of global population. This created substantial computational inefficiencies, as all segments require roughly equivalent computation.

[8] The '1:10m' label indicates the scale of the physical vector layers, which can also be thought of as the maximum length of coastline across which simplification of complex coastlines into straight line segments can occur. 1:10m coastlines are the most granular product provided by Natural Earth.

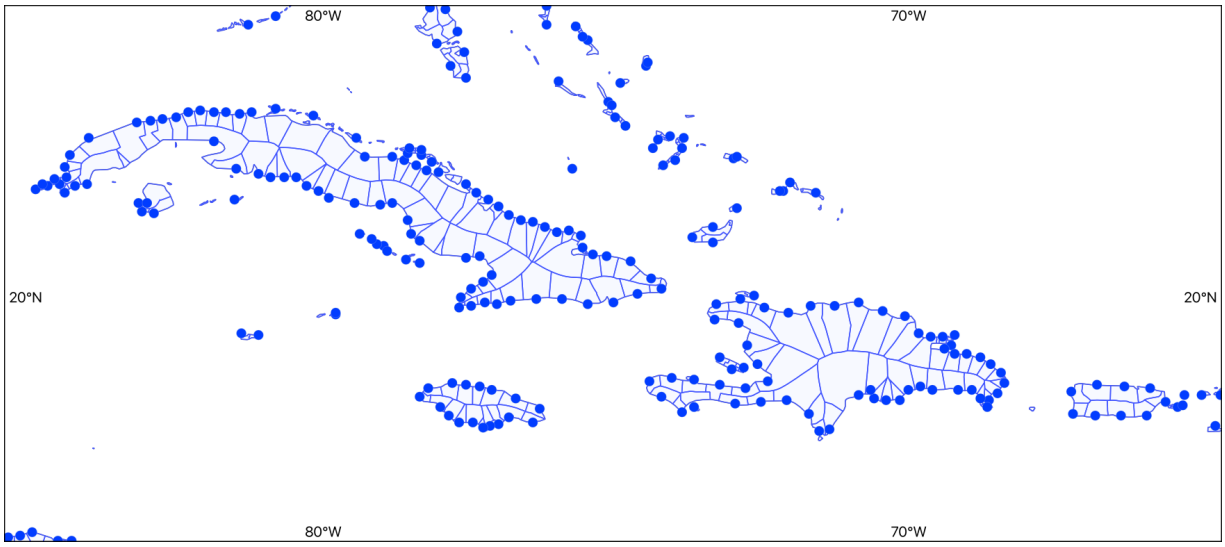

Figure 3. pyCIAM coastal segment centroids (points) and areas for a subregion of the Caribbean.

2.5.2 Extreme Sea Levels

We obtained ESL distributions from CoDEC v1 (https://doi.org/10.5281/zenodo.3660927), which uses the third generation Global Tide and Surge Model (GTSM) combined with the ERA5 reanalysis to create a reanalysis product of historical sea levels (Muis et al., 2020). The CoDEC data provide the location and scale parameters of a Gumbel extreme value distribution fit to modeled ESLs at each coastline point, which we used to obtain the return periods required by CIAM (1, 10, 100, 1000, 10000-year). In validation analysis that compares CoDEC to observed tide gauge values, CoDEC values slightly underestimate annual ESL maxima by an average of 0.04m across all observed tide gauge stations, with 1-in-10 year mean ESL heights underestimated by 0.10m. Certain areas exhibit greater model bias, with 25% of tide gauge stations included in the validation showing absolute biases greater than 0.2m and 0.3m for annual and decadal maxima, respectively. In regions with a large tidal range and/or frequent tropical cyclones, biases are generally larger. See Muis et al. (2020) for a full discussion of CoDEC model validity.

2.5.3 Elevation

The use of accurate elevation data is crucial to appropriately representing sea level rise impacts (Scott A. Kulp and Strauss 2019). We have implemented an updated elevation model used to define the population and physical capital exposed to SLR in pyCIAM in the following manner:

1. We utilize the CoastalDEM v2.1 dataset (Kulp and Strauss, 2021) to define elevations at 1 arc-second resolution (roughly 30m). The v2.1 release of CoastalDEM represents further improvements to the initially-released product (v1.1) (Kulp and Strauss, 2018), though both datasets represent substantial accuracy improvements to prior DEMs, such as the widely used SRTM DEM. In addition to higher resolution elevation estimates compared to the 30-arc-second GLOBE DEM used in Diaz (2016), CoastalDEM

significantly reduces bias found in SRTM, as presented in a comparative analysis based on CoastalDEM's initial release (v1.1) (Kulp and Strauss, 2019). Compared to SRTM, CoastalDEM v1.1 suggests that roughly three times the amount of present day population resides below projected high tide levels under low emissions sea level rise scenarios by 2100 globally (Kulp, and Strauss 2019). It should be noted that the high-resolution version of CoastalDEM v2.1 is the only input used in this study that is not publicly available. It is obtained via license with Climate Central, the developers of the DEM, though lower-resolution versions of the dataset are freely available for academic use. For the small number of regions that we model where CoastalDEM does not exist (e.g. above and below 60N and 60S, respectively), we derive elevations from the SRTM15+ v2.5 dataset (Tozer et al., 2019).

2. We pair this DEM with our 30 arc-second population (LandScan, 2021, Sims et al., 2022) and capital stock (LitPop (Eberenz et al., 2020)) rasters, which allows for independent calculations of the distribution of land area, capital, and population with respect to elevation. We also rescale LitPop at the country-level to match more recently available data from Penn World Table 10.0 (Feenstra et al., 2015) and other sources (see Section 1.6.3). This approach differs from that of Diaz (2016), where population and capital stock densities were defined at the segment level and assumed to be homogeneously distributed within a segment.
3. We discretize the distributions of population and capital to 0.1m elevation slices, rather than 1.0m.
4. We remove all pixels present in our coastal DEM from 0-20m that are not hydraulically-connected to the ocean from analysis.

2.5.4 Wetlands and Mangroves

For wetland areas, pyCIAM utilizes the European Space Agency's GLOBCOVER v2.3 global land cover dataset from 2009, offered at a 300m resolution (obtained in May 2021 from http://due.esrin.esa.int/page_globcover.php) (European Space Agency and UCLouvain 2010). Three different land cover classifications from this layer, as defined in (Hu et al., 2017), were coded as "wetlands":

1. Closed to open (>15%) broadleaved forest regularly flooded (semi-permanently or temporarily) - Fresh or brackish water
2. Closed (>40%) broadleaved forest or shrubland permanently flooded - Saline or brackish water
3. Closed to open (>15%) grassland or woody vegetation on regularly flooded or waterlogged soil - Fresh, brackish or saline water

Mangrove extents were updated using values from UNEP's Global Mangrove Watch 2016 dataset (Bunting et al., 2018) (obtained from https://data.unep-wcmc.org/datasets/45 in May 2021). The final wetland area used in pyCIAM consists of the spatial union of these two datasets.

2.5.5 Sea Level Rise

We integrate local SLR projections from 23 different future scenarios drawn from six different global and regional sea level change research efforts conducted in recent years. These are detailed in Table 1. We model and present results for the median (i.e. 50th percentile) reported trajectories for each of these 23 future SLR scenarios in the main text of this paper, although we also ran pyCIAM using the 17th and 83rd percentile SLR runs for all 23 scenarios, the results of which are available in the model output dataset and summarized along with median results in Tables C3, C4. We also note that pyCIAM is also configurable to run a probabilistic large ensemble of SLR trajectories on a multi-core computing platform, an approach used in recent research efforts using pyCIAM (Climate Impact Lab (CIL) 2022).

Our modeled future SLR pathways include the seven principal projections underlying the future sea level change trajectories detailed in the Intergovernmental Panel on Climate Change's (IPCC) Sixth Assessment Report (AR6) (Fox-Kemper et al., 2021). The data for these projections were generated using the Framework for Assessing Changes To Sea Level (FACTS) and were obtained from the report's public data repository (https://doi.org/10.5281/zenodo.6382554) (Garner et al., 2022). These seven trajectories represent different combinations of future emissions and underlying physical processes that influence sea levels. These scenarios are partitioned into two groups: *low confidence* (n=2) and *medium confidence* (n=5), which refer to the relative level of confidence of the underlying physical processes reflected in each future scenario. *Medium confidence* scenarios are considered to be of higher likelihood but do not incorporate less-certain physical processes, such as marine ice cliff instability, that could have large impacts on future sea levels, particularly in higher emission scenarios. These processes are represented in the *low confidence* AR6 projections and project higher end-of-century GMSL values compared to their *medium confidence* counterparts (Table 1).

It should be noted that each of the AR6 emissions scenarios were originally constructed using Integrated Assessment Models (IAMs) driven by a single socioeconomic trajectory (i.e. a single SSP). However, when assessing economic impacts of climate change it is often useful to separate future changes in welfare caused by non-climate-related socioeconomic trends from climate impacts. This is done by holding baseline growth rates fixed across emissions scenarios. For this reason, we assess damages from each of the AR6 emissions scenarios under each of the 5 SSPs, even though some emissions trajectories may be more or less plausible under different SSPs.

We also incorporate the five main SLR scenarios represented in the U.S. inter-agency Sea Level Rise Technical Report (2022), led by the National Oceanic and Atmospheric Administration (NOAA) (Sweet et al., 2022) and derived from the FACTS-based projections in Garner et al., (2022). The SLR pathways in this report were organized by their projected GMSL value in 2100, rather than by global emissions trajectories. As such, they are grouped into five bins, based on different plausible GMSL values in 2100: Low (0.3m), Intermediate-Low (0.5m), Intermediate (1.0m), Intermediate-High (1.5m) and High (2.0m)[9]. These data were obtained from the report's public data repository (https://doi.org/10.5281/zenodo.6382554).

[9] These GMSL values are expressed relative to GMSL in 2000, while pyCIAM expresses GMSL relartive to 2005, making its end-of-century values associated with these scenarios in pyCIAM approximately 2cm lower (Table 1) than those specified in Sweet et al. (2022).

The remaining 11 SLR projections are derived from the LocalizeSL framework (Kopp et al., 2014, 2017) (https://doi.org/10.5281/zenodo.6029807). LocalizeSL was used in the IPCC AR5 report (Church et al., 2013) and in subsequent publications (e.g. Kopp et al. (2017), Sweet et al. (2017), Rasmussen et al. (2018), Bamber et al. (2019), DeConto et al. (2021), Tebaldi et al. (2021)) prior to the introduction of FACTS. Similar to the AR6 SLR projections derived from FACTS, these based on LocalizeSL reflect a distribution across emissions scenarios, as well as across the component models used to represent the various contributing factors to SLR. These differences in component models refer to alternate assumptions and process representations regarding all contributors to sea level rise, with particularly influential differences in assumptions relating to ice sheet contributions.

Overall, these 23 scenarios cover a likely range of plausible SLR trajectories in the 21st century and allow us to estimate the marginal welfare costs of additional SLR across this full range (Fig. 4). Scenarios based on emissions trajectories may be most relevant for users interested in evaluating the benefits of emissions mitigation while those based on GMSL levels may be most relevant for local planners seeking to design adaptation strategies.

Notably, each of these scenarios contains a Monte Carlo sampling of a distribution of local SLR projections. However, because the 23 scenarios we reflect in this analysis cover a broad range of outcomes, for the purposes of this paper, we present results only for the median SLR projection at each coastal segment. In other words, the presented results reflect impacts in a world in which all regions experience the median projected RSLR for that scenario. Given the computational improvements in pyCIAM and its scalable design, it is suited for execution on a full Monte Carlo distribution. Climate Impact Lab (CIL) (2022), for example, applies CIAM to a 110,000-sample ensemble, using 10,000 draws from each of the 11 LocalizeSL-based SLR projections.

In addition to projections of climate change-induced SLR, and in alignment with Diaz (2016), we run a “no climate change” counterfactual scenario in which all SLR components are set to 0 except for a spatially heterogeneous and empirically estimated background rate of change parameter that includes drivers assumed to be unaffected by climate change (e.g. glacial isostatic adjustment, tectonics, sediment compaction, and other processes contributing to vertical land motion). This is a probabilistic parameter in the LocalizeSL and FACTS frameworks that is held fixed across all scenarios from a given modeling framework. The impacts estimated under these scenarios are subtracted from those in the climate change-driven scenarios to isolate the contributions of climate change to global 21st century coastal economic impacts (see Fig. 4).

To estimate local sea level extremes, we linearly combine the fixed ESL distributions from CoDEC with an annually interpolated version of the decadal SLR projections from each of these 23 scenarios. This allows us to maintain a globally consistent representation of extremes at reasonably fine resolution. Limitations of this “local bathtub” approach are described in Section 2.3.

Values for median GMSL rise throughout the 21st century are detailed in Table 2 below. Equivalent tables for the 17th and 83rd percentile SLR projections for each scenario are provided as Supplemental Tables C1, C2.

Table 2. GMSL rise between 2005 and 2100 for each median SLR scenario used in the pyCIAM and Diaz (2016) models, representing the x-axis positions of costs by scenario displayed in Fig. 4.

ID	SLR Scenario	Model Used	GMSL in 2100 [m] (median)
NCC	No Climate Change*	CIAM, pyCIAM	0.00
AR6-Med	IPCC AR6 *Medium Confidence* (2021): SSP1-1.9, SSP1-2.6, SSP2-4.5, SSP3-7.0, SSP5-8.5	pyCIAM	0.38, 0.44, 0.56, 0.68, 0.77
AR6-Low	IPCC AR6 *Low Confidence* (2021): SSP1-2.6, SSP5-8.5	pyCIAM	0.45, 0.88
NOAA	US Inter-agency SLR Technical Report (2022): Low, Int-Low, Int, Int-High, High	pyCIAM	0.28, 0.48, 0.98, 1.48, 1.98
K14	Kopp et al. (2014): RCP 2.6, RCP 4.5, RCP 8.5	CIAM, pyCIAM	0.48, 0.58, 0.78
SR	IPCC-SROCC (2019): RCP 2.6, RCP 4.5, RCP 8.5	pyCIAM	0.49, 0.60, 0.88
B19	Bamber et al. (2019): Low (C), High (C)	pyCIAM	0.68, 1.10
D21	DeConto et al. (2021): RCP 2.6, RCP 4.5, RCP 8.5	pyCIAM	0.52, 0.62, 1.10

*Includes local background rates of relative sea level rise at each segment due to non-climatic background processes. Because of model differences, the FACTS-based projections (AR6 and NOAA) will use slightly different no-climate-change scenarios than those based on LocalizeSL.

2.6 Socioeconomic Variables

2.6.1 Population

In SLIIDERS, we use information from LandScan 2021 (Sims et al., 2022) to represent the present-day spatial distribution of population, scaled such that the aggregated country level population estimates match the 2019 estimates contained within the Penn World Table (PWT) v10.0 (Feenstra et al., 2015). In pyCIAM, we then maintain this within-country distribution and scale the country totals to match the SSPs (Riahi et al., 2017), exponentially interpolated between 5-year projections to annual values. Because the SSPs begin in 2010 and pyCIAM

begins in 2005, we must scale populations back to 2005. To do so, we use observed country-level growth rates from 2005 to 2010 and apply these backcast from the 2010 SSP projections, which are constant across all SSPs. Observed rates are drawn primarily from PWT, with missing countries filled through a variety of sources including the 2022 UN World Population Prospects (UN DESA, 2022), multiple iterations of the CIA World Factbook (Agency, 2021), World Bank World Development Indicators (WDI, Bank (2021)), and local government statistics for some small island states. To project population forward For countries and territories not covered by the SSP data, we use global average population growth rates applied to 2010 estimates.

2.6.2 GDP

pyCIAM combines SSP-consistent, country-level GDP projections from two growth models - one from IIASA (Crespo Cuaresma, 2017) and one from the Organisation for Economic Co-operation and Development (OECD, Dellink et al., (2017)) OECD) and population projections from IIASA (Kc and Lutz, 2017) to create country-level GDP per capita projections. These data are available on the SSP Database (Riahi et al., 2017). SSP interpolation and extrapolation approaches match those used for population values. Observed values for 2005-2010 are again drawn from PWT 10.0 where available, with alternative sources including (Fariss et al., 2021), OECD Regional Statistics (OECD, 2020), the 2021 International Monetary Foundation World Economic Outlook (IMF, 2021), and the WDI. Where and when country-level estimates are unavailable but estimates do exist for associated sovereign entities, we use a regression estimator described in Bertram (2004) to estimate per capita GDP for the territories. For the countries and territories not covered by IIASA and OECD projections, we take the global-average per capita estimates in 2010 and interpolate/extrapolate using the global average yearly growth rates for missing years.

To create per capita GDP estimates (*ypc*) for coastal segments in pyCIAM for each year (*t*), we use the same national-to-segment downscaling approach as Diaz (2016), which relates population density to income. See Equation 8 in the Diaz (2016) Supplemental Information for further details. In Diaz (2016) population density is assumed to be homogeneous within segment, which implies that all elevation slices within a coastal segment are prescribed the same local income. In pyCIAM, each elevation slice within each region has a unique population density. Thus, we apply this downscaling approach separately to each elevation slice.

2.6.3 Physical Capital

In addition to assessing the exposure of human population to SLR-related hazards, pyCIAM also assesses the exposure of physical capital stock to these threats. Both the IIASA and OECD GDP growth models utilize projections of physical capital; however, neither model has publicly released these projections. Therefore, to create future capital stock estimates, we extract the relevant growth equations for OECD's Env-Growth model as described in Dellink et al. (2017). The capital growth trajectory in the IIASA model is exogenously specified, constant across SSP scenario, and yielded implausibly large capital stocks in later years. For instance, the IIASA model projects that Macau reaches $30.8 quadrillion in 2100 capital stock, which is 23 times that of the U.S. in 2100 ($1.3 quadrillion) and 200,000 times that of Macau in 2010 ($134 billion) (all

values in constant 2019 PPP USD). Due to such implausible growth rates, we do not use the IIASA capital growth trajectory in pyCIAM.

We use country-level capital stock estimates up through 2020 and then use 2020 estimates as the initial conditions for this growth model. Like with population and GDP, historical estimates of capital come primarily from PWT 10.0. Where these values are missing and outside of the special cases of Cuba and North Korea, SLIIDERS uses estimates of the ratios of non-financial wealth (NFW) to GDP derived from multiple vintages of the Credit Suisse Global Wealth Databook (Suisse, 2021), combined with nominal GDP information from United Nations System of National Accounts (Nations 2021). Following the approach taken in (Eberenz et al., 2020), we then multiply PPP GDP by these NFW-to-GDP ratios to acquire proxies of physical capital. For Cuba, we use the ratio of Cuban and the U.S. capital stock values from Berlemann and Wesselhöft (2017) and multiply this ratio with the U.S. capital stock values from PWT 10.0. For North Korea, we multiply the capital-to-GDP ratio in Pyo and Kim (2020) with PPP GDP.

Then, we apply the OECD capital stock equations with the estimated 2020 capital stock values and SSP-consistent GDP projections to obtain projections of capital stock for each SSP scenario and for each GDP growth model. To parameterize these equations, we use a value for the partial elasticity of GDP with respect to capital taken from Crespo Cuaresma (2017) (0.326), since this is not reported in Dellink et al. (2017). We also estimate country-specific initial conditions for the marginal product of capital using a modified Cobb-Douglas production function fit to the historical capital data. See Sect. 4.3 for further methodological detail.

pyCIAM uses the LitPop dataset (Eberenz et al., 2020) to represent within-country spatial distribution of physical capital stock at 30 arc-second resolution. LitPop combines population information from the Gridded Population of the World dataset (v4.1) with nightlight intensity (Román et al., 2018) to downscale country-level estimates of total physical assets. In some countries, e.g. Libya and Syria, LitPop does not provide any downscaled estimates. In these locations, we use the downscaled estimates provided by the GEG-15 dataset (Bono and Chatenoux, 2014). For the small number of island countries that do not have capital distributions reflected in either dataset, we assume homogeneous capital stock.

In pyCIAM, the ratio of mobile to immobile capital is used to determine costs of inundation. Diaz (2016) used a fixed ratio of 10%. However, PWT 10.0 contains country-level information that can be used to estimate across-country heterogeneity in this ratio. PWT decomposes physical capital into four categories:

- Residential and non-residential structures
- Machinery and non-transport equipment
- Transport equipment
- Other assets

For SLIIDERS, we assume that the first category (residential and non-residential structures) represents immobile capital and the others represent mobile capital. We take the average mobile fraction from 2000-2019 and apply this at the country level. These country specific values vary from 1% (Haiti) to 52% (Equitorial Guinea) with 25th, 50th, and 75th percentiles of 14, 18, and 20%, respectively.

2.6.4 Construction Costs

We maintained the same reference unit cost of coastal protection utilized in CIAM but updated the national construction cost index scaling factors by using the ratio of construction cost indices from ICP 2017 (World Bank, 2020) instead of 2011. For countries not included in this dataset, we augment with the country-level construction cost indices used in Lincke and Hinkel (2021), averaged across the rural and urban distinction.

2.7 Other Features

2.7.1 Model Duration

Diaz (2016) runs from 2000-2200. However, the SSPs stop at 2100 and thus the SLIIDERS dataset does as well. Because of this, and because the AR6 SLR scenarios begin in 2005, we limit pyCIAM to 2005-2100. Using the 4% discount rate employed in Diaz (2016) and pyCIAM, the discount factors for 2100-2200 costs vary from 2% in 2100 to 0.03% in 2200, so the exclusion of these additional years is unlikely to have a substantial effect on the optimal adaptation option selected by each segment.

2.7.2 Timesteps and Planning Periods

We increase temporal resolution from the decadal timesteps used in Diaz (2016) to annual. In addition to the exponential interpolation of 5-year SSP inputs described above, decadal SLR projections are linearly interpolated to yield annual values. The 40-50 year planning periods used in Diaz (2016) yield substantial step-changes in realized costs at mid-century and end-of-century due to substantial simultaneous global adaptation actions. To generate a smoother time series of costs, we use decadal planning periods. A potential trade-off of using shorter planning periods is that this may overestimate the frequency with which governments and populations are able to update major adaptation actions. An unrealistically agile representation of large-scale adaptation actions may underestimate associated net present cost because some adaptation costs can be postponed to future years with lower discount factors. Future work may empirically estimate the frequency at which adaptation approaches are updated and explore further options for incorporating planning periods that are not globally simultaneous and thus do not lead to substantial step-changes in global SLR costs at the start of each period.

2.7.3 Net Present Value Calculation

In pyCIAM, the NPV each segment uses to calculate an optimal adaptation approach is calculated from 2010-2200, excluding the initial planning period of 2000-2009. In this way, each segment is allowed a “free” initial relocation or protection action. For example, if a segment chooses to protect to the 1-in-10,000 year sea level height, which is 3 meters in 2000, they do not consider the costs of building a corresponding seawall when calculating the NPV of this action. They only consider the marginal cost of extensions to this seawall to remain at the 1-in-10,000 year height as local sea levels increase.

The rationale for this initial "spin-up" period in Diaz (2016) was to allow each segment to choose an optimal adaptation approach without including costs for adaptation measures that may already exist but are not reflected in observed values due to the lack of high quality global input data describing population distribution and coastal protection measures. In other words, segments were allowed to choose their optimal adaptation approach based only on adaptation costs associated with *updating* adaptation (e.g. through height increases of protection or additional managed retreat) but not based on the costs of initial implementation (e.g. the initial protection construction or managed retreat).

By using finer resolution population and capital stock estimates, SLIIDERS partially ameliorates this need by providing more accurate observed measures of coastal exposure. In addition, we argue that any existing adaptation measures would have to have been implemented at some point in history when they were presumably determined to be a cost-effective approach, even including the initial costs of implementation. Assuming that this adaptation was allowed to occur "for free", as in Diaz (2016), is likely to overestimate the state of present-day adaptation.

For these reasons, in the configuration of pyCIAM presented here, each segment uses costs from the entire model duration of 2005-2100, inclusive of the initial adaptation costs, to calculate NPV and choose an optimal adaptation approach. This configuration is applied to costs from all scenarios, including those from the "no climate change" counterfactual scenario that are subtracted from the "with climate change" scenarios in order to isolate the climate change contributions to coastal welfare impacts.

Because of this consistency in application, the choice of the initial NPV year is likely to have a minimal effect on the estimated climate change costs. However, it will substantially affect the "un-differenced", total costs associated with both the "with climate change" and "no climate change" in the initial adaptation period. This is reflected in substantially different NPV calculations between this paper and Diaz (2016) in this un-differenced context (see Fig. B1). pyCIAM provides users with a configurable parameter to determine whether initial adpatation costs should be accounted for in each segments NPV calculation or not.

In addition to modifying the starting year of the NPV calculation, we make one change to the application of a discount rate. Diaz (2016) applied the discount rate at the start of each decadal timestep to the full 10 years of costs incurred in that timestep. This overestimates the discounted cost for all years after the first. We avoid this issue by using annual timesteps; however, when comparing NPV results to Diaz (2016) (Fig. 4), we apply annually varying discount rates to the Diaz (2016) outputs as well.

2.7.4 Manual Correction Factors

In pyCIAM, the following manual correction factors in the original code underlying Diaz (2016) have been removed. These correction factors were originally used by Diaz (2016) in order to correct for certain limitations in data availability or quality that are no longer necessary after incorporating the data updates in SLIIDERS:

- Doubling the price of construction on all "island" segments. The new construction cost index values utilized in pyCIAM should reflect any increased construction costs on island

nations. Additionally, segments defined as “island” in CIAM were not entirely consistent, with some islands receiving the label and others not.

- Halving the protection heights under the protection adaptation scenario corresponding to 10-year ESL heights. This was originally implemented to account for elevation profiles found in the GLOBE DEM that were deemed physically implausible (extremely high area totals from 0-1m), but is no longer required following the updated CoastalDEM elevation values.
- Averaging of the inundated land area-by-elevation bins for the first two (0-1m, 1-2m) bins in order to smooth the elevation profile due to the high 0-1m area totals in the GLOBE DEM values. This adjustment, too, is no longer required following the updated CoastalDEM elevation values.

3 - Results and Discussion

Upon implementing the changes described above, global costs estimated by pyCIAM diverge modestly from those in Diaz (2016). Additionally, we obtain estimates for a greater breadth of socioeconomic and SLR trajectories that reflect deep uncertainty in these processes. Fig. 4 displays estimated global costs for the following global SLR-driven cost metrics reported in Diaz (2016): (i) global net present costs under an optimal adaptation scenario using a 4% discount rate, (ii) end-of-century annual total costs under that same scenario, (iii) end-of-century annual total costs under a “reactive retreat only” scenario, and (iv) end-of-century annual costs of wetland loss under the optimal adaptation scenario. Global NPV and end-of-century costs for the highlighted scenarios in Fig. 4, averaged by SSP and economic growth model are shown in Table 3.

Results are shown for the pyCIAM model both in its replicated CIAM configuration and after all the above changes were applied. Values are expressed such that each vertical group of points comprise the spread of results between the different socioeconomic projections for a given SLR scenario, with the position along the x-axis representing that scenario’s median GMSL value in 2100. As described in Sect. 1.5.5, all of the pyCIAM results use a constructed “median” SLR trajectory where each location experiences the median RSLR across the probabilistic projected distribution. This matches the approach used in Diaz (2016).

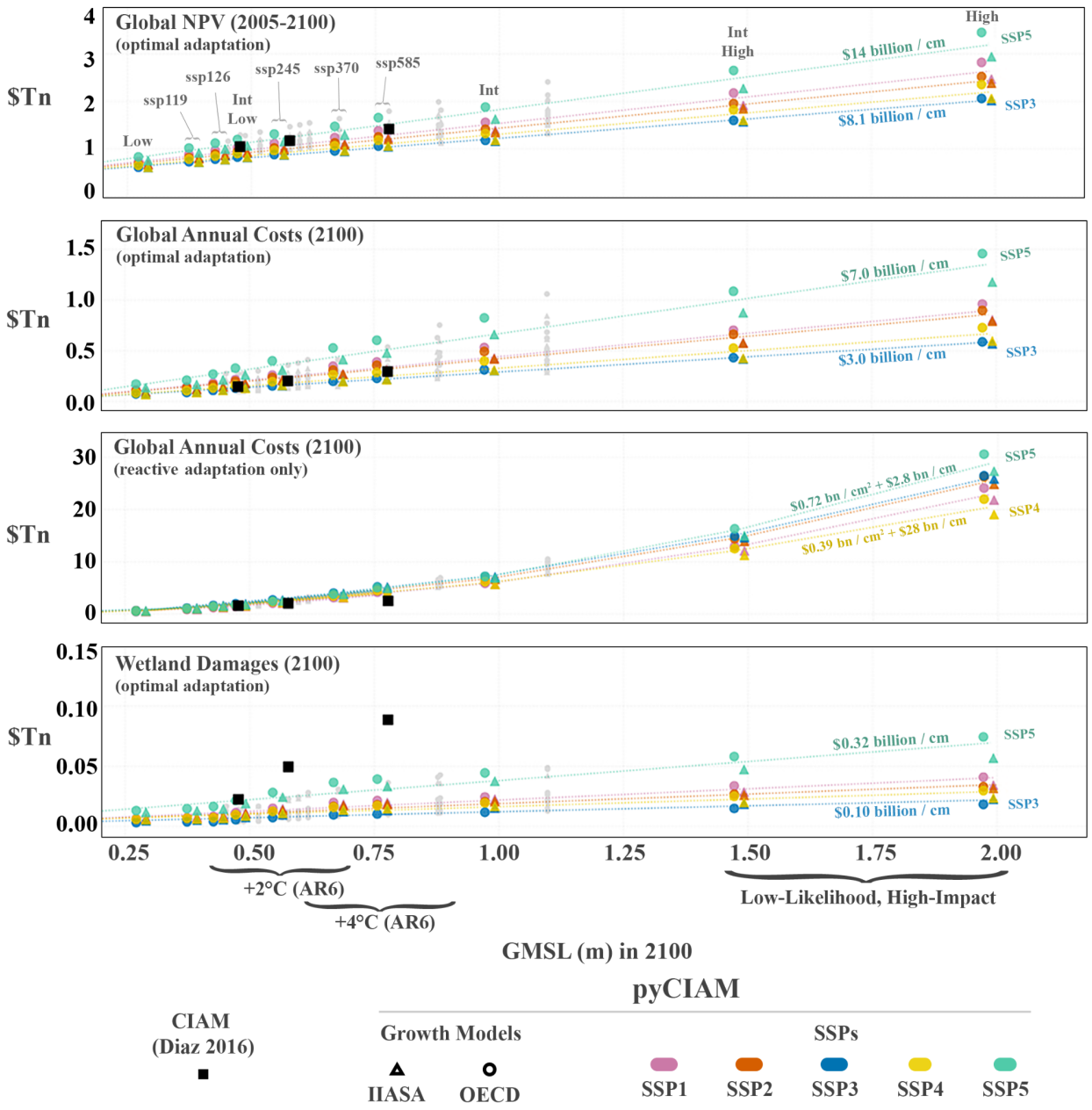

Figure 4. Comparison of global cost estimates under each SLR scenario. Values are costs from climate change induced SLR only, i.e. after differencing the costs under a "no climate change" scenario that reflects median projections of non-climatic RSLR rates and no GMSL rise. All costs are expressed in constant 2019 PPP USD. Each vertical group of points describes a single SLR scenario, with each point in the group representing a unique combination of SSP and economic growth model. For visual clarity, only medium confidence AR6 (ssp119, ssp126, ...) and Sweet et al. (2022) scenarios (Low, IntLow, ...) are indicated with colored markers and jittered slightly along the x-axis based on runs using the OECD (-1cm) or IIASA (+1cm) economic growth model. The remaining SLR scenarios are shown in grey without jitter. Dashed lines represent fitted relationships between the cost metric and 2100 GMSL across the full set of SLR scenarios. Relationships are estimated for each SSP scenario and are linear for all metrics except for global annual costs under a reactive adaptation scenario.

Table 3. Global NPV and annual costs of climate-driven SLR in 2100, expressed in constant 2019 PPP USD, for the medium confidence AR6, Sweet et al. (2022) (NOAA) and Diaz (2016) SLR scenarios. Each metric is presented for both the optimal adaptation and reactive retreat modeling configurations.

SLR Scenario	**GMSL [m] (2100)**	**NPV $Tn (Optimal)**	**NPV $Tn (Reactive)**	**Costs (2100 $Tn (Optimal)**	**Costs (2100 $Tn (Reactive)**
Low (NOAA)	0.28	0.683	1.24	0.103	0.550
SSP1-1.9 (AR6-Med)	0.38	0.820	2.03	0.128	1.01
SSP1-2.6 (AR6-Med)	0.44	0.889	2.43	0.160	1.43
RCP 2.6 (CIAM)	0.48	1.05	6.84	0.146	1.58
Int-Low (NOAA)	0.48	0.945	2.50	0.193	1.70
SSP2-4.5 (AR6-Med)	0.56	1.02	3.30	0.230	2.40
RCP 4.5 (CIAM)	0.58	1.17	7.93	0.202	2.04
SSP3-7.0 (AR6-Med)	0.68	1.12	4.18	0.300	3.57
SSP5-8.5 (AR6-Med)	0.77	1.25	5.27	0.341	4.68
RCP 8.5 (CIAM)	0.78	1.42	9.70	0.293	2.50
Int (NOAA)	0.98	1.41	6.23	0.469	6.52
Int-High (NOAA)	1.48	1.94	13.7	0.629	13.8
High (NOAA)	1.98	2.51	24.9	0.857	24.9

3.0.1 Global NPV with Varying Discount Rates

It should be highlighted that in the estimates of NPV presented throughout the text, in Fig. 4 and Table 3 above were calculated assuming an annual discount rate of 4% from 2005-2100. This was originally done to both match the methods employed by Diaz (2016) and also to match the discount rate of 4% that underpins coastal segments' adaptation decision-making, whereby potential future damages are assessed and valued by each coastal segment (i.e. decision agent) in each planning period and valued using a 4% discount rate. This discount rate is similar but, importantly, distinct from that used to estimate net present global costs for the entire 2005-2100 from the full set of model results. Therefore, these values can in theory differ from one another, as they represent different evaluations of future damages in different contexts. It is valid to assume that individual coastal segment decision agents may place a higher premium on near-term future costs and discount longer-term potential impacts when deciding optimal adaptation strategies (i.e. with a 4% rate).

One can think of the model results, optimal adaptation behavior and associated costs as being the product of agent-based future damage discounting. However, these resultant raw cost values from 2005-2100 can then be converted to global net present costs using any discount rate deemed appropriate, which need not necessarily equal the rate employed by coastal agents in their adaptation decision-making. Here we present three alternate methods for computing global NPV from 2005-2100, all of which correspond to model results in which adaptation decisions were made using a constant 4% discount rate in each case, but with varying discount rates applied post-hoc to calculate global net present costs. We applied discount rates of 4%, 2% and 1.5%, the latter two of which reflect a growing consensus in the climate impacts research community that future damages are more appropriately valued using discount rates below 4% (Rode et al., 2021). Ranges of global NPV across all 230 model scenarios for climate-driven SLR and total damages, as well as for optimal and reactive retreat-only adaptation scenarios are presented in Table 4 and in Fig. 5. Similarly to previously-presented results, these values reflect median SLR trajectories in each of the scenarios.

Table 4. Range of net present costs from 2005 to 2100 in constant 2019 PPP USD across all 230 socioeconomic and SLR scenarios for multiple discount rates used to calculate NPV. Cost ranges reflect all combinations of cost type (climate-driven SLR versus total) and adaptation practice (optimal versus reactive retreat alone).

NPV (2005-2100) ($Trillion)	**Climate-Driven SLR** (optimal)	**Climate-Driven SLR** (reactive)	**Total** (optimal)	**Total** (reactive)
Disc. Rate = 4%	0.606-3.45	1.13-29.9	6.37-10.6	35.4-80.8
Disc. Rate = 2%	1.35-11.0	3.71-129	8.36-21.7	37.2-170
Disc. Rate = 1.5%	1.71-15.1	2.25-116	9.23-27.6	38.1-233

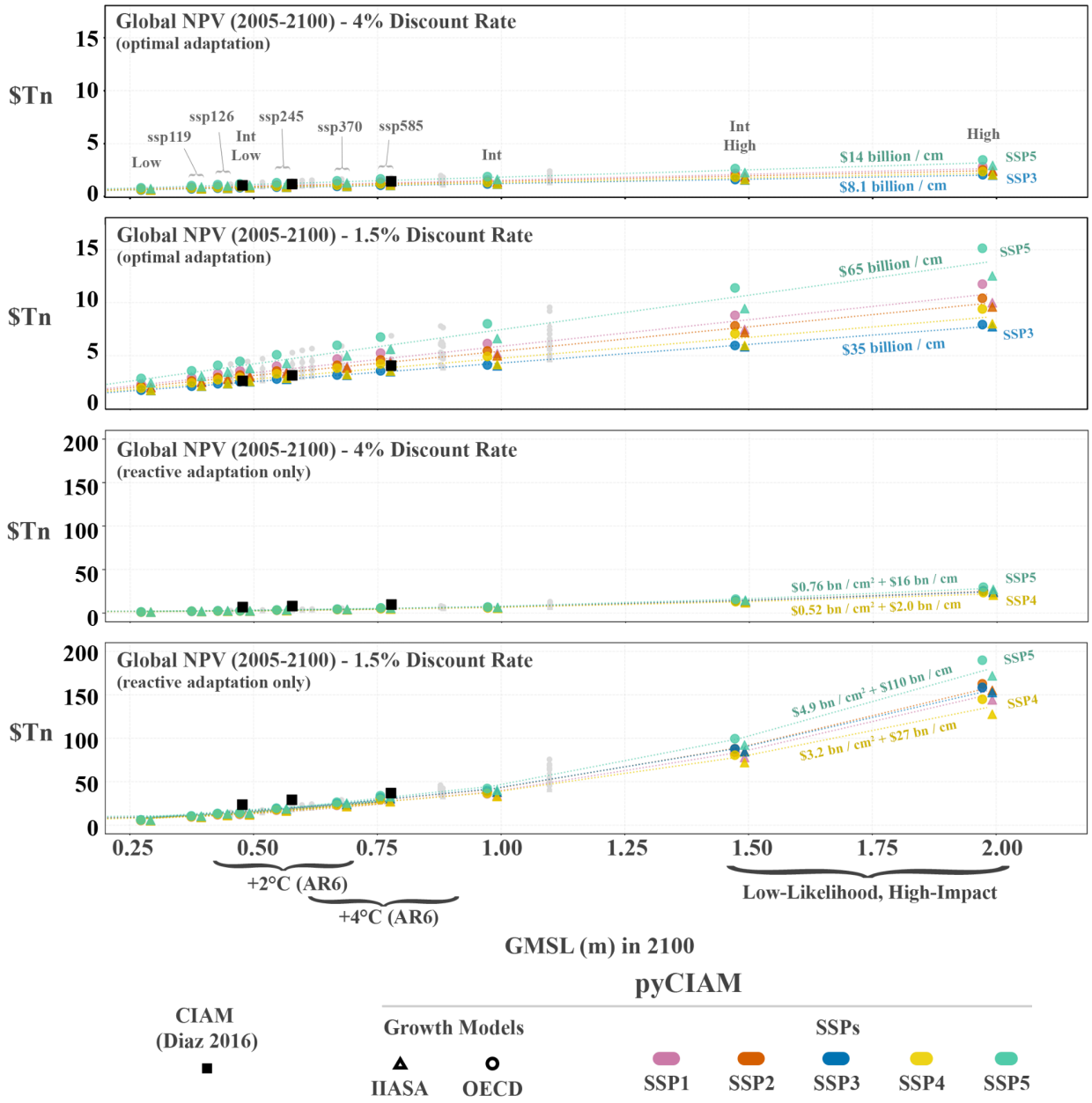

Figure 5. Comparison of global NPV values for median model results under each scenario for climate-driven SLR impacts. Values are expressed in constant 2019 PPP USD and reflect two discount rate alternatives (4% and 1.5%) for computing net present costs from 2005-2100. Results from utilizing both discount rates and both optimal and reactive retreat adaptation model configurations are displayed. Plot layout is equivalent to Fig. 4.

From Table 4 and Fig. 5, we can see that the choice of discount rate for calculating NPV from 2005-2100 heavily influences the global estimates of 21st-century net present coastal impacts, both under climate-driven SLR alone and overall. Using a 4% discount rate, as in Diaz (2016), yields global NPV values that range from roughly $610 billion to $3.5 trillion for climate-driven

damages under optimal adaptation. However, these values increase to $1.7 to $15 trillion using a discount rate of 1.5% (i.e. a near-quintupling of high-end net present costs). This trend is observed for all other types of NPV, especially for high-end scenarios, with the highest-cost model configuration (total costs, reactive retreat only) ranging from $35-81 trillion with a 4% rate, but jumping to $38-233 trillion under a 1.5% rate.

It is important to observe that NPVs for low-end SLR scenarios are much less sensitive to changing discount rates compared to high-end SLR rates. This is primarily due to the temporal distribution of SLR and related damages across the 2005-2100 period. Scenarios in which NPVs are less sensitive to alternate discount rates indicate the bulk of costs being borne at the start of the modeling period, or at least not disproportionately weighted towards the end-of-century. For example, in the case of climate-driven SLR costs with reactive retreat alone, NPV values for the low-end SLR scenario (NOAA-Low) only increase by roughly 2x ($1.13 to $2.25 trillion) between a 4% and 1.5% discount rate, while NPVs associated with the highest-end scenario (NOAA-High) exhibit a nearly 4x increase ($29.9 to $116 trillion). This is due to the fact that under high-end SLR scenarios, the majority of impacts are borne near the end of the century when GMSL is highest. For the total-cost/reactive-retreat scenario, this disparity is even more pronounced, with low-end (non-climate, background rates of sea level change alone) NPV increasing just 7.6% ($35.4 to $38.1 trillion), while high-end (NOAA-High) NPV increases 290% ($80.8 to $233 trillion).

3.1 Total SLR Costs

The global distribution of end-of-century average annual costs of climate-driven SLR under optimal adaptation, aggregated to “admin 1” regions (equivalent to state-level in the U.S.), is shown in Fig. 6, using the AR6 (medium confidence) SSP2-4.5 SLR scenario and SSP2-IIASA socioeconomic trajectory. Fig. 7 similarly demonstrates spatial heterogeneity in the annual cost savings realized through optimal adaptation, relative to costs in the reactive retreat scenario.

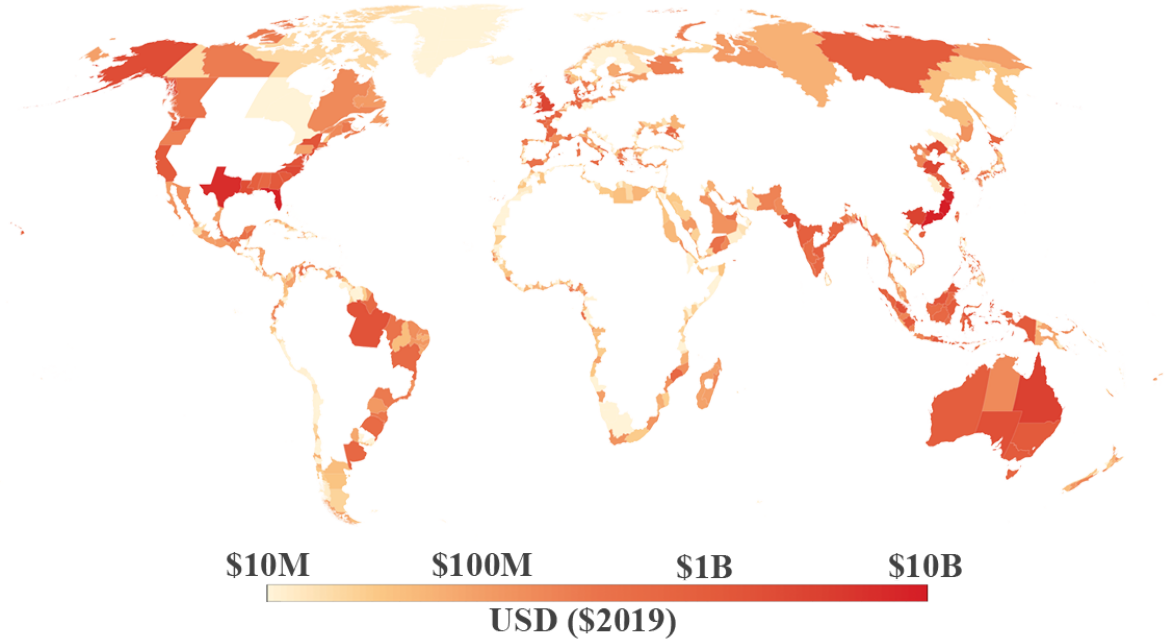

Figure 6. Estimated annual average costs in 2100 by "admin 1" region (equivalent to state-level in the U.S.). Results shown reflect optimal adaptation, using the AR6 (medium confidence) SSP2-4.5 SLR scenario and SSP2, IIASA socioeconomic projections.

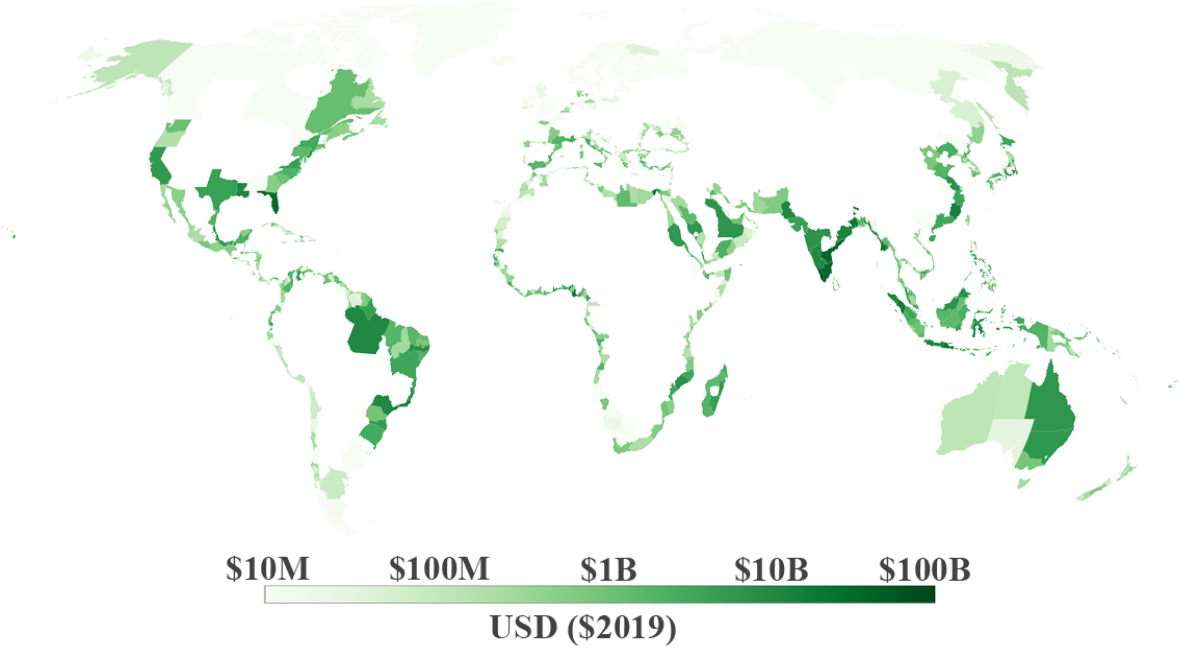

Figure 7. Estimated annual adaptation benefits in 2100 by "admin 1" region (equivalent to state-level in the U.S.). Results shown reflect the AR6 (medium confidence) SSP2-4.5 SLR scenario and SSP2, IIASA socioeconomic projections.

Median global NPV values from 2005-2100 under optimal adaptation ranges from $610 billion to $3.4 trillion in pyCIAM across its 230 SLR-SSP-economic growth model scenarios, corresponding to end-of-century GMSL rise values between 0.28 and 1.98m, relative to 2005 mean sea level (Fig. 4). Estimates of global NPV from Diaz (2016) range from $1.0 to $1.4 trillion in the three SLR scenarios considered (end-of-century GMSL rise from 0.48 to 0.78m, Table 2). Comparing the three SLR scenarios used in pyCIAM that match those employed in Diaz (2016) (K14 RCPs 2.6, 4.5, 8.5), pyCIAM's median global NPV values from 2005-2100 are fairly similar to those estimated by CIAM (Fig. 4).

When considering total damages, rather than the difference between them, pyCIAM estimates significantly higher global NPV (median values are 5-6x higher) and moderately higher (2x) end-of-century costs compared to Diaz (2016) (Fig. B1). This may be largely attributed to the fact that projected capital stock and population in SLIIDERS across its SSP and growth model scenarios are significantly higher than those modeled in Diaz (2016). For example, the mid-century global capital stock located between 0 and 15 meters above sea level ranges from $220 to $370 trillion (2019 USD) across the five SSPs and two growth models in SLIIDERS, compared to $97 trillion in Diaz (2016). Similarly, SLIIDERS' mid-century population ranges from 1.19 to 1.35 billion people across the five SSPs (population is equivalent in each economic growth model), compared to 1.18 billion in Diaz (2016). The SSP-based ranges differ most from the Diaz (2016) trajectories around mid-century before beginning to converge toward end-of-century. This behavior aligns with the observation that end-of-century annual costs are more similar across pyCIAM and Diaz (2016) than total NPV. Another reason for higher modeled costs in pyCIAM may be the updated topographic maps and other physical input datasets used for estimating exposure to SLR in pyCIAM. Finally, the decision to include initial adaptation costs in the NPV calculation and optimal adaptation selection for each segment contributes to the substantially higher NPV values seen in pyCIAM (see Section 1.7.3). Annual global costs due to climate-driven SLR in 2100 under optimal adaptation range from $70 billion to $1.5 trillion across all pyCIAM scenarios, and from $100 billion to $540 billion across the K14-pyCIAM scenarios that correspond to those used in Diaz (2016). The corresponding values from Diaz (2016) range from $150 billion to $290 billion. Under a reactive retreat scenario, pyCIAM values are generally similar to those of Diaz (2016) for low and medium-SLR scenarios and higher for high-end SLR scenarios (Fig. 4).

Considering the AR6 (*low* and *medium-confidence*) warming scenarios and associated ranges of global SLR by 2100, we estimate that under 2° C of warming by 2100 (+0.40-0.69m GMSL), annual end-of-century costs will be between $110 billion and $530 billion, depending on SSP, economic growth model, and SLR magnitude and assuming optimal adaptation. For AR6's 4° C scenario (+0.58-0.91m GMSL), these costs range from $200 billion to $750 billion. Also, for two low-likelihood, high-impact scenarios (NOAA-IntHigh, NOAA-High), which incorporate more uncertain physical processes like accelerated marine ice sheet and marine ice cliff instability, and correspond to GMSL rises of 1.5-2.0m by 2100, global annual costs range from $420 billion to $1.5 trillion by end-of-century under the same set of assumptions.

Upon projecting costs across this wide range of SLR scenarios, we find a strongly linear relationship for both NPV and annual end-of-century wetland and total damages with respect to end-of-century GMSL. Depending on socioeconomic projections, the marginal NPV costs associated with 1 cm of end-of-century GMSL range from $8.1 billion to $14 billion, the marginal annual end-of-century total costs range from $3 billion to $7 billion, and the marginal annual end-of-century wetland costs range from $100 million to $320 million. In a scenario with only reactive adaptation, annual end-of-century costs are not only much higher in absolute terms but also increase in a much sharper (quadratic) manner with respect to GMSL.

3.2 Adaptation Costs and Benefits

The global distribution of optimal adaptation strategies is displayed in Fig. 8 for the AR6 (*medium confidence*) SSP2-4.5 SLR and SSP2, IIASA scenario. Notably, the majority of segments that protect are located in Asia, where coastal population densities are generally high and construction costs, at least as parameterized by CIAM and pyCIAM, are relatively low. Scattered high-density areas across OECD countries in Europe and North America are protected as well. The fact that most protecting segments opt for the maximum level of protection (1-in-10,000-year ESL height) also suggests that, for segments where protection is optimal, the marginal costs of building higher protection are almost always lower than the benefits they provide, up to the point where the protection heights have provided safety from an exceedingly rare event. Future work should further explore the empirical validity of the construction cost functions used in Diaz (2016) and ported to pyCIAM, as these may control the spatial distribution of protection. Similar to the dominance of maximum protection, there is a common preference to retreat to the 1-in-10-year ESL height amongst segments that adopt retreat as their optimal strategy. This suggests that increasing the resolution of retreat options around this level may better reflect heterogeneity in optimal retreat height. Finally, segments for which reactive retreat is optimal are generally sparsely populated or unpopulated, as seen in the low percentages of global population residing in these segments (Fig. 9).

Fig. 9 displays the proportion of global segment populations adopting different adaptation strategies (protection, proactive retreat, and reactive retreat), across the various socioeconomic and SLR scenarios for both pyCIAM/SLIIDERS and CIAM. In general, while CIAM indicates that roughly 50% of the world's population would be protected under optimal adaptation and 50% would be relocated, pyCIAM, paired with SLIIDERS inputs, finds these ratios to be closer to 80% and 20%, respectively. This is largely due to our increased relocation cost parameter (Sect. 1.3), which disincentivizes retreat relative to protection. In contrast to the influence of relocation cost on adaptation type, little variance is observed in these percentages across pyCIAM's different socioeconomic scenarios. This high stability is seen even within individual segments' adaptation choices and suggests that particular choices of adaptation strategy (protection versus retreat) and the return value to which the chosen adaptation strategy is enacted may be robust to a range of future socioeconomic and SLR trajectories for most coastal regions. Similar results are shown normalized by coastline length rather than population in Fig. B2.

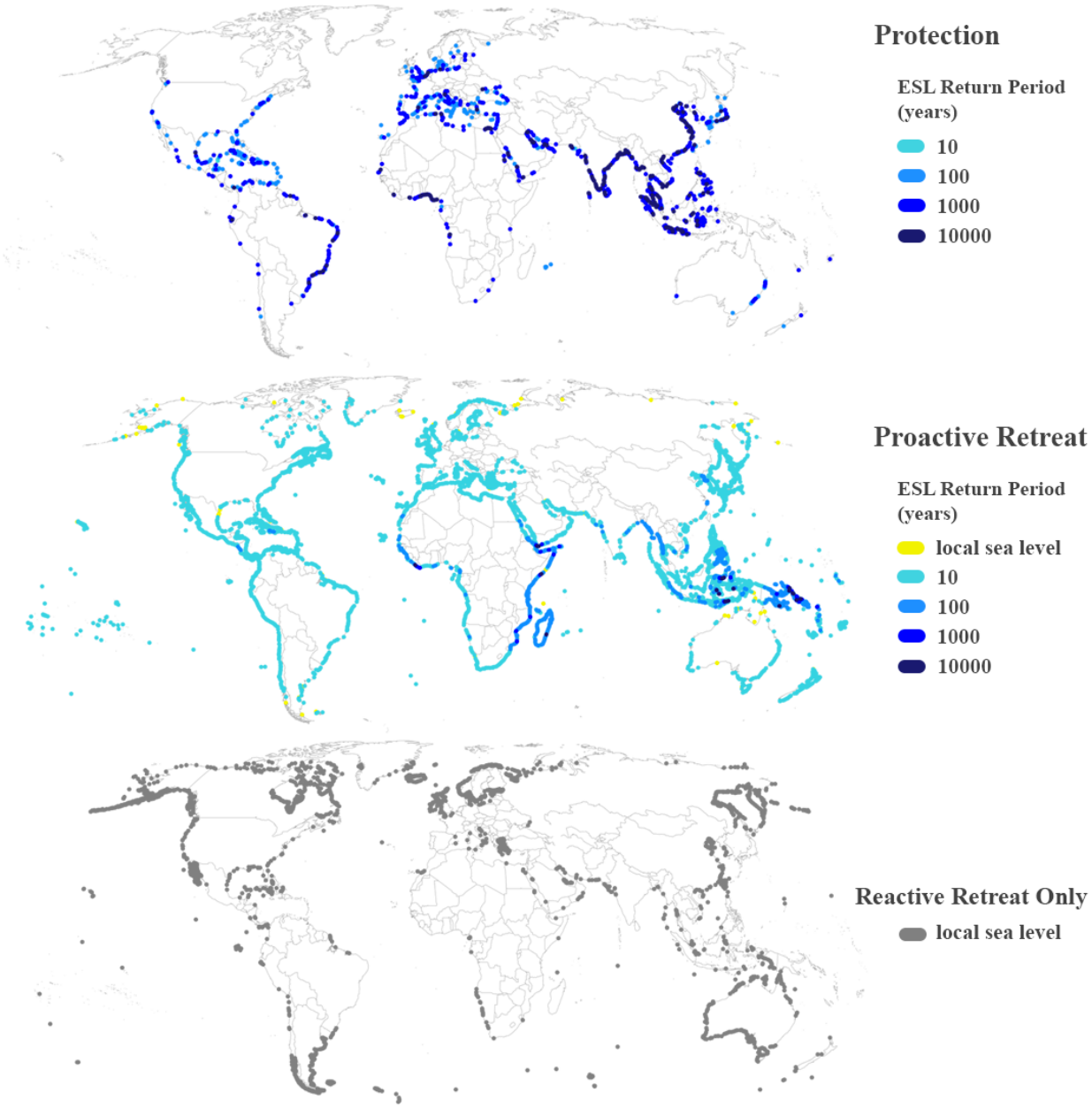

Figure 8. Adaptation strategies chosen by each segment in the optimal adaptation scenario. Results reflect the AR6 (medium confidence) SSP2-4.5 SLR scenario and SSP2 and IIASA socioeconomic growth projections.

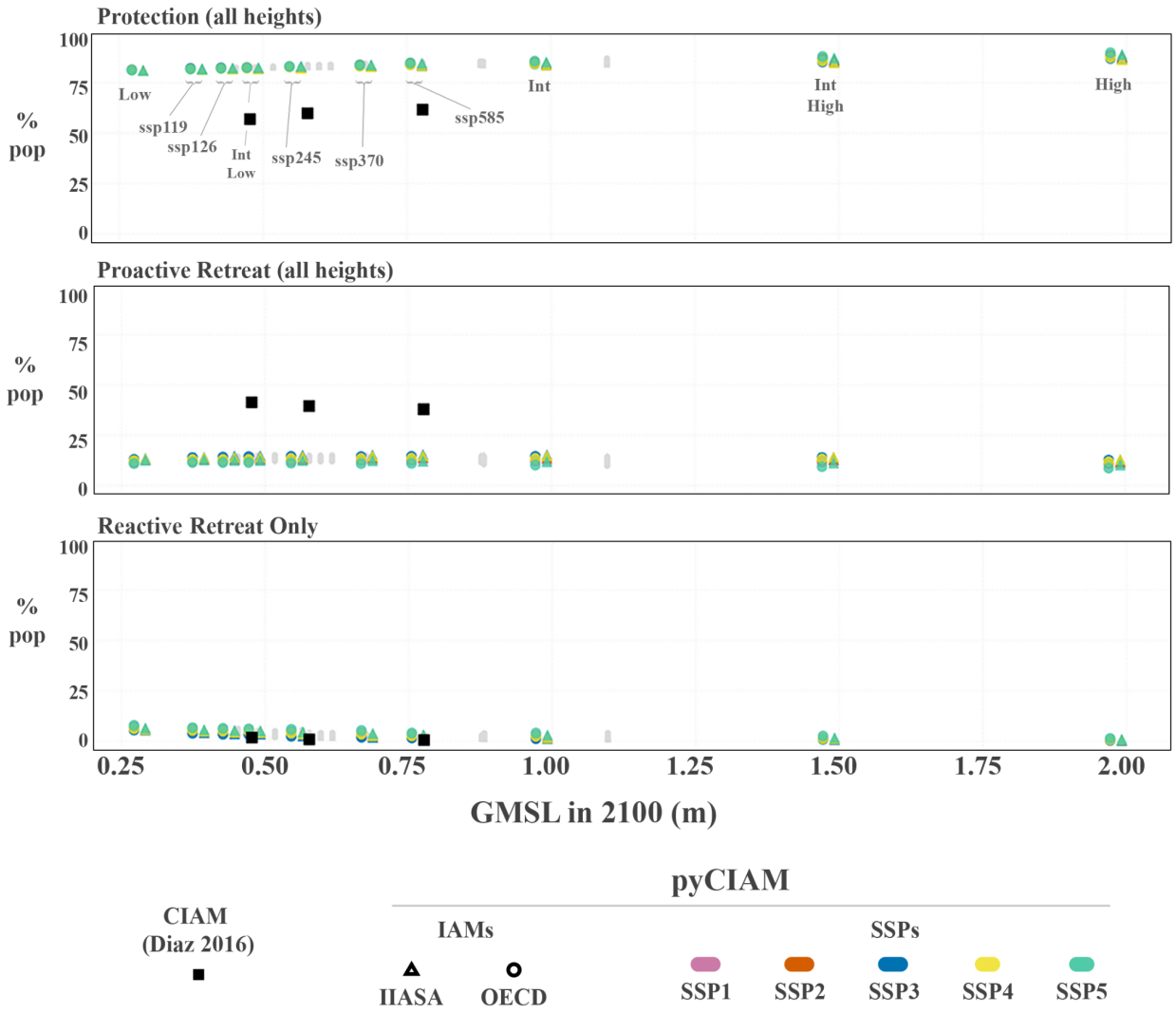

Figure 9. Comparison of optimal adaptation strategies adopted across all segments. Values represent percentages of global population residing at elevations below 15 meters in segments adopting each respective adaptation strategy. Proactive retreat and protection values are aggregates of all possible heights for each. Solid black squares represent the results from (Diaz, 2016). For visual clarity, only the medium confidence AR6 (ssp119, ssp126, ...) and W. Sweet et al. (2022) scenarios (Low, IntLow, ...) are indicated with colored markers, with the remaining SLR scenarios shown in grey and all scenario values are jittered based on runs using the OECD (-1cm) or IIASA (+1cm) economic growth model.

3.2.1 Global Coastal Retreat

In this section, we highlight the estimated relocation of populations from coastal segments inland throughout the modeling period. It is important to note that while the results and figures presented above reflect monetary costs associated with 'climate change-only' SLR projections, where the no-climate change baseline costs are differenced from the model totals, this section focuses on the total retreating population and associated cost estimates. The rationale for this is that it is preferable to identify how future inland human migration may manifest in the coming decades, irrespective of specific attributability to climate change-driven SLR.

Overall, pyCIAM estimates that 16.2-46.0 million people are projected to relocate inland by 2100 if optimal adaptation actions are employed, dependent on SLR, SSP and economic growth scenarios. However, under the scenario where the only adaptation strategy employed is reactive retreat (i.e. least optimal), these estimates increase to 28.2-204 million people. Table 5 presents estimated population relocation quantities, aggregated by World Bank regional units and averaged across SLR scenarios, within the 2° C, 4° C and high-end GMSL ranges. We see that under 2° C of warming by 2100, projected relocated population ranges from 24.6-48.3 million, depending on the degree of adaptation optimality adopted. Under 4° C of warming, this range increases to 28.8-68.1 million, and under the high-end SLR scenarios becomes 38.8-167 million.

The East Asia & Pacific region is predicted to have the highest retreat totals, ranging from 22.2-74.6 million people, depending on adaptation optimality, under the high-end GMSL scenario. However, the highest rates of retreat as a share of present-day (2019) coastal populations under high-end scenarios with sub-optimal adaptation are projected to occur in the Middle-East & North Africa (MENA) and Europe & Central Asia regions, with 18.5% and 17.3% of their present-day coastal populations projected to move inland by 2100, respectively. Other regions exhibit high shares of coastal population retreat under high-end, reactive adaptation only scenarios, with South Asia and Sub-Saharan Africa's shares projected as 15.7% and 14.9%, respectively.

However, most regions have a much lower projected share of relocated population if they choose to adapt optimally, as opposed to reactive retreat alone (e.g. 0.81% versus 18.5% in the MENA region). Two regions where these avoided-relocation adaptation gains are less substantial, however, are Sub-Saharan Africa and Latin America & the Caribbean, where relocation totals for optimal and least-optimal adaptation are much closer to one another than in other regions, suggesting that it may not be economical for these regions to build protective infrastructure under most scenarios, even when permitted to do so in the model.

It is also notable that estimated relocation totals under optimal adaptation are only mildly sensitive to magnitude of GMSL change by 2100, with retreat population only increasing from 24.6 to 38.8 million people (~60% increase) between the 2° C and high-end SLR scenarios, which represents a difference of roughly a full meter of GMSL by 2100. Without proactive adaptation, however, these estimates are much more sensitive to changes in GMSL, ranging from 48.3 million under 2° C to 167 million under high-end SLR (~250% increase). This is due to the fact that the primary optimal adaptation strategy for densely populated coastal segments is the construction of protection to minimize exposure to SLR and ESLs. However, when protective adaptation is not implemented, population centers are forced to move inland en masse as land is lost to permanent inundation. Table 6 provides a disaggregation of projected net present costs from 2005-2100 for each modeled cost-type.

Table 5. Modeled estimates of the number of people (in millions) living in coastal regions (elevations of 0-20m relative to 2005 MSL) that would retreat inland from 2005-2100. Totals are summed by the World Bank's 'regional units' and averaged by 2° C, 4° C and high-end SLR scenarios groups, under both optimal and reactive retreat-only adaptation. Parenthetical values indicate the percentages of these totals as percentages of each ADM1 region's total coastal population in 2019.

		Retreating Coastal Population (million), 2005-2100					
Region	**Coastal Pop. (2019)** ***(million)***	**2° C** ***(optimal)***	**2° C** ***(reactive)***	**4° C** ***(optimal)***	**4° C** ***(reactive)***	**High-end** ***(optimal)***	**High-end** ***(reactive)***
East Asia & Pacific	625.77	12.99 *(2.08%)*	17.00 *(2.72%)*	15.86 *(2.53%)*	26.35 *(4.21%)*	22.15 *(3.54%)*	74.61 *(11.9%)*
Europe & Central Asia	91.39	1.90 *(2.08%)*	8.35 *(9.13%)*	2.13 *(2.33%)*	10.34 *(11.3%)*	2.94 *(3.22%)*	15.81 *(17.3%)*
Latin America & Caribbean	89.88	2.87 *(3.19%)*	3.05 *(3.39%)*	3.27 *(3.63%)*	4.37 *(4.86%)*	4.52 *(5.03%)*	10.85 *(12.1%)*
Middle East & North Africa	66.12	0.32 *(0.49%)*	4.71 *(7.13%)*	0.39 *(0.59%)*	6.33 *(9.58%)*	0.54 *(0.81%)*	12.20 *(18.5%)*
North America	58.76	1.30 *(2.21%)*	2.36 *(4.02%)*	1.55 *(2.64%)*	3.01 *(5.12%)*	1.89 *(3.22%)*	4.78 *(8.13%)*
South Asia	233.47	0.99 *(0.42%)*	7.96 *(3.41%)*	1.16 *(0.50%)*	11.55 *(4.95%)*	1.33 *(0.57%)*	36.54 *(15.7%)*
Sub-Saharan Africa	80.48	4.19 *(5.20%)*	4.88 *(6.06%)*	4.40 *(5.47%)*	6.18 *(7.68%)*	5.39 *(6.70%)*	11.98 *(14.9%)*
Total	**1245.87**	**24.56** ***(1.97%)***	**48.31** ***(3.88%)***	**28.76** ***(2.31%)***	**68.13** ***(5.47%)***	**38.75** ***(3.11%)***	**166.76** ***(13.4%)***

In terms of net present costs, the higher magnitudes of retreating populations in least-optimal adaptation scenarios are associated with much higher relocation costs (~10x) as compared to those costs under optimal adaptation (Table 6). We also see that many more people are projected to be killed (reflected in 'storm mortality' costs) and the cost of permanently-inundated land loss much higher under reactive-only compared to optimal adaptation, due to the absence of protective barriers. That said, the NPV of wetland loss is estimated to be lower under suboptimal adaptation (roughly half compared to optimal) due to the fact that building protection is currently assumed to disconnect wetlands from the ocean and therefore render them destroyed, although wetland ecosystem processes are more complex than this representation. Cost of building protection is also inherently lower (i.e. zero) in the reactive retreat adaptation scenarios, compared to optimal, but our results indicate that the cost of building this infrastructure is worth the investment in order to avert much higher imparted costs in the face of SLR.

Table 6. Net present values (using a 4% discount rate) from 2005-2100 for each cost-type, averaged across SSPs and economic growth models within the 2° C, 4° C and high-end SLR scenarios groups under optimal and reactive retreat-only adaptation, corresponding scenario columns in Table 5.

	Global Net Present Value (Trillions, $2019), 2005-2100					
Cost Type	**2° C** ***(optimal)***	**2° C** ***(reactive)***	**4° C** ***(optimal)***	**4° C** ***(reactive)***	**High-end** ***(optimal)***	**High-end** ***(reactive)***
Relocation	2.04	20.7	2.11	20.8	2.37	21.7

Protection	3.81	0.0	3.99	0.0	4.60	0.0
Storm Mortality	0.36	3.12	0.34	4.84	0.31	14.3
Storm Capital Damage	0.10	0.34	0.10	0.64	0.11	3.69
Permanent Inundation	1.03	14.7	1.04	14.7	1.07	15.0
Wetland Loss	0.37	0.15	0.39	0.17	0.46	0.22
Total	**7.71**	**39.0**	**7.96**	**41.1**	**8.92**	**55.0**

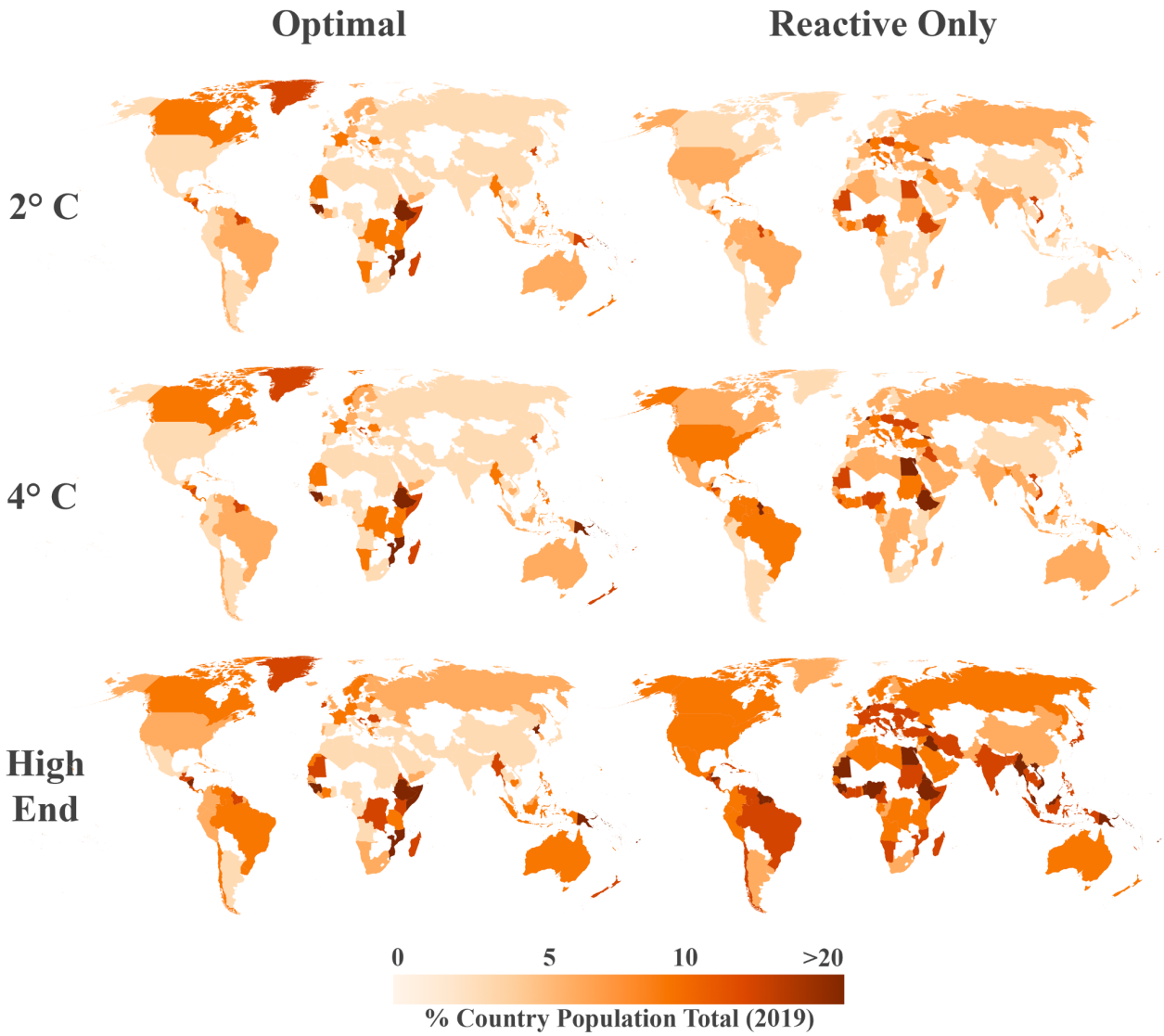

Figure 10. Global map of populations, expressed as percentages of country population totals in 2019, that are estimated to retreat inland by 2100, averaged across SSPs and economic growth models within the 2° C, 4° C and high-end SLR projection groups under optimal and reactive retreat-only adaptation.

3.3 Model Limitations and Planned Improvements

pyCIAM is subject to some of the same limitations as its predecessor CIAM. First, adaptation is limited to the ten possible options introduced in (Diaz, 2016) - four protection heights, five proactive retreat heights and a reactive retreat action. Second, segments are only allowed one protection or retreat standard throughout the model duration. They cannot, for example, retreat to the 1-in-10 year ESL height for the first 20 years and then retreat to the 1-in-100 year height. Rather a single optimal standard is chosen given the full distribution of potential future outcomes. Similarly, segments cannot combine both retreat and protection. More flexible approaches may enable lower-cost outcomes (Kopp et al., 2019; Haasnoot et al., 2019), though computational constraints have limited the implementation of more dynamic adaptation approaches to models with local domains (Lickley et al., 2014). A preliminary approach to this problem, such as allowing for a one time, mid-century alteration of adaptation strategies, could be a simple scheme to allow for some level of dynamic adaptation strategies. Third, insurance, subsidies or other policies may discourage proactive retreat even when the NPV would be positive, and these interventions are not taken into account by segment agents in the model when determining the least cost adaptation path. Fourth, many cost functions and parameters in the model are based on limited empirical evidence, as little evidence at fine resolution and global scale is available to inform the magnitude and heterogeneity of these costs.

Existing coastal protections are not directly modeled due to a lack of globally consistent data. Instead, existing protections are assigned in the model like those of any other year based on the least cost adaptation scenario for each segment. This means that protection costs in the initial year of the model will include the cost of constructing these existing structures, though these additional costs will be differenced out of our climate impact estimates because they will occur in both the “with climate change” and “no climate change” SLR trajectories.

Retreat or protection heights within each decadal planning period are chosen under perfect foresight of projected RSLR at that segment during the entire period, such that any maximum projected change in ESL return values due to RSLR is perfectly anticipated and incorporated into adaptation cost considerations and decisions. Notably, segments also chose their optimal adaptation strategy (e.g. protection to the 1-in-100 year ESL height) based on an NPV calculation that utilizes perfect foresight over the entire model duration. While this assumption cannot be correct in its extreme form, Fig. 9 suggests that these choices are very robust to uncertainty in future sea level and socioeconomic change.

pyCIAM also does not currently represent accommodation measures (e.g., infrastructure hardening and building elevation), which in some cases may be more cost-effective than either protection or retreat (Oppenheimer et al., 2019; Kopp et al., 2019; Rasmussen et al., 2020). Accommodation encompasses a broad range of actions and is thus difficult to parameterize within the model. To our knowledge, accommodation is not represented in other coastal modeling platforms but could be the subject of future updates to pyCIAM. Additionally, the potential changing feasibility of both adaptation and accommodation measures in future decades, due to potential factors unrelated to climate change, like shifting supply chain and/or labor

market dynamics, are not currently represented. These may prove to be relevant to society's capacity to effectively adapt in the future.

Our current estimation of the non-market costs of relocation detailed in Sect. 1.3 is intended to represent the fact that many coastal areas are observed to currently be under-adapted to present ESL hazards (Houser et al., 2015; McNamara and Keeler, 2013; McNamara et al., 2015; Armstrong et al., 2016; Haer et al., 2017; Hinkel et al., 2018; Suckall et al., 2018; Lorie et al., 2020). However, improved estimates of these non-market relocation costs could potentially be guided by more detailed empirical assessments of present-day under-adaptation to coastal hazards. Other forms of adaptation-related behavioral "inertia" preventing or delaying economically rational action may exist as well. Mendelsohn et al., (2020) estimated the cost-benefit ratio of building seawalls to be at least 2:1 in East Haven, CT, estimates this ratio for elevating coastal homes up to 9:1 in some U.S. locations, and Bakkensen and Mendelsohn, (2016) found that the U.S., in particular, may be up to 14x less adapted to tropical cyclone hazards than other OECD countries threats presently. While some of this under-adaptation is rationalized by our non-market costs of relocation, other factors including challenges of permitting and funding costly infrastructure projects, subsidized insurance (Craig, 2019) or limited risk information may play a role as well. We are aware of efforts to further understand adaptation costs and the reasons for under-adaptation (Bower and Weerasinghe, 2021; Berrang-Ford et al., 2021), but the current extent of empirical evidence quantifying sub-optimal adaptation is limited. If and when such evidence is available, the modularity of pyCIAM enables future integration of these estimates to improve its adaptation cost-benefit implementation.

Better global data describing existing coastal protection infrastructure would improve the accuracy of pyCIAM. Spatially resolved data on constructed protection around the globe is sparse. To overcome this, some studies assume a certain level of protection as being present in all coastal regions, making stylized assumptions based on population densities and national GDP (Sadoff et al., 2015). Other studies develop statistical models to empirically ground such relationships (Scussolini et al., 2016), and these have been incorporated in other global coastal adaptation models (Tiggeloven et al., 2020) and could be evaluated for use in future versions of pyCIAM. Further improvements to certain regions could also be made using protection data collected by Hallegatte et al. (2013) for 136 coastal cities.

Our reflection of local mean and extreme sea levels is limited by the resolution of our local MSL projections (1 degree in FACTS, 2 degrees in LocalizeSL) and our ESL distributions from CoDEC (50km coastline spacing). Because of the desire to build a globally consistent model using these inputs, we employ a "local bathtub" model in which all points nearest to a given pair of ESL and MSL prediction points receive the same mean and extreme sea level projections. While this local model preserves the substantial large-scale spatial heterogeneity in SLR and ESL, sub-grid-scale variation is ignored. In particular, bathtub models are known to overestimate storm surge in inland areas largely due to the deceleration of flows caused by surface roughness (Bootsma, 2022; Vousdoukas et al., 2016). A more sophisticated, dynamic representation of ESL based on local hydrodynamic simulations for each MSL/ESL combination is beyond the computational scope of this analysis but may yield improved future results and could be incorporated either "on-the-fly" within the pyCIAM model or in a pre-processing step that updates the ESL distributions in SLIIDERS.

Such an approach would also address a second limitation in our local sea level estimation. By linearly combining present-day ESL estimates and SLR predictions, our current approach ignore changing ESL distributions due to (a) climate-driven changes to storm surge distributions from, for example, altered tropical cyclone patterns; and (b) the dynamic interaction between storm surge and MSL, moderated by local topography.

Despite these limitations in estimating sea levels, it is important to note that when isolating climate change-induced coastal costs, we difference the costs of a no-climate change baseline scenario that uses the same local bathtub flood model. This differencing also serves as a bias correction step, partially mitigating any over-estimates of flooding damages potentially introduced by the bathtub approach, though some high or low bias may still be present in the final results. Total (un-differenced) cost estimates (Fig. 9), however, will reflect any bias associated with the bathtub flood model.

Finally, additional geophysical dynamics associated with SLR inundation and related flooding, such as erosion, salinization of aquifers and estuaries, are also not currently addressed in our approach.

4 - Conclusion

Modeling the social and economic impact of future sea level rise can inform our understanding of costs in different climate change mitigation scenarios and support the analysis of adaptation policies. To construct global estimates, modelers face the dual challenge of developing a global approach capable of representing the detailed local information relevant to accurately estimating SLR impacts and adaptation. Prior modeling studies have developed frameworks for conducting such analyses; however, continued iteration of these data and models is necessary in order to improve the accuracy and precision of projections and to keep pace with relevant advancements in data, modeling, and computing. Achieving this through community-wide collaboration requires a collection of open-source and transparent datasets as well as modeling tools.

This paper has summarized improvements to the quality and accessibility of both coastal impact data products and related modeling platforms. The Sea Level Impacts Input Dataset by Elevation, Region and Scenarios (SLIIDERS) represents a globally comprehensive and consistent collection of physical, ecological and socioeconomic variables for roughly 10,000 coastal localities. SLIIDERS is a segment-wise data product for coastal impacts, similar to previous products like DIVA (Vafeidis et al., 2008), but with significant improvements to the quality of represented variables. It is available as an open-source resource following FAIR guidelines (Wilkinson et al., 2016). Any researcher can download, inspect and alter SLIIDERS to utilize in their own coastal modeling studies.

The Python-Coastal Impacts and Adaptation Model (pyCIAM), a companion model that utilizes SLIIDERS as an input, was developed as an open-source update to the original Coastal Impacts and Adaptation Model Diaz (2016) and incorporates numerous improvements to model functionality and efficiency. pyCIAM is also made available as a modular, open-source tool meant to be modified by users seeking to add functionality or improve input sources, with users able to combine the model with their own input datasets, provided they are formatted similarly to SLIIDERS. An additional key advance of pyCIAM is that it is designed to simulate impacts from

tens to hundreds of thousands of future SLR scenarios in parallel, facilitating scalable probabilisitic impact modeling research.

Results from pyCIAM v1.1, paired with SLIIDERS v1.1, show the model produces roughly similar estimates of the global net present cost of SLR to those of CIAM (Diaz, 2016) under the SSP5 socioeconomic scenario, with all other SSP-economic growth model configurations producing slightly smaller values (Fig. 4). Median annual, end of century costs under optimal adaptation in pyCIAM are also very similar to CIAM when averaging across all SSPs and growth models. When prohibiting proactive adaptation, costs are higher in pyCIAM for almost all scenarios as compared to CIAM. However, when comparing total yearly coastal damages, rather than just the climate-driven component, pyCIAM projects global NPV of all coastal damages between 2000-2100 to be roughly 3-4 those of CIAM (Fig. B1), likely due to greater population and capital stock estimates in these SSPs as compared to the trajectories used in Diaz (2016). The median annual, end of century total costs under optimal adaptation in pyCIAM are also higher than CIAM for all scenarios, with only the SSP4-IIASA scenario producing similar values.

Despite the improvements represented by the SLIIDERS data product and pyCIAM platform, there are aspects of them that should be improved in the future. We believe that a priority for future work should be to incorporate empirical evidence on coastal damages and adaptation behavior due to rising and extreme sea levels in order to better inform model assumptions. We hope that improvements to SLIIDERS can be made regularly as new, higher quality data sources for each of its constituent variables are made available. Additionally, the segmentation of coastlines in SLIIDERS v1.1 can likely be improved beyond a uniform (50km) spacing nested at the country level to better delineate between coastal regions that are more likely to represent autonomous, decision making units, such as extents of coastal urban centers. We intend to make many of these improvements moving forward, and will make updated versions available as such efforts are carried out. However, our hope is that the open-source nature of both SLIIDERS and pyCIAM will enable community-driven development to spur more rapid and substantial improvements to both tools.

Code and data availability

Version 1.1 of SLIIDERS, is associated with the results presented in this manuscript. These two datasets, along with the code to create them and the pyCIAM source code, are available at https://doi.org/10.5281/zenodo.6449231. Code to create SLIIDERS is also available at https://github.com/ClimateImpactLab/sliiders, and the 1.1 release corresponds to the version used in this manuscript (and uploaded at the aforementioned Zenodo link). Similarly, the pyCIAM source code is available at https://github.com/ClimateImpactLab/pyCIAM, with release 1.1 again corresponding to this manuscript. pyCIAM is also available on PyPI as the python-CIAM package. Scripts and notebooks associated with running pyCIAM and creating the results contained in this manuscript are also included in the pyCIAM GitHub repository and the Zenodo repository.

Author contributions

Project conceptualized by IB, SH, REK. Data curation by DA, IB, JC, ND, AH. Methodology development, investigation, and formal analysis conducted by DA, IB, JC, ND. Map and figure visualizations were done by ND. Code base developed by DA, 940 IB, JC, ND. Software developed by DA, IB, JC and ND. Model validation performed by IB and ND. Project administered by IB, ND, SH. Original draft written by IB, JC, DA, ND. Manuscript review and editing by DA, IB, JC, ND, SH, REK, MG. Funding acquisition by MG, SH, TH, REK. Supervision by MD, MG, SH, REK.

Acknowledgements

We thank Maya Norman for conducting her review and evaluation of relevant exposure datasets. Thank you also to Delavane Diaz, who contributed invaluable assistance in the access and interpretation of the CIAM model. We also thank members of the Climate Impact Lab who provided important feedback and guidance during frequent discussions about model objectives and developments. This project is an output of the Climate Impact Lab that gratefully acknowledges funding from the Energy Policy Institute of Chicago (EPIC), International Growth Centre, National Science Foundation (ICER-1663807), Sloan Foundation, Carnegie Corporation, and Tata Center for Development.

Appendix A: Supplemental Information

A1 - Coastlines Creation and Length Calculation

To create each segment represented in SLIIDERS and used in pyCIAM, we assembled a set of polylines according to the following steps[10]:

1. Downloaded highly-resolved 1:10m Natural Earth Coastlines (www.naturalearthdata.com/downloads/), which were used for all segments
2. Removed Caspian Sea borders from both coastline layers to avoid modeling along this inland sea.
3. Removed all line segments south of 60S (Antarctica) from both coastline layers to avoid inclusion of these coastlines in any final coastal segments, due to the lack of population and capital exposure any latitudes below 60S.
4. Converted coastlines layers to polygons in order to get land areas that correspond to the 1:10m scale coastline resolutions.
5. Intersected resulting polygon layer of land masses with exposure grid of population and capital assets, and removed land masses that contained no capital or population exposure. In these completely unpopulated areas, we cannot accurately represent value of lost land within the pyCIAM framework, nor is this value likely to be large.
6. Converted this 1:10m land area polygon layer back to polylines for use as our final vector layer of global coastlines.

[10] Steps 2-6 and 8 used the Quantum Geographical Information Systems (QGIS) v3.16 software.

7. Constructed a set of Voronoi polygons from the CoDEC-derived coastal segment centroids and intersected these with the coastlines layer constructed in Steps 1-8. This partitioned coastlines according to segment, allowing for the calculation of the total length (in kilometers) of coastline by coastal segment.

A2 - Aligning geographic and socioeconomic datasets to build SLIIDERS

Socioeconomic variables expressed in SLIIDERS and used in pyCIAM are defined at various geographic aggregation levels, from the fine “elevation bin by admin-1 region” scale to the coarse country scale. Input data sources also come in various formats, from gridded estimates of coastal elevation, population and capital distribution, and wetland area, to country-level SSP-based projections of income, population, and capital growth trajectories, to vector representations of country boundaries and coastlines. To create SLIIDERS, we must harmonize these various input sources. We start by assigning admin-1 and country labels to each grid cell in the gridded elevation and exposure input sources, using boundaries from GADM v3.6. Notably, GADM considers as a "country" any region with an ISO country code, regardless of sovereignty.

There are 199 such countries that are coastal and contain non-zero land under 20 m elevation. The boundaries of the admin-1 regions within these 199 countries are overlaid on gridded elevation and exposure datasets, including those defining spatial distributions of population (LandScan 2021) and physical capital (LitPop and GEG-15), to assign elevations and admin-1 labels to each grid cell. The gridded dryland and wetland area, population, and physical capital estimates are then binned by 10 cm elevation increments and grouped within admin-1 regions and coastal segments. Each admin-1 region is then assigned its corresponding country label, which is matched to the SSP-based country-level growth trajectories.

A3 - Imputing initial-year (2010) capital stock values

Out of the 199 countries included in SLIIDERS, 146 have capital stock values in 2010 in PWT 10.0 that we use as initial conditions for projecting capital stock consistent with the SSPs. We must impute the 53 remaining values; while only 2010 values are needed to seed the capital growth model, we take an approach that allows for simultaneous estimation of a time series of capital stock beginning in 1950. This approach generates estimates of historical capital consistent with those of other ongoing work. Our estimation process consists of the following steps:

1. We impute any missing historical GDP estimates from 1950-2020 (Sect. 4.3.1) within our aggregation of GDP data sources (Sect. 1.6.2).
2. We estimate the relationship between historical investment-to-GDP ratio, income, and population share values, and impute historical investment, following (Higgins, 1998) (Sect 4.3.2).
3. For the countries with 2005 capital stock estimates in GEG-15 (Bono and Chatenoux, 2014) and 2014 estimates in LitPop (Eberenz et al., 2020), but with no estimates in PWT 10.0, we exponentially interpolate to 2010.

4. For the remaining countries with 2005 estimates in GEG-15 but no 2014 estimates in LitPop, we use the perpetual inventory method with historical investment estimates from Step 2 to estimate 2010 capital stock.
5. For the remaining countries with 2014 estimates in LitPop but no 2005 estimates in GEG-15 or PWT 10.0, we first estimate the 1950 capital stock values following (Inklaar et al., 2019) using the actual and estimated GDP and investment-to-GDP ratio. Then, we exponentially interpolate to 2010.
6. For the final set of countries with no capital stock estimates in any of these three sources, we follow (Eberenz et al., 2020) and estimate the 2014 capital stock values by multiplying GDP estimates by a capital-to-GDP ratio of 1.24724 from (Credit Suisse Research Institute, 2017). Then, we follow Step 5 to obtain 2010 estimates.

In the parts below, we describe the processes for imputing missing historical GDP and income values, historical investment-to-GDP ratios, and missing capital depreciation rates, and for estimating the missing 1950 capital stock values.

A3.1 - Imputing missing historical (1950-2020) GDP

The capital stock imputation described above relies, in some cases, on a complete time series of GDP. While this exists for many countries after aggregating across the multiple data sources described in Sect 1.6.2, some countries and territories are missing observations for some of this time series. For territories, whose growth often converges to that of the corresponding sovereign state (Bertram 2004), we impute GDP in missing years using the average ratio of the territory's GDP to that of the sovereign state during non-missing years. For other cases, we find five "nearest" countries, such that the sum of squared differences of yearly GDP growth rates to that of the target country are minimized across all non-missing years. We then impute the growth rates for missing years using a weighted average of these five end members, weighted by the inverse of the SSEs, and interpolate/extrapolate around non-missing observation using these growth rates.

A3.2 - Imputing missing historical (1950-2020) investment-to-GDP ratios

Investment-to-GDP ratios are imputed via a regression across non-missing years of this ratio on per capita GDP levels and growth rates as well as population age distributions. The regression used is borrowed from Foure et al., (2012) and adjusted , AIC, and BIC are compared across models with and without the age distribution variables. The model that includes those variables performs better and thus we use that model for the necessary imputations. See the code repository that accompanies this manuscript for further details on method and for a summary of regression results.

A3.3 - Imputing missing capital depreciation rates

We use PWT 10.0 as our main source for historical capital depreciation rates. However, many of the countries considered in our workflow are either not included in PWT 10.0, or they are included but are missing values for certain years. In these cases, we impute the depreciation rate

of each country each year by taking an unweighted average of the available depreciation rates across all countries and years. To project future capital depreciation for each country, necessary to project future capital stock levels, we simply extend our estimates of 2010 capital depreciation rates to all future years. The projection method described in Dellink et al., (2017) also requires a global capital depreciation rate used when deriving long-run investment-to-GDP ratios, for which we use the 2010 global average depreciation rate in PWT 10.0, which is approximately 4.416%, comparable to the 5% global depreciation rate used in (Dellink et al., 2017).

A3.4 - Imputing 1950 capital stock

We follow the method used in PWT 10.0 (Inklaar et al., 2019) to estimate capital stock in 1950 where needed for imputation, using GDP and investment-to-GDP ratios estimated from the data sources compiled in Sect. 1.6.2 and imputed via the previously described approaches. We update the bounds and annual increment of capital intensity (a.k.a. capital-to-GDP ratio) used in the algorithm based on the compiled data. Inklaar et al. (2019) sets bounds of [0.5, 4.0] and an annual increment of 0.02; however, capital intensities and their increments vary greatly across countries. Thus, we apply a -means clustering analysis of the 2014-2020 capital intensity values to classify countries into three groups based on their capital intensity values and growth rates. As a result, we use the following triples of lower bound, upper bound, and annual increment of capital intensity for each cluster: (0.861, 3.902, 0.014), (1.810, 6.298, 0.037), and (2.616, 13.853, 0.166). Note that as opposed to using minimum and maximum values as the lower and upper capital intensity bounds as in (Inklaar et al., 2019), we use bottom and top decile within each cluster due to heavy tailed distributions of capital intensity in PWT 10.0.

A4 - Projecting SSP-consistent (2010-2100) capital stock values

Using actual and imputed historical 2010 country-level capital stocks as initial conditions, we extract the capital portion of the OECD Env-Growth model (Dellink et al., 2017) and apply it to the SSP trajectories of GDP and population. The model requires global GDP elasticity of capital and 2010 country-level marginal products of capital (MPK), which are not described in (Dellink et al., 2017). We use a global GDP elasticity of capital of 0.326 from Crespo Cuaresma (2017) and estimate 2010 MPKs using a modified Cobb-Douglas production function that contains only capital inputs. Coefficients of the function are derived by fitting to the compiled dataset of historical GDP and capital. Alternative approaches for obtaining these necessary inputs, including the use of a production function with labor and capital inputs and deriving the global elasticity directly from the production function, were also evaluated; however, these approaches yielded greater discrepancies in projected capital stocks when compared with the limited set of results presented in (Dellink et al., 2017).

Appendix B: Supplemental Figures

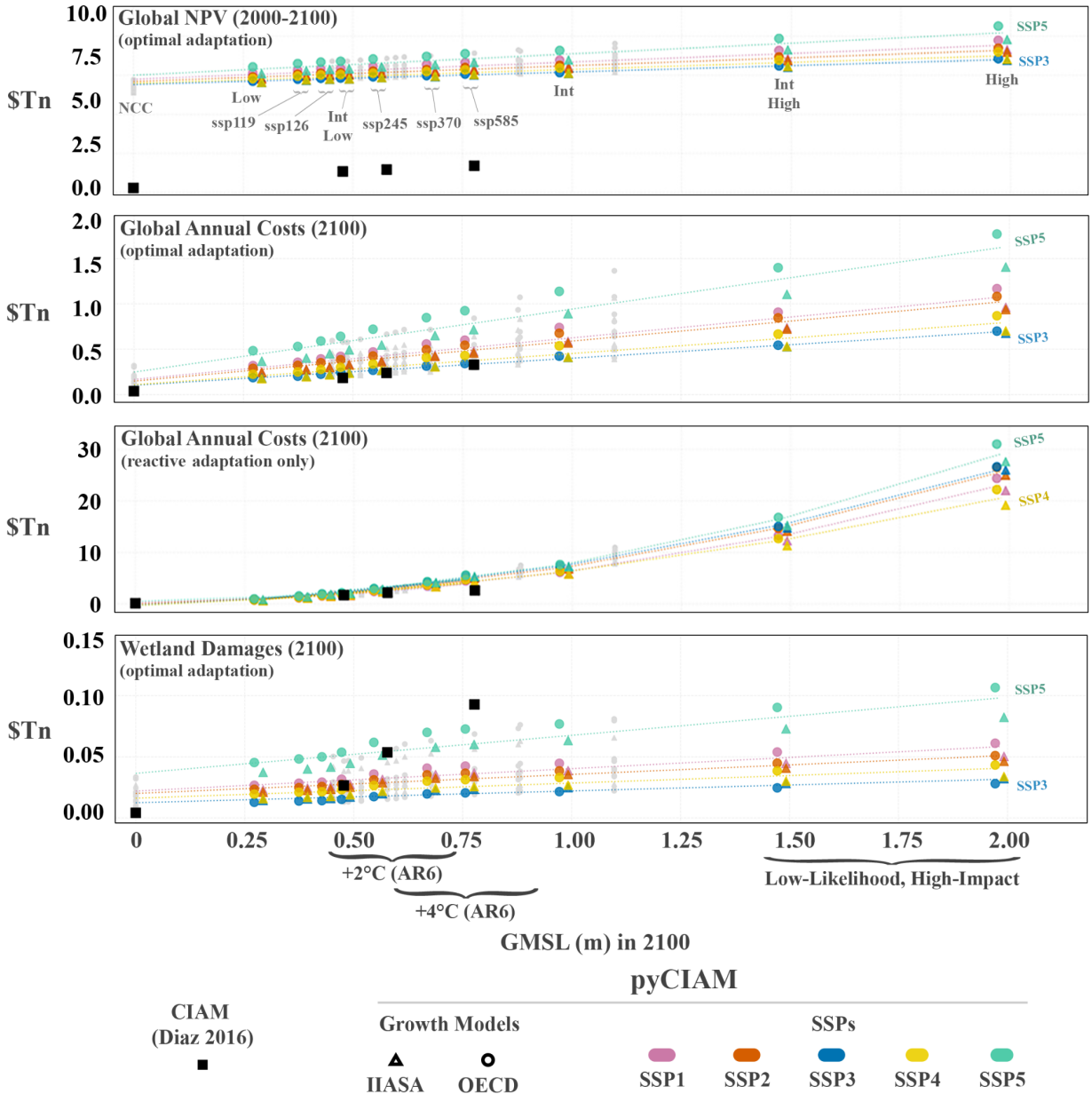

Figure B1. Comparison of global cost metrics for median model results under each SLR scenario. Values are total coastal losses (inclusive of hazards not attributable to climate change), expressed in constant 2019 PPP USD. Each vertical group of points is a single SLR scenario, with each point in the group representing a unique combination of SSP-economic growth model. Differencing values associated with 0 GMSL rise from the other values yields Fig. 4. For visual clarity, only medium confidence AR6 (ssp119, ssp126, ...) and W. Sweet et al. (2022) scenarios (Low, IntLow, ...) are indicated with colored markers and jittered based on runs using the OECD (-1cm) or IIASA (+1cm) economic growth model, with the remaining SLR scenarios shown in grey without jitter.

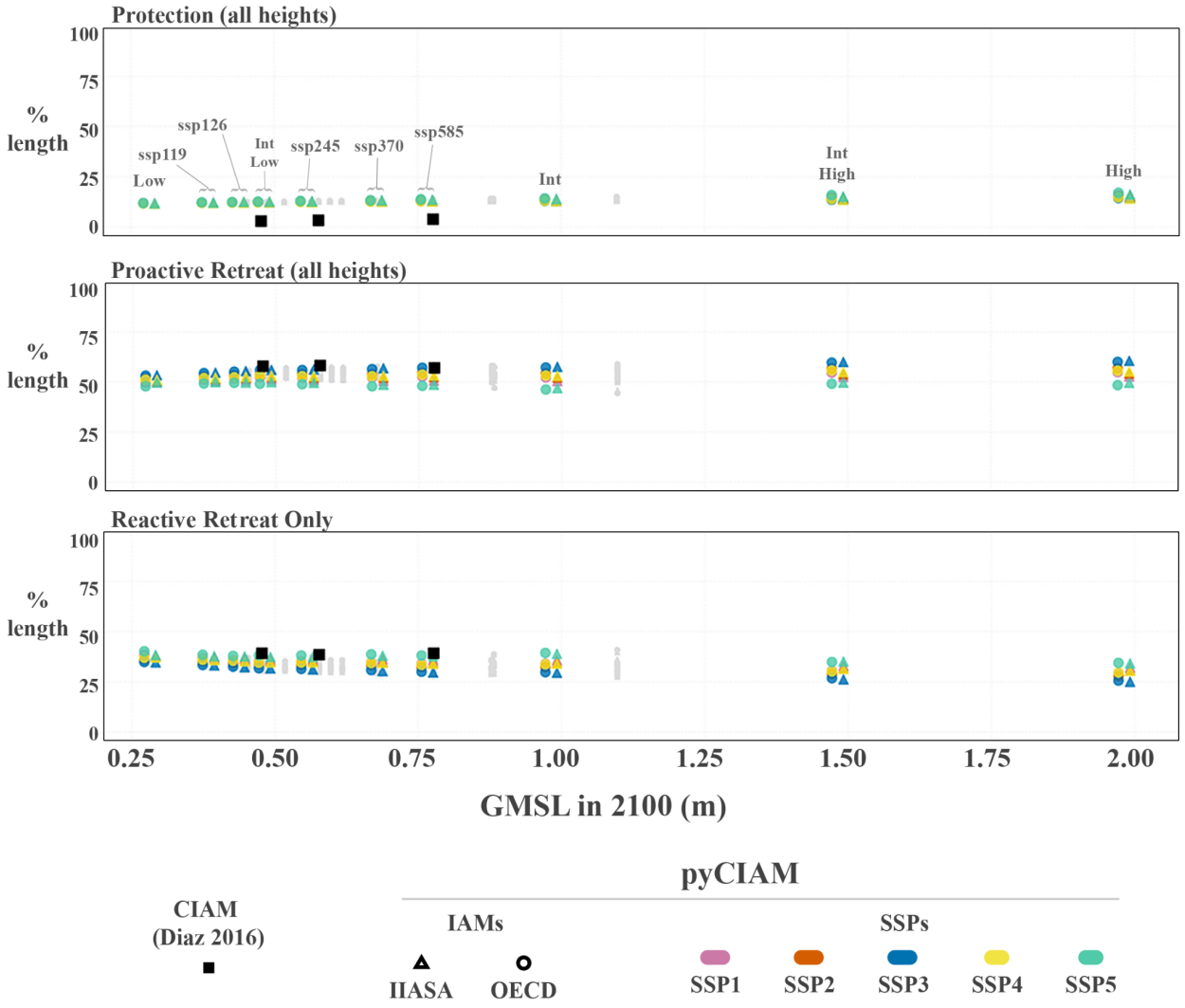

Figure B2. Comparison of optimal adaptation strategies adopted across all segments. Values represent percentages of global coastline associated with segments adopting each respective adaptation strategy. Proactive retreat and protection values are aggregates of all possible heights for each. Solid black squares represent the results from (Diaz, 2016) and the colored circle and triangle markers represent pyCIAM/SLIIDERS results for all SLR (differentiated by GMSL values), SSP and economic growth model. For visual clarity, only the medium confidence AR6 (ssp119, ssp126, ...) and Sweet et al. (2022) scenarios (Low, IntLow, ...) are indicated with colored markers, with the remaining SLR scenarios shown in grey and all scenario values are jittered based on runs using the OECD (-1cm) or IIASA (+1cm) economic growth model.

Appendix C: Supplemental Tables

Table C1. GMSL rise between 2005 and 2100 for each 17th-percentile SLR scenario used in the pyCIAM and Diaz (2016) models, representing the x-axis positions of costs by scenario displayed in Fig. 4.

ID	SLR Scenario	Model Used	GMSL in 2100 [m] (17th-percentile)

NCC	No Climate Change*	CIAM, pyCIAM	0.00
AR6-Med	IPCC AR6 *Medium Confidence* (2021) (SSP1-1.9, SSP1-2.6, SSP2-4.5, SSP3-7.0, SSP5-8.5)	pyCIAM	0.28, 0.32, 0.44, 0.55, 0.63
AR6-Low	IPCC AR6 *Low Confidence* (2021) (SSP1-2.6, SSP2-4.5, SSP5-8.5)	pyCIAM	0.32, 0.44, 0.63
NOAA	US Inter-agency SLR Technical Report (2022) (Low, Int-Low, Int, Int-High, High)	pyCIAM	0.28, 0.48, 0.98, 1.47, 1.95
K14	Kopp et al. (2014) (RCP 2.6, RCP 4.5, RCP 8.5)	CIAM, pyCIAM	0.35, 0.43, 0.61
SR	IPCC-SROCC (2019) (RCP 2.6, RCP 4.5, RCP 8.5)	pyCIAM	0.39, 0.48, 0.71
B19	Bamber et al. (2019) (Low, High)	pyCIAM	0.48, 0.79
D21	DeConto et al. (2021) (RCP 2.6, RCP 4.5, RCP 8.5)	pyCIAM	0.43, 0.52, 0.90

**Includes local background rates of relative sea level rise at each segment due to non-climatic background processes.*

Table C2. GMSL rise between 2005 and 2100 for each 83rd-percentile SLR scenario used in the pyCIAM and Diaz (2016) models, representing the x-axis positions of costs by scenario displayed in Fig. 4.

ID	**SLR Scenario**	**Model Used**	**GMSL in 2100 [m] (83rd-percentile)**
NCC	No Climate Change*	CIAM, pyCIAM	0.00
AR6-Med	IPCC AR6 *Medium Confidence* (2021) (SSP1-1.9, SSP1-2.6, SSP2-4.5, SSP3-7.0, SSP5-8.5)	pyCIAM	0.55, 0.61, 0.76, 0.90, 1.02
AR6-Low	IPCC AR6 *Low Confidence* (2021) (SSP1-2.6, SSP2-4.5, SSP5-8.5)	pyCIAM	0.79, 0.88, 1.61

NOAA	US Inter-agency SLR Technical Report (2022) (Low, Int-Low, Int, Int-High, High)	pyCIAM	0.29, 0.49, 0.99, 1.50, 2.02
K14	Kopp et al. (2014) (RCP 2.6, RCP 4.5, RCP 8.5)	CIAM, pyCIAM	0.65, 0.76, 1.00
SR	IPCC-SROCC (2019) (RCP 2.6, RCP 4.5, RCP 8.5)	pyCIAM	0.60, 0.76, 1.11
B19	Bamber et al. (2019) (Low, High)	pyCIAM	0.96, 1.71
D21	DeConto et al. (2021) (RCP 2.6, RCP 4.5, RCP 8.5)	pyCIAM	0.61, 0.74, 1.32

**Includes local background rates of relative sea level rise at each segment due to non-climatic background processes.*

NPV (2005-2100) *($Trillion)*	**CIAM median SLR** *(min-max)*	**pyCIAM median SLR** *(min-max)*	**pyCIAM 17th-percentile SLR** *(min-max)*	**pyCIAM 83rd-percentile SLR** *(min-max)*
Optimal Adaptation	1.05-1.42	0.606-3.45	0.363-2.70	0.802-3.94
Reactive Adaptation Only	6.84-9.70	1.13-29.9	0.533-17.2	2.69-44.2

Table C3. Range of net present costs of climate-driven SLR from 2005 to 2100 in constant 2019 PPP USD across all 230 socioeconomic and SLR scenarios. Minimum and maximum NPV values are shown for the fully updated pyCIAM model, as well as CIAM as configured in Diaz (2016).

Annual Costs in 2100 *($Trillion)*	**CIAM median SLR** *(min-max)*	**pyCIAM median SLR** *(min-max)*	**pyCIAM 17th-percentile SLR** *(min-max)*	**pyCIAM 83rd-percentile SLR** *(min-max)*
Optimal Adaptation	0.146-0.293	0.070-1.46	0.035-1.49	0.078-1.46
Reactive Adaptation Only	1.58-2.50	0.458-30.6	0.166-24.4	1.36-36.7

Table C4. Range of end-of-century average annual costs of climate-driven SLR in the year 2100 in constant 2019 PPP USD across all 230 socioeconomic and SLR scenarios. Minimum and maximum values are shown for the fully updated pyCIAM model, as well as CIAM as configured in Diaz (2016).

Table C5. Summary of SLIIDERS datasets and pyCIAM inputs for physical variables.

Input Dataset	**Source & Description**	**DOI**
Coastal Segments	CoDEC, Natural Earth (Muis et al., 2020) Thinned European coastal points in CoDEC from 10km spacing to 50km and made 15 manual additions to ensure all countries contain at least one segment. Coastline shapes were taken from Natural Earth (1:10m).	10.5281/zenodo.3660927 (Unaltered CoDEC)
Extreme sea levels (ESLs)	CoDEC (Muis et al., 2020) ESL values in CoDEC are calculated from the Global Tide and Surge Model (GTSMv3.0)	10.5281/zenodo.3660927 (Unaltered CoDEC)
Elevation	CoastalDEM v1.1 (Scott A. Kulp and Strauss 2019) Corrects significant high bias of coastal elevations found in previous DEMs (e.g. SRTM) SRTM15+ v2.3 (Tozer et al., 2019) Global topography and bathymetry at 15 arc-second resolution. Used wherever CoastalDEM is undefined MDT Global CNES-CLS18 (Mulet et al., 2021) Mean dynamic topography at resolution XGM2019e (Zingerle et al., 2020) Experimental gravity field model at 2 arc-minute resolution	10.1038/s41467-019-12808-z 10.1029/2019EA000658 10.5194/os-17-789-2021 10.1007/s00190-020-01398-0
Wetland and Mangrove Extent	GLOBCOVER v2.3 (European Space Agency and UCLouvain 2010) (wetlands) Global Mangrove Watch 2016 (Bunting et al., 2018) (mangroves)	N/A 10.3390/rs1010669

Sea level rise projections	LocalizeSL (projections corresponding to Kopp et al., 2014; Bamber et al., 2019; Oppenheimer et al., 2019; DeConto et al., 2021)] Localized probabilistic estimates of global SLR at each coastal segment conditional on a certain level of global SLR in a certain year and under a variety of physical assumptions	10.5281/zenodo.6029807

Table C6. Summary of SLIIDERS datasets and pyCIAM inputs for socioeconomic variables.

Input Dataset	**Source & Description**
Current Population	LandScan 2021 (Sims et al., 2022) Spatial distribution of global population in 2019 at a 30 arc-second resolution (1km at equator) PWT 10.0 (Feenstra et al., 2015), UN World Population Prospects (UN DESA 2019) Country-level population estimates
Current Income	PWT 10.0 (Feenstra, Inklaar, and Timmer 2015) World Bank World Development Indicators (World Bank, 2021) IMF World Economic Outlook (IMF, 2021) Maddison Project Database (Bolt and Zanden, 2020) OECD regional statistics (Economic Cooperation and Development 2020) CIA World Factbook (Agency 2021) Collection of contemporary datasets to estimate national income levels
Physical capital	LitPop (Eberenz et al., 2020), 2015 Global Assessment Report (GEG-15) (Bono and Chatenoux, 2014) Spatially downscaled (30 arc-second and , respectively) estimates of physical capital stock PWT 10.0 (Feenstra et al., 2015) Country-level physical capital stock levels
Mobile capital fraction	PWT 10.0 (Feenstra et al., 2015) Capital is reported in PWT by category; structures are assumed to be immobile, with all other categories assumed as mobile
Economic growth trajectories	Shared Socioeconomic Pathways (Riahi et al., 2017) and capital growth modeled by Dellink et al. 2017 (Dellink et al., 2017) Updated growth trajectories to match those used by the IPCC
Construction cost indices	World Bank ICP (World Bank, 2020; Lincke and Hinkel, 2021)

References

Agency, Central Intelligence. 2021. “The World Factbook.”

Armstrong, Scott B., Eli D. Lazarus, Patrick W. Limber, Evan B. Goldstein, Curtis Thorpe, and Rhoda C. Ballinger. 2016. “Indications of a Positive Feedback Between Coastal Development and Beach Nourishment.” Earth’s Future 4 (12): 626–35.

Bakkensen, Laura A., and Robert O. Mendelsohn. 2016. “Risk and Adaptation: Evidence from Global Hurricane Damages and Fatalities.” Journal of the Association of Environmental and Resource Economists 3 (3): 555–87.

Bakkensen, Laura A, Doo-Sun R Park, and Raja Shanti Ranjan Sarkar. 2018. “Climate Costs of Tropical Cyclone Losses Also Depend on Rain.” Environmental Research Letters 13 (7): 074034.

Bamber, Jonathan L., Michael Oppenheimer, Robert E. Kopp, Willy P. Aspinall, and Roger M. Cooke. 2019. “Ice Sheet Contributions to Future Sea-Level Rise from Structured Expert Judgment.” Proceedings of the National Academy of Sciences 116 (23): 11195–200.

Bank, The World. 2021. “World Development Indicators.”

Berlemann, Michael, and Jan-Erik Wesselhöft. 2017. “Aggregate Capital Stock Estimations for 122 Countries: An Update.” Review of Economics 68 (2): 75–92.

Berrang-Ford, Lea, A. R. Siders, Alexandra Lesnikowski, Alexandra Paige Fischer, Max W. Callaghan, Neal R. Haddaway, Katharine J. Mach, et al. 2021. “A Systematic Global Stocktake of Evidence on Human Adaptation to Climate Change.” Nature Climate Change 11 (11): 989–1000.

Bertram, Geoffrey. 2004. “On the Convergence of Small Island Economies with Their Metropolitan Patrons.” World Development 32 (2): 343–64.

Bolt, Jutta, and Jan Luiten van Zanden. 2020. “Maddison Style Estimates of the Evolution of the World Economy. A New 2020 Update.” Maddison-Project Working Paper, no. WP-15 (August): 1–43.

Bono, Andrea De, and Bruno Chatenoux. 2014. “A Global Exposure Model for GAR 2015.” Input {Paper prepared for the Global Assessment Report on Disaster Risk Reduction. Geneva, Switzerland: The United Nations Office for Disaster Risk Reduction.

Bootsma, J. 2022. “Evaluating Methods to Assess the Coastal Flood Hazard on a Global Scale : A Comparative Analysis Between the Bathtub Approach and the LISFLOOD-AC Model.”

Bower, Erica, and Sanjula Weerasinghe. 2021. “Enhancing the Evidence Base on Planned Relocation Cases in the Context of Hazards, Disasters, and Climate Change,” no. March.

Bunting, Pete, Ake Rosenqvist, Richard M. Lucas, Lisa-Maria Rebelo, Lammert Hilarides, Nathan Thomas, Andy Hardy, Takuya Itoh, Masanobu Shimada, and C. Max Finlayson. 2018. “The Global Mangrove Watch—A New 2010 Global Baseline of Mangrove Extent.” Remote Sensing 10 (10): 1669.

Carleton, Tamma A., Amir Jina, Michael T. Delgado, and Others. 2020. “VALUING THE GLOBAL MORTALITY CONSEQUENCES OF CLIMATE CHANGE ACCOUNTING FOR ADAPTATION COSTS AND BENEFITS.” NBER WORKING PAPER SERIES.

Church, J. A., P.U. Clark, A. Cazenave, J.M. Gregory, S. Jevrejeva, A. Levermann, M.A. Merrifield, et al. 2013. “2013: Sea Level Change.” In Climate Change 2013: The Physical Science Basis. Contribution of Working Group I to the Fifth Assessment Report of the Intergovernmental Panel on Climate Change, edited by T. F. Stocker, D. Qin, G.-K. Plattner, M. Tignor, S.K. Allen, J. Boschung, A. Nauels, Y. Xia, V. Bex, and P.M. Midgley. Cambridge, United Kingdom; New York, NY, USA: Cambridge University Press.

Climate Impact Lab (CIL). 2022. “Data-Driven Spatial Climate Impact Model User Manual, Version 092022-EPA.”

Council, Multihazard Mitigation. 2017. “Natural Hazard Mitigation Saves: 2017 Interim Report,” 22.

Craig, Robin Kundis. 2019. “Coastal Adaptation, Government-Subsidized Insurance, and Perverse Incentives to Stay.” Climatic Change 152 (2): 215–26.

Credit Suisse Research Institute. 2017. “Global Wealth Report 2017: Where Are We Ten Years After the Crisis?”

Crespo Cuaresma, Jesús. 2017. “Income Projections for Climate Change Research: A Framework Based on Human Capital Dynamics.” Global Environmental Change 42 (January): 226–36.

DeConto, Robert M., David Pollard, Richard B. Alley, Isabella Velicogna, Edward Gasson, Natalya Gomez, Shaina Sadai, et al. 2021. “The Paris Climate Agreement and Future Sea-Level Rise from Antarctica.” Nature 593 (7857): 83–89.

Dellink, Rob, Jean Chateau, Elisa Lanzi, and Bertrand Magné. 2017. “Long-Term Economic Growth Projections in the Shared Socioeconomic Pathways.” Global Environmental Change 42 (January): 200–214.

Diaz, Delavane B. 2016. “Estimating Global Damages from Sea Level Rise with the Coastal Impact and Adaptation Model (CIAM).” Climatic Change 137 (1-2): 143–56.

Dronkers, J., J. T. E. Gilbert, L. W. Butler, J. J. Carey, J. Campbell, E. James, C. Mckenzie, et al. 1990. “Strategies for Adaptation to Sea Level Rise.”

Eberenz, Samuel, Dario Stocker, Thomas Röösli, and David N. Bresch. 2020. “Asset Exposure Data for Global Physical Risk Assessment.” Earth System Science Data 12 (2): 817–33.

Economic Cooperation and Development, Organisation for. 2020. “Regions and Cities: OECD Statistics.”

European Space Agency, and UCLouvain. 2010. “Globcover 2009.”

Fariss, Christopher J, Therese Anders, Jonathan Markowitz, and Miriam Barnum. 2021. “New Estimates of Over 500 Years of Historic GDP and Population Data.” Preprint. SocArXiv.

Feenstra, Robert C., Robert Inklaar, and Marcel P. Timmer. 2015. “The Next Generation of the Penn World Table.” American Economic Review 105 (10): 3150–82.

Foure, Jean, Agnès Bénassy-Quéré, and Lionel Fontagne. 2012. “The Great Shift: Macroeconomic Projections for the World Economy at the 2050 Horizon.” {SSRN} {Scholarly} {Paper} ID 2004332. Rochester, NY: Social Science Research Network.

Fox-Kemper, B., H. T. Hewitt, C. Xiao, G. Aðalgeirsdóttir, S. S. Drijfhout, T. L. Edwards, N. R. Golledge, M. Hemer, R. E. Kopp, and G. Krinner. 2021. “Ocean, Cryosphere and Sea Level Change.” Climate Change 2021: The Physical Science Basis. Contribution of Working Group I to the Sixth

Assessment Report of the Intergovernmental Panel on Climate Change [Masson-Delmotte, V., P. Zhai, A. Pirani, S.L. Connors, C. Péan, S. Berger, N. Caud, Y. Chen, L. Goldfarb, M.I. Gomis, M. Huang, K. Leitzell, E. Lonnoy, J.B.R. Matthews, T.K. Maycock, T. Waterfield, O. Yelekçi, R. Yu, and B. Zhou (Eds.)], no. Cambridge University Press, Cambridge, United Kingdom and New York, NY, USA: 1211–1362.

Garner, G. G., T. Hermans, R. E. Kopp, A. B. A. Slangen, T. L. Edwards, A. Levermann, S. Nowicki, et al. 2022. "IPCC AR6 WGI Sea Level Projections," December.

Gregory, Jonathan M., Stephen M. Griffies, Chris W. Hughes, Jason A. Lowe, John A. Church, Ichiro Fukimori, Natalya Gomez, et al. 2019. "Concepts and Terminology for Sea Level: Mean, Variability and Change, Both Local and Global." Surveys in Geophysics 40 (6): 1251–89.

Haasnoot, Marjolijn, Sally Brown, Paolo Scussolini, Jose A. Jimenez, Athanasios T. Vafeidis, and Robert J. Nicholls. 2019. "Generic Adaptation Pathways for Coastal Archetypes Under Uncertain Sea-Level Rise." Environmental Research Communications 1 (7).

Haer, Toon, W. J.Wouter Botzen, Hans de Moel, and Jeroen C. J. H. Aerts. 2017. "Integrating Household Risk Mitigation Behavior in Flood Risk Analysis: An Agent-Based Model Approach." Risk Analysis 37 (10): 1977–92.

Hallegatte, Stephane, Colin Green, Robert J. Nicholls, and Jan Corfee-Morlot. 2013. "Future Flood Losses in Major Coastal Cities." Nature Climate Change 3 (9): 802–6.

Hastings, David A., and Paula K. Dunbar, eds. 1999. "Global Land One-Kilometer Base Elevation (GLOBE)." Documentation. Boulder, CO: National Oceanic; Atmospheric Administration.

Heston, Alan, Robert Summers, and Bettina Aten. 2011. "Penn World Table Version 7.0." Center for International Comparisons of Production, Income; Prices at the University of Pennsylvania.

Higgins, Matthew. 1998. "Demography, National Savings, and International Capital Flows." International Economic Review 39 (2): 343–69.

Hinkel, Jochen, Jeroen C. J. H. Aerts, Sally Brown, Jose A. Jiménez, Daniel Lincke, Robert J. Nicholls, Paolo Scussolini, Agustín Sanchez-Arcilla, Athanasios Vafeidis, and Kwasi Appeaning Addo. 2018. "The Ability of Societies to Adapt to Twenty-First-Century Sea-Level Rise." Nature Climate Change 8 (7): 570–78.

Hinkel, Jochen, and Richard J. T. Klein. 2009. "Integrating Knowledge to Assess Coastal Vulnerability to Sea-Level Rise: The Development of the DIVA Tool." Global Environmental Change 19 (3): 384–95.

Hinkel, Jochen, Daniel Lincke, Athanasios T. Vafeidis, Mahé Perrette, Robert James Nicholls, Richard S. J. Tol, Ben Marzeion, Xavier Fettweis, Cezar Ionescu, and Anders Levermann. 2014. "Coastal Flood Damage and Adaptation Costs Under 21st Century Sea-Level Rise." Proceedings of the National Academy of Sciences of the United States of America 111 (9): 3292–97.

Hinkel, Jochen, Detlef P. van Vuuren, Robert J. Nicholls, and Richard J. T. Klein. 2013. "The Effects of Adaptation and Mitigation on Coastal Flood Impacts During the 21st Century. An Application of the DIVA and IMAGE Models." Climatic Change 117 (4): 783–94.

Hoozemans, Frank M. J., M. Marchand, and H. A. Pennekamp. 1993. "A Global Vulnerability Analysis: Vulnerability Assessment for Population, Coastal Wetlands and Rice Production on a Global Scale." Technical Report 2nd Edition. The Netherlands: Delft Hydraulics.

Houser, Trevor, Solomon Hsiang, Robert Kopp, Kate Larsen, Michael Delgado, Amir Jina, Michael Mastrandrea, et al. 2015. Economic Risks of Climate Change: An American Prospectus. Columbia University Press.

Hu, Shengjie, Zhenguo Niu, and Yanfen Chen. 2017. “Global Wetland Datasets: A Review.” Wetlands 37 (5): 807–17.

IMF, International Monetary. 2011. “World Economic Outlook Database 2011.”

IMF, I. M.: World Economic Outlook Database, April 2021. 2021.

Inklaar, Robert, Pieter Woltjer, and Daniel Gallardo Albarrán. 2019. “The Composition of Capital and Cross-Country Productivity Comparisons.” International Productivity Monitor 36: 34–52.

Jones, B., and B. C. O’Neill. 2016. “Spatially Explicit Global Population Scenarios Consistent with the Shared Socioeconomic Pathways.” Environmental Research Letters 11 (8): 084003.

Jonkman, S. N., and J. K. Vrijling. 2008. “Loss of Life Due to Floods.” Journal of Flood Risk Management 1: 43–56.

Kc, Samir, and Wolfgang Lutz. 2017. “The Human Core of the Shared Socioeconomic Pathways: Population Scenarios by Age, Sex and Level of Education for All Countries to 2100.” Global Environmental Change 42 (January): 181–92.

Kopp, Robert E., Robert M. DeConto, Daniel A. Bader, Carling C. Hay, Radley M. Horton, Scott Kulp, Michael Oppenheimer, David Pollard, and Benjamin H. Strauss. 2017. “Evolving Understanding of Antarctic Ice-Sheet Physics and Ambiguity in Probabilistic Sea-Level Projections.” Earth’s Future 5 (12): 1217–33.

Kopp, Robert E., Elisabeth A. Gilmore, Christopher M. Little, Jorge Lorenzo-Trueba, Victoria C. Ramenzoni, and William V. Sweet. 2019. “Usable Science for Managing the Risks of Sea-Level Rise.” Earth’s Future 7 (12): 1235–69.

Kopp, Robert E., Radley M. Horton, Christopher M. Little, Jerry X. Mitrovica, Michael Oppenheimer, D. J. Rasmussen, Benjamin H. Strauss, and Claudia Tebaldi. 2014. “Probabilistic 21st and 22nd Century Sea level Projections at a Global Network of Tide‐gauge Sites.” Earth’s Future 2 (8): 383–406. ht

Krogh, Georg von, and Eric von Hippel. 2006. “The Promise of Research on Open Source Software.” Management Science 52 (7): 975–83.

Kulp, Scott A., and Benjamin H. Strauss. 2018. “CoastalDEM: A Global Coastal Digital Elevation Model Improved from SRTM Using a Neural Network.” Remote Sensing of Environment 206 (March): 231–39.

Kulp, S. A. and Strauss, B. H.: 2019. “New Elevation Data Triple Estimates of Global Vulnerability to Sea-Level Rise and Coastal Flooding.” Nature Communications 10 (1).

Kulp, Scott A, and Benjamin H Strauss. 2021. “CoastalDEM V2.1: A High-Accuracy and High-Resolution Global Coastal Elevation Model Trained on ICESat-2 Satellite Lidar,” September, 17.

Lickley, Megan J., Ning Lin, and Henry D. Jacoby. 2014. “Analysis of Coastal Protection Under Rising Flood Risk.” Climate Risk Management 6 (January): 18–26.

Lincke, Daniel, and Jochen Hinkel. 2018. “Economically Robust Protection Against 21st Century Sea-Level Rise.” Global Environmental Change 51 (July): 67–73.

Lincke, D. and Hinkel, J.: 2021. “Coastal Migration Due to 21st Century Sea-Level Rise.” Earth’s Future 9 (5): e2020EF001965.

Lorie, Mark, James E. Neumann, Marcus C. Sarofim, Russell Jones, Radley M. Horton, Robert E. Kopp, Charles Fant, et al. 2020. “Modeling Coastal Flood Risk and Adaptation Response Under Future Climate Conditions.” Climate Risk Management 29 (January): 100233.

McNamara, Dylan E., Sathya Gopalakrishnan, Martin D. Smith, and A. Brad Murray. 2015. “Climate Adaptation and Policy-Induced Inflation of Coastal Property Value.” PLoS ONE 10 (3): 1–12.

McNamara, Dylan E., and Andrew Keeler. 2013. “A Coupled Physical and Economic Model of the Response of Coastal Real Estate to Climate Risk.” Nature Climate Change 3 (6): 559–62.

Mendelsohn, Robert O., Joseph G. Schiavo, and Alex Felson. 2020. “Are American Coasts Under-Protected?” Coastal Management 48 (1): 23–37.

Merkens, Jan-Ludolf, Lena Reimann, Jochen Hinkel, and Athanasios T. Vafeidis. 2016. “Gridded Population Projections for the Coastal Zone Under the Shared Socioeconomic Pathways.” Global and Planetary Change 145 (October): 57–66.

Muis, Sanne, Maialen Irazoqui Apecechea, Job Dullaart, Joao de Lima Rego, Kristine Skovgaard Madsen, Jian Su, Kun Yan, and Martin Verlaan. 2020. “A High-Resolution Global Dataset of Extreme Sea Levels, Tides, and Storm Surges, Including Future Projections.” Frontiers in Marine Science 7: 263.

Muis, Sanne, Martin Verlaan, Hessel C. Winsemius, Jeroen C. J. H. Aerts, and Philip J. Ward. 2016. “A Global Reanalysis of Storm Surges and Extreme Sea Levels.” Nature Communications 7 (June): 11969.

Mulet, Sandrine, Marie-Hélène Rio, Hélène Etienne, Camilia Artana, Mathilde Cancet, Gérald Dibarboure, Hui Feng, et al. 2021. “The New CNES-CLS18 Global Mean Dynamic Topography.” Ocean Science 17 (3): 789–808.

Nations, United. 2021. “National Accounts—Analysis of Main Aggregates (AMA).” UN Statistics Division.

Neumann, Barbara, Athanasios T. Vafeidis, Juliane Zimmermann, and Robert J. Nicholls. 2015. “Future Coastal Population Growth and Exposure to Sea-Level Rise and Coastal Flooding - A Global Assessment.” PLoS ONE 10 (3).

Nicholls, Robert J. 2002. “Analysis of Global Impacts of Sea-Level Rise: A Case Study of Flooding.” Physics and Chemistry of the Earth, Parts A/B/C 27 (32): 1455–66.

Nicholls, R. J.: 2004. “Coastal Flooding and Wetland Loss in the 21st Century: Changes Under the SRES Climate and Socio-Economic Scenarios.” Global Environmental Change 14 (1): 69–86.

Nicholls, Robert, Richard Klein, and Richard Tol. 2006. “Managing Coastal Vulnerability and Climate Change: A National to Global Perspective.” In.

O’Neill, Brian C., Elmar Kriegler, Kristie L. Ebi, Eric Kemp-Benedict, Keywan Riahi, Dale S. Rothman, Bas J. van Ruijven, et al. 2017. “The Roads Ahead: Narratives for Shared Socioeconomic Pathways Describing World Futures in the 21st Century.” Global Environmental Change 42 (January): 169–80.

Oppenheimer, Michael, Bruce Glavovic, J. Hinkel, R. van de Wal, Alexandre K. Magnan, Amro Abd-Elgawad, Rongshuo Cai, et al. 2019. “Chapter 4: Sea Level Rise and Implications for Low Lying

Islands, Coasts and Communities." In IPCC Special Report on the Ocean and Cryosphere in a Changing Climate.

Pardaens, A. K., J. A. Lowe, S. Brown, R. J. Nicholls, and D. de Gusmão. 2011. "Sea-Level Rise and Impacts Projections Under a Future Scenario with Large Greenhouse Gas Emission Reductions." Geophysical Research Letters 38 (12).

Pyo, Hak K., and Minjung Kim. 2020. "Estimating Capital Stock in North Korea and Its Implications." {SSRN} {Scholarly} {Paper}. Rochester, NY.

Rasmussen, D. J., Klaus Bittermann, Maya K. Buchanan, Scott Kulp, Benjamin H. Strauss, Robert E. Kopp, and Michael Oppenheimer. 2018. "Extreme Sea Level Implications of 1.5 °C, 2.0 °C, and 2.5 °C Temperature Stabilization Targets in the 21st and 22nd Centuries." Environmental Research Letters 13 (3): 034040.

Rasmussen, D. J., Maya K. Buchanan, Robert E. Kopp, and Michael Oppenheimer. 2020. "A Flood Damage Allowance Framework for Coastal Protection With Deep Uncertainty in Sea Level Rise." Earth's Future 8 (3): e2019EF001340.

Riahi, Keywan, Detlef P. van Vuuren, Elmar Kriegler, Jae Edmonds, Brian C. O'Neill, Shinichiro Fujimori, Nico Bauer, et al. 2017. "The Shared Socioeconomic Pathways and Their Energy, Land Use, and Greenhouse Gas Emissions Implications: An Overview." Global Environmental Change 42 (January): 153–68.

Rode, Ashwin, Tamma Carleton, Michael Delgado, Michael Greenstone, Trevor Houser, Solomon Hsiang, Andrew Hultgren, et al. 2021. "Estimating a Social Cost of Carbon for Global Energy Consumption." Nature 598 (7880): 308–14.

Rodriguez, Ernesto, C. S. Morris, J. E. Belz, E. C. Chapin, J. M. Martin, W. Daffer, and S. Hensley. 2005. "An Assessment of the SRTM Topographic Products."

Román, Miguel O., Zhuosen Wang, Qingsong Sun, Virginia Kalb, Steven D. Miller, Andrew Molthan, Lori Schultz, et al. 2018. "NASA's Black Marble Nighttime Lights Product Suite." Remote Sensing of Environment 210 (June): 113–43.

Sadoff, C. W., J. W. Hall, D. Grey, J. C. J. H. Aerts, M. Ait-Kadi, C. Brown, A. Cox, et al. 2015. "Securing Water, Sustaining Growth. Report of the GWP/OECD Task Force on Water Security and Sustainable Growth." University of Oxford.

Scussolini, Paolo, Jeroen C. J. H. Aerts, Brenden Jongman, Laurens M. Bouwer, Hessel C. Winsemius, Hans de Moel, and Philip J. Ward. 2016. "FLOPROS: An Evolving Global Database of Flood Protection Standards." Natural Hazards and Earth System Sciences 16 (5): 1049–61.

Sims, Kelly, Andrew Reith, Edward Bright, Jacob McKee, and Amy Rose. 2022. "LandScan Global 2021." Oak Ridge National Laboratory.

Suckall, Natalie, Emma L. Tompkins, Robert J. Nicholls, Abiy S. Kebede, Attila N. Lázár, Craig Hutton, Katharine Vincent, et al. 2018. "A Framework for Identifying and Selecting Long Term Adaptation Policy Directions for Deltas." Science of the Total Environment 633: 946–57.

Suisse, Credit. 2021. "Global Wealth Databook 2021." Zurich: Crédit Suisse.

Sweet, W. V., R. Horton, R. E. Kopp, A. N. LeGrande, and A. Romanou. 2017. “Ch. 12: Sea Level Rise. Climate Science Special Report: Fourth National Climate Assessment, Volume I.” U.S. Global Change Research Program.

Sweet, WV, BD Hamlington, RE Kopp, CP Weaver, PL Barnard, D Bekaert, W Brooks, et al. 2022. “Global and Regional Sea Level Rise Scenarios for the United States: Updated Mean Projections and Extreme Water Level Probabilities Along US Coastlines.” NOAA Technical Report.

Taylor, Karl E., Ronald J. Stouffer, and Gerald A. Meehl. 2012. “An Overview of CMIP5 and the Experiment Design.” Bulletin of the American Meteorological Society 93 (4): 485–98.

Tebaldi, Claudia, Roshanka Ranasinghe, Michalis Vousdoukas, D. J. Rasmussen, Ben Vega-Westhoff, Ebru Kirezci, Robert E. Kopp, Ryan Sriver, and Lorenzo Mentaschi. 2021. “Extreme Sea Levels at Different Global Warming Levels.” Nature Climate Change 11 (9): 746–51.

Tiggeloven, Timothy, Hans de Moel, Hessel C. Winsemius, Dirk Eilander, Gilles Erkens, Eskedar Gebremedhin, Andres Diaz Loaiza, et al. 2020. “Global-Scale Benefit-Cost Analysis of Coastal Flood Adaptation to Different Flood Risk Drivers Using Structural Measures.” Natural Hazards and Earth System Sciences 20 (4): 1025–25.

Tol, Richard S. J. 1996. “The Damage Costs of Climate Change Towards a Dynamic Representation.” Ecological Economics 19 (1): 67–90.

Tozer, B, D T Sandwell, W H F Smith, C Olson, J R Beale, and P Wessel. 2019. “Global Bathymetry and Topography at 15 Arc Sec: SRTM15+.” Earth and Space Science 6 (August): 1–18.

UN DESA, Department of Economic and Social Affairs, P. U. N.: 2012. “World Population Prospects 2012: Volume I: Comprehensive Tables.”

UN DESA, Department of Economic and Social Affairs, P. U. N.: 2019. “World Population Prospects 2019: Volume I: Comprehensive Tables.”

United Nations, Department of Economic and Social Affairs, Population Division. 2022. “World Population Prospects 2022, Online Edition.”

University, Center For International Earth Science Information Network-CIESIN-Columbia. 2016. “Gridded Population of the World, Version 4 (GPWv4): Population Density.” Palisades, NY: NASA Socioeconomic Data; Applications Center (SEDAC).

Vafeidis, Athanasios T., Robert J. Nicholls, Loraine McFadden, Richard S. J. Tol, Jochen Hinkel, Tom Spencer, Poul S. Grashoff, Gerben Boot, and Richard J. T. Klein. 2008. “A New Global Coastal Database for Impact and Vulnerability Analysis to Sea-Level Rise.” Journal of Coastal Research 24 (4): 917–24.

Vousdoukas, Michalis I., Evangelos Voukouvalas, Lorenzo Mentaschi, Francesco Dottori, Alessio Giardino, Dimitrios Bouziotas, Alessandra Bianchi, Peter Salamon, and Luc Feyen. 2016. “Developments in Large-Scale Coastal Flood Hazard Mapping.” Natural Hazards and Earth System Sciences 16 (8): 1841–53.

Wilkinson, Mark D., Michel Dumontier, IJsbrand Jan Aalbersberg, Gabrielle Appleton, Myles Axton, Arie Baak, Niklas Blomberg, et al. 2016. “The FAIR Guiding Principles for Scientific Data Management and Stewardship.” Scientific Data 3 (1): 160018.

World Bank. 2020. “International Comparison Program 2017.” Database..

Yohe, Gary, James Neumann, and Holly Ameden. 1995. “Assessing the Economic Cost of Greenhouse-Induced Sea Level Rise: Methods and Application in Support of a National Survey.” Journal of Environmental Economics and Management 29 (3): S78–97.

Yohe, Gary, and Richard S. J. Tol. 2002. “Indicators for Social and Economic Coping Capacity - Moving Toward a Working Definition of Adaptive Capacity.” Global Environmental Change 12 (1): 25–40..

Zingerle, P., R. Pail, T. Gruber, and X. Oikonomidou. 2020. “The Combined Global Gravity Field Model XGM2019e.” Journal of Geodesy 94 (7): 1–12.

Conclusion

While the projects detailed above provide important insights specific to certain climatic hazards and geographic regions, there is much more research that needs to be conducted in this space to better define, identify, and quantify climate-migration links. Increased internal and international mobility resulting from climatic and environmental hazards will likely strain existing political, economic and social institutions and warrants comprehensive attention from the international humanitarian and governance communities. Migrating in the face of deteriorating regional environmental conditions is, in many cases, an important form of adaptation, especially when investing in the kinds of resiliency measures needed to stay in place is not physically possible or prohibitively expensive. Humane, comprehensive policymaking to accommodate and/or facilitate these growing migratory trends within countries and in multilateral contexts needs to be informed by the best possible scientific understanding of climate hazards, their impacts, links to migration and the feasibility of different adaptive pathways.

It may not be necessary, and indeed is likely impossible, to create rigid definitions of 'climate migrants' or 'climate displaced persons', such that a given individual falls squarely in or out of this classification. The number of risk multiplying factors and spectra of socioeconomic factors along which each person exists means that many migrants will be compelled to move due to more than climatic hazards alone. Therefore, research and governance efforts should utilize the best available data to predict future climate-migration dynamics and should be part of a broader conversation about human mobility that is not singularly climate focused.

The advances made in the research work detailed above represent steps towards filling the knowledge and data gaps that are crucial for informing global climate and migration policy discussion. Though uncertainties regarding the magnitude and spatiotemporal patterns of future climate hazards and human migration will always be present, the range of this uncertainty can be reduced and relative likelihoods of different pathways can be converged upon with improved modeling efforts, integration of newly available data products and robust, empirically-grounded research. My work constitutes important advances towards achieving these goals, summarized below.

I. New regional drought projections in a Central American region that is becoming increasingly afflicted by severe dry spells, contains a high proportion of rain-dependent agricultural communities and is a major source region for out-migration, primarily to the United States and Mexico. This is done using a suite of contemporary climate models for multiple future scenarios, new sources of historical, gridded climate reanalysis data and through the creation of a novel comprehensive drought stress metric. This analysis was done for seasonal and annual scale droughts and finds that both drought types are projected to become more frequent, lengthy and severe throughout the remainder of the 21st-century.

II. Drought stress metrics, along with other physical and socioeconomic variables linked to international out-migration and internal movement in Guatemala from 2002-2018, as reported in their latest 2018 national census report. This predictive modeling exercise finds drought stress to be a significant predictor of international out-migration and points

to the need to continue similar such studies with improved migration data and potentially in a framework of causal identification.

III. A comprehensive, historical assessment of the evidence base regarding multiple climate shocks and stressors and their direct and indirect impacts on human displacement in the United States. This evaluation underscores important aspects of socioeconomic inequities in terms of hazard exposure, resilience and the ability to recover following climate impacts across the country.

IV. An improved method for creating downscaled, gridded maps of population distributions in a U.S. context for multiple sociodemographic variables. Using census data, satellite-detected building rooftop footprints and fine-scale residential parcel boundaries, 2020 census data for California was disaggregated to 100-meter (sub-census block) pixel estimates. These resultant gridded data products, though not directly applied to migration-relevant research, have been used in multiple environmental justice, sea level rise and social inequity-oriented studies and have the potential to inform migration studies in the state moving forward, as well as serving as a methodological template for similar data product efforts elsewhere.

V. A novel methodological approach to assess post-hurricane power outages in the context of Puerto Rico following Hurricane Maria. Utilizing new collections of satellite-detected nighttime lights imagery before and after the storm made landfall, it was possible to create a high-resolution mapping of outage severity experienced across the island and build a predictive model that identifies physical and socioeconomic predictors of those outages. Population change between 2010 and 2020 on the island, largely reflecting out-migration in that period to the mainland United States, was also evaluated as potential links to post-Maria outages were explored.

VI. Creation of a global, open-source coastal impacts and adaptation modeling platform that integrates the most contemporary climate projections and socioeconomic and physical input datasets at a granular resolution for roughly ten-thousand coastline segments. The initial model results provide important insight into the magnitude of projected economic impacts of rising sea levels and present a compelling case for likely adaptation pathways. These potential adaptive behaviors undertaken by coastal regions throughout the 21st-century include constructing protective sea walls or migrating inland. Based on the optimality of adaptation decision making, the magnitude of potential coastal out-migrants varies dramatically, but could amount to up to 200 million people fleeing inland by 2100.

The findings of these two Central American studies can help inform the discussion around the scope, magnitude and potential solutions with respect to the nature of drought hazards in Central America and can give credence to policy agendas that seek to acknowledge the role of climate as an influencing factor in migratory decision-making in the region. The complexity of the migration modeling results also highlights the need for a nuanced discussion that recognizes the interplay of both climatic and non-climatic factors as potential migration drivers.

The results of these U.S.-based studies provide additional synthesis, dataset development, methodological improvement and modeling progress that can be used to guide continued

research efforts in this and adjacent fields, and enrich ongoing climate migration and displacement discussions in policy spheres. The global coastal impacts modeling platform represents a significant improvement upon the modeling methods and dataset utilization of prior studies in the space, providing both a useful publicly-accessible tool for interested researchers and supplying plausible estimates of damages, investment in protective infrastructure and potential out-migration from the world's coastlines. These advances all represent important improvements in the fields of climate impacts, migration and human geography and can constitute useful tools for policymakers attempting to craft consensus and legislation in these realms.